LOCKHEED MARTIN ENERGY RESEARCH LIBRARIES

3 4456 0515105 5

ORNL-5020

Cy 91

Theoretical and Experimental Stress Analyses of ORNL Thin-Shell Cylinder-to-Cylinder Model 3

R. C. Gwaltney
S. E. Bolt
J. M. Corum
J. W. Bryson

OAK RIDGE NATIONAL LABORATORY
CENTRAL RESEARCH LIBRARY
DOCUMENT COLLECTION
LIBRARY LOAN COPY
DO NOT TRANSFER TO ANOTHER PERSON
If you wish someone else to see this document, send in name with document and the library will arrange a loan.

OAK RIDGE NATIONAL LABORATORY
OPERATED BY UNION CARBIDE CORPORATION • FOR THE U.S. ATOMIC ENERGY COMMISSION

Printed in the United States of America. Available from
National Technical Information Service
U.S. Department of Commerce
5285 Port Royal Road, Springfield, Virginia 22161
Price: Printed Copy $7.60; Microfiche $2.25

This report was prepared as an account of work sponsored by the United States Government. Neither the United States nor the Energy Research and Development Administration, nor any of their employees, nor any of their contractors, subcontractors, or their employees, makes any warranty, express or implied, or assumes any legal liability or responsibility for the accuracy, completeness or usefulness of any information, apparatus, product or process disclosed, or represents that its use would not infringe privately owned rights.

ORNL-5020
UC-79, -79h, -79k

Contract No. W-7405-eng-26

Reactor Division

THEORETICAL AND EXPERIMENTAL STRESS ANALYSES OF ORNL THIN-SHELL CYLINDER-TO-CYLINDER MODEL 3

R. C. Gwaltney J. M. Corum
S. E. Bolt J. W. Bryson

JUNE 1975

OAK RIDGE NATIONAL LABORATORY
Oak Ridge, Tennessee 37830
operated by
UNION CARBIDE CORPORATION
for the
U.S. ENERGY RESEARCH AND DEVELOPMENT ADMINISTRATION

LOCKHEED MARTIN ENERGY RESEARCH LIBRARIES

3 4456 0515105 5

CONTENTS

Page

ABSTRACT 1

1. INTRODUCTION 1

2. EXPERIMENTAL ANALYSIS 4

2.1 Model Construction 5

2.2 Strain-Gage Layout 5

2.3 Test Description 8

2.4 Data Acquisition and Reduction 13

2.5 Variations of Maximum Measured Stresses Around Nozzle-Cylinder Junction 14

3. FINITE-ELEMENT ANALYSIS 22

3.1 Background 22

3.2 Finite-Element Method 23

3.3 Finite-Element Idealization of Model 29

4. COMPARISON OF THEORY AND EXPERIMENT 30

4.1 Internal Pressure 31

4.2 Out-of-Plane Moment Loading, M_{XN}, on Nozzle 36

4.3 Torsional Moment Loading, M_{YN}, on Nozzle 42

4.4 In-Plane Moment Loading, M_{ZN}, on Nozzle 42

4.5 In-Plane Force, F_{XN}, on Nozzle 53

4.6 Axial Force, F_{YN}, on Nozzle 53

4.7 Out-of-Plane Force, F_{ZN}, on Nozzle 53

4.8 Torsional Moment Loading, M_{XC}, on Cylinder 54

4.9 Out-of-Plane Moment Loading, M_{YC}, on Cylinder 54

4.10 In-Plane Moment Loading, M_{ZC}, on Cylinder 55

4.11 Axial Force, F_{XC}, on Cylinder 55

4.12 In-Plane Force, F_{YC}, on Cylinder 56

4.13 Out-of-Plane Force, F_{ZC}, on Cylinder 56

5. CONCLUSIONS 102

ACKNOWLEDGMENTS 104

REFERENCES 105

APPENDIX. TABULATION OF EXPERIMENTAL DATA 109

THEORETICAL AND EXPERIMENTAL STRESS ANALYSES OF ORNL THIN-SHELL CYLINDER-TO-CYLINDER MODEL 3

R. C. Gwaltney J. M. Corum
S. E. Bolt J. W. Bryson

ABSTRACT

The third in a series of four thin-shell cylinder-to-cylinder models was tested, and the experimentally determined elastic stress distributions were compared with theoretical predictions obtained from a thin-shell finite-element analysis. The models are idealized thin-shell structures consisting of two circular cylindrical shells that intersect at right angles. There are no transitions, reinforcements, or fillets in the junction region. This series of model tests serves two basic purposes: (1) the experimental data provide design information directly applicable to nozzles in cylindrical vessels, and (2) the idealized models provide test results for use in developing and evaluating theoretical analyses applicable to nozzles in cylindrical vessels and to thin piping tees.

The cylinder of model 3 had an outside diameter of 10 in., and the nozzle had an outside diameter of 1.29 in., giving a d_o/D_o ratio of 0.129. The OD/thickness ratios for the cylinder and the nozzle were 50 and 7.68 respectively. Thirteen separate loading cases were analyzed. In each, one end of the cylinder was rigidly held. In addition to an internal pressure loading, three mutually perpendicular force components and three mutually perpendicular moment components were individually applied at the free end of the cylinder and at the end of the nozzle. The experimental stress distributions for all the loadings were obtained using 158 three-gage strain rosettes located on the inner and outer surfaces.

The loading cases were also analyzed theoretically using a finite-element shell analysis developed at the University of California, Berkeley. The analysis used flat-plate elements and considered five degrees of freedom per node in the final assembled equations. The comparisons between theory and experiment show reasonably good agreement for this model.

1. INTRODUCTION

Intersecting cylindrical shells are common configurations in structural components for nuclear reactor systems, specifically piping tees and nozzles. However, despite their common occurrence, proven elastic stress

analysis methods for such configurations have not been generally available, and only recently have potential analyses been developed. This is true even for an idealized configuration consisting of two thin-shell cylinders intersecting normally with no transitions, reinforcements, or fillets in the junction region.

To meet the need for experimental data obtained from carefully machined models, Oak Ridge National Laboratory (ORNL) tested a series of four thin-shell cylinder-to-cylinder models. In addition to providing test results for use in developing and evaluating potential analytical techniques, the models in the series will provide design information directly applicable to nozzles in cylindrical vessels and to a class of thin piping tees as well. The test results will be particularly applicable to liquid-metal-cooled fast breeder reactor components in which relatively low internal pressures and high thermal transients dictate thin-walled structures.

All the models have been tested, and the experimentally determined stress distributions have been compared with the predictions of a thin-shell finite-element analysis. This report describes the complete tests and analyses of model 3 and presents comparisons of theory and experiments. Some of the tests and analyses of model 3 were described in Ref. 1. The complete tests and analyses for models 1 and 4 are described in Refs. 2 and 3 respectively.

Model 3 is shown in Fig. 1 along with a list of the significant dimensions of all four models. As indicated by the figure, these models are truly idealized shell structures with no transitions, fillets, or reinforcing in the junction region. The outside diameter D_o of the cylinder of model 3 was 10 in. and the outside diameter d_o of the nozzle was 1.29 in., giving a d_o/D_o ratio of 0.129. The cylinder thickness T was 0.2 in., and the nozzle thickness t was 0.168 in. Thus the OD/thickness ratios of the cylinder and the nozzle were 50 and 7.68 respectively. Model 4 was obtained from the third by boring out the nozzle to provide a thinner wall thickness.

Model 3 is shown schematically in Fig. 2, along with the applied forces and moments to which it was subjected and the major dimensions. One end of the model was rigidly fixed, or "built-in," as shown, while external loads

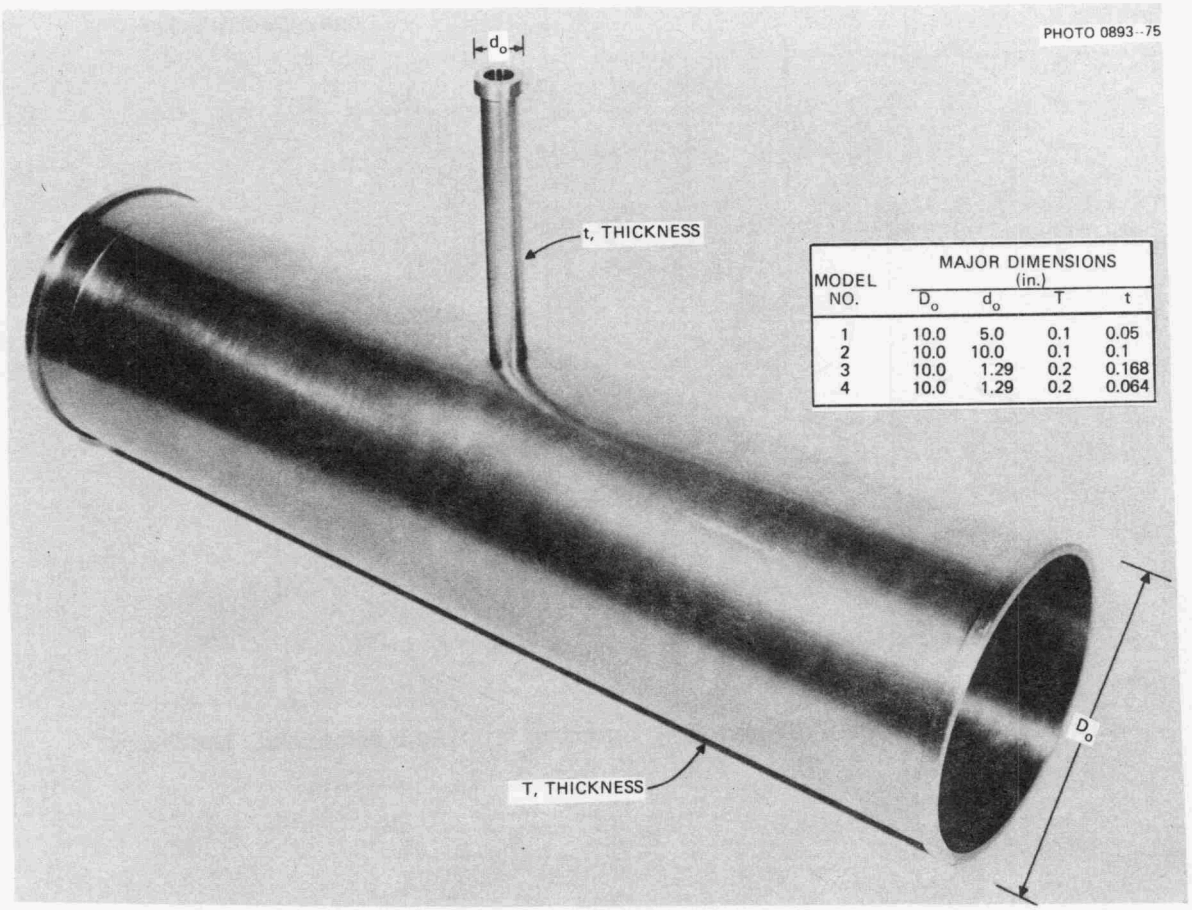

MODEL NO.	MAJOR DIMENSIONS (in.) D_o	d_o	T	t
1	10.0	5.0	0.1	0.05
2	10.0	10.0	0.1	0.1
3	10.0	1.29	0.2	0.168
4	10.0	1.29	0.2	0.064

Fig. 1. Thin-shell cylinder-to-cylinder model 3 and dimensions of all four models in test series.

were applied to the free end of the cylinder and to the end of the nozzle. Three mutually perpendicular force components and three mutually perpendicular moment components were applied individually at each location. Thus, including internal pressure, there was a total of 13 loading cases. These loading cases were examined both experimentally and analytically, and the results were compared for each case.

Chapter 2 of this report describes the testing aspects of the experimental analysis and also the strain-gage data-acquisition and -reduction techniques used. Representative experimental results in the form of maximum measured stress distributions around the nozzle-cylinder junction are presented for each loading. The finite-element analysis is discussed in Chap. 3 along with a brief description of the formulation used and the

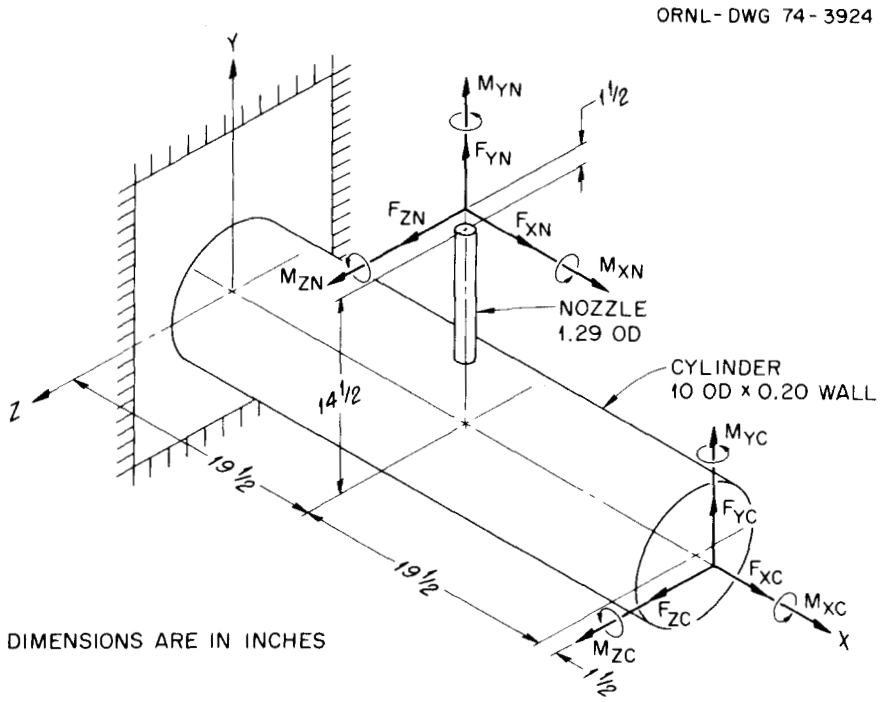

Fig. 2. Schematic of model 3 showing applied external loadings.

specific element layout for the model. Complete comparisons of theory and experiment for all 13 loading cases are discussed in Chap. 4, and Chap. 5 contains a concise summary of the conclusions drawn from the study of model 3. For the benefit of the reader who wishes to use the experimental data for comparisons with his own analyses, an appendix is included that gives a complete set of experimental data for each of the 13 loading cases.

2. EXPERIMENTAL ANALYSIS

In experimental investigations of thin-shell cylinder-to-cylinder pressure vessel configurations, both strain-gage metal models and photoelastic models have been used. Strain-gage model studies for internal pressure and for external nozzle loadings have been carried out by Hardenbergh, Zamrik, and Edmondson,[4] by Hardenbergh and Zamrik,[5] and by Riley.[6] Contoured and reinforced outlets were used in the first two studies; in

the third, the model was fabricated from hot rolled sheet steel by welding. In photoelastic studies carried out by Taylor and Lind[7] and by Leven,[8] reinforced openings were examined. Thus, of the previous studies, only that of Riley[6] used a thin-shell idealized cylinder-to-cylinder metal model, and it was of welded construction rather than being carefully machined.

2.1 Model Construction

One of the primary objectives of the experimental analysis described in this report was to obtain experimental data on a carefully machined cylinder-to-cylinder model so that the effects of geometrical imperfections would be minimized.

The basic configuration was obtained by forging a carbon steel billet into the shape of a tee and then annealing it. The forging was then bored out to the rough inside dimensions, the outside was rough machined, and the structure was reannealed. To maintain the correct dimensions during annealing, a tight-fitting graphite mandrel was machined and inserted in both the nozzle and cylinder. The inside surfaces were then machined to the final dimensions by boring. The final machining on the outside surface was done on a tracing-type milling machine using a carefully constructed mahogany wood pattern.

2.2 Strain-Gage Layout

Model 3 was instrumented with electric resistance strain gages on both the outside and inside surfaces. A sufficient number of gages was used on this model to provide a good description of the stress distributions for comparisons with predictions and for identifying the high-stress regions.

The strain-gage layouts for the outer and inner surfaces are shown in Figs. 3 and 4 respectively. A total of 158 three-gage strain-gage rosettes was used, making 474 individual strain gages. There were 85 rosettes on the outer surface and 73 on the inner surface. These were, in most cases, located "back to back" at the locations shown in Figs. 3 and 4.

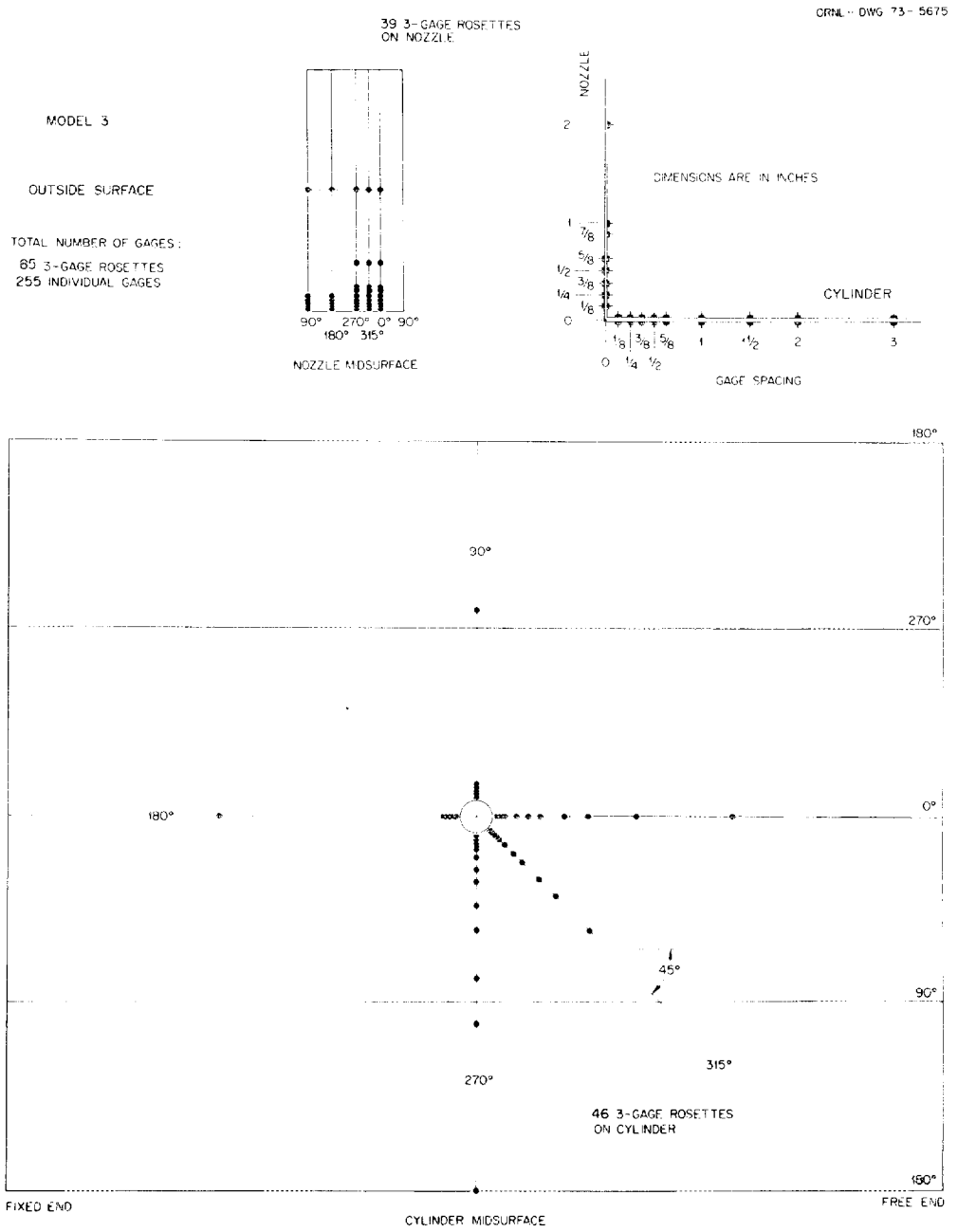

Fig. 3. Strain-gage layout on the outer surface.

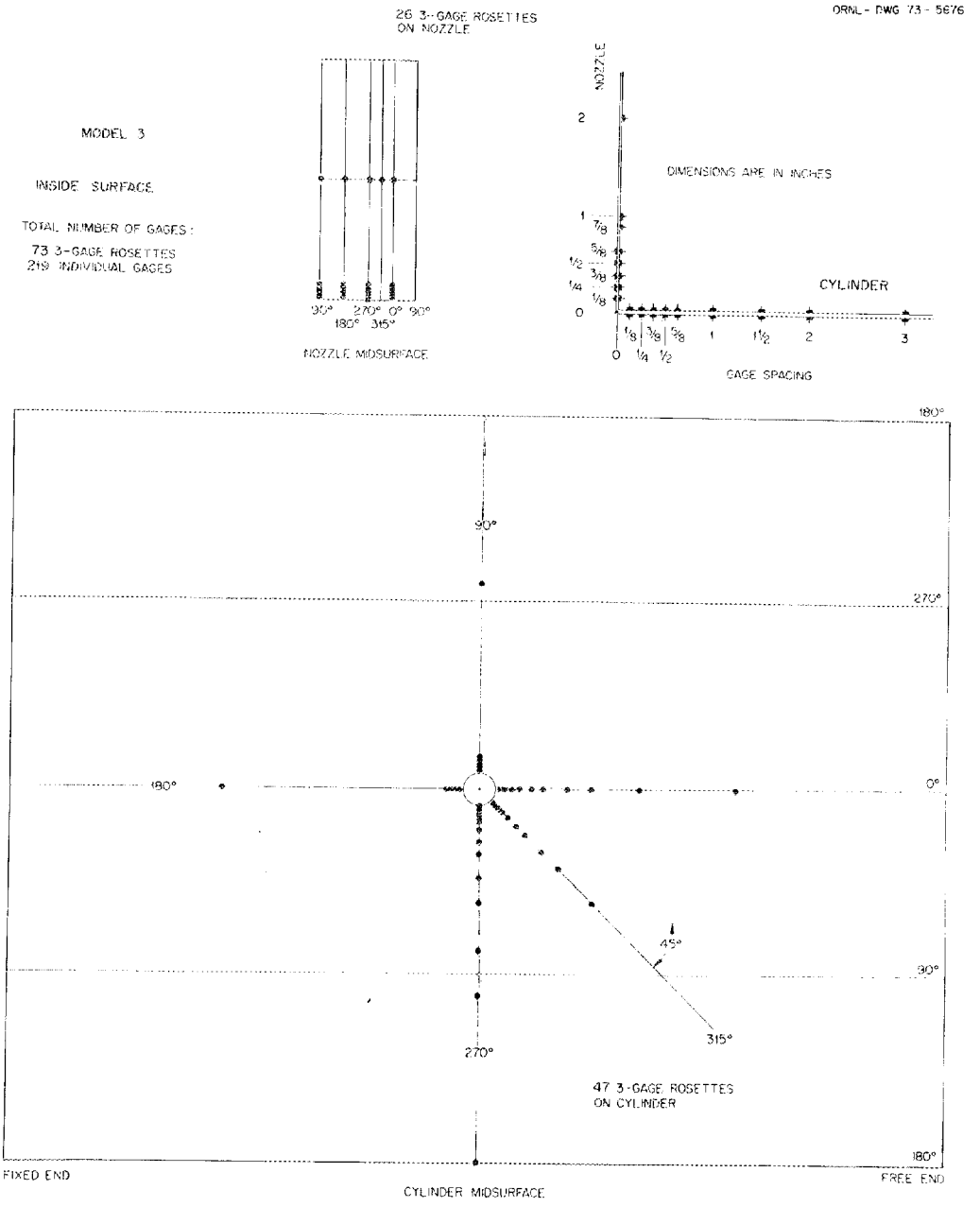

Fig. 4. Strain-gage layout on the inner surface.

The gages were arranged in two opposite quadrants along lines running from the junction of the nozzle and cylinder. One quadrant has three lines of gages at 45° intervals and the other has two lines of gages at 90° intervals with only six rosettes in a line on each surface.

There were two principal reasons for gaging two opposite quadrants. First, the behavior in the two quadrants was expected to be different for the majority of the 13 loadings. Second, for loadings such as internal pressure, where the behavior should be identical, experimental data from two supposedly identical quadrants allow a check of the data and provide some indication of the effects of geometrical imperfections in the model.

The three-gage rosettes used were Micro-Measurements type EA-06-030YB-120, option SE, which are very compact three-gage foil rosettes. The three individual gages are arranged in a "Y" pattern and have an individual gage length of 0.030 in. As can be seen in the inset in the upper right-hand corner of Fig. 3, five complete rosettes were located along each gage line within the first 5/8 in. from the junction. These first five rosettes were supplied mounted on a common backing by the gage manufacturer. These assemblies have the same designation as the single rosettes except that the option becomes B27. One of the five-rosette assemblies is shown in Fig. 5.

The rosettes were applied with an epoxy adhesive, BR-610, which is available from W. T. Bean, Inc. Curing times and temperatures ranged from 10 hr at 250°F to 24 hr at 200°F. Uninsulated 4-mil-diam wire was used to connect the gages to terminal tabs to which larger lead wires were connected.

The model is shown in Fig. 6 with the strain gages applied but not completely wired. The three lines of gages in the fourth quadrant can be clearly seen. They are in the longitudinal plane at 0°, at 45° around from the longitudinal plane, and in the transverse plane at 90° from the longitudinal plane. A closeup of the rosettes in the junction region is shown in Fig. 7.

2.3 Test Description

Figure 8 shows the instrumented model in a loading frame being subjected to an in-plane moment loading on the nozzle. The right end of the

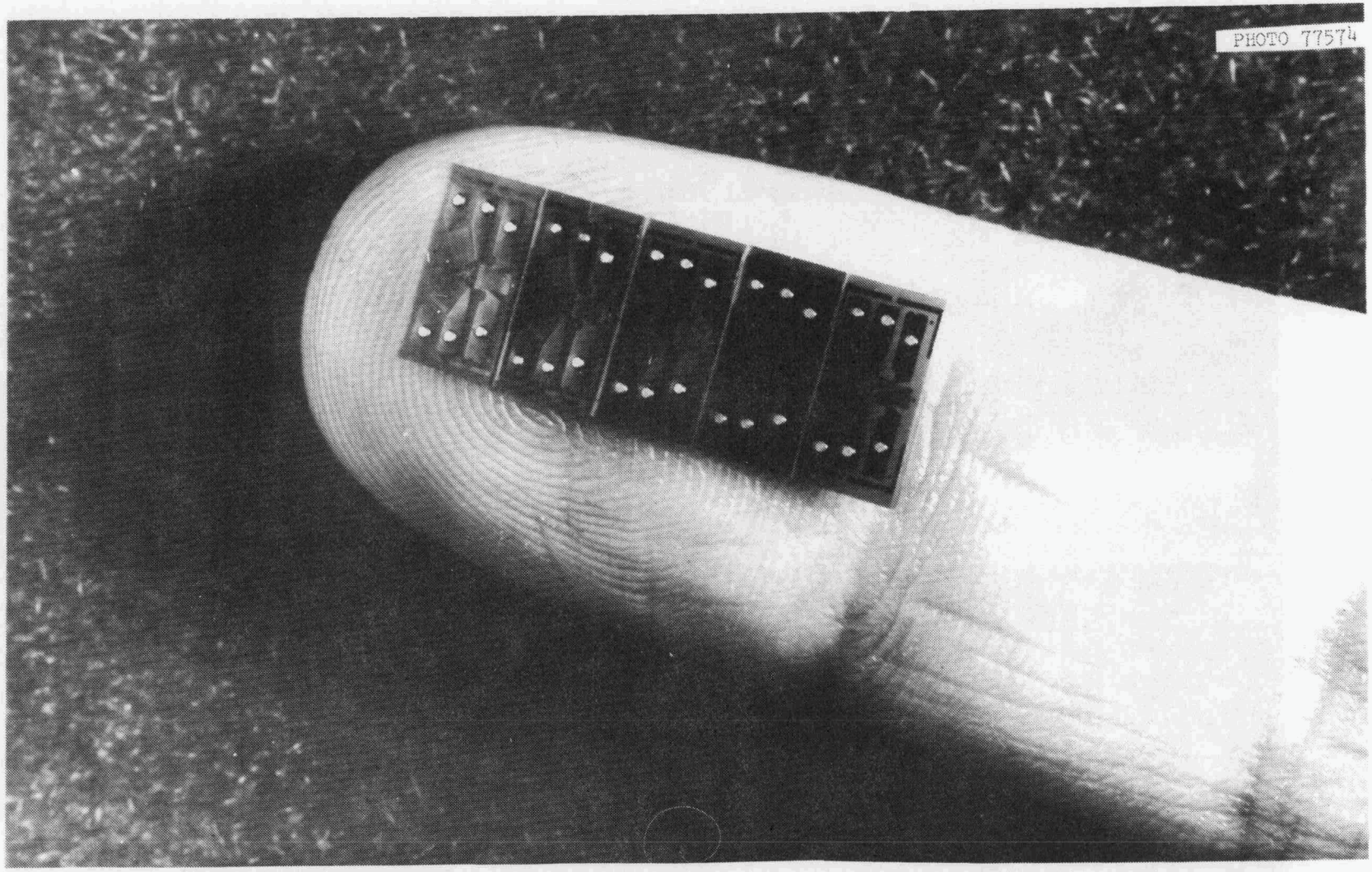

Fig. 5. Closeup of assembly of five strain-gage rosettes on a common foil backing.

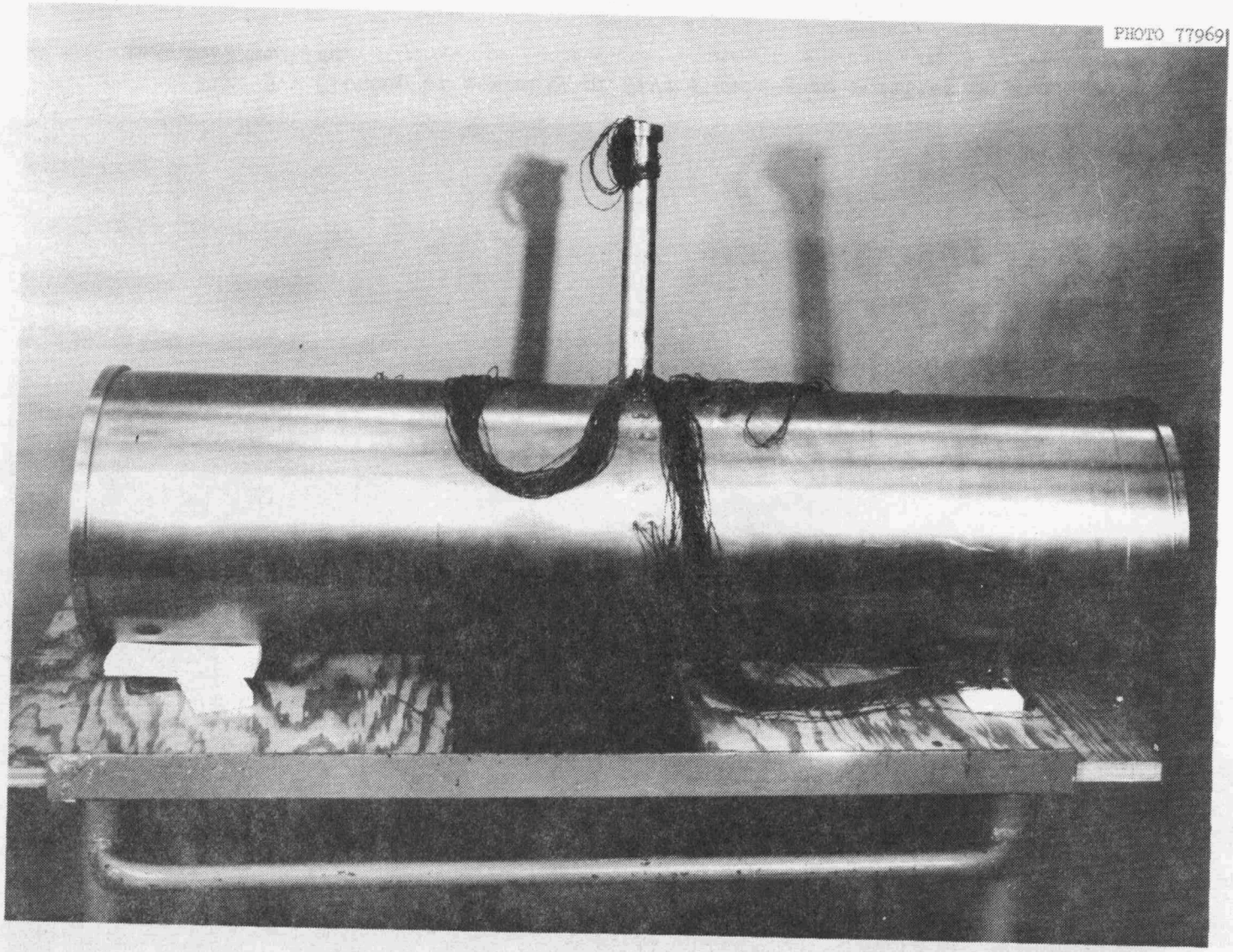

Fig. 6. Model during instrumentation.

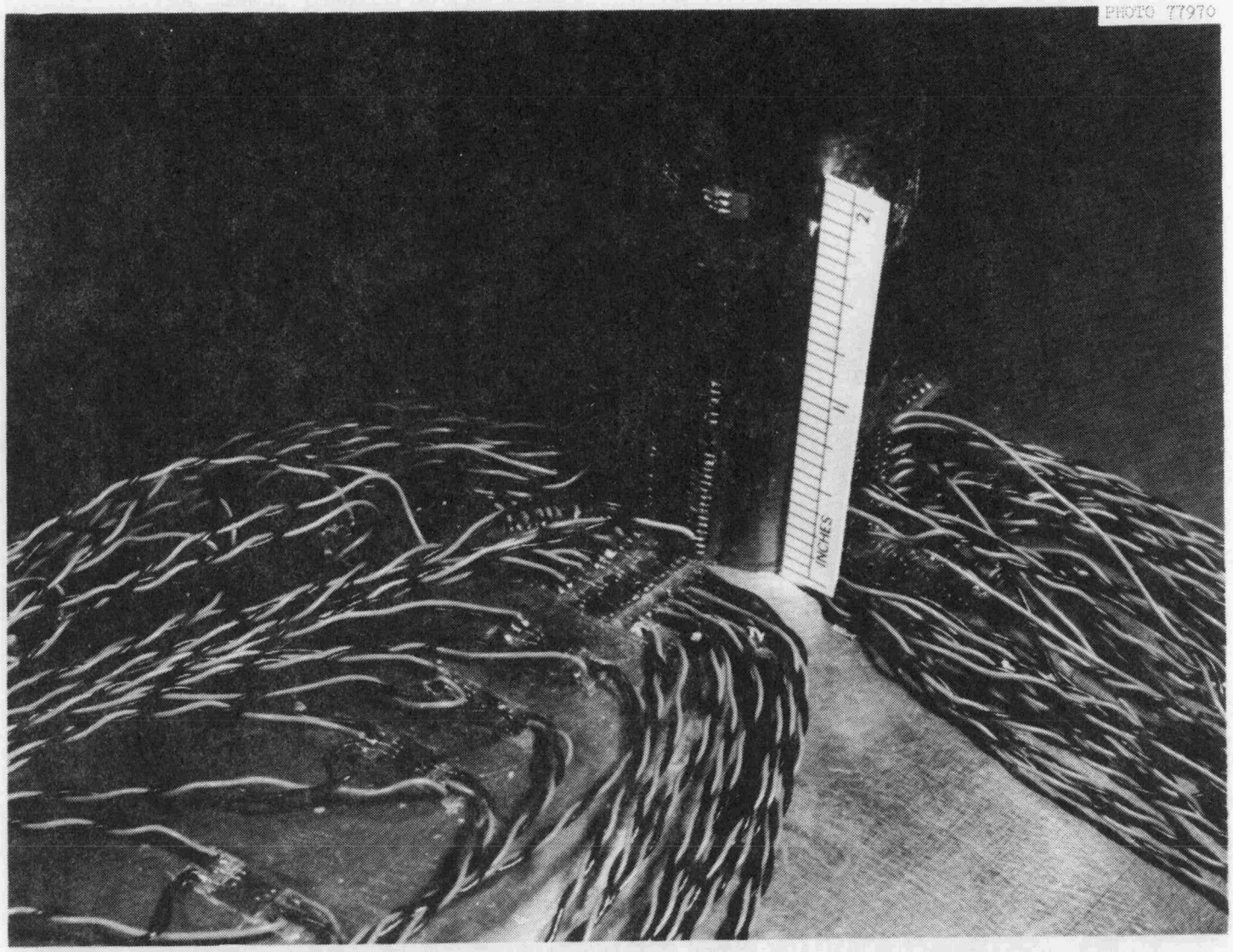

Fig. 7. Closeup of gages in junction region.

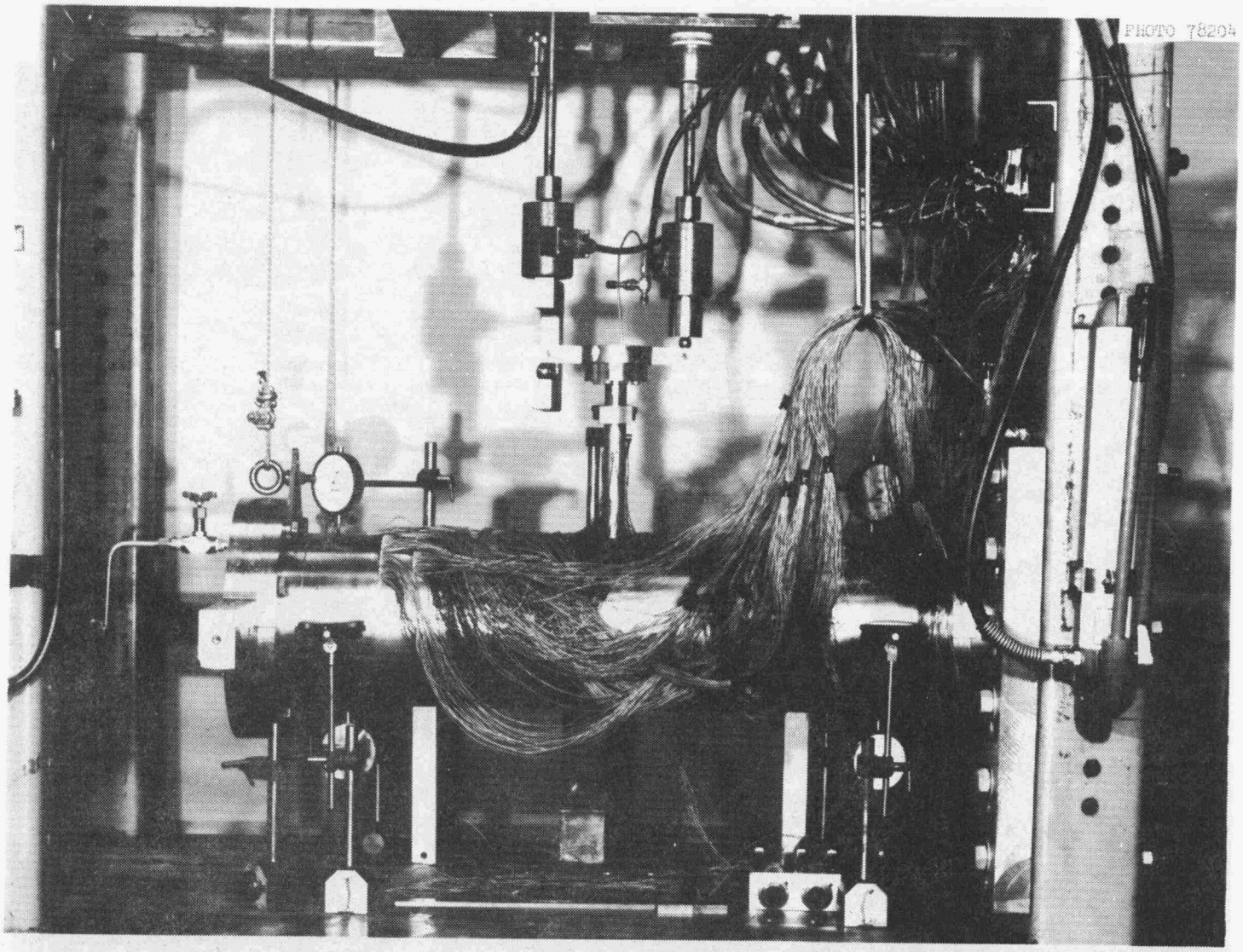

Fig. 8. Instrumented model in test frame being subjected to an in-plane moment loading on the nozzle.

cylinder was rigidly clamped to the heavy flat plate using a split ring arrangement acting over the flange on the end of the cylinder. The loading fixtures on the other end of the cylinder and on the end of the nozzle were attached in a similar manner. These heavy fixtures in effect constrained the end circles of the shell to remain plane circles. The end fixtures were counterbalanced by weights attached to the cables (Fig. 8).

The external loads were applied by hydraulic rams acting through load cells, and the loads were controlled by the load cell indications. The pressure loading was applied using a hydraulic fluid. To avoid undue straining of the model, weights were used to counterbalance the weight of the pressurizing fluid in the model.

For all 13 loading cases, data were taken in eight steps. In most cases the data were taken at 0, 25, 50, 75, 100, 75, 50, 25, 0% of full load. The procedure was then repeated, so that two complete sets of data were taken for each gage every loading.

2.4 Data Acquisition and Reduction

The strain-gage data were recorded by a Datum Computer-Controlled Data Acquisition System (CCDAS). The system consists of a data-acquisition unit composed of a data-acquisition control module controlled by a PDP-8/I computer with the following capabilities: (1) magnetic tape input/output system, (2) in-core calculation ability, and (3) teletypewriter input and output.

The system records the strain data in millivolt readings on magnetic tape. The PDP-8/I computer converts the millivolt reading on the tape into engineering units (strains in this case) and stores them on a second tape which is compatible with the ORNL IBM 360-91 computer. This second tape is sent to the ORNL 360-91 computer, and stresses are calculated for each rosette by stripping the strains off the second tape.

The experimental results presented later in this report and tabulated in the appendix are generally based on the strain-gage readings at maximum load and on the first of the two sets of data taken from each gage and loading. If the first set of data was questionable, the second set was used. The strain-gage readings at fractional values of the maximum load

were used to check linearity and drift of the gages. In cases where nonlinearity or drift was excessive or where an individual gage or circuit was otherwise obviously malfunctioning, the rosette of which the gage was a part was not used in the final results for the specific loading case under consideration. In some instances, a gage that behaved erratically during one loading behaved normally during others. Thus, in the final plots showing the experimental stresses, results from a given rosette may be included for some loadings but not for others.

Stresses were calculated from the experimental strains by using a modulus of elasticity value of 30×10^6 psi and a Poisson ratio of 0.3.

2.5 Variations of Maximum Measured Stresses Around Nozzle-Cylinder Junction

In all but two cases, the maximum measured stresses occurred at the nozzle-cylinder junction. Consequently, representative experimental results in the form of maximum measured stress distributions around the nozzle-cylinder junction are presented and discussed here for each loading. Plots of all the experimental points along each gage line are presented in Chap. 4 for each loading and compared with theoretical predictions.

To examine the maximum stresses, stress ratios were considered. These ratios were determined by dividing the maximum absolute principal stress value at a point by a nominal membrane stress value. The membrane hoop stress in the cylinder and in the nozzle was used as the nominal stress level for the pressure loading. For the moment loadings, the maximum membrane bending stresses (computed by Mc/I) or the membrane shear stress (computed by Tc/J and equal to the maximum normal stress) in the nozzle or cylinder were used as the nominal stresses. For the axial forces on the nozzle and the cylinder, the axial membrane stress (calculated by P/A) was used. For the in-plane and out-of-plane forces on the nozzle, the nominal stress was somewhat arbitrarily chosen as the maximum bending stress in the nozzle (calculated by Mc/I) at the level of the top of the cylinder. For the in-plane and out-of-plane forces on the cylinder, the nominal stress was chosen as the maximum bending stress in the cylinder at its midlength (at the center line of the nozzle).

The applied loads used in the experimental analyses are given in Table 1, together with the nominal membrane stress levels calculated by the above procedures.

The variations in the experimentally determined maximum stresses around the nozzle-cylinder junction are shown in Figs. 9 through 21 for each of the 13 individual loading cases. In each case, the stresses were determined from the strain-gage rosettes immediately adjacent to the junction, and of the four possible maximum stress distributions – cylinder inside and outside and nozzle inside and outside – those shown produced the largest stresses in each case.

The points labeled "extrapolated maximum" in the figures are estimated maximum stress ratios at the junction obtained by extrapolating the experimentally determined principal stress distributions along each gage line to the peak stresses at the junction. It should be emphasized that the maximum stress estimates are based on the stresses along gage lines only; this

Table 1. Applied loads and nominal stress levels

Loading case	Load level	Nominal membrane stress (psi)
Internal pressure	300 psi	7350
Out-of-plane moment, M_{XN}	800 in.-lb	4820
Torsional moment, M_{YN}	2400 in.-lb	7220
In-plane moment, M_{ZN}	1200 in.-lb	7220
In-plane force, F_{XN}	120 lb	6860
Axial force, F_{YN}	500 lb	850
Out-of-plane force, F_{ZN}	80 lb	4580
Torsional moment, M_{XC}	40,000 in.-lb	1330
Out-of-plane moment, M_{YC}	40,000 in.-lb	2650
In-plane moment, M_{ZC}	40,000 in.-lb	2650
Axial force, F_{XC}	10,000 lb	1620
In-plane force, F_{YC}	3000 lb	3880
Out-of-plane force, F_{ZC}	3000 lb	3880

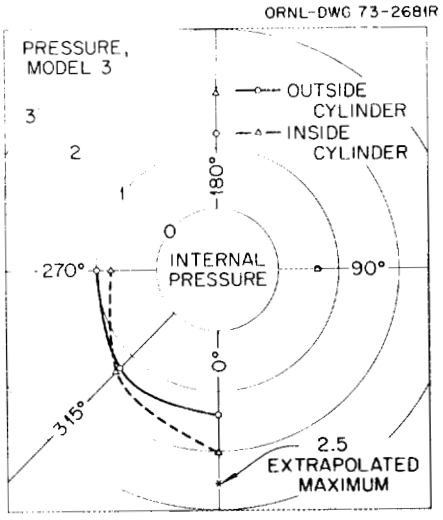

Fig. 9. Variation of maximum principal stress ratios around the nozzle-cylinder junction for internal pressure.

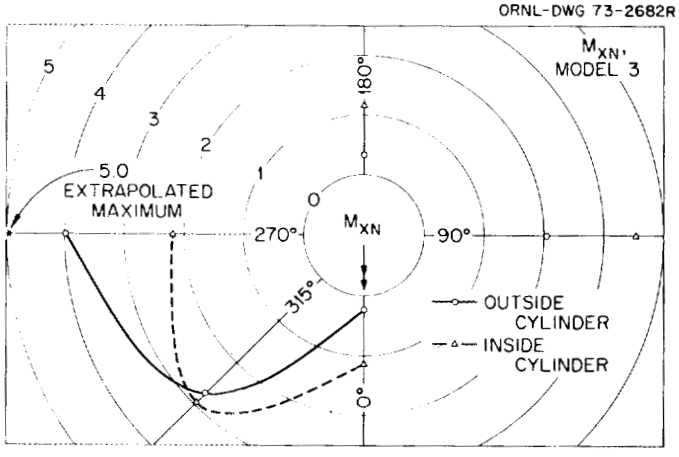

Fig. 10. Variation of maximum principal stress ratios around the nozzle-cylinder junction for out-of-plane moment, M_{XN}, on the nozzle.

does not preclude the existence of slightly higher stresses at locations between gage lines. The maximum stress ratios and the locations of the maximum stresses based on both the experimental and the finite-element analyses are tabulated and compared in Chap. 5.

Figures 9 through 21 indicate that, in general, the maximum measured stresses varied in a reasonably smooth and consistent manner around the

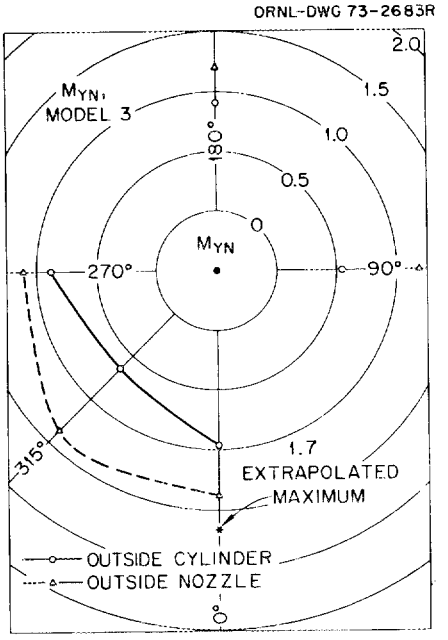

Fig. 11. Variation of maximum principal stress ratios around the nozzle-cylinder junction for torsional moment, M_{YN}, on the nozzle.

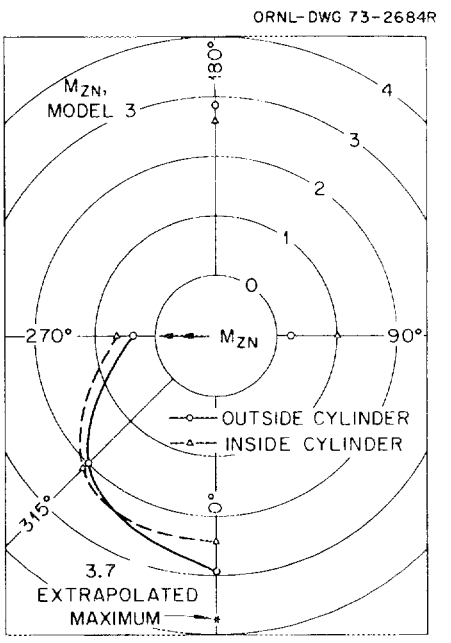

Fig. 12. Variation of maximum principal stress ratios around the nozzle-cylinder junction for an in-plane moment, M_{ZN}, on the nozzle.

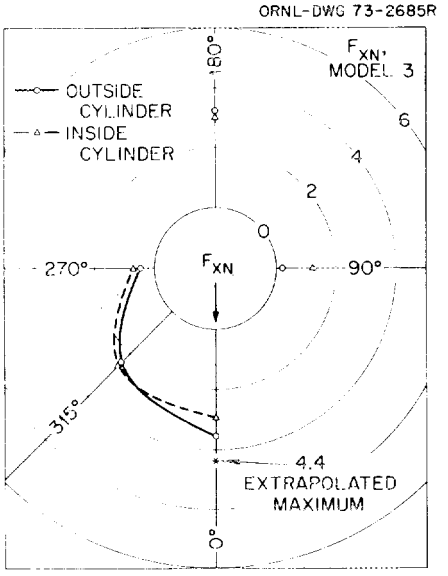

Fig. 13. Variation of maximum principal stress ratios around the nozzle-cylinder junction for an in-plane force, F_{XN}, on the nozzle.

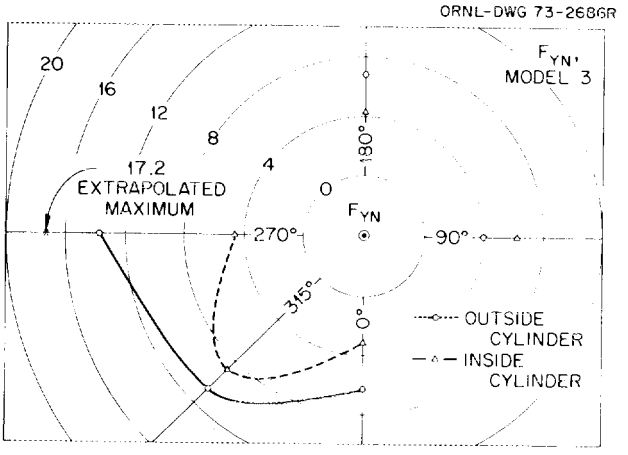

Fig. 14. Variation of maximum principal stress ratios around the nozzle-cylinder junction for an axial force, F_{YN}, on the nozzle.

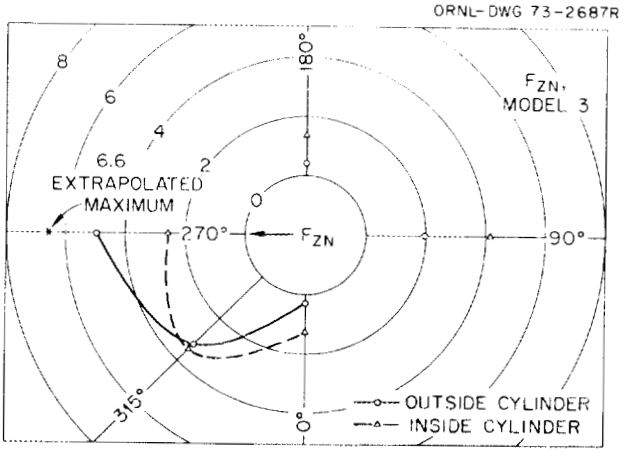

Fig. 15. Variation of maximum principal stress ratios around the nozzle-cylinder junction for an out-of-plane force, F_{ZN}, on the nozzle.

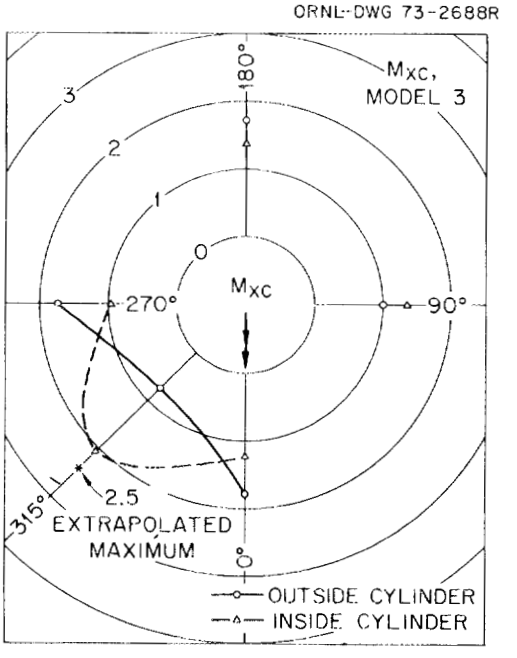

Fig. 16. Variation of maximum principal stress ratios around the nozzle-cylinder junction for a torsional moment, M_{XC}, on the cylinder.

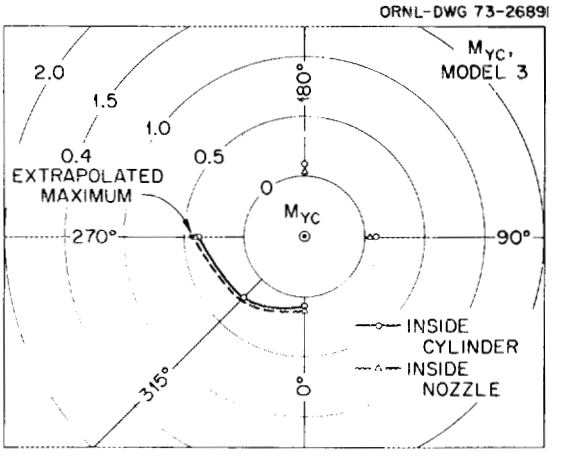

Fig. 17. Variation of maximum principal stress ratios around the nozzle-cylinder junction for an out-of-plane moment, M_{YC}, on the cylinder.

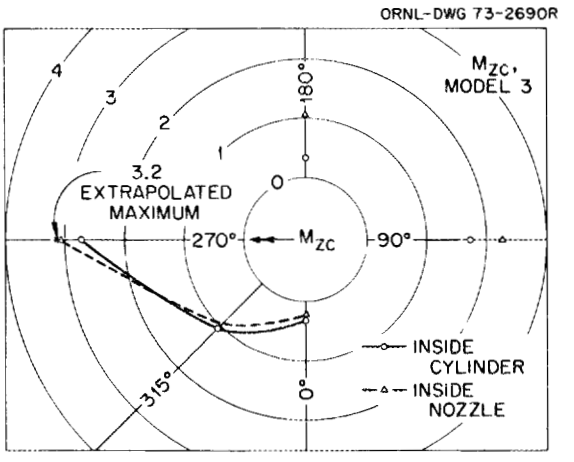

Fig. 18. Variation of maximum principal stress ratios around the nozzle-cylinder junction for an in-plane moment, M_{ZC}, on the cylinder.

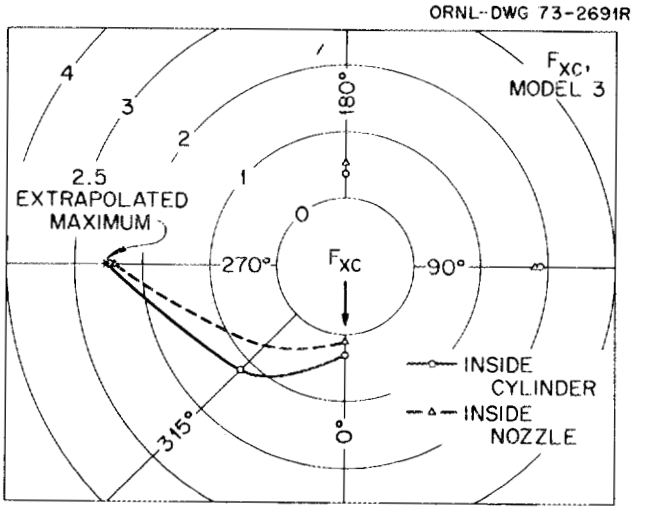

Fig. 19. Variation of maximum principal stress ratios around the nozzle-cylinder junction for an axial force, F_{XC}, on the cylinder.

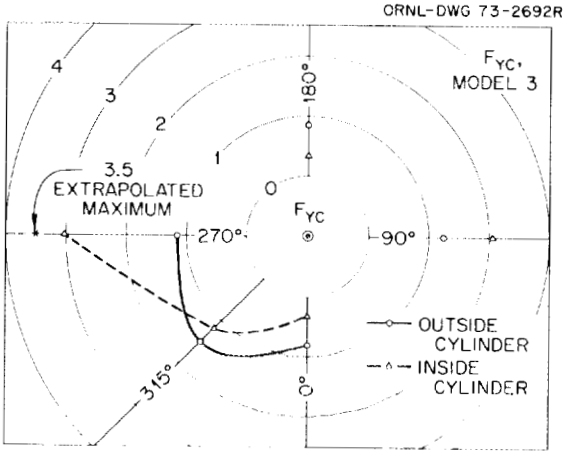

Fig. 20. Variation of maximum principal stress ratios around the nozzle-cylinder junction for an in-plane force, F_{YC}, on the cylinder.

nozzle-cylinder junction. It is particularly significant to note that the maximum stress occurred in the longitudinal plane of symmetry only for the internal pressure case, in-plane force and moment, and torsional moment on the nozzle. For all other loadings, the maximum occurred in the transverse plane of symmetry or at an intermediate position between the two planes of symmetry.

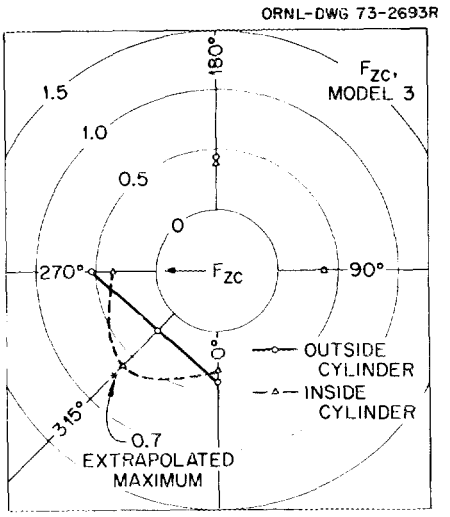

Fig. 21. Variation of maximum principal stress ratios around the nozzle-cylinder junction for an out-of-plane force, F_{ZC}, on the cylinder.

3. FINITE-ELEMENT ANALYSIS

3.1 Background

Thin-shell cylinder-to-cylinder intersection problems have, in recent years, been a favorite with the stress analyst. Their popularity stems not only from the common occurrence of such configurations in practical design, but also from the challenge that they present as complex shell analysis problems. In addition to their use in piping and pressure vessel configurations, thin-shell cylinder-to-cylinder intersections occur in the petroleum industry, which uses tubular structural members extensively in off-shore oil-drilling towers. Much of the cylinder-to-cylinder intersection research, both experimental and theoretical, that has been done was motivated by the off-shore oil-drilling tower application. The literature associated with the latter application is reviewed in Ref. 9.

Both analytical and numerical analyses have been developed and applied to thin-shell cylinder-to-cylinder intersection problems. In 1961, Reidelbach[10] developed the first analytical solution for two perpendicularly intersecting cylindrical shells subjected to internal pressure. Eringen[11-14] and his co-workers corrected some errors and approximations

in Reidelbach's solutions and formulated a solution in which the intersection curve was approximated by a circle. These solutions consisted of products of Krylov functions and Hankel functions of the first kind. A collocation method was used whereby the boundary conditions were satisfied in a least-squares sense at selected boundary points.

In 1969, Hansberry and Jones[15] used the method developed by Reidelbach and Eringen et al. to develop a solution for an in-plane bending moment applied to the nozzle of a nozzle-to-cylinder configuration. In 1970, Maye and Eringen[16] developed a solution using Fourier series involving Bessel functions in place of the Krylov functions. In 1973, Hansberry and Jones[17] expanded their solution to include the case of an axial force applied to the nozzle. As in the case of earlier solutions, however, the nozzle diameter was limited relative to the cylinder diameter.

In 1967, Bijlaard, Dohrmann, and Wang[18] formulated the problem to include the case where the nozzle and cylinder are of equal diameter. They indicated a solution in the form given by Flügge for closed cylindrical shells. In 1969, Pan[19] developed a numerical solution to the differential equations of Flügge and Donnell that is applicable to the equal-diameter case. He compared his predictions with the experimental results obtained by Riley[6] for a nozzle-diameter/cylinder-diameter ratio of 1/2. By careful choice of some of the factors used in the solution, he obtained predictions that agreed reasonably well with experiment.

In 1968, Herrmann and Campbell[20] presented a finite-element shell analysis formulation using flat-plate elements, and as a sample problem they used the 1/2 diameter ratio model tested by Riley.[6] The limited comparisons shown were for internal pressure and indicated reasonably good agreement between theory and experiment. In 1969, Prince and Rashid[21] also presented a flat-plate finite-element shell analysis using the cylinder-to-cylinder intersection as a sample problem. Their shell analysis program was developed under subcontract to ORNL as a part of the ORNL Prestressed Concrete Reactor Vessel Program.

3.2 Finite-Element Method

The finite-element program used for the analysis of this model was chosen as being reasonably representative of currently available and

widely used finite-element shell formulations. The program was developed at the University of California, Berkeley, under the direction of Professor R. W. Clough. The original program was written for general shell analysis by Johnson[22,23] and was later modified and adopted by Greste[9,24] for treating the "K" joints of cylindrical shells found in off-shore oil-drilling towers.

The basic elements used in the program, shown in Fig. 22, are non-planar quadrilaterals that are built up of an assemblage of four component triangles. Within each component triangle, the in-plane displacements u and v are assumed to vary quadratically over the plane of the triangle, except that they are constrained to vary linearly along the one exterior edge. The resulting membrane element, referred to as a constrained linear strain triangle (CLST), has two degrees of freedom (u and v) at each of the five nodes.

The plate bending portion of the component triangle elements has three degrees of freedom at each of the three corner nodes – two rotations about axes in the plane of the element and the transverse, or normal, displacement w. The displacement expansion for this element is due to Hsieh, Clough, and Tocher,[25] and the element is referred to as the HCT triangle. Full compatibility of displacements and slopes between triangular element boundaries is achieved by dividing the element into three subtriangles and

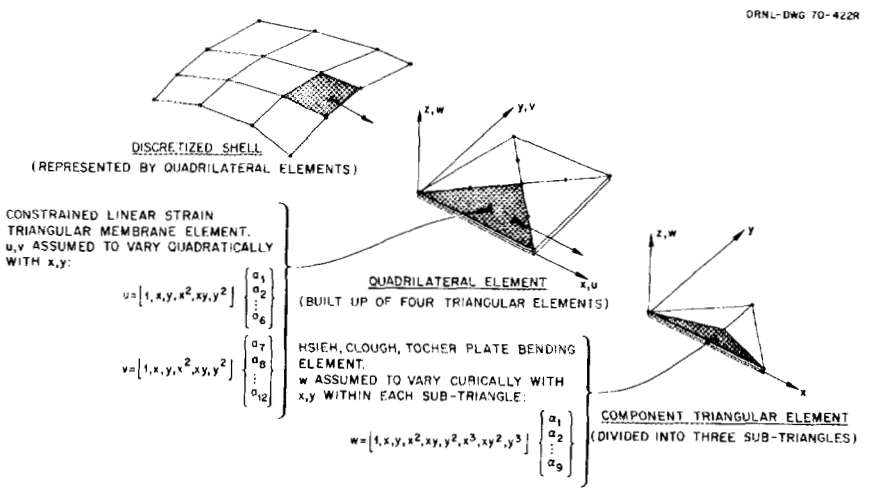

Fig. 22. Quadrilateral element and component triangles.

assuming an independent cubic variation for w within each subtriangle. One of the ten terms of the general cubic is neglected in each subtriangle, so that in the final assembled component triangle the normal slope varies linearly along each exterior edge. This feature ensures slope compatibility in the resulting element system for plate bending problems. The 27 constants in the three cubic expressions for w within the triangular element are reduced to 9 (and related to the 9 nodal degrees of freedom) by internal compatibility considerations. With w varying as a cubic polynomial within each subtriangle, the three components of curvature, and hence the bending and twisting moments, vary linearly.

The total stiffness (membrane plus bending) of the triangular elements that form the components of the quadrilateral is obtained by superposition of the plate bending element and the membrane element. The membrane plus bending stresses vary piecewise linearly over the surface of the resulting triangular element.

The quadrilateral element stiffness is obtained from that of the four component triangles. In general, due to the curvature of the shell that is being discretized, an arbitrary quadrilateral will be nonplanar. This introduces a complication in the transformation of the triangular element stiffness, because on the element level only two bending rotations per node are defined. When transformed from the element coordinates to some other coordinate system, a third bending rotation quantity is introduced, and in the transformed system three rotational degrees of freedom should be considered at each node. This consideration regarding the third rotational degree of freedom also arises in the subsequent assembly of the quadrilateral elements into the total structural stiffness, since adjacent elements are generally not coplanar. In his formulation, Johnson[22] chose to retain only two rotations per node in the total element assemblage. He argued that since the element plane in a sufficiently fine mesh lies close to the shell tangent plane at each node, the rotations could be transformed from the element coordinates (in the plane of the element) to coordinates in the shell tangent plane and the small transformed component of bending rotation about the normal to the shell could be neglected. This is perhaps a reasonable assumption everywhere except at the junction of intersecting shells.

The stiffness formulation for the quadrilateral element, as well as for the CLST membrane element and the HCT plate bending element, was summarized by Greste.[9] The quadrilateral element has five degrees of freedom at each node: u, v, w, and the two rotations. In the final assembled structure, the five degrees of freedom per node are u, v, w, and the two rotations about the shell tangent coordinates at each node.

The task of the finite-element method is to determine the unknown coefficients of the assumed element displacement functions for u, v, and w. This is done by connecting the quadrilateral elements at discrete points, the corner nodes, and requiring compatibility of displacements and rotations and equilibrium of forces and moments at these nodes. Unfortunately, when the elements are assembled into a curved-shell structure, compatibility and equilibrium are not completely achieved along the element interfaces. Thus there are inherent small errors involved. However, studies by Johnson[22] have shown that these errors are not too significant provided a sufficiently fine element mesh is used.

There is an error in intersecting shell problems which is not diminished by mesh refinement. This error arises from the aforementioned neglect of the rotation about the shell normal. At the junction nodes in the cylinder-to-cylinder intersection problem, there are three nonzero rotational components, but only two of these can be retained as nodal degrees of freedom. Greste[9] chose to define the tangent plane, and hence the two rotational degrees of freedom, at the junction nodes as the cylinder tangent plane. The manner in which he treated the junction nodes thus constrained the normal rotation about the cylindrical shell normal to be zero at the junction. This rotational constraint unrealistically constrains the bending deformation of the adjacent nozzle elements.

This constraint did not greatly affect the analysis of model 1, but its effect was significant in the analysis of model 3. A problem arose in the analysis of model 3, with its small slender nozzle, that was not encountered in the analysis of model 1 or in similar models with relatively large nozzles. In the cases of the in-plane and out-of-plane forces and moments applied to the end of the nozzle, it was found that the membrane-type axial bending stresses, which should have been constant

along the nozzle, were dissipated with distance from the end of the nozzle. This dissipation was traced to the neglect of the rotational degree of freedom about normals to the nozzle surface and occurred in model 3 because of the relatively large deformations of the small slender nozzle. This problem was overcome by redefining the neglected sixth degree of freedom for these loading cases.

The difficulty is illustrated by the example problem shown in Fig. 23, in which the nozzle of model 3 was analyzed by fixing a row of nodes near the junction.[1] The mesh shown in Fig. 24 for the nozzle was used, and the nozzle was subjected to a bending moment at the free end. The distribution of normalized bending stress in the outer wall of the nozzle is shown in Fig. 23 for three different analyses. Also shown is the predicted stress based on simple beam theory with $I = \pi a^3 h$ and $c = a$, where a is the radius of the midsurface and h is the nozzle thickness.

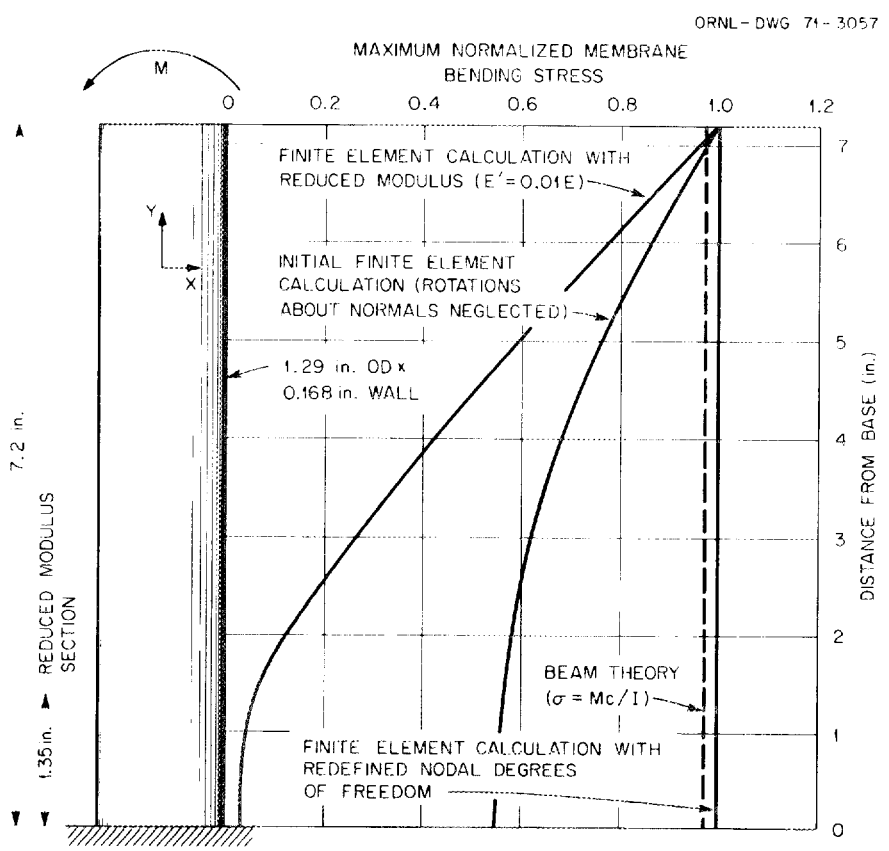

Fig. 23. Example problem demonstrating effects of neglecting component of bending rotation about normals to the surface of a slender nozzle.

The middle curve in Fig. 23 was obtained with the component of bending rotation about normals to the nozzle surface neglected. These neglected rotations are small and are in effect set to zero in the assembled set of equations. Overall equilibrium implicitly requires that small moments be imposed at each node to maintain zero bending rotation. These small constraints combine to counteract a portion of the applied moment and result in the decrease in membrane bending stress depicted in Fig. 23.

To illustrate the dependence of these nodal constraints on the deflection of the nozzle, the problem was reexamined using a reduced elastic modulus for a section near the fixed end. The nozzle deflection produced by the applied moment was thus increased, and the bending moment was dissipated more rapidly as shown by the left-hand curve in Fig. 23.

The problem was overcome by redefining the neglected degree of freedom in the nozzle.[1] Rather than setting the rotations about normals equal to zero, the rotations about lines parallel to the nozzle axis were set equal to zero in the final assembled set of equations. The assumption of zero bending rotation about lines parallel to the nozzle axis is reasonable and is equivalent to the assumption, often made in analyzing the local bending in cylindrical shells, that changes in curvature in the hoop direction are negligible compared with those in the axial direction. Bailey and Hicks,[26] for example, made the latter assumption in examining the effects of a bending moment applied to the nozzle of a nozzle-to-spherical-shell attachment. With this modification, the membrane bending moment remained constant, as shown by the right-hand curve in Fig. 23. This modification was used in the analysis of the in-plane and out-of-plane forces and moments on the nozzle.

In conclusion, two significant points should be made. First, even though a computer program may be checked for some geometries and conditions, there can be other cases for which it does not function properly. Thus, structural analysis programs must be thoroughly validated for the range of parameters over which they are expected to apply. Second, the problems introduced by considering only five degrees of freedom per node could be eliminated by retaining six degrees of freedom in the final assembled equations. However, for large systems, the five degrees of

freedom per node has a distinct advantage from the standpoint of economy of computer time.

3.3 Finite-Element Idealization of Model

The finite-element representation chosen for model 3 is depicted in Fig. 24, which shows developed views of one-half of the nozzle, cylinder, and end plates. It was necessary to consider only one-half of the structure because of symmetry considerations. This mesh layout was developed

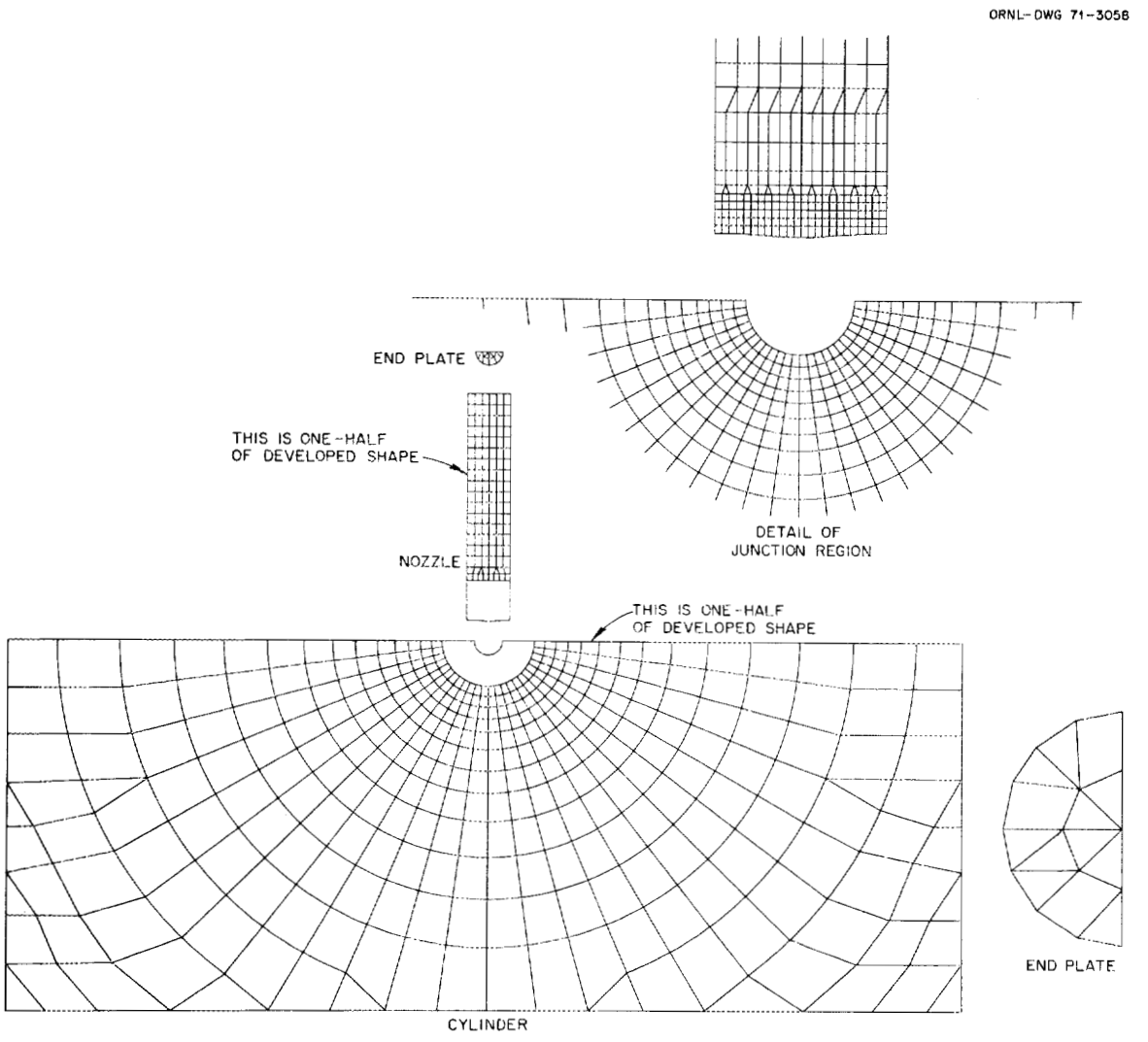

Fig. 24. Finite-element idealization of model 3.

manually and was arranged so that lines of nodes corresponded to the lines of strain gages in the experimental model. There were 993 nodes, resulting in approximately 4500 linear algebraic simultaneous equations to be solved for the unknown displacement parameters. There were 25 nodes along the (half) junction line between the nozzle and the cylinder. All 13 loading cases considered experimentally were analyzed using this mesh, and the theoretical predictions were compared with the experimentally determined stresses (Chap. 4).

Seven of the 13 loadings – pressure, axial forces on cylinder and nozzle, and in-plane moments and forces on cylinder and nozzle – produce behavior that is theoretically symmetric about the longitudinal plane of symmetry of the model. For these symmetric loadings, it is correct to consider just one-half of the model in the finite-element representation. The boundary conditions on nodal displacements and rotations are those commonly associated with symmetry conditions.

For the remaining six loadings – out-of-plane moments and forces on cylinder and nozzle and torsional moments on cylinder and nozzle – asymmetric conditions exist, and to consider just one-half of the model in the finite-element representation requires assumptions, or approximations, in establishing nodal displacement and rotational boundary conditions. Basically, the boundary conditions used were based on the assumption that the projection on the X-Y plane (see Fig. 2) of the boundary remained fixed in the X-Y plane. In other words, the displacements in the X and Y directions and the rotation about the Z axis were assumed to be zero for the nodes along the boundary in the X-Y plane. Although these conditions are obviously not strictly correct, they nonetheless seem to be reasonable assumptions that are useful for reducing the size of the problem to be solved.

4. COMPARISON OF THEORY AND EXPERIMENT

The theoretical predictions, based on the finite-element layout shown in Fig. 24, are compared in this chapter with experimentally determined distributions for all 13 loading cases. The theoretical and experimental stress distributions along the five gage lines on the cylinder and nozzle

(see Figs. 3 and 4) are presented for each loading. The stresses shown are always those parallel (longitudinal) and those perpendicular (transverse) to the gage lines.

4.1 Internal Pressure

The measured and predicted stress distributions determined for an internal pressure of 300 psi applied to the model are shown in Figs. 25 through 29. Figure 25 shows the measured and predicted stress distributions on the outside and inside surfaces of the cylinder and on the outside and inside surfaces of the nozzle along the 0° gage line, which is

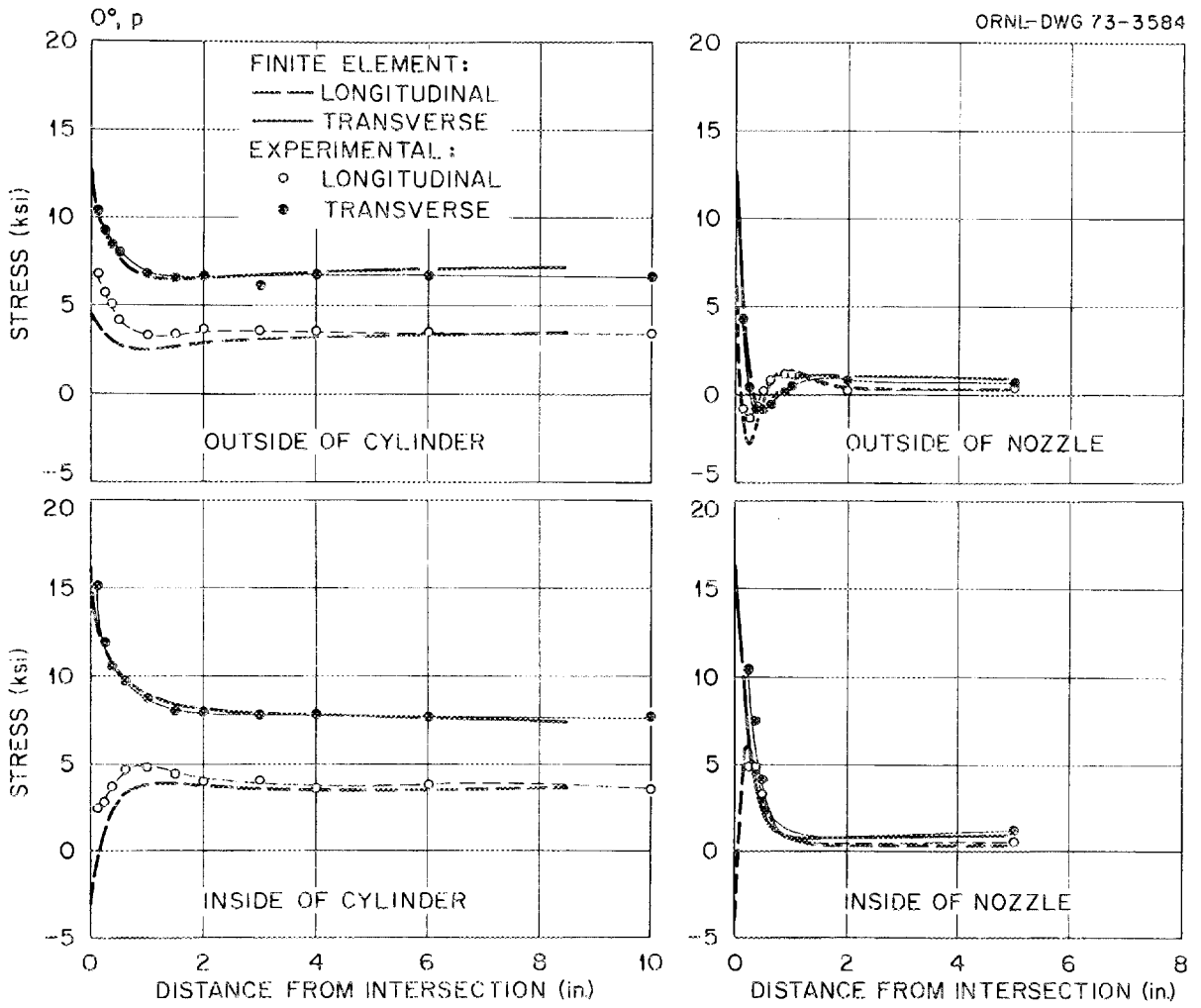

Fig. 25. Measured and predicted stress distributions at 0° for internal pressure of 300 psi.

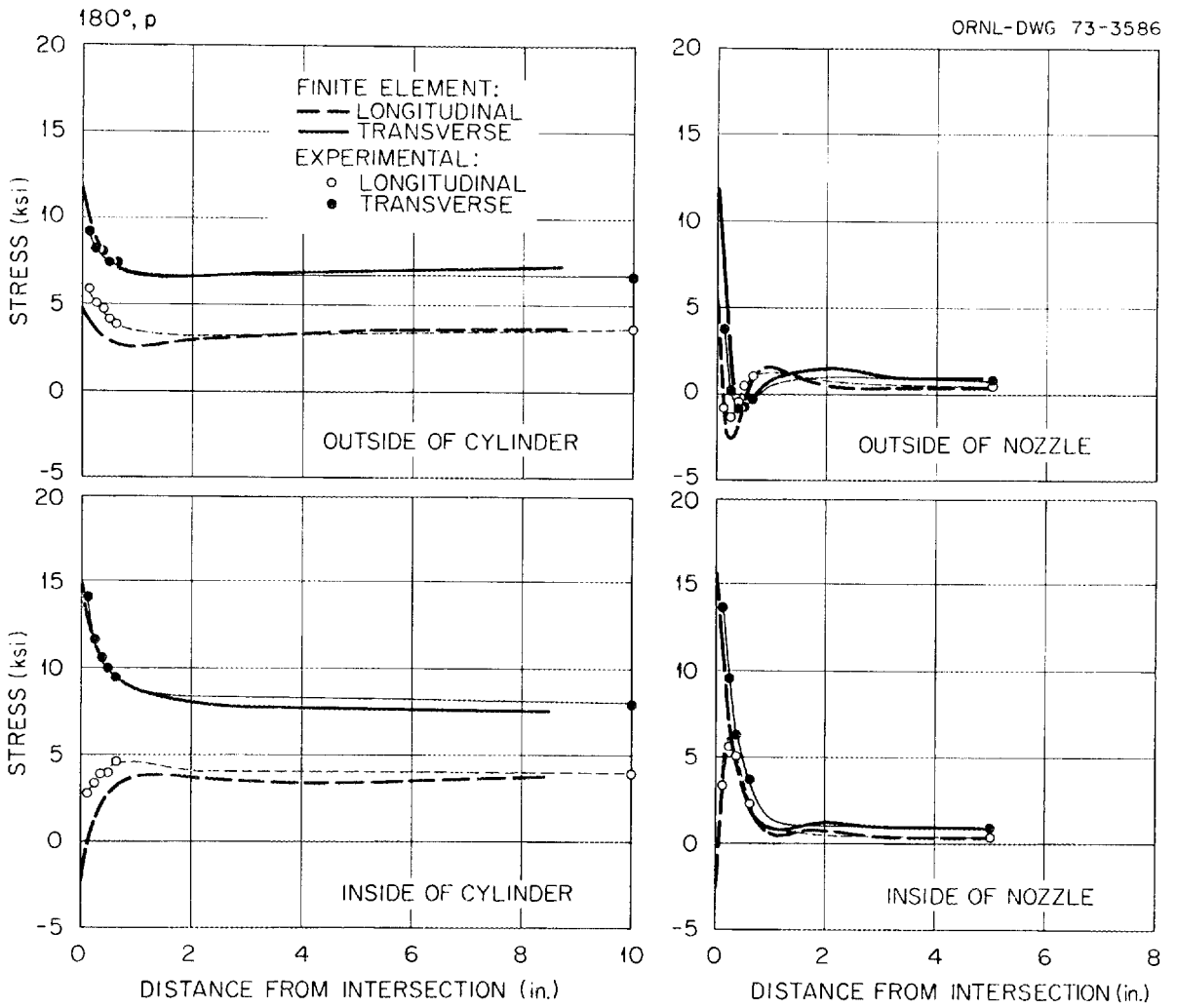

Fig. 26. Measured and predicted stress distributions at 180° for internal pressure of 300 psi.

the longitudinal plane of symmetry (see Figs. 3 and 4). The stresses are shown as a function of distance from the junction of nozzle and cylinder midsurfaces. The heavy lines are the predicted stresses, while the fine lines through the experimental points show the measured distributions. The solid lines in each case represent the transverse stresses, which are perpendicular to the gage lines. The dashed lines represent the longitudinal stresses, which are parallel to the gage lines. Thus, we can compare the solid lines with each other and the dashed lines with each other.

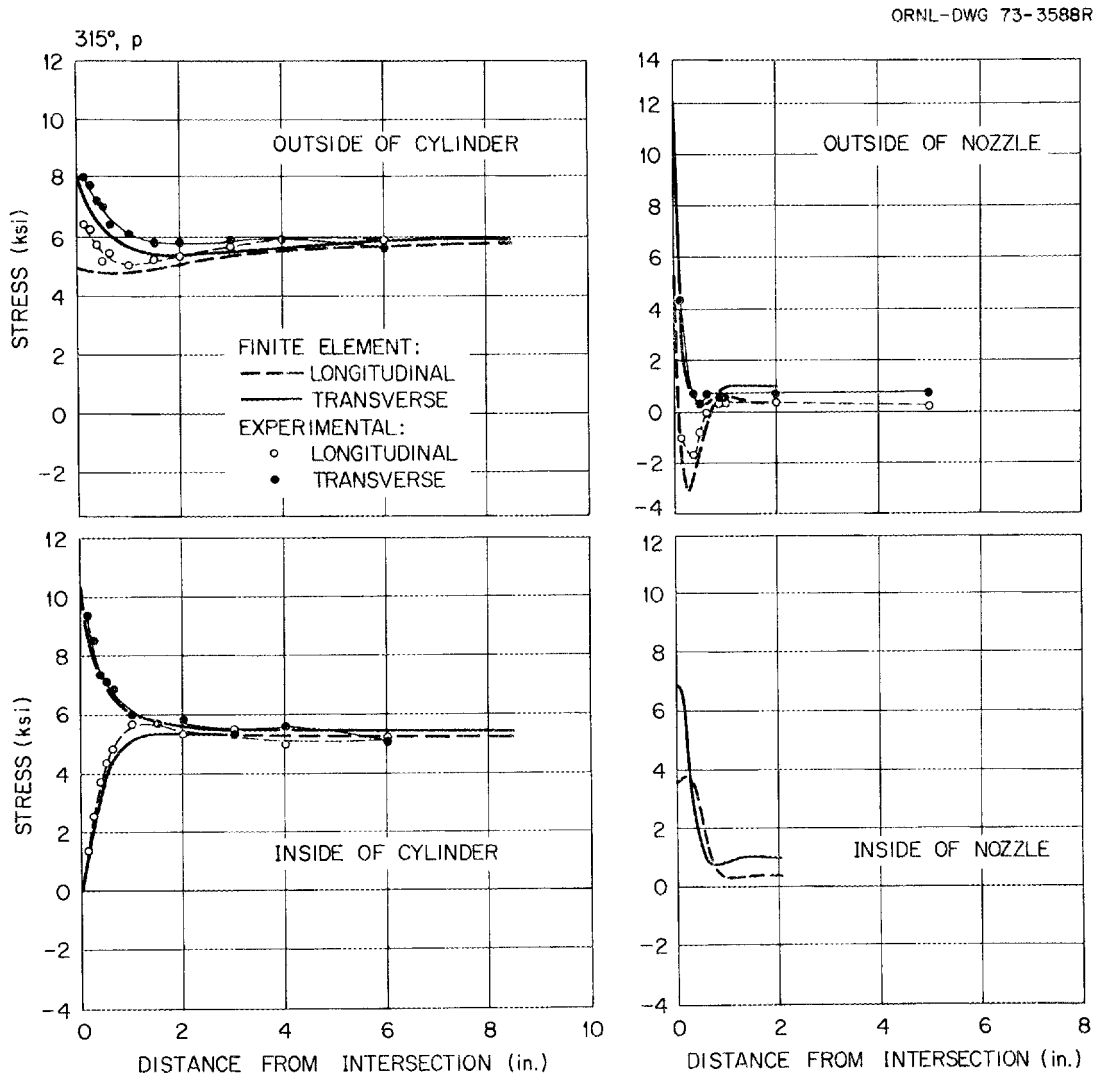

Fig. 27. Measured and predicted stress distributions at 315° for internal pressure of 300 psi.

The agreement between theory and experiment is good in Fig. 25, except that the stresses at the junction, where the maximums occur, are at times underestimated somewhat by the finite-element predictions. However, the general shape and distributions of the stresses are well predicted by the theory.

The remaining internal pressure comparisons (Figs. 26 through 29) are arranged to facilitate ready comparison of comparable results. Figure 26 shows the stresses along the 180° gage line, which is opposite the

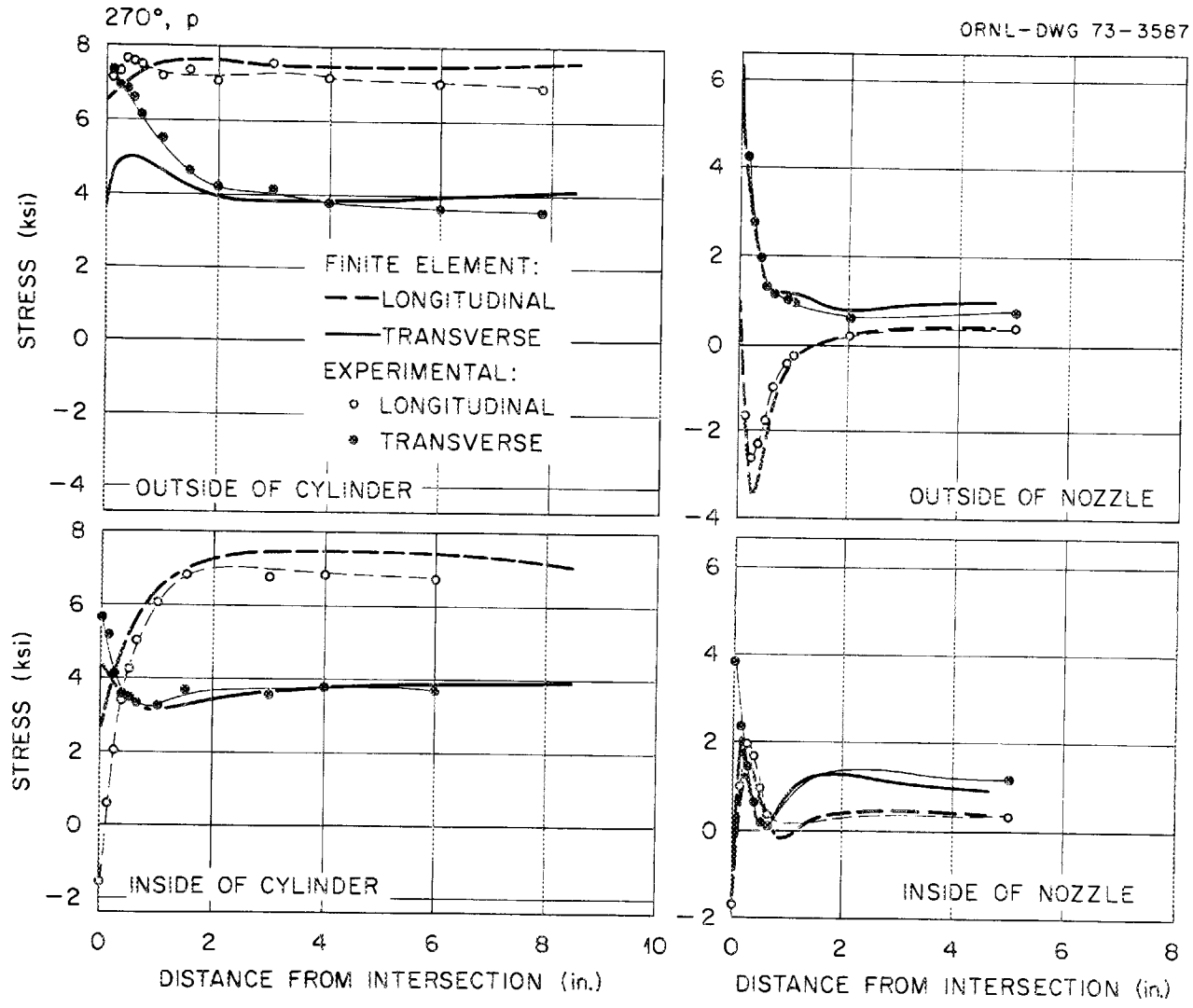

Fig. 28. Measured and predicted stress distributions at 270° for internal pressure of 300 psi.

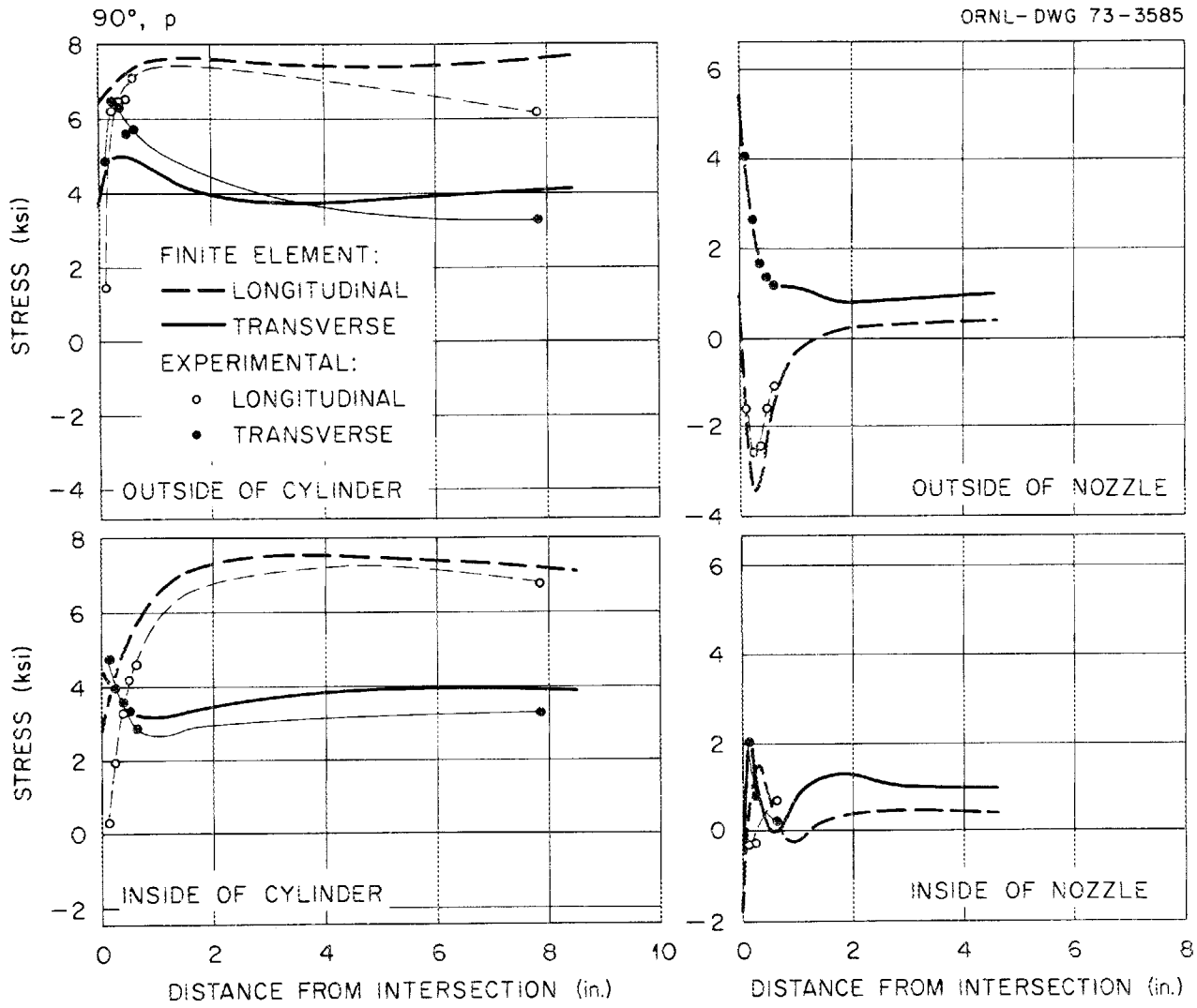

Fig. 29. Measured and predicted stress distributions at 90° for internal pressure of 300 psi.

0° gage line in the longitudinal plane of symmetry. Because of symmetry, the stresses along the 180° gage line are almost the same as those along the 0° gage line shown in Fig. 25. Comparison of the two figures shows excellent agreement between results for opposite sides of the nozzle in the longitudinal plane of symmetry.

The results for a gage line 45° from the longitudinal plane of symmetry (see Figs. 3 and 4) are shown in Fig. 27. Figure 27 shows the results for the 315° gage line, which is in the fourth quadrant. Agreement between theory and experiment is as good here as for the previous two figures.

The internal pressure loading results for the 270 and 90° gage lines, in the transverse plane of symmetry, are shown in Figs. 28 and 29 respectively. Here the agreement between theory and experiment is relatively poor on the transverse plane. However, since the stresses are low, the disagreement is perhaps not too significant. The overall agreement between theory and experiment is generally good.

The method used to determine the estimated maximum experimental stresses and stress ratios was described in Sect. 2.5. The maximum theoretically predicted stresses were obtained in the same manner; that is, they were taken as the largest absolute values of the principal stresses. To match the experimental maximums, the search for the theoretical maximums was limited to gage lines only.

The maximum experimentally determined stress occurred on the inside surface of the nozzle at 0°, and the maximum stress ratio was 2.5. The theoretical maximum stress was on the outer surface of the nozzle at 0°, and the maximum stress ratio was 2.3.

4.2 Out-of-Plane Moment Loading, M_{XN}, on Nozzle

The measured and predicted stress distributions for an out-of-plane moment loading of 800 in.-lb applied to the nozzle are shown in Figs. 30 through 34. Results for the five gage lines are arranged in the same manner as for the internal pressure case, although the fourth and second quadrant results are not theoretically the same.

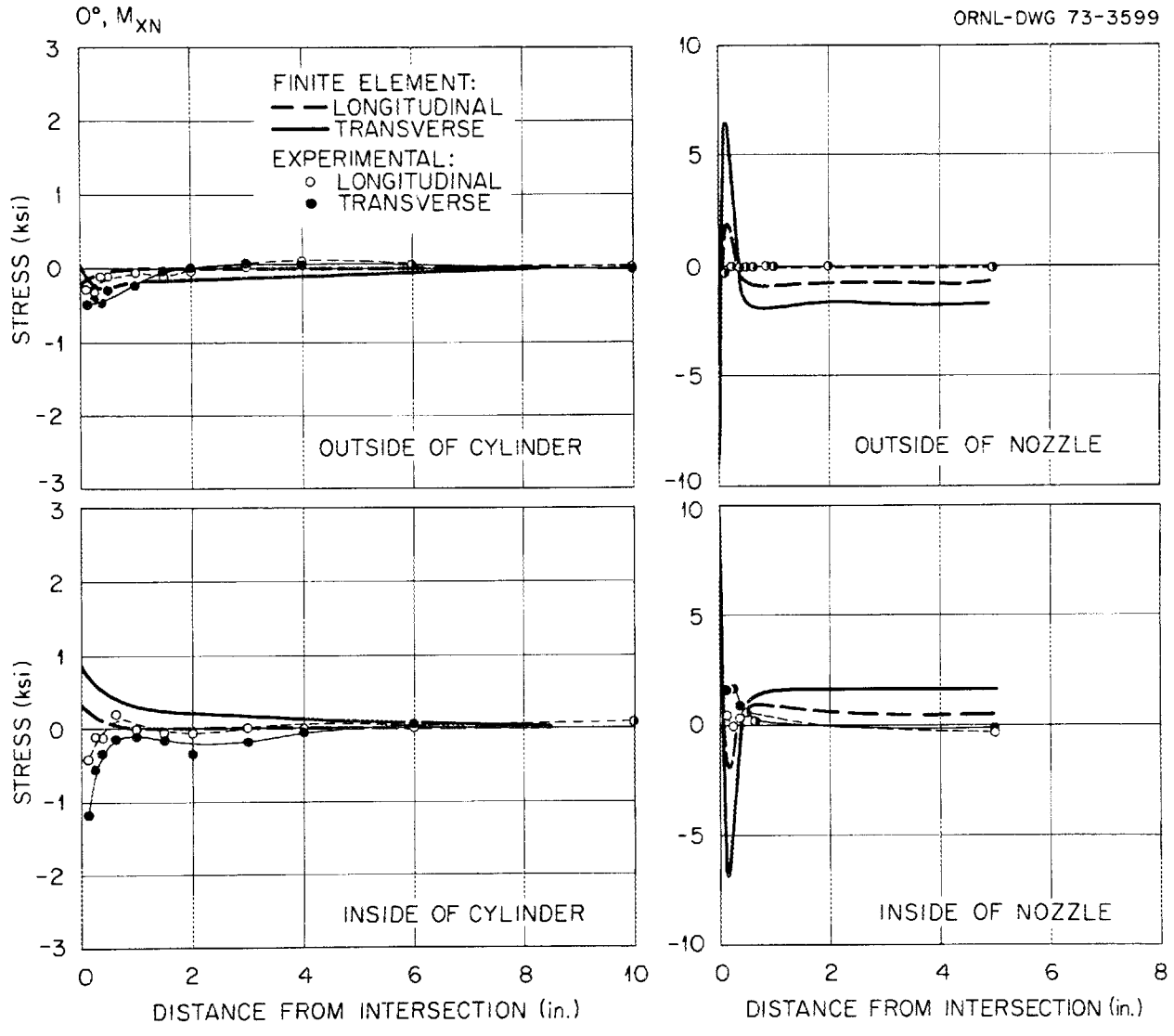

Fig. 30. Measured and predicted stress distributions at 0° for an out-of-plane moment of 800 in.-lb on the nozzle.

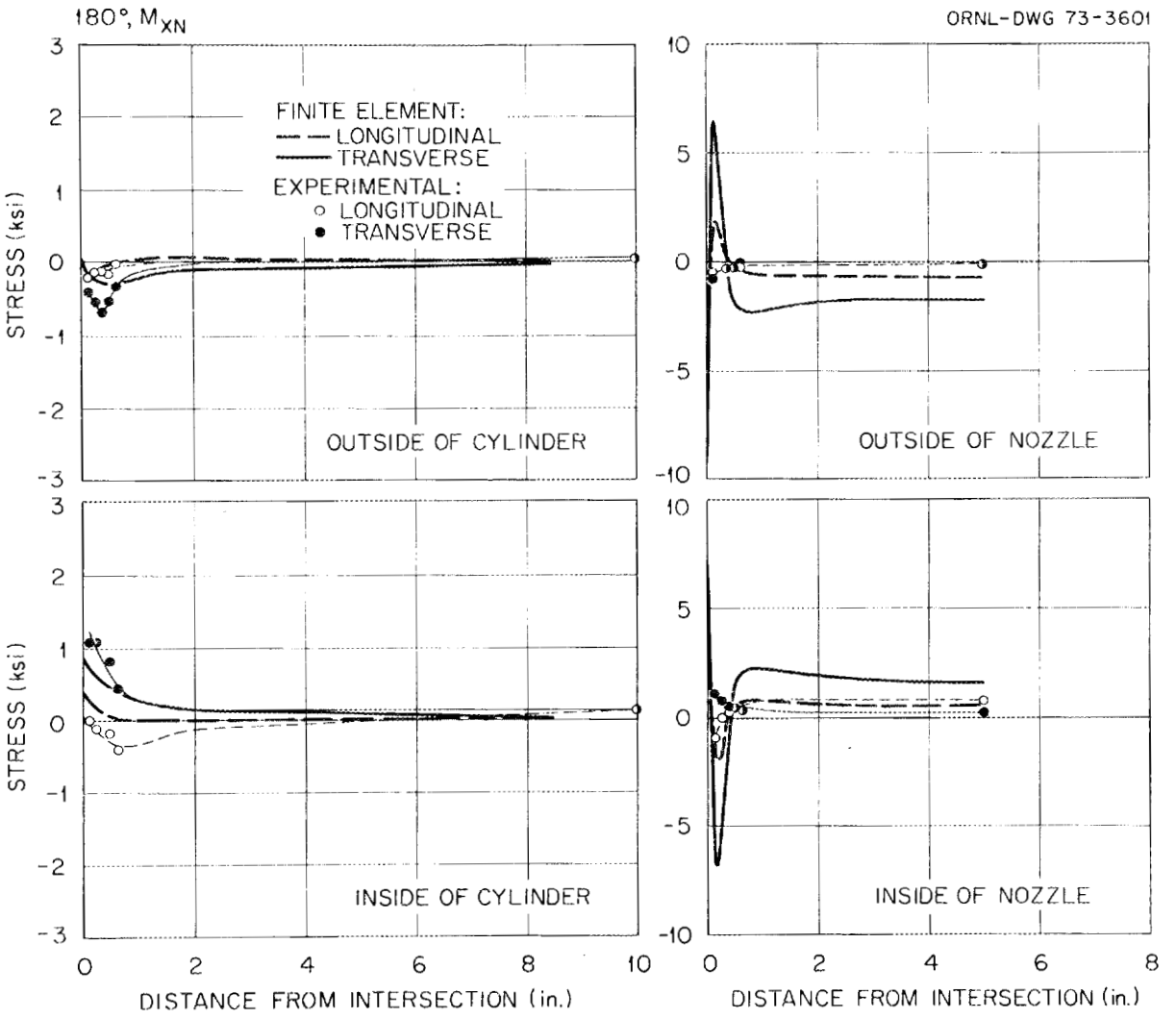

Fig. 31. Measured and predicted stress distributions at 180° for an out-of-plane moment of 800 in.-lb on the nozzle.

The results in Figs. 30 and 31 are for 0 and 180°, respectively, in the longitudinal plane of symmetry. As expected, the stresses are small since these locations are somewhat analogous to the neutral axis of a beam in bending. The results for the 315° gage line, which is 45° from the longitudinal plane of symmetry, are shown in Fig. 32. At this location the stresses are larger, and the agreement between theory and experiment is very good.

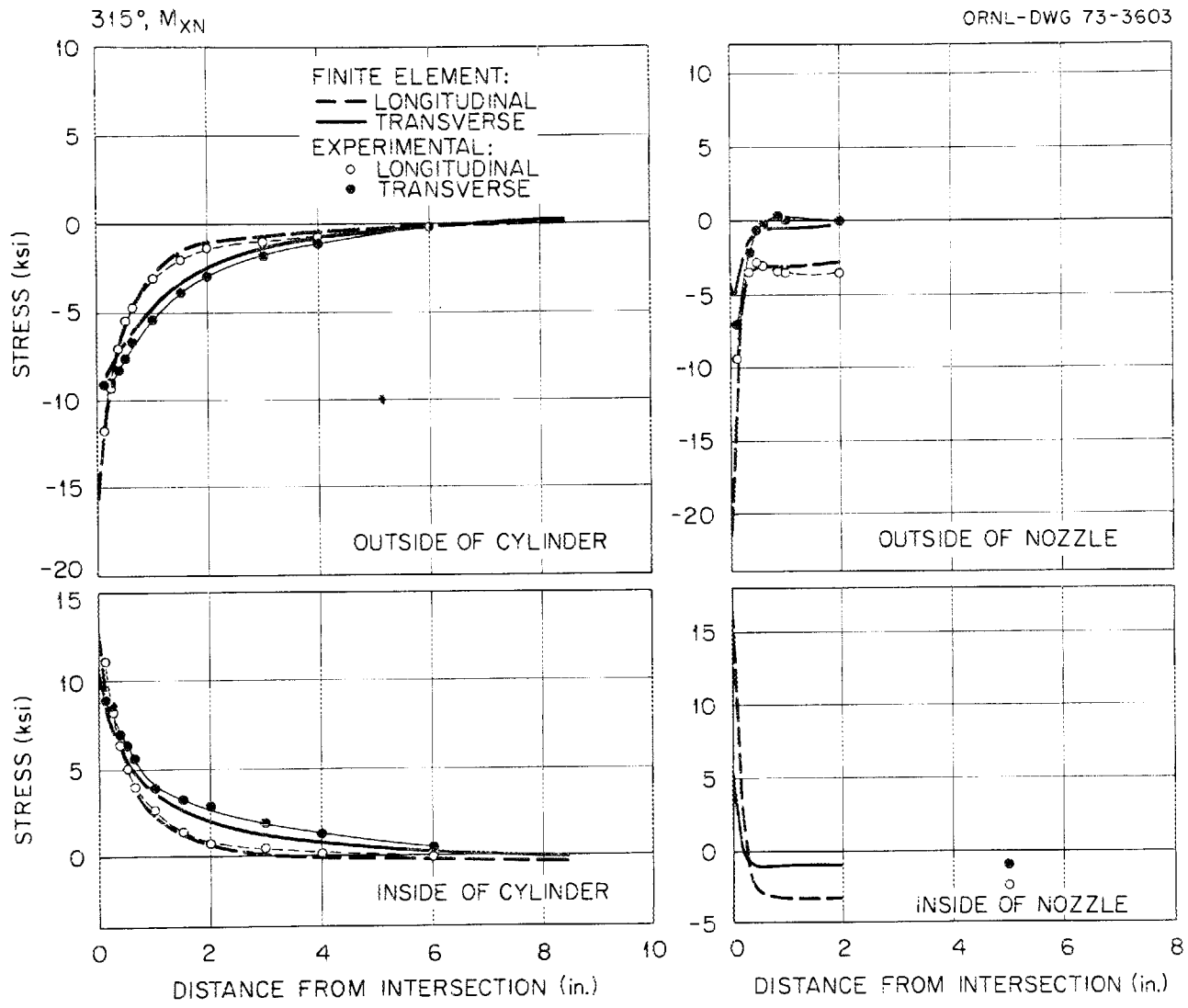

Fig. 32. Measured and predicted stress distributions at 315° for an out-of-plane moment of 800 in.-lb on the nozzle.

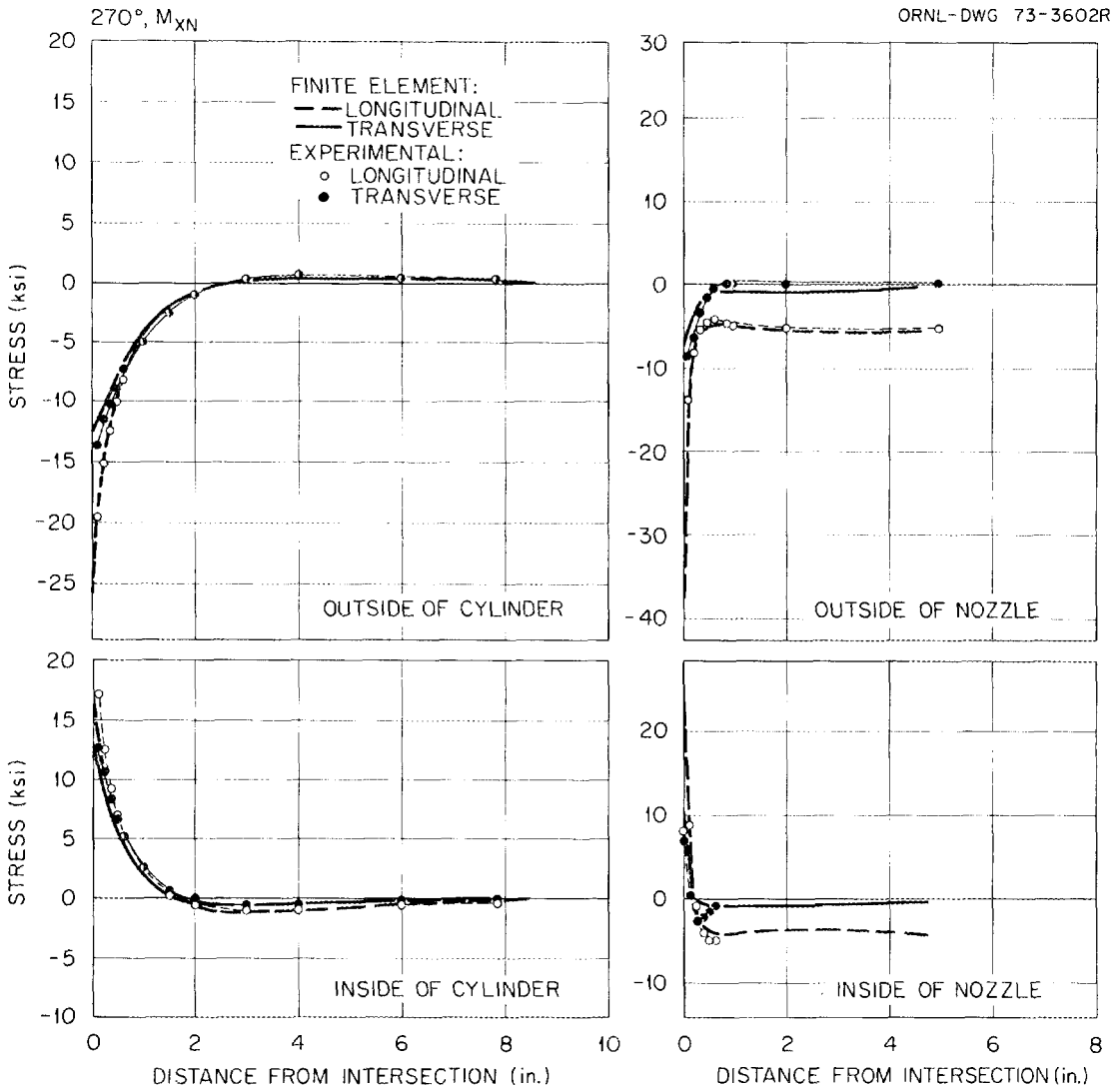

Fig. 33. Measured and predicted stress distributions at 270° for an out-of-plane moment of 800 in.-lb on the nozzle.

The results for the 270 and 90° gage lines, which are located in the transverse plane of symmetry, are shown in Figs. 33 and 34 respectively. Here the stresses are a maximum, and the agreement between theory and experiment is very good. The maximum experimental stress is on the outer surface of the cylinder and is closely predicted by the analysis.

The maximum experimentally determined principal stress ratio was 5.0, with the maximum stress occurring on the outer surface of the cylinder at the junction on the 270° gage line. The theoretical maximum was on the

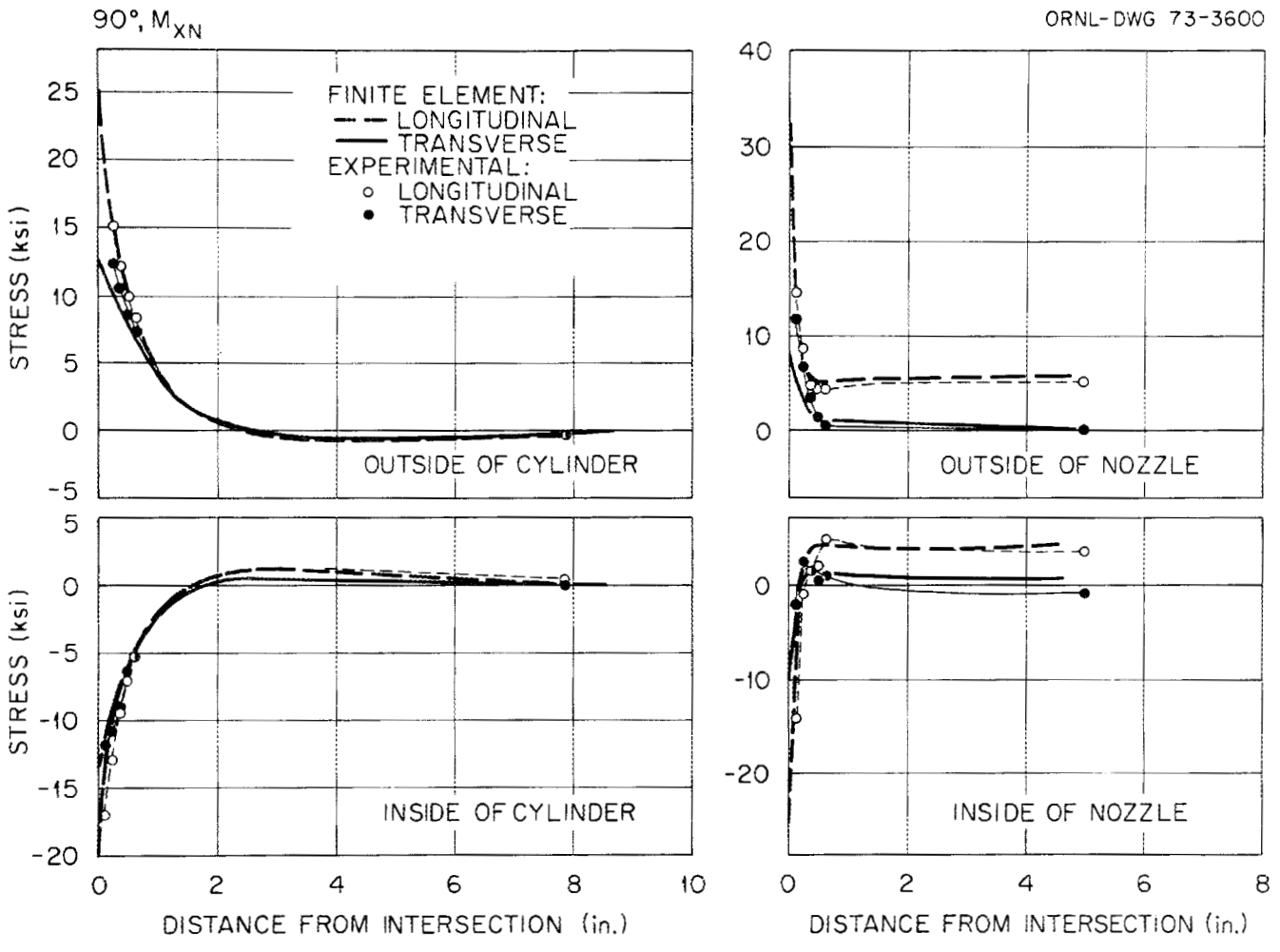

Fig. 34. Measured and predicted stress distributions at 90° for an out-of-plane moment of 800 in.-lb on the nozzle.

outer surface of the nozzle at the junction on the 270° gage line, and the maximum stress ratio was 7.3.

4.3 Torsional Moment Loading, M_{YN}, on Nozzle

The measured and predicted stress distributions for a torsional moment loading of 2400 in.-lb applied to the nozzle are shown in Figs. 35 through 39. As in the previous case, the fourth and second quadrant results are not theoretically the same. Here the experimental stresses in the longitudinal and transverse planes of symmetry are low and rise to their maximum levels on the intermediate gage line. The distribution of stresses along the intermediate gage line, which is 45° around from the longitudinal plane of symmetry, is shown in Fig. 37. Here the agreement is very poor. In general, the distributions show very poor quantitative agreement between theory and experimental results.

The maximum experimentally determined stress ratio was 1.7, with the maximum stress located on the outer surface of the nozzle at the junction on the 0° gage line. The maximum theoretical stress was also on the inner surface of the nozzle at the same location, and the maximum theoretical stress ratio was 0.6.

4.4 In-Plane Moment Loading, M_{ZN}, on Nozzle

The measured and predicted stress distributions for an in-plane moment loading of 1200 in.-lb applied to the nozzle are shown in Figs. 40 through 44. Here the stresses are large in the longitudinal plane of symmetry, as shown in Figs. 40 and 41, and the agreement between theory and experiment is very good for the gage lines in the longitudinal plane of symmetry.

The stresses are lower along the gage line 45° around from the longitudinal plane of symmetry. In the transverse plane of symmetry the stresses are very low, as shown in Figs. 43 and 44. For this loading the transverse plane is somewhat similar to the neutral axis of a beam.

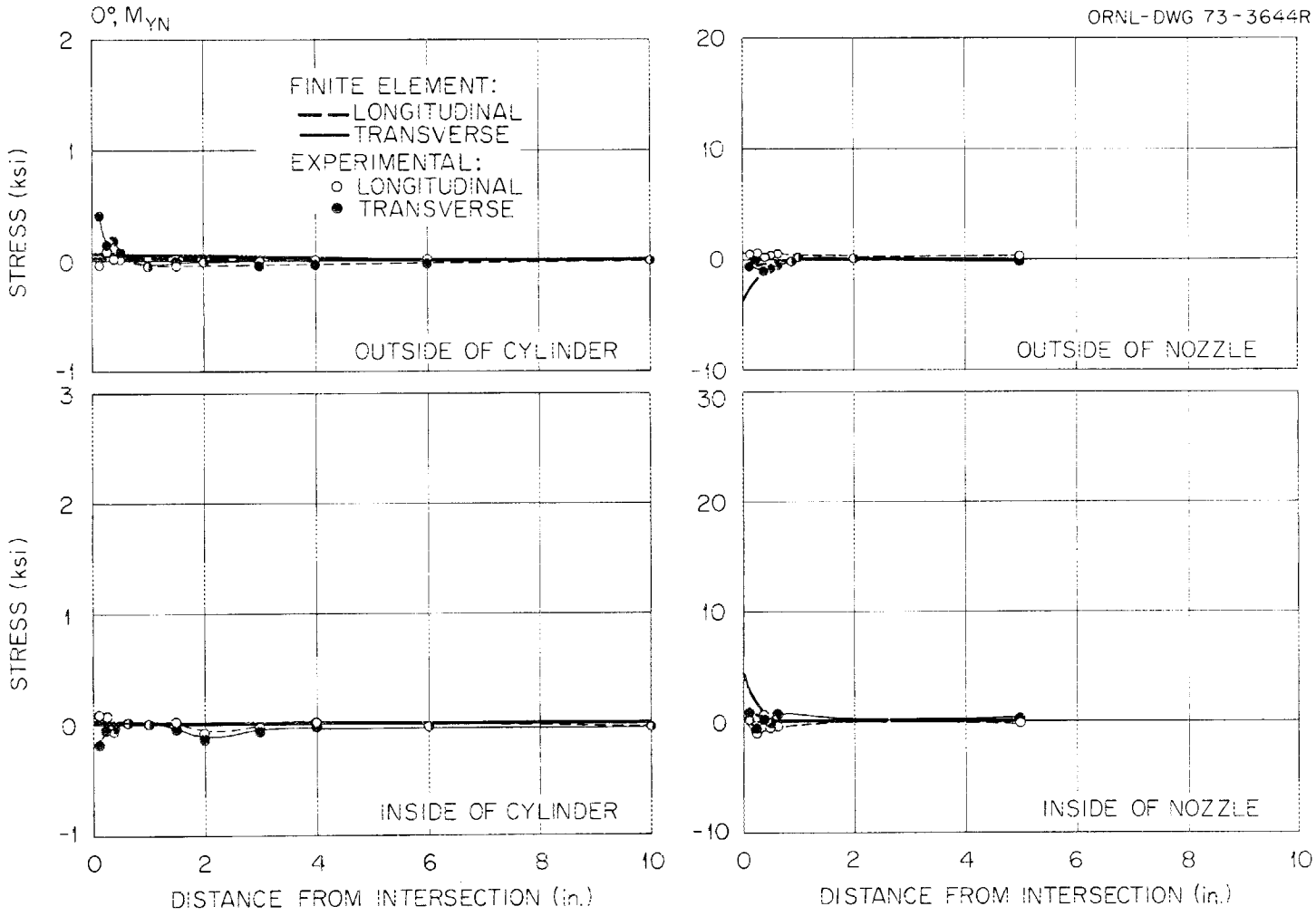

Fig. 35. Measured and predicted stress distributions at 0° for a torsional moment of 2400 in.-lb on the nozzle.

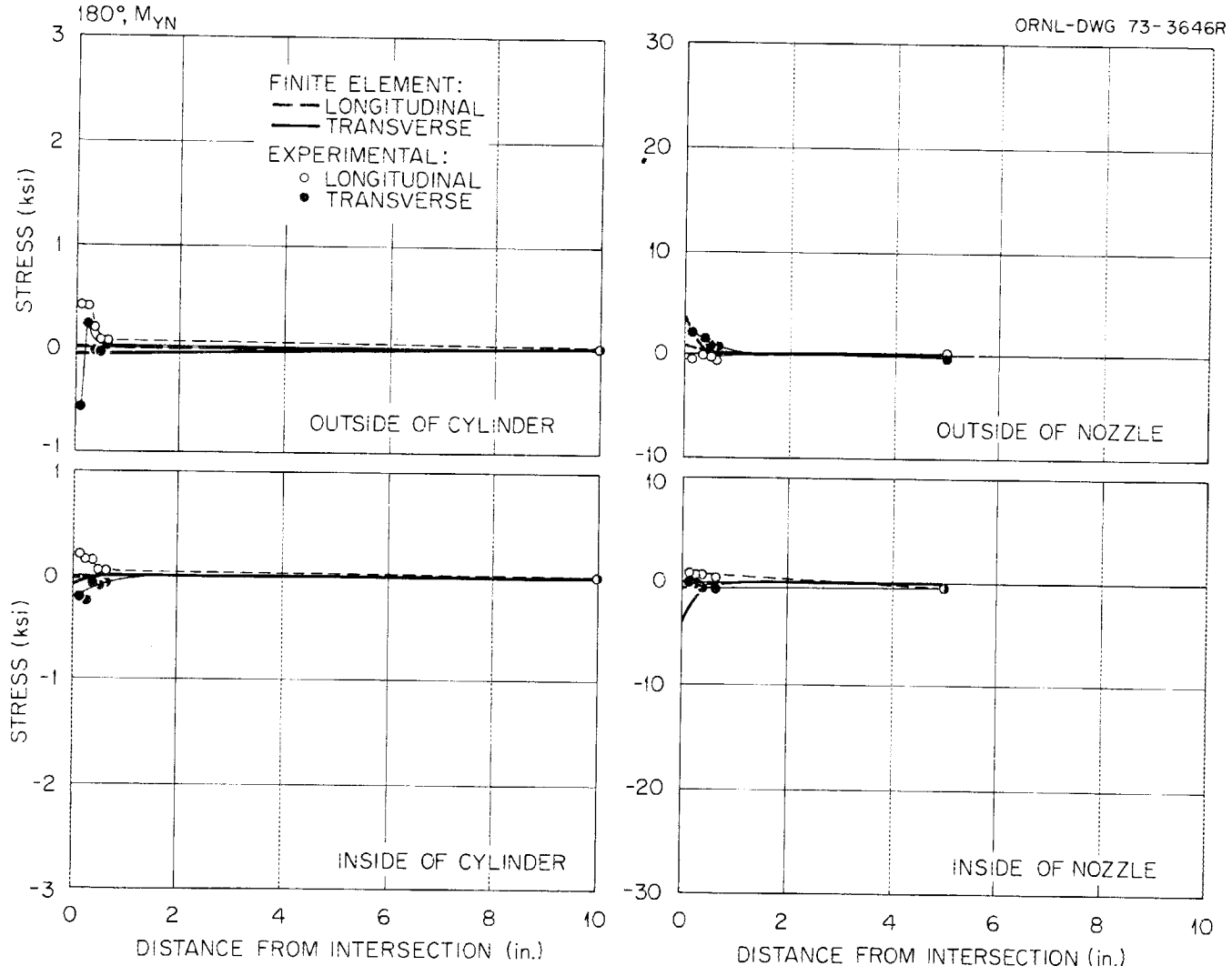

Fig. 36. Measured and predicted stress distributions at 180° for a torsional moment of 2400 in.-lb on the nozzle.

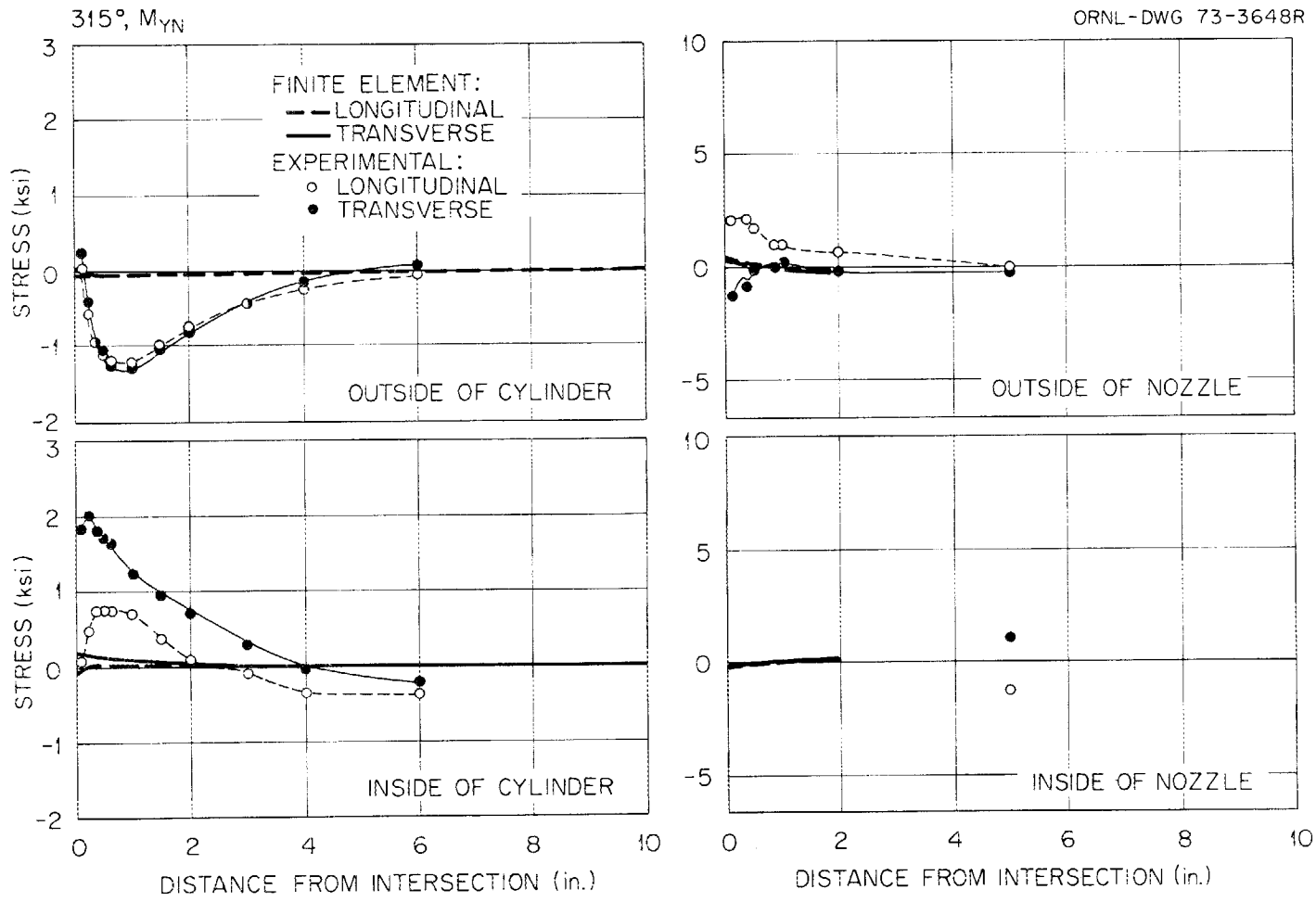

Fig. 37. Measured and predicted stress distributions at 315° for a torsional moment of 2400 in.-lb on the nozzle.

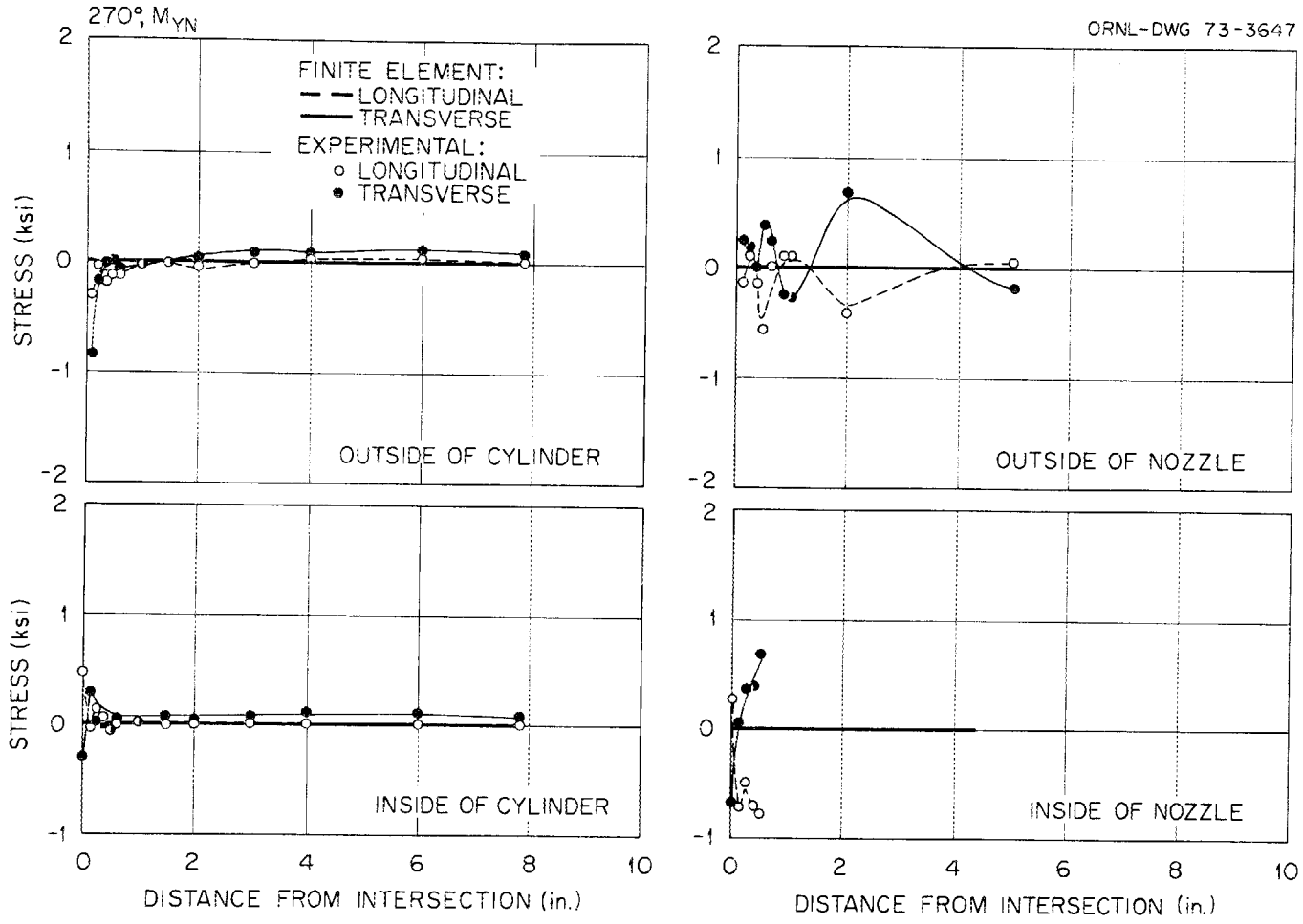

Fig. 38. Measured and predicted stress distributions at 270° for a torsional moment of 2400 in.-lb on the nozzle.

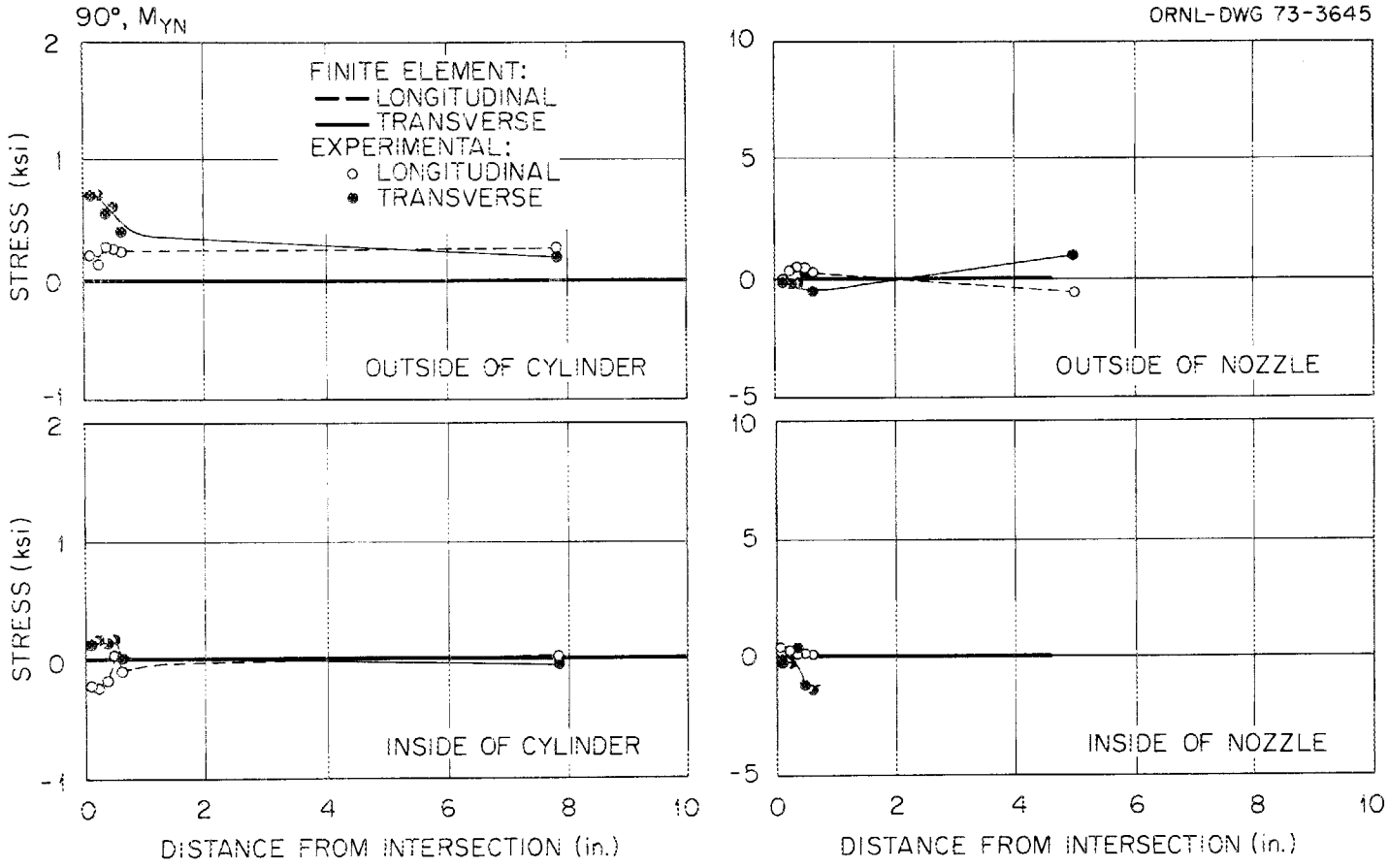

Fig. 39. Measured and predicted stress distributions at 90° for a torsional moment of 2400 in.-lb on the nozzle.

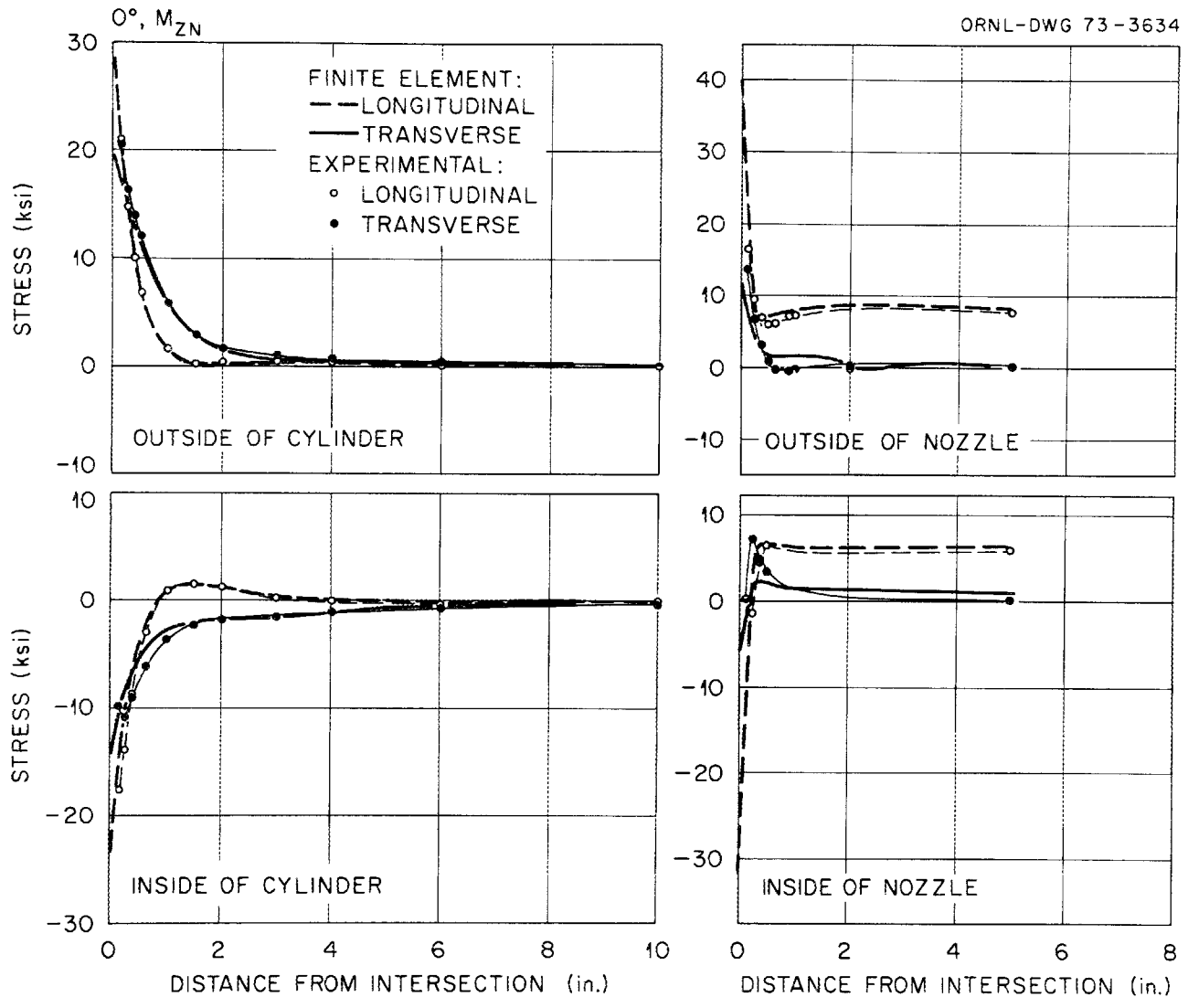

Fig. 40. Measured and predicted stress distributions at 0° for an in-plane moment of 1200 in.-lb on the nozzle.

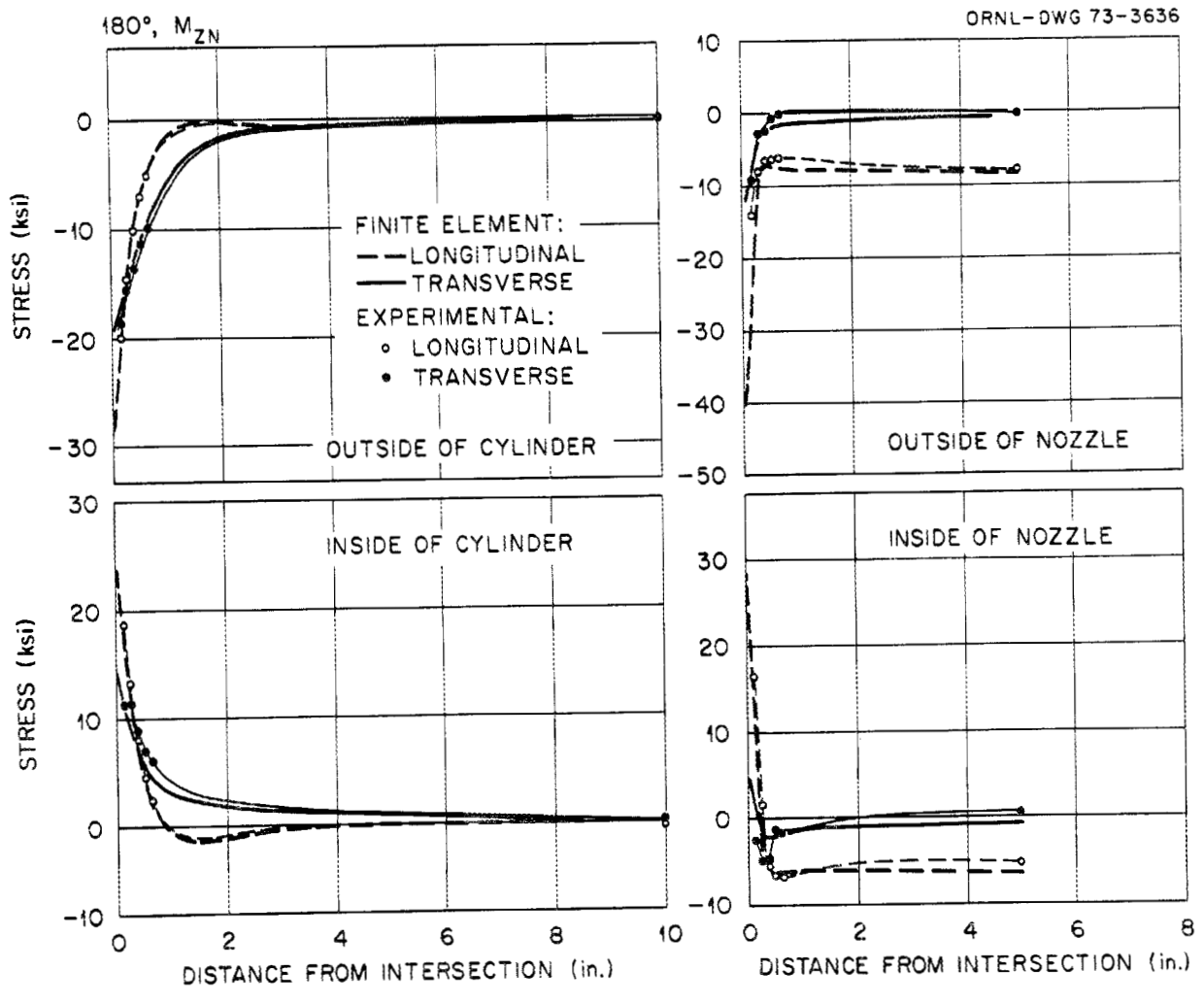

Fig. 41. Measured and predicted stress distributions at 180° for an in-plane moment of 1200 in.-lb on the nozzle.

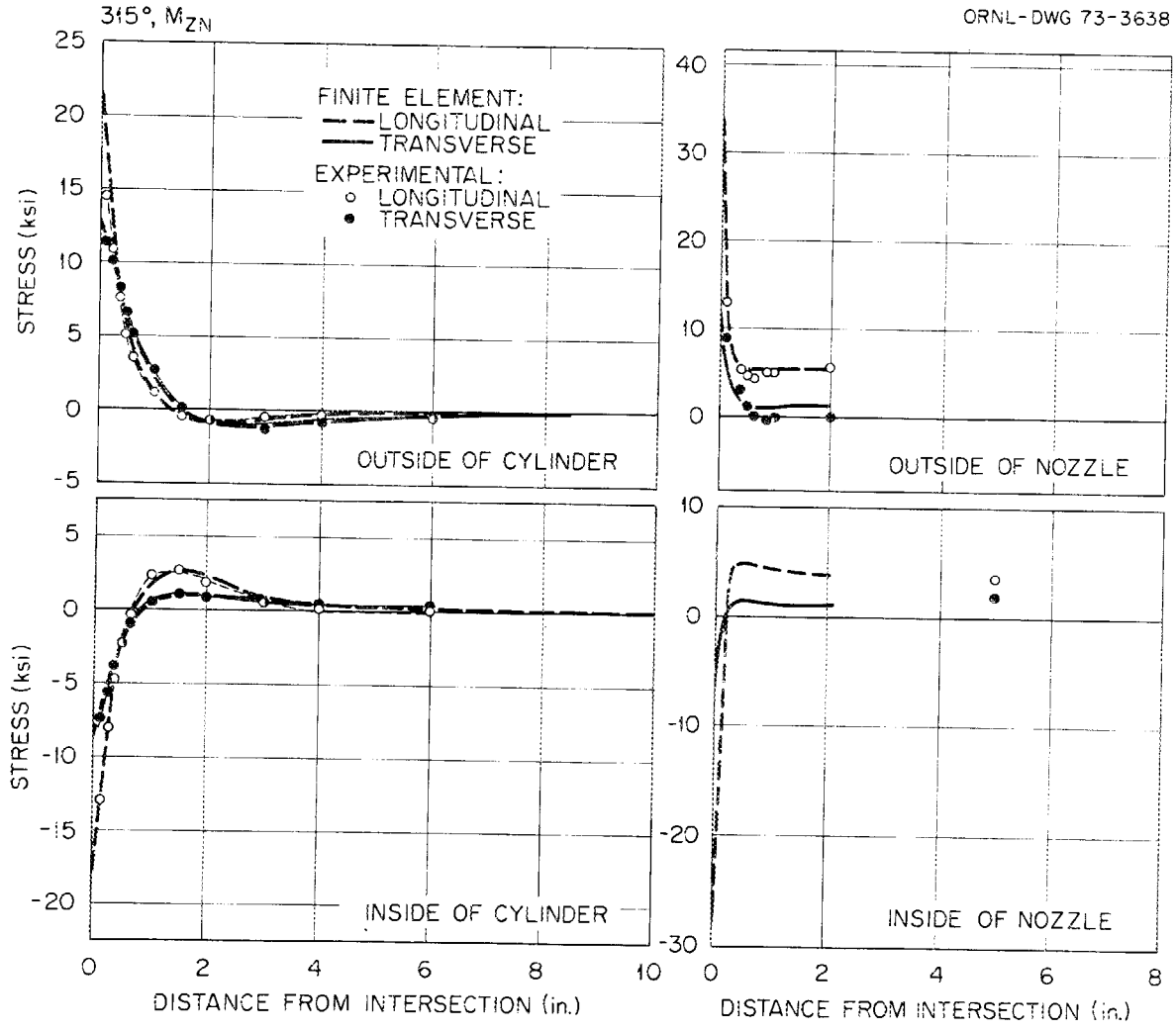

Fig. 42. Measured and predicted stress distributions at 315° for an in-plane moment of 1200 in.-lb on the nozzle.

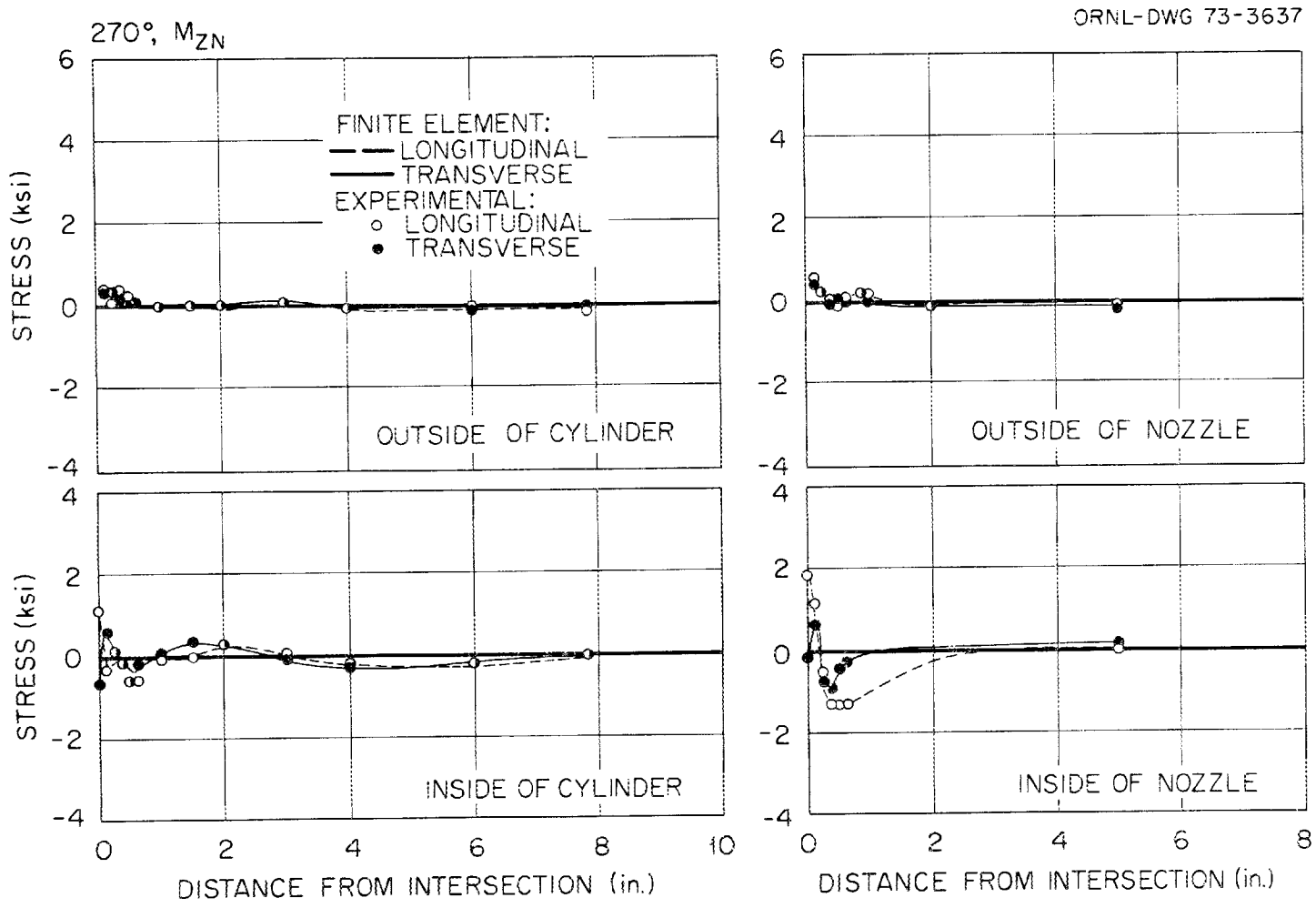

Fig. 43. Measured and predicted stress distributions at 270° for an in-plane moment of 1200 in.-lb on the nozzle.

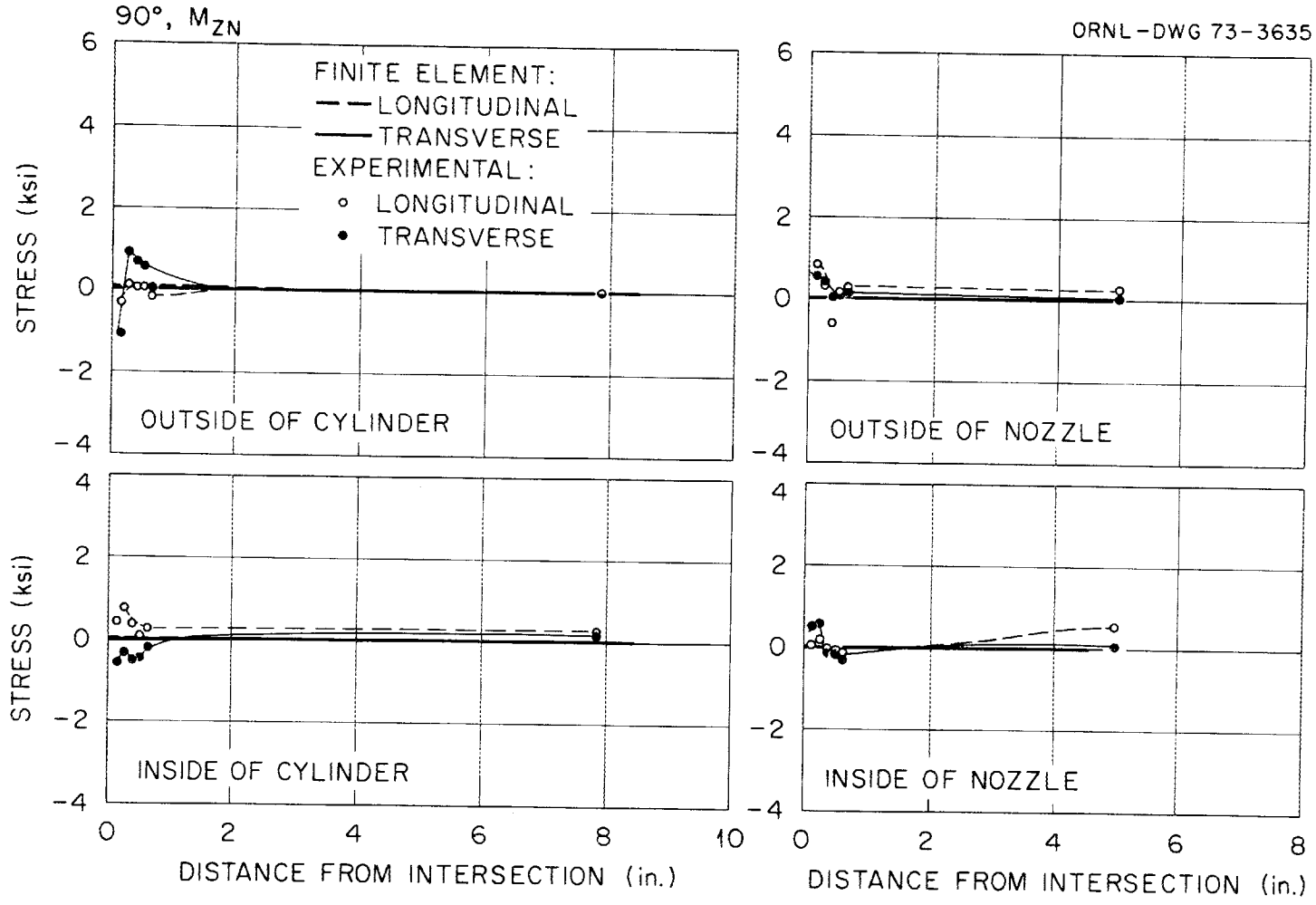

Fig. 44. Measured and predicted stress distributions at 90° for an in-plane moment of 1200 in.-lb on the nozzle.

The maximum experimentally determined stress ratio was 3.7, with the maximum stress occurring on the outer surface of the cylinder at the junction along the 0° gage line. The maximum theoretical stress occurred on the outer surface of the nozzle at the junction along the 0° gage line; the stress ratio was 5.6.

4.5 In-Plane Force, F_{XN}, on Nozzle

The in-plane force applied to the nozzle had a value of 120 lb. The comparisons of theory and experiment for the eight gage lines are shown in Figs. 45 through 49. The results here are very similar to the previous case of the in-plane bending moment on the nozzle, and the overall agreement is very good.

The maximum experimentally determined stress (ratio of 4.4) occurred on the outer surface of the cylinder at the junction along the 0° gage line. The maximum theoretical stress occurred on the outer surface of the nozzle at the junction along the 0° gage line; the ratio was 6.2.

4.6 Axial Force, F_{YN}, on Nozzle

The comparisons of theory and experiment for an axial force of 500 lb applied to the nozzle are presented in Figs. 50 through 54. The agreement between theory and experiment is very good, particularly as the larger stress levels are approached on the transverse plane of symmetry (Figs. 53 and 54).

The experimentally determined maximum stress occurred on the outer surface of the cylinder on the 270° plane at the junction; the ratio was 17.2. The theoretically determined maximum stress occurred on the outer surface of the nozzle on the 270° gage line at the junction; the ratio was 19.4.

4.7 Out-of-Plane Force, F_{ZN}, on Nozzle

The comparisons of theory and experimental data for an out-of-plane force of 80 lb applied to the nozzle are presented in Figs. 55 through 59. These results are very similar to those for the out-of-plane moment

on the nozzle, and the overall agreement between theory and experiment is again good. The stresses are very small on the 0 and 180° gage lines, and the agreement naturally does not look as good as along other gage lines.

The experimentally determined maximum stress ratio was 6.6 with the maximum stress occurring on the outer surface of the cylinder along the 270° gage line at the junction. The theoretically determined maximum stress (ratio of 8.1) occurred on the outer surface of the nozzle along the 270° gage line.

4.8 Torsional Moment Loading, M_{XC}, on Cylinder

The comparisons of theory and experiment for a torsional moment of 40,000 in.-lb applied to the cylinder are presented in Figs. 60 through 64. In general, the experimental stresses are low in the longitudinal and transverse planes of symmetry and rise to their maximum levels on the intermediate gage line. The agreement between theory and experiment is satisfactory on the intermediate line. However, the stresses are not very large anywhere in the model.

The experimentally determined maximum stress occurred on the inner surface of the cylinder along the 315° gage line at the junction, and the maximum stress ratio was 2.5. The theoretically determined maximum stress occurred on the outer surface of the nozzle along the 180° gage line at the junction, and the maximum stress ratio was 5.6.

4.9 Out-of-Plane Moment Loading, M_{YC}, on Cylinder

The comparisons of theory and experiment for an out-of-plane moment loading of 40,000 in.-lb applied to the cylinder are presented in Figs. 65 through 69. Here the 0 and 180° gage lines on the longitudinal plane of symmetry are analogous to the neutral axis of a beam in bending, and the stresses are thus low. However, the stresses are not very large anywhere in the model. As a result of the relatively low stress levels, the

stress distributions are not too well defined on the 0, 180, and 315° gage lines, and the agreement between theory and experiment appears to be relatively poor. However, on the gage lines of maximum stress (270 and 90°) the agreement between theory and experiment is good.

The experimentally determined maximum stress (ratio of 1.2) occurred on the outer surface of the cylinder along the 270° plane. The theoretical maximum stress ratio (1.1) occurred on the outside surface of the nozzle at the junction on the 0° gage line.

4.10 In-Plane Moment Loading, M_{ZC}, on Cylinder

The comparisons of theory and experiment for an in-plane moment loading of 40,000 in.-lb applied to the cylinder are presented in Figs. 70 through 74. Here the experimental stress levels are a maximum in the transverse plane of symmetry, as shown in Figs. 73 and 74. The comparisons on the cylinder were good, while those on the nozzle were fair.

The experimentally determined maximum stress (ratio of 3.2) occurred on the inside surface of the nozzle at the junction on the 270° gage line, while the theoretical maximum stress (ratio of 2.5) occurred on the inside surface of the nozzle both on the 90 and 270° gage lines.

4.11 Axial Force, F_{XC}, on Cylinder

The axial force applied to the cylinder had a value of 10,000 lb. The comparisons of theory and experiment for the five gage lines are presented in Figs. 75 through 79. Even considering the relatively low stresses, the agreement between theory and experiment is poor, since only along a few gage lines is the agreement satisfactory.

The experimentally determined maximum stress occurred on the inner surface of the cylinder at the junction on the 270° gage line, while the theoretical maximum stress occurred on the inner surface of the nozzle at the junction on the 270 and 90° planes. The experimental and theoretical stress ratios were 2.5.

4.12 In-Plane Force, F_{YC}, on Cylinder

The comparisons of theory and experiment for an in-plane force of 3000 lb applied to the cylinder are shown in Figs. 80 through 84. The agreement between theory and experiment is very good for this loading case.

Both the experimentally determined and the theoretically determined maximum stresses occurred on the inside surface of the nozzle at the junction. The experimental maximum was on the 270° gage line, while the theoretical maximum was on both the 270 and 90° gage lines. The maximum experimental stress ratio was 3.5, and the maximum theoretical ratio was 2.6.

4.13 Out-of-Plane Force, F_{ZC}, on Cylinder

The comparisons of theory and experiment for an out-of-plane force of 3000 lb applied to the cylinder are shown in Figs. 85 through 89. The 0 and 180° gage lines, in the longitudinal plane of symmetry, are analogous to the neutral axis of a beam, so that the stresses are low along these gage lines. However, they build up for the other gage lines, and the agreement between theory and experiment is very good along gage lines 90 and 270°.

The experimentally determined maximum stress occurred on the outer surface of the cylinder along the 270° gage line, and the theoretical maximum occurred on the outer surface of the nozzle along the 315° gage line. The ratios were 1.3 and 1.5 respectively.

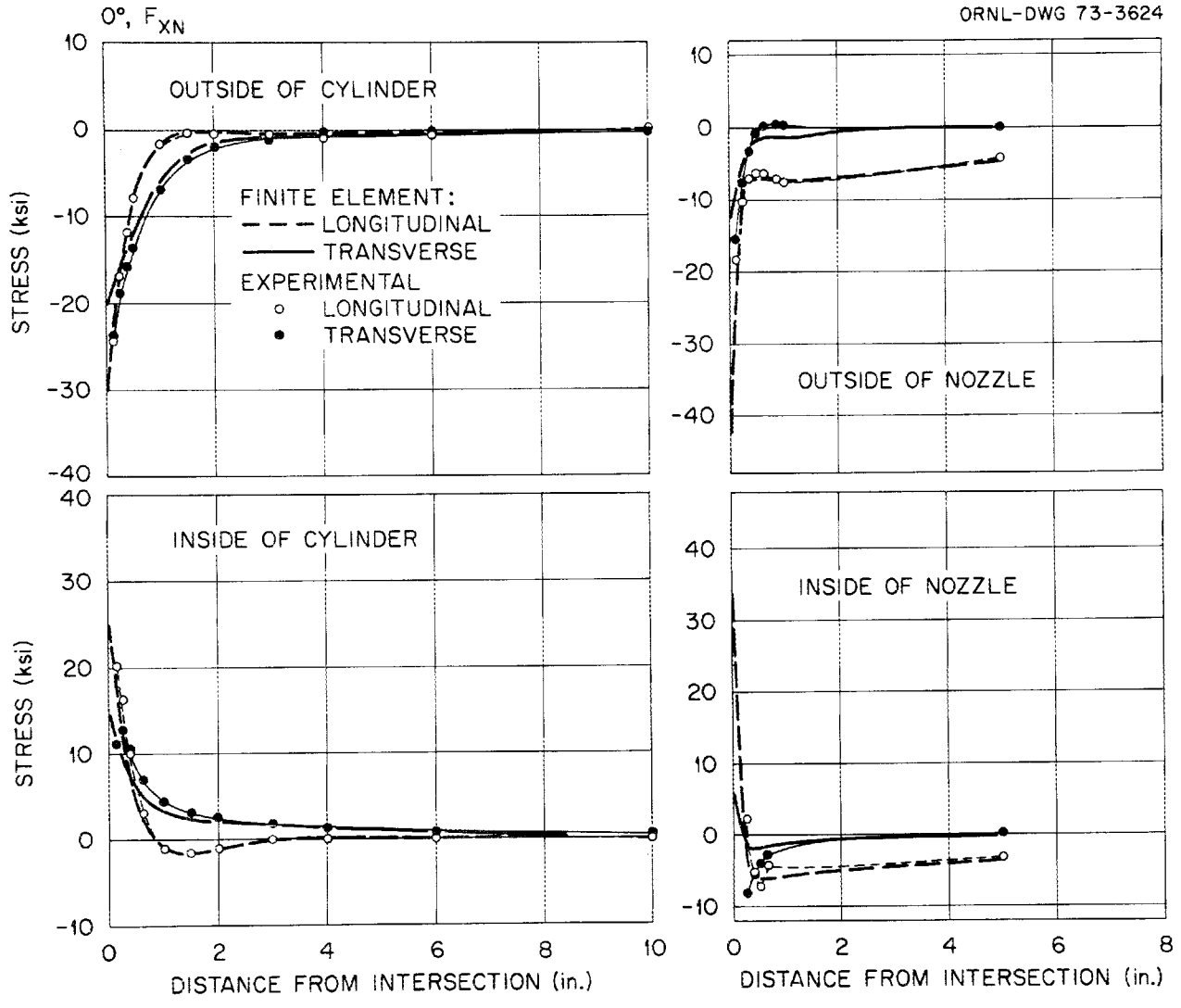

Fig. 45. Measured and predicted stress distributions at 0° for an in-plane force of 120 lb on the nozzle.

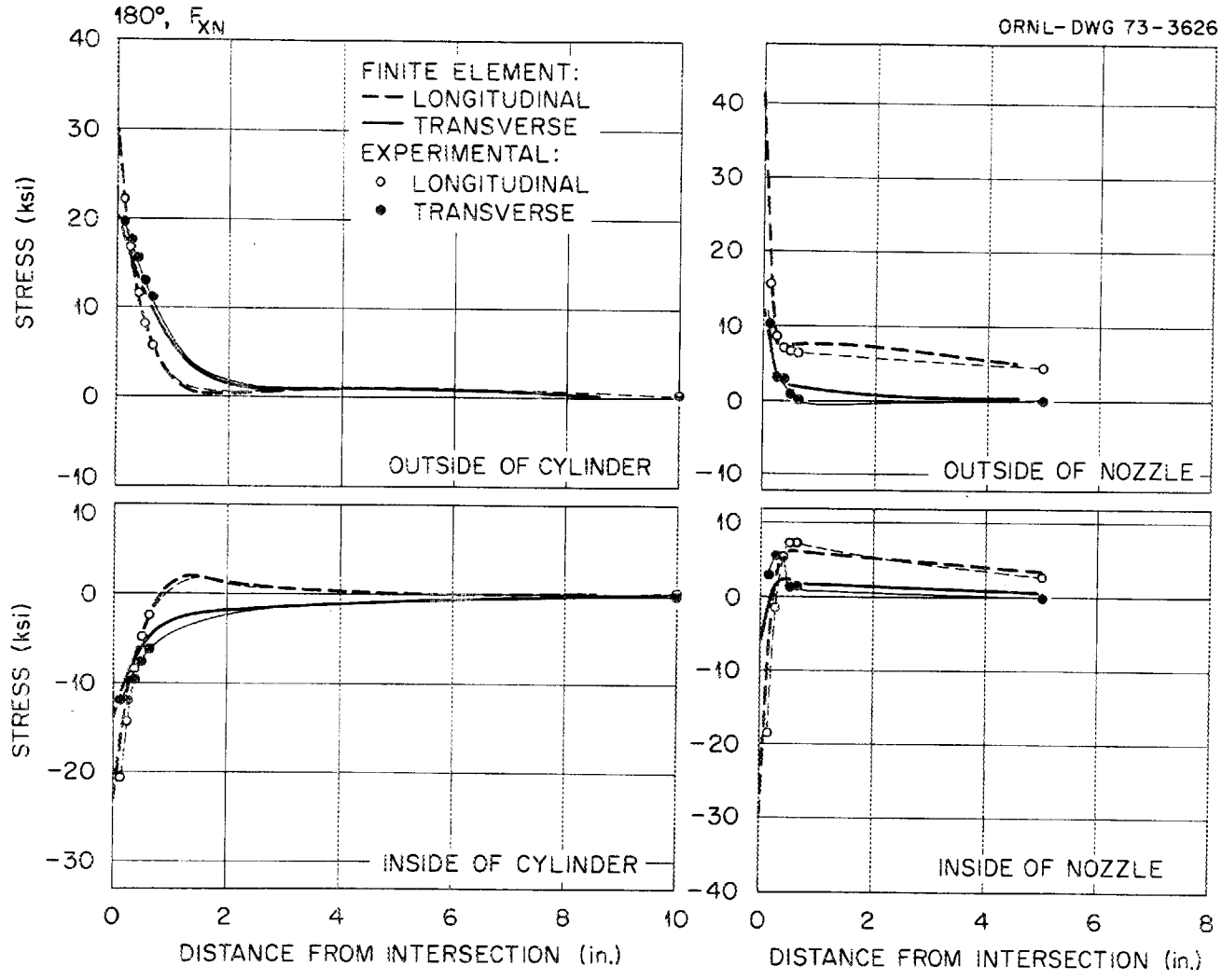

Fig. 46. Measured and predicted stress distributions at 180° for an in-plane force of 120 lb on the nozzle.

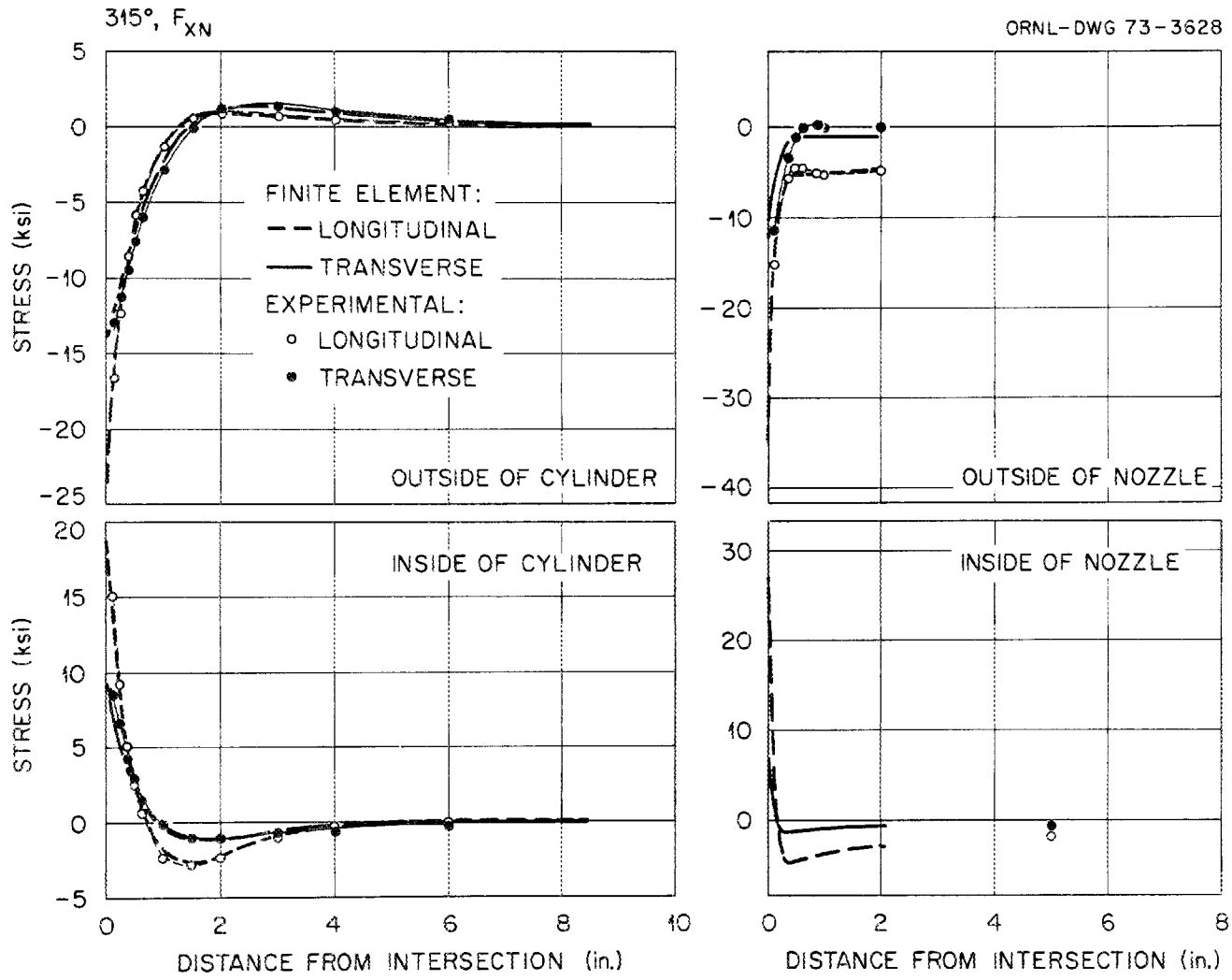

Fig. 47. Measured and predicted stress distributions at 315° for an in-plane force of 120 lb on the nozzle.

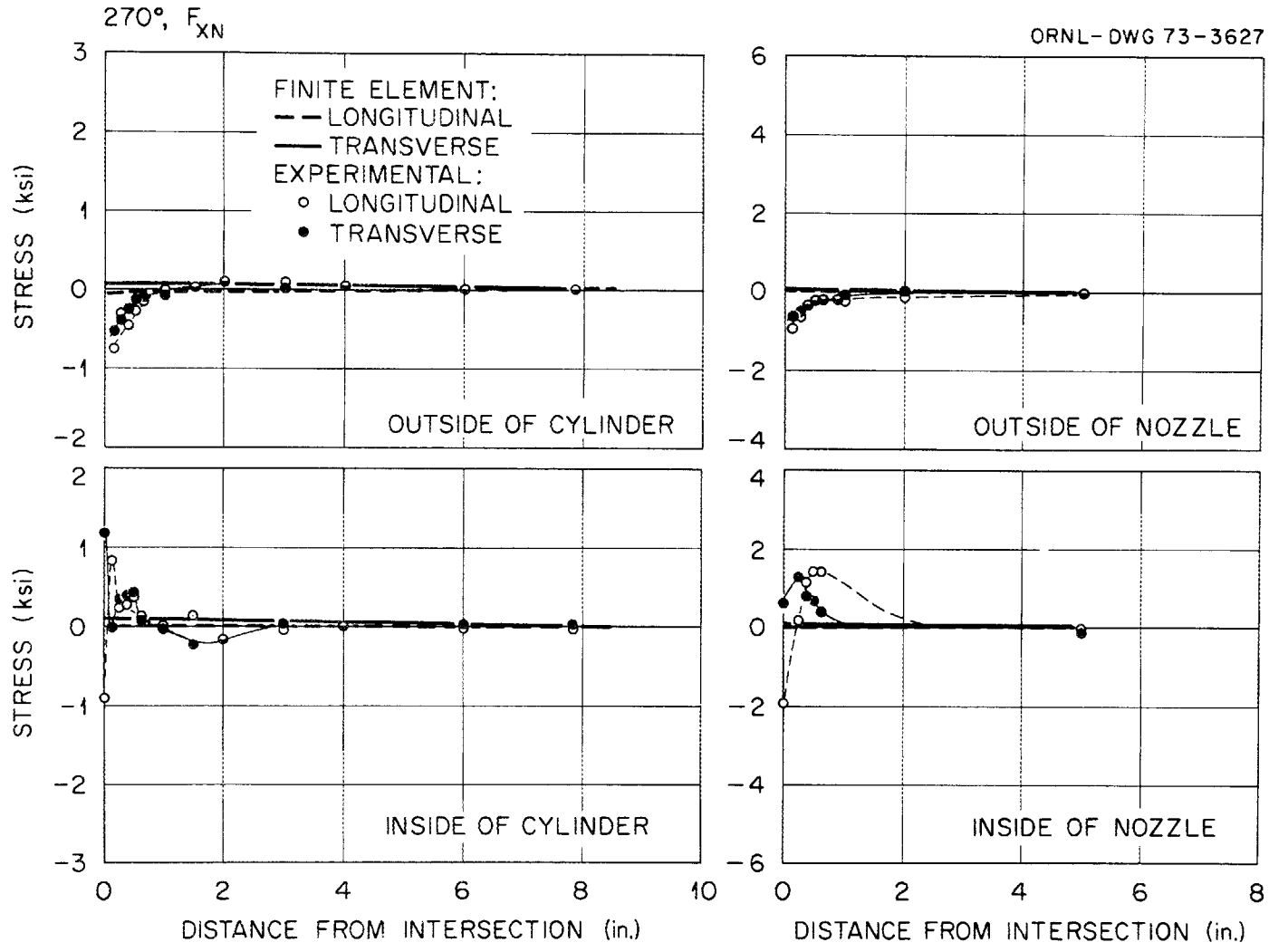

Fig. 48. Measured and predicted stress distributions at 270° for an in-plane force of 120 lb on the nozzle.

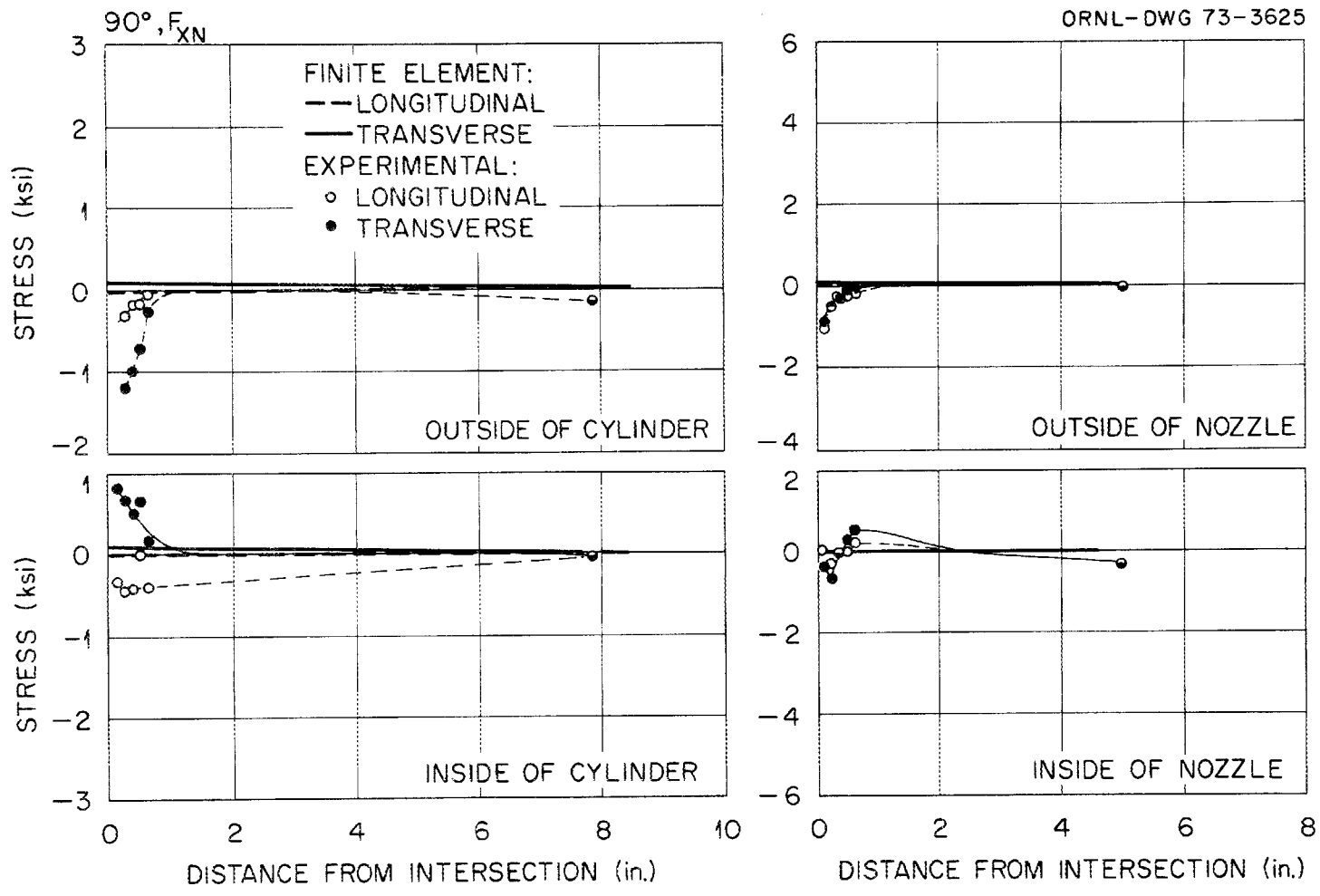

Fig. 49. Measured and predicted stress distributions at 90° for an in-plane force of 120 lb on the nozzle.

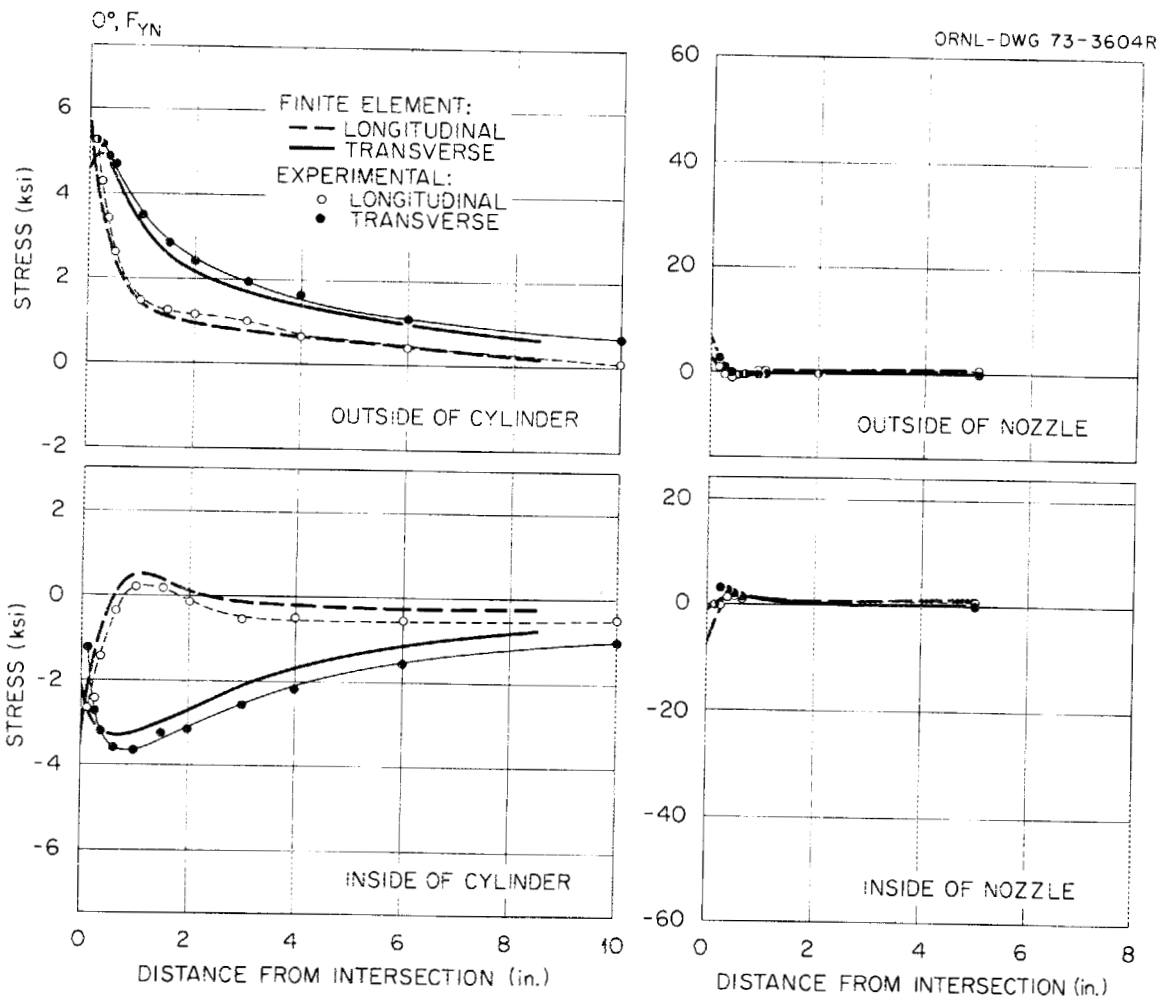

Fig. 50. Measured and predicted stress distributions at 0° for an axial force of 500 lb on the nozzle.

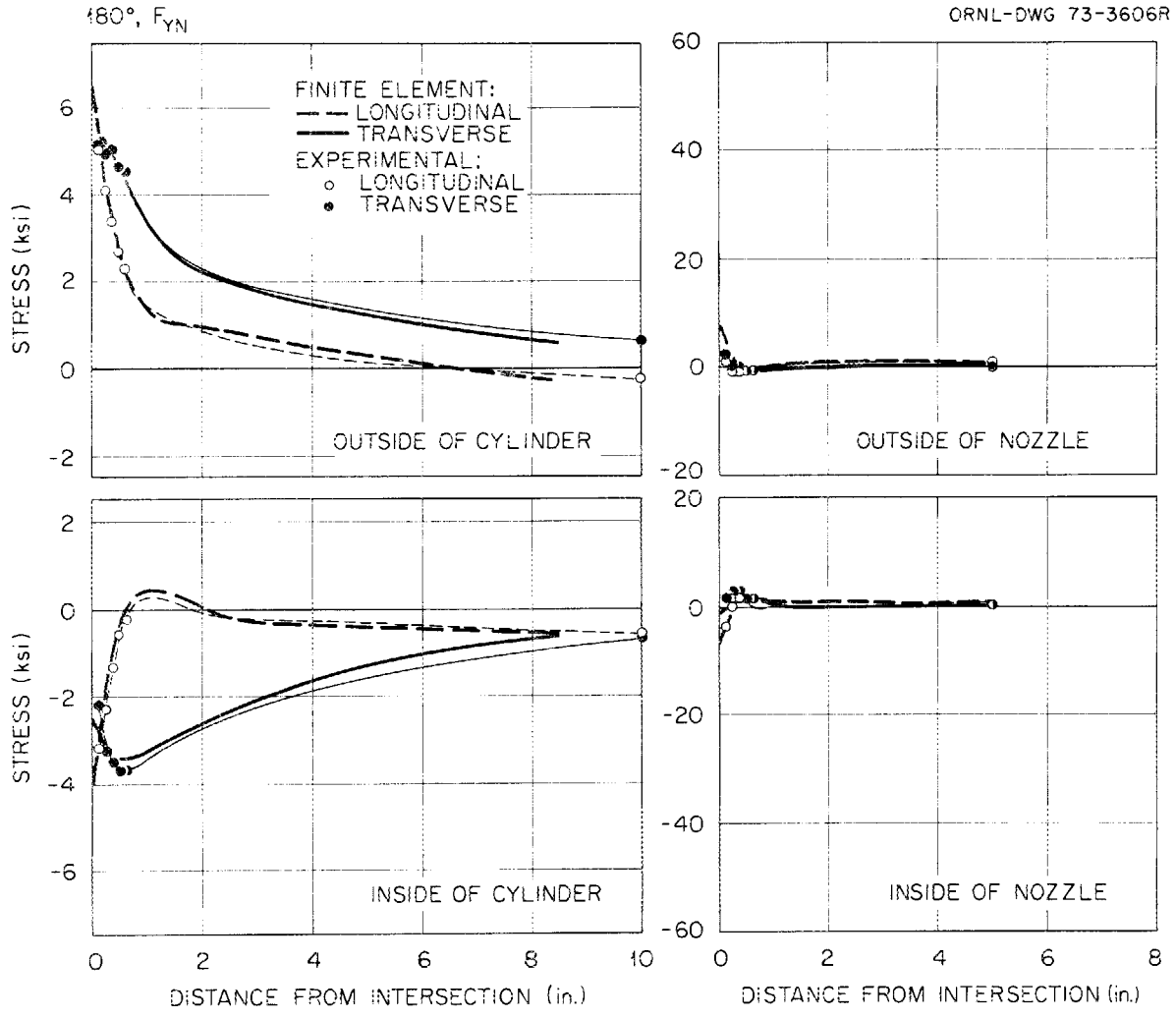

Fig. 51. Measured and predicted stress distributions at 180° for an axial force of 500 lb on the nozzle.

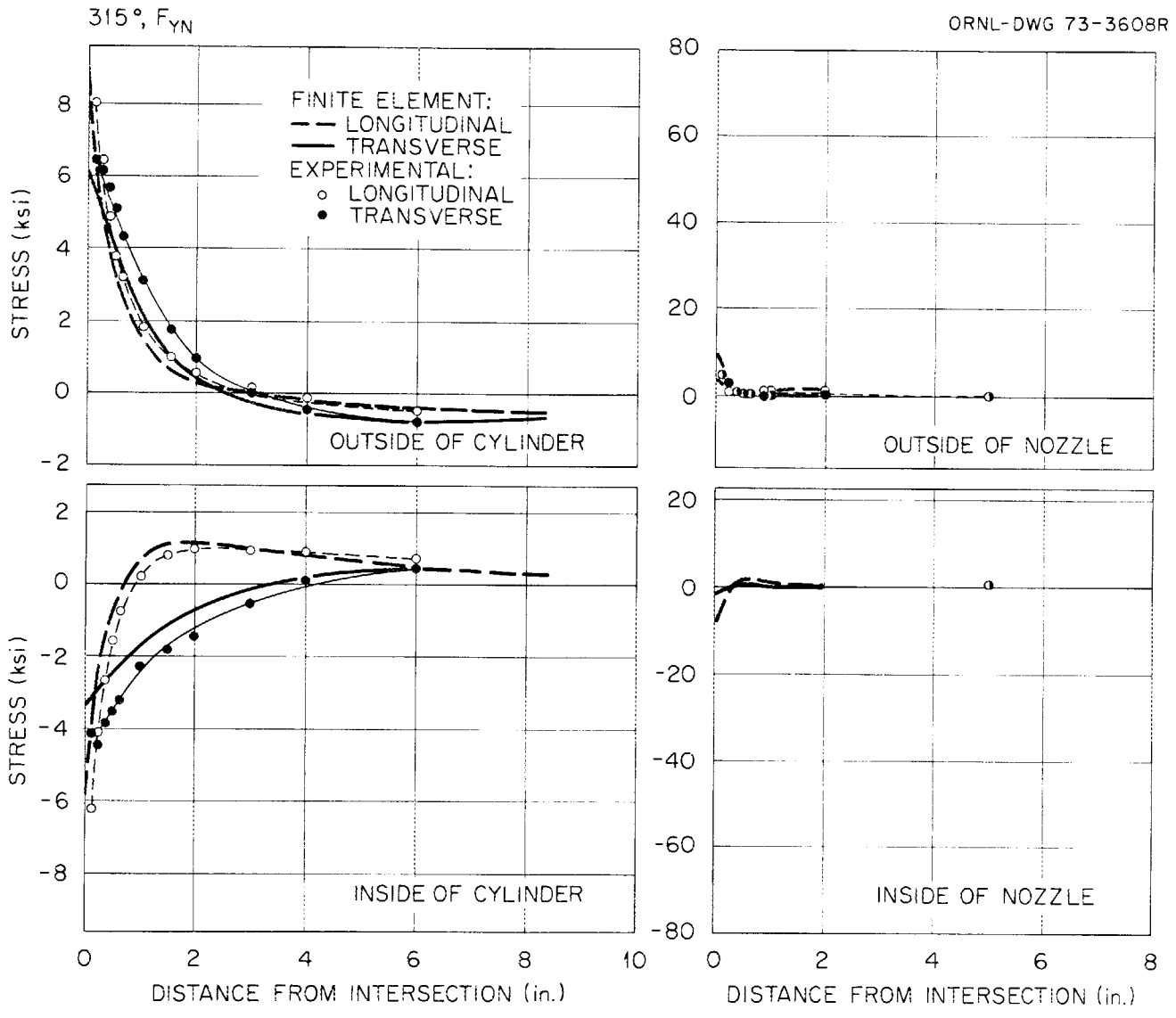

Fig. 52. Measured and predicted stress distributions at 315° for an axial force of 500 lb on the nozzle.

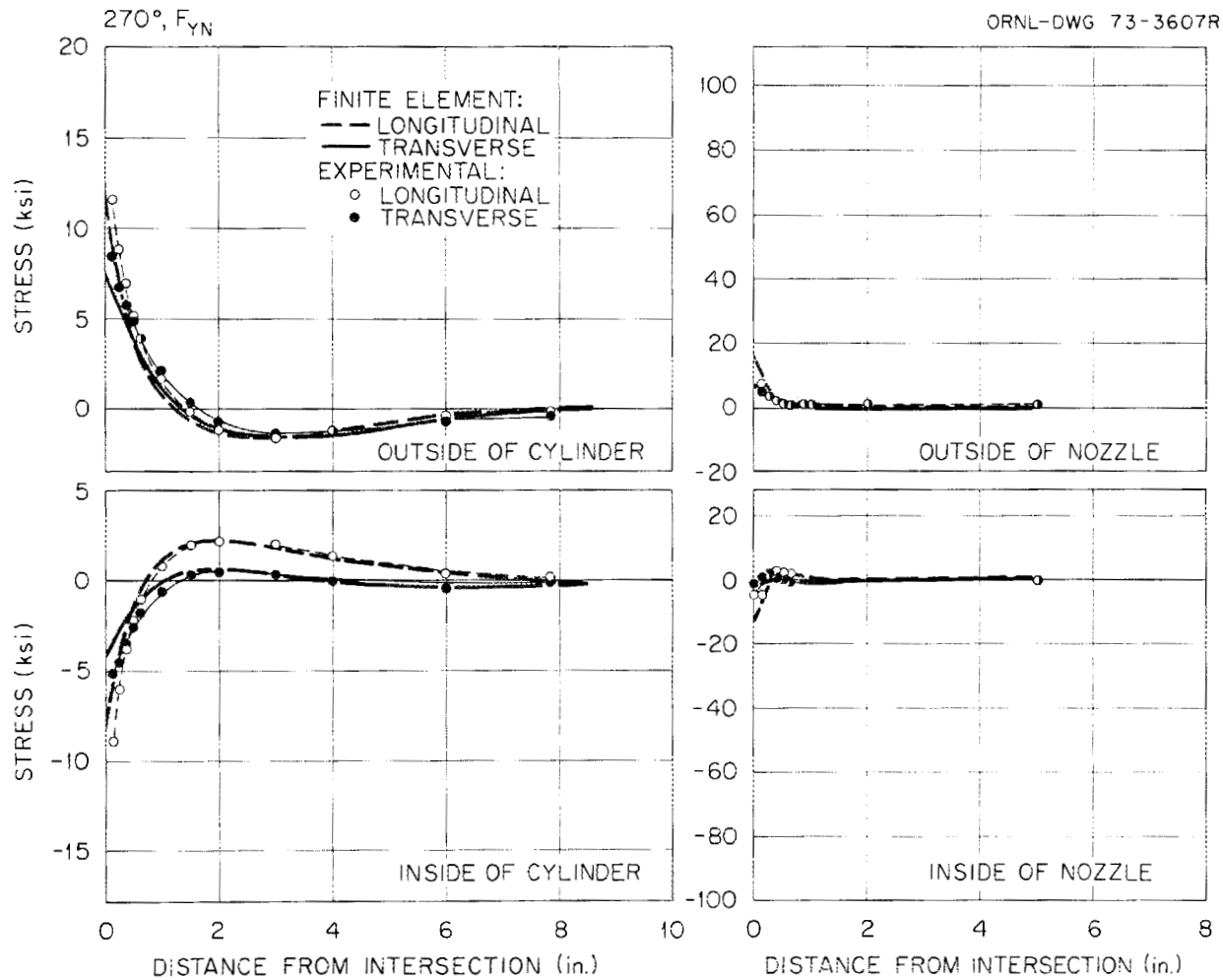

Fig. 53. Measured and predicted stress distributions at 270° for an axial force of 500 lb on the nozzle.

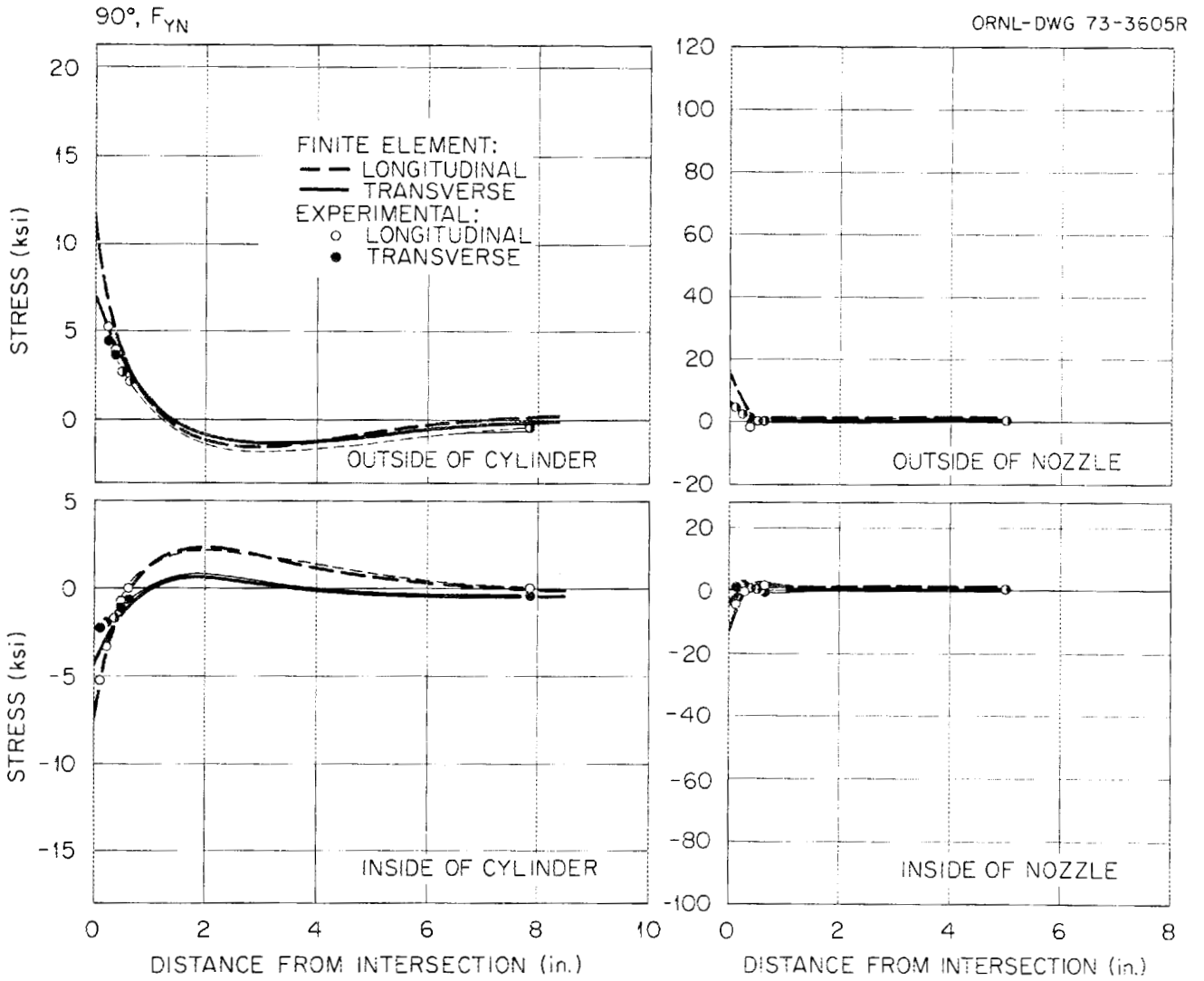

Fig. 54. Measured and predicted stress distributions at 90° for an axial force of 500 lb on the nozzle.

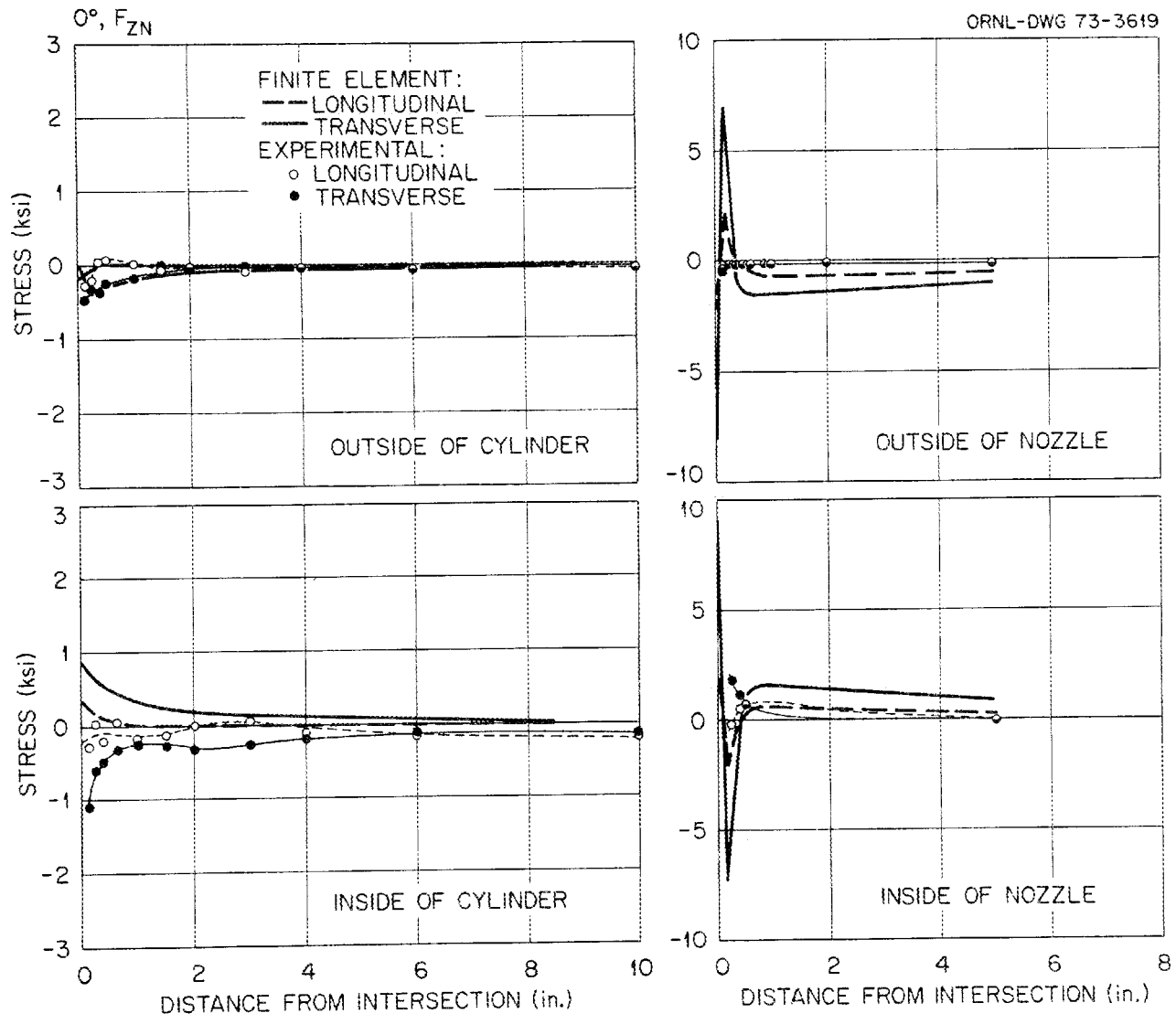

Fig. 55. Measured and predicted stress distributions at 0° for an out-of-plane force of 80 lb on the nozzle.

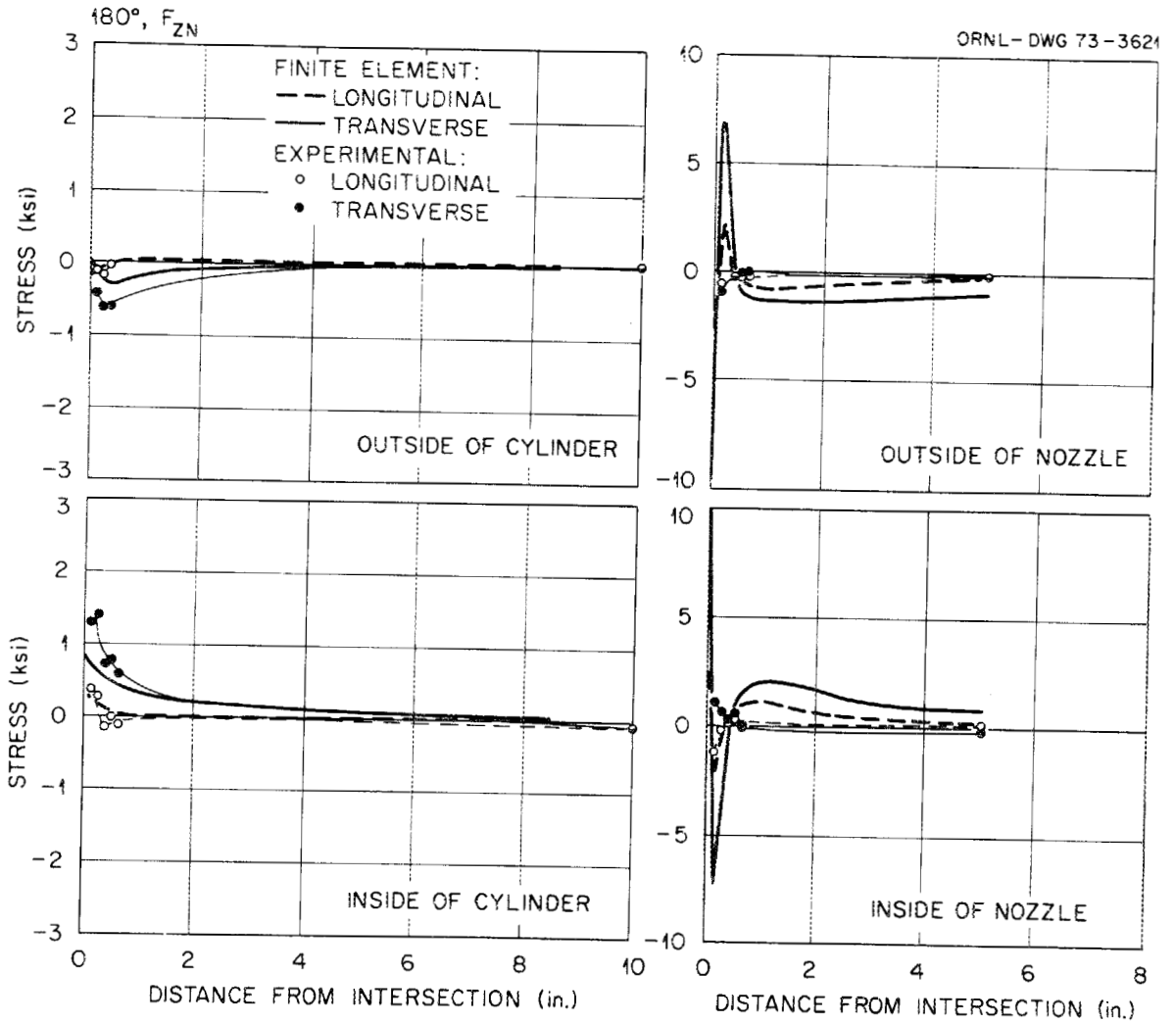

Fig. 56. Measured and predicted stress distributions at 180° for an out-of-plane force of 80 lb on the nozzle.

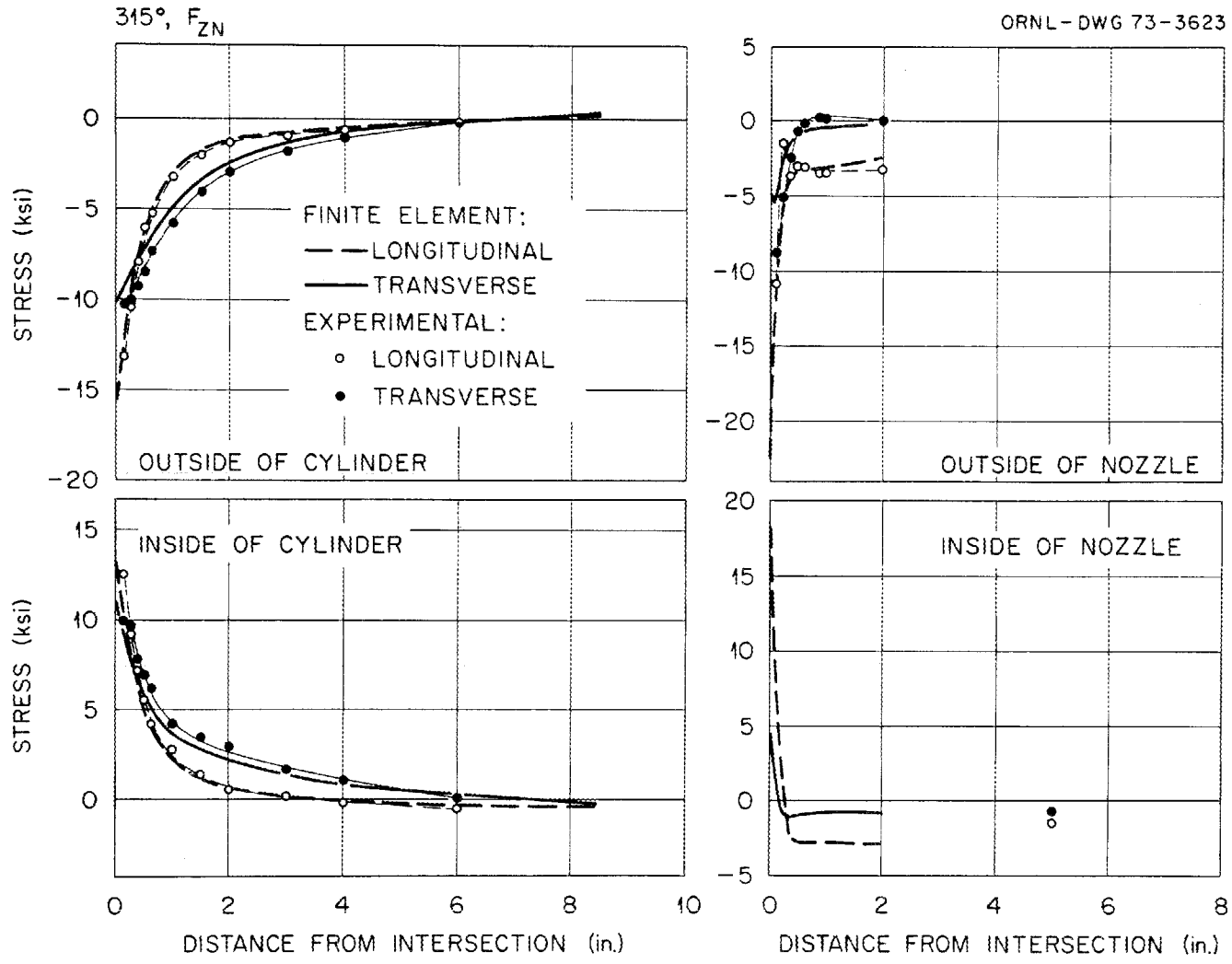

Fig. 57. Measured and predicted stress distributions at 315° for an out-of-plane force of 80 lb on the nozzle.

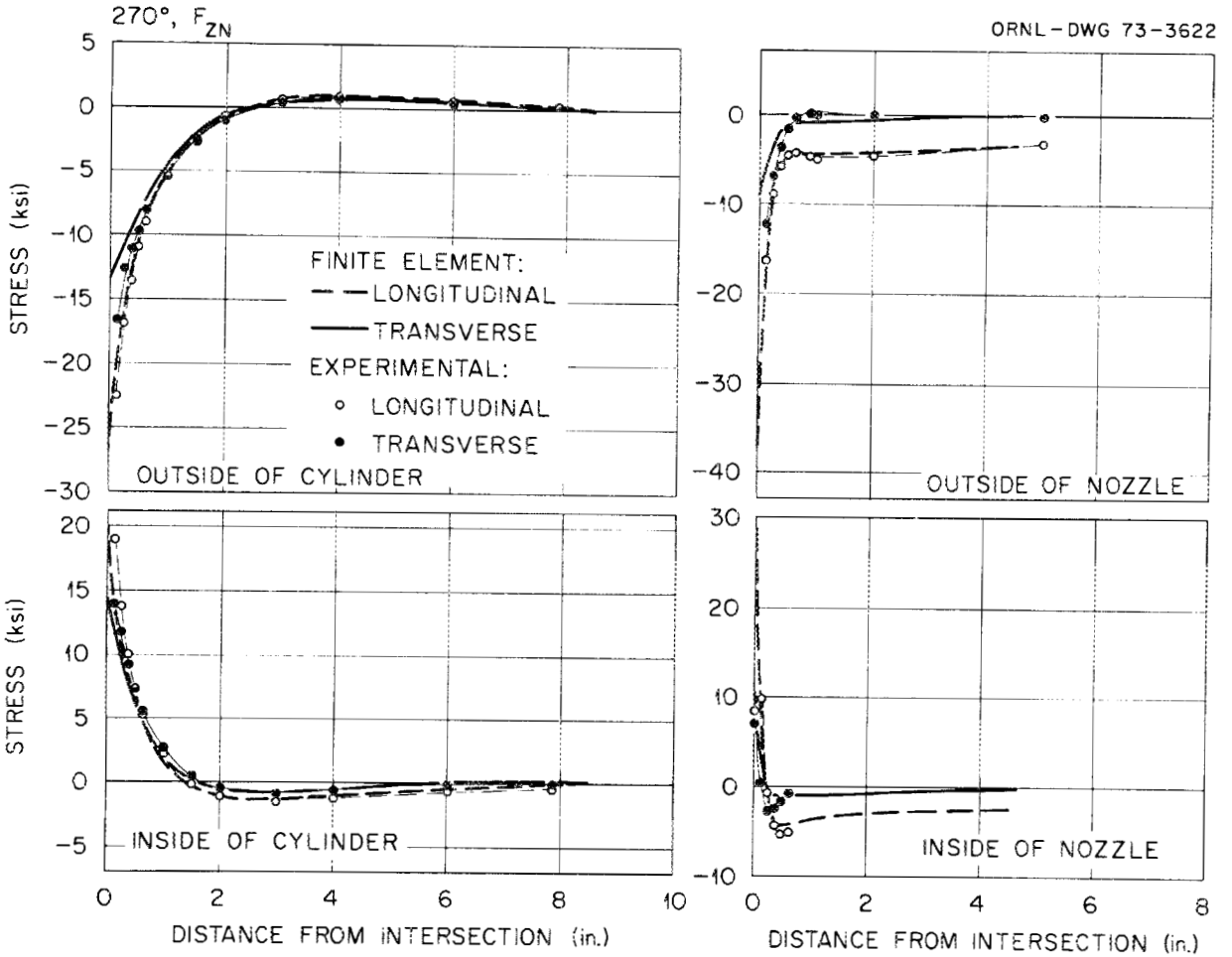

Fig. 58. Measured and predicted stress distributions at 270° for an out-of-plane force of 80 lb on the nozzle.

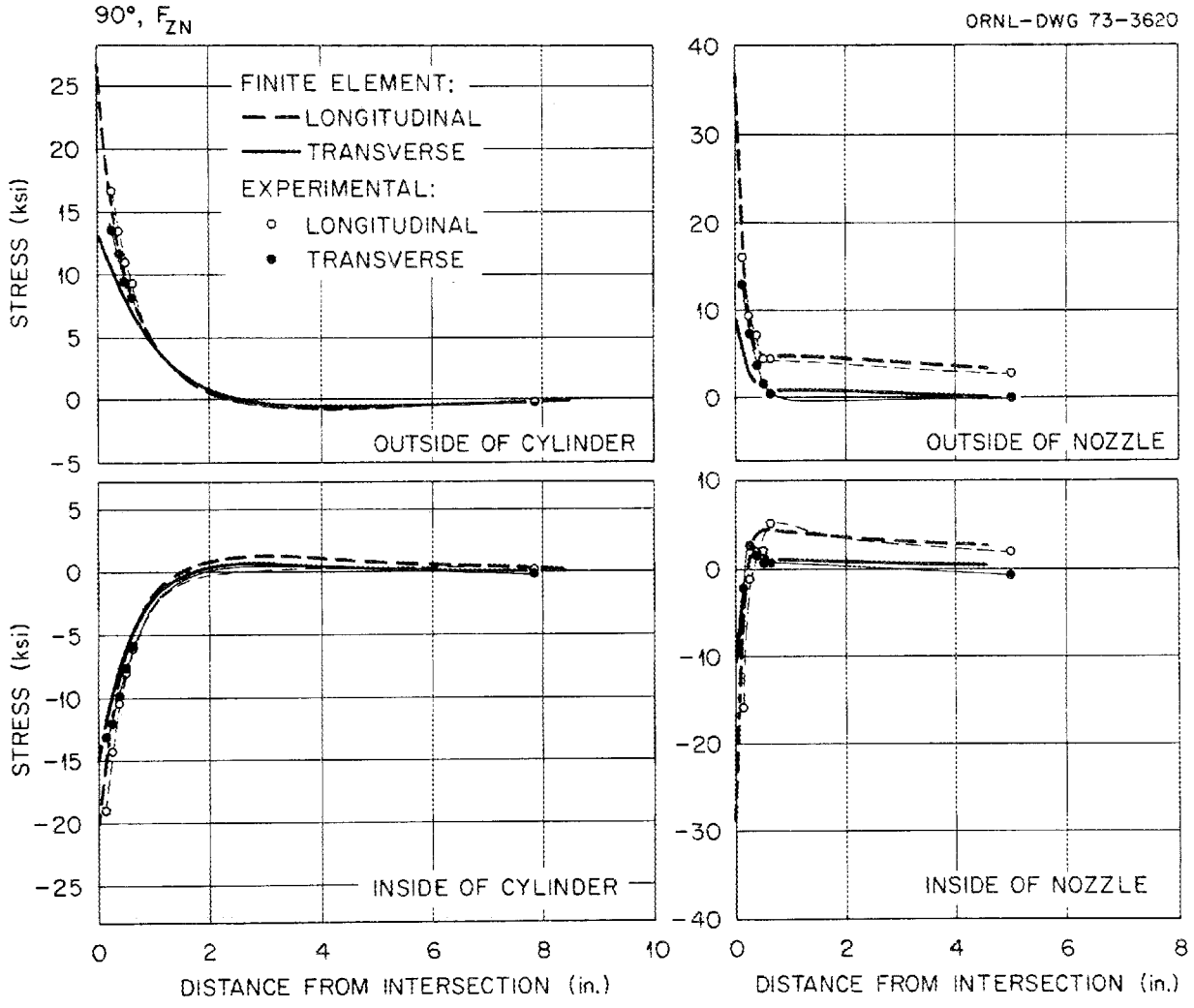

Fig. 59. Measured and predicted stress distributions at 90° for an out-of-plane force of 80 lb on the nozzle.

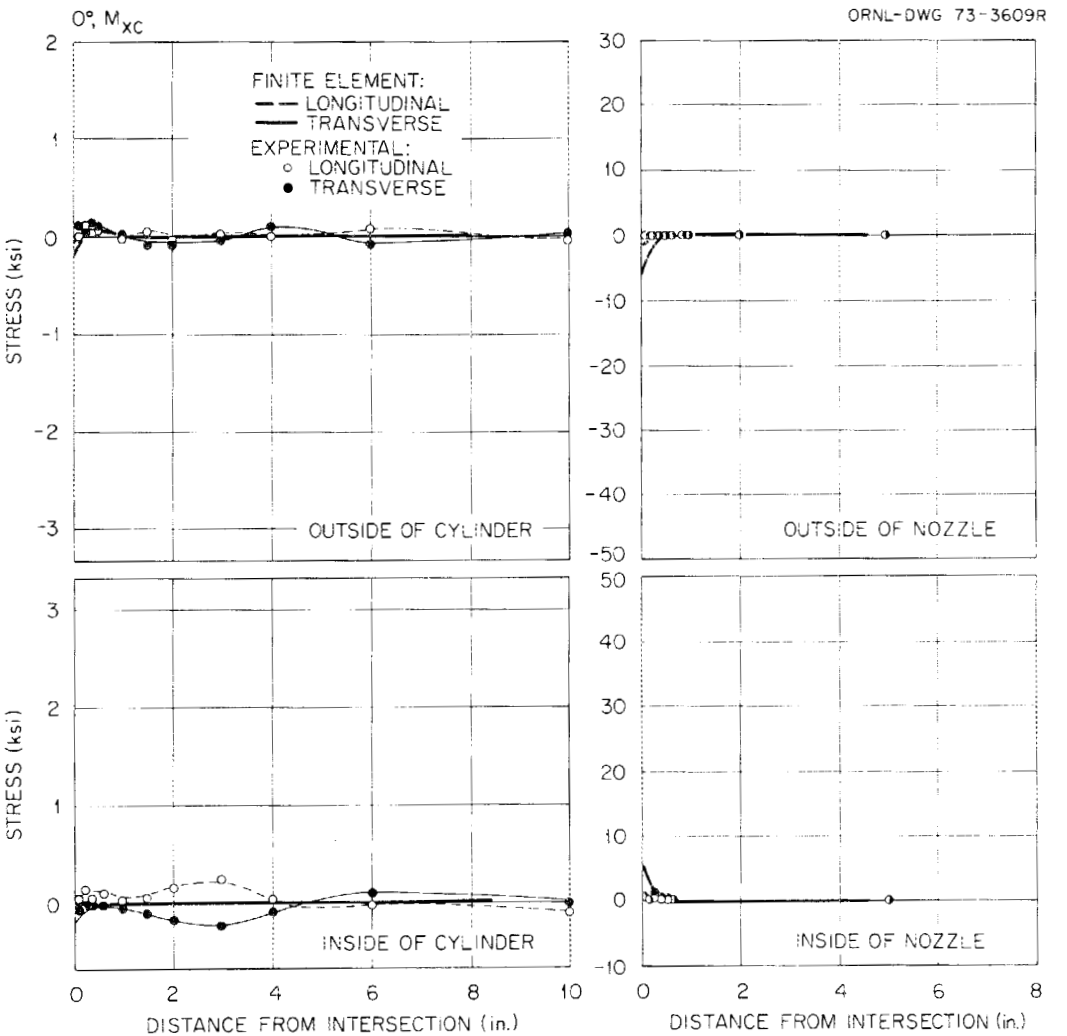

Fig. 60. Measured and predicted stress distributions at 0° for a torsional moment of 40,000 in.-lb on the cylinder.

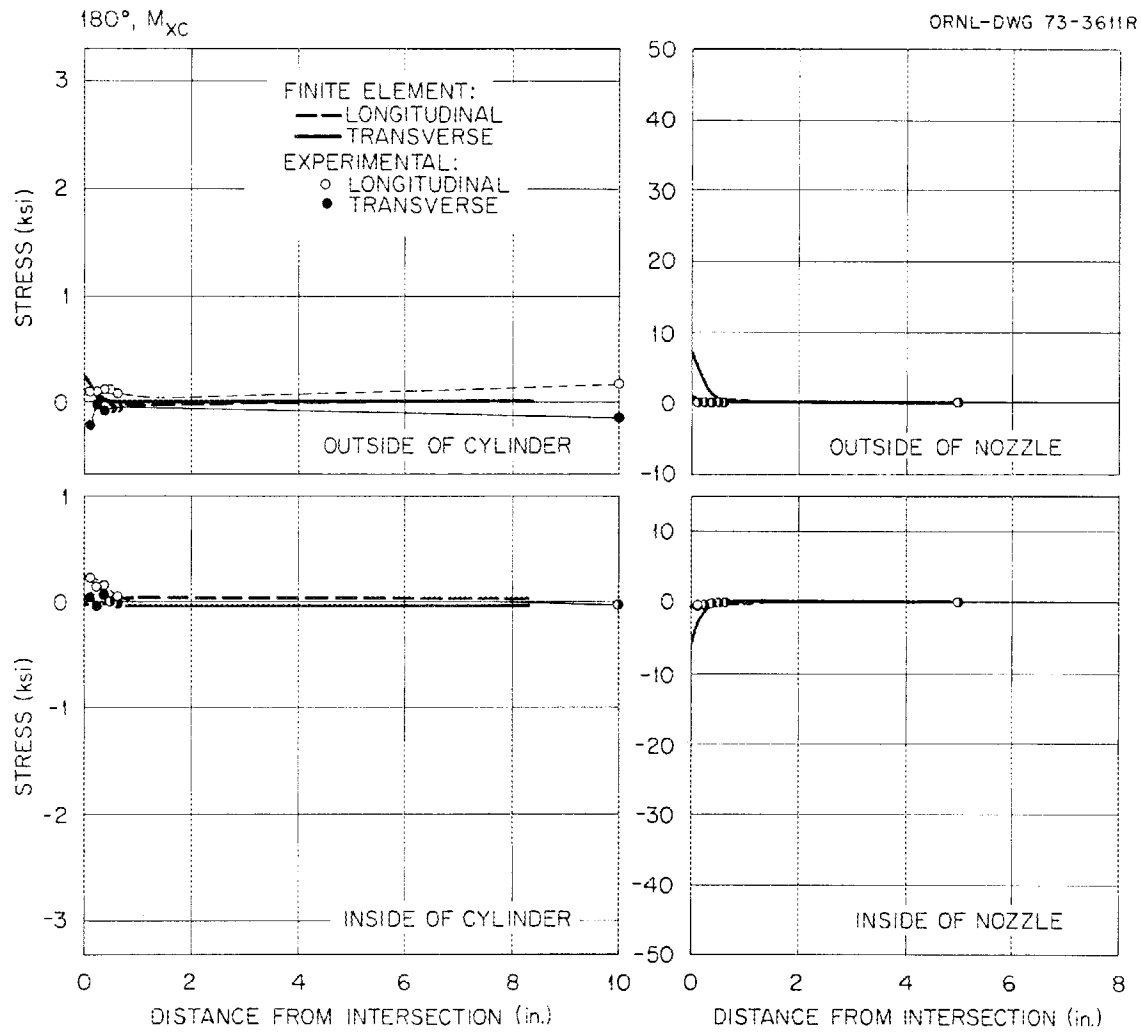

Fig. 61. Measured and predicted stress distributions at 180° for a torsional moment of 40,000 in.-lb on the cylinder.

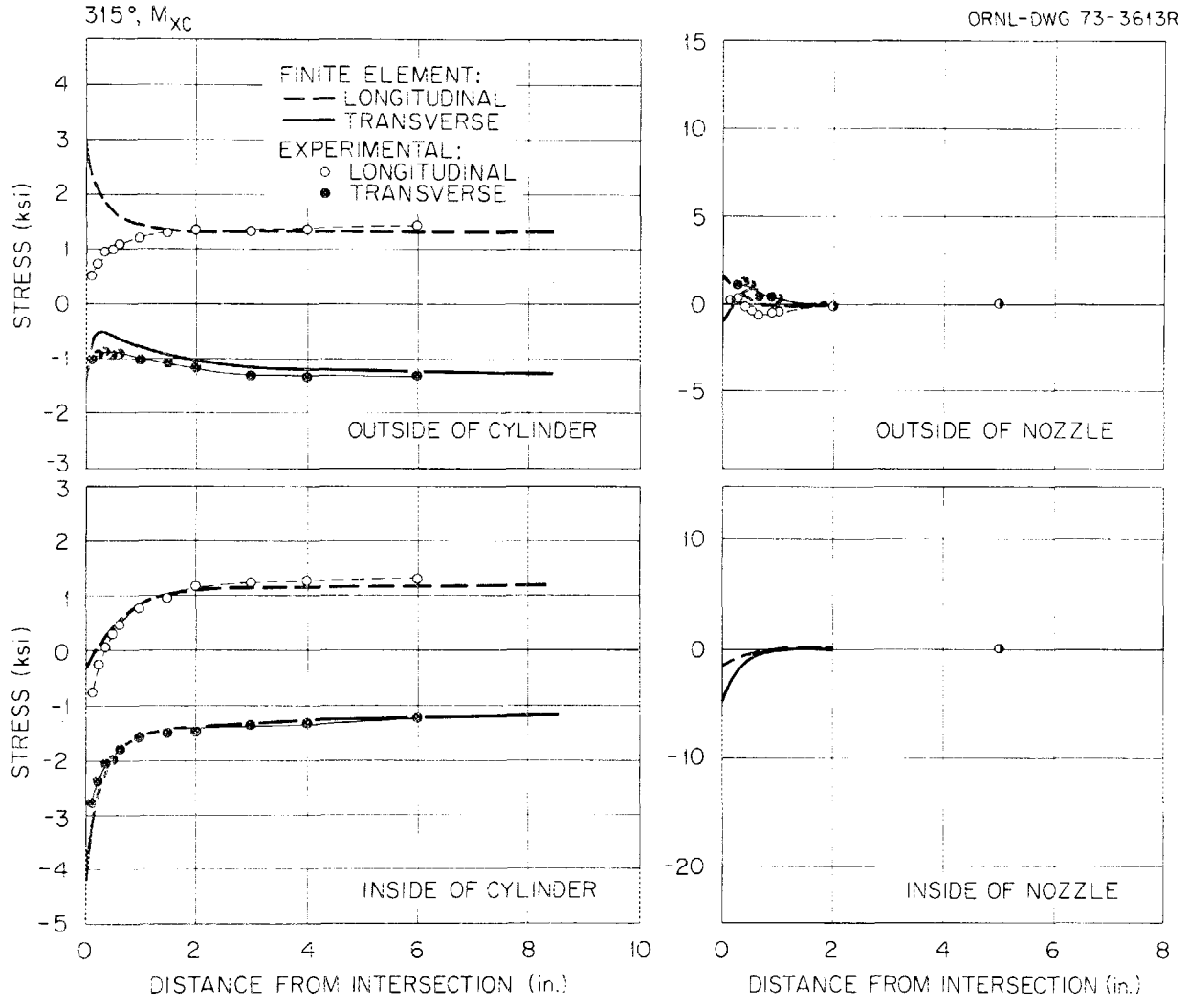

Fig. 62. Measured and predicted stress distributions at 315° for a torsional moment of 40,000 in.-lb on the cylinder.

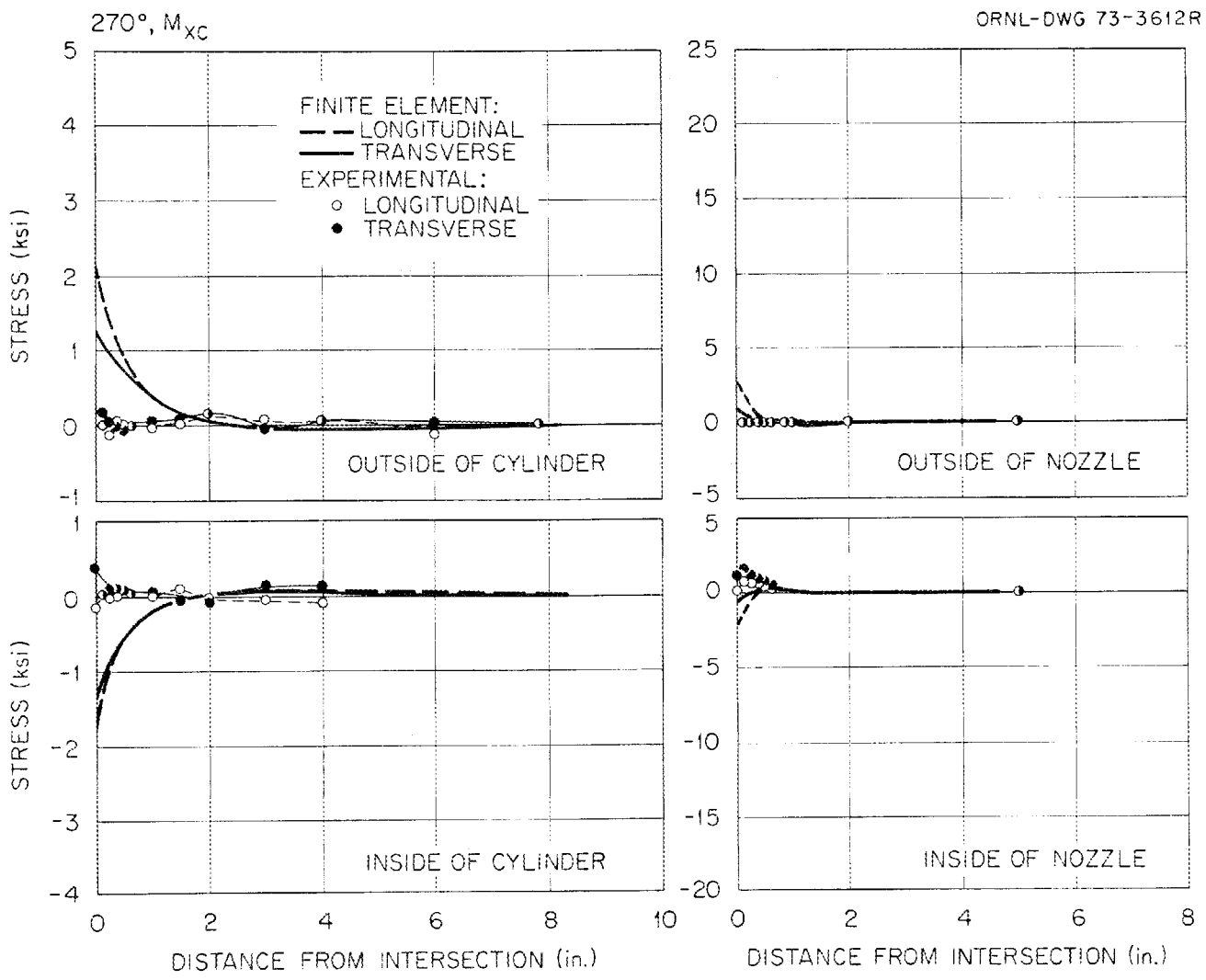

Fig. 63. Measured and predicted stress distributions at 270° for a torsional moment of 40,000 in.-lb on the cylinder.

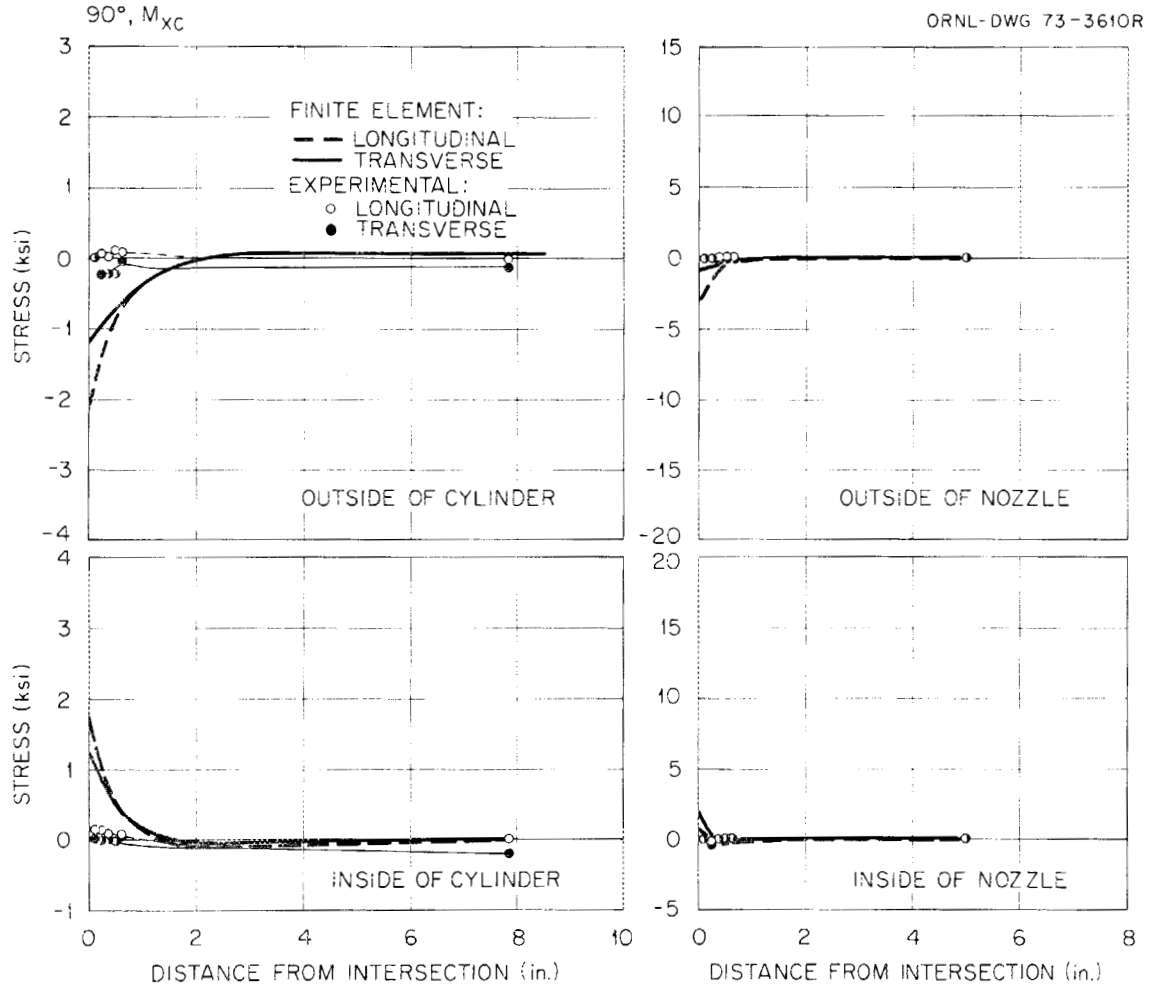

Fig. 64. Measured and predicted stress distributions at 90° for a torsional moment of 40,000 in.-lb on the cylinder.

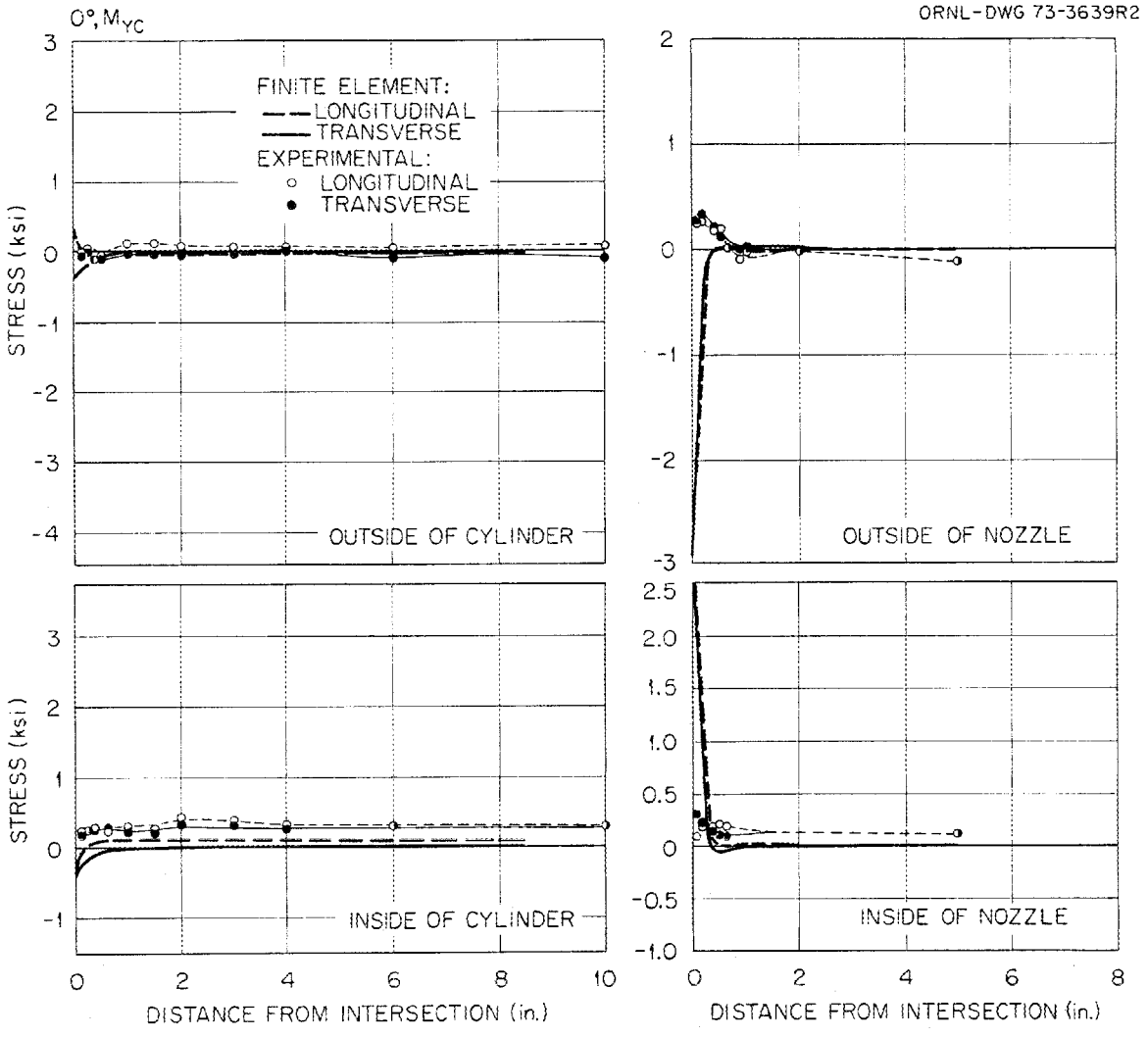

Fig. 65. Measured and predicted stress distributions at 0° for an out-of-plane moment of 40,000 in.-lb on the cylinder.

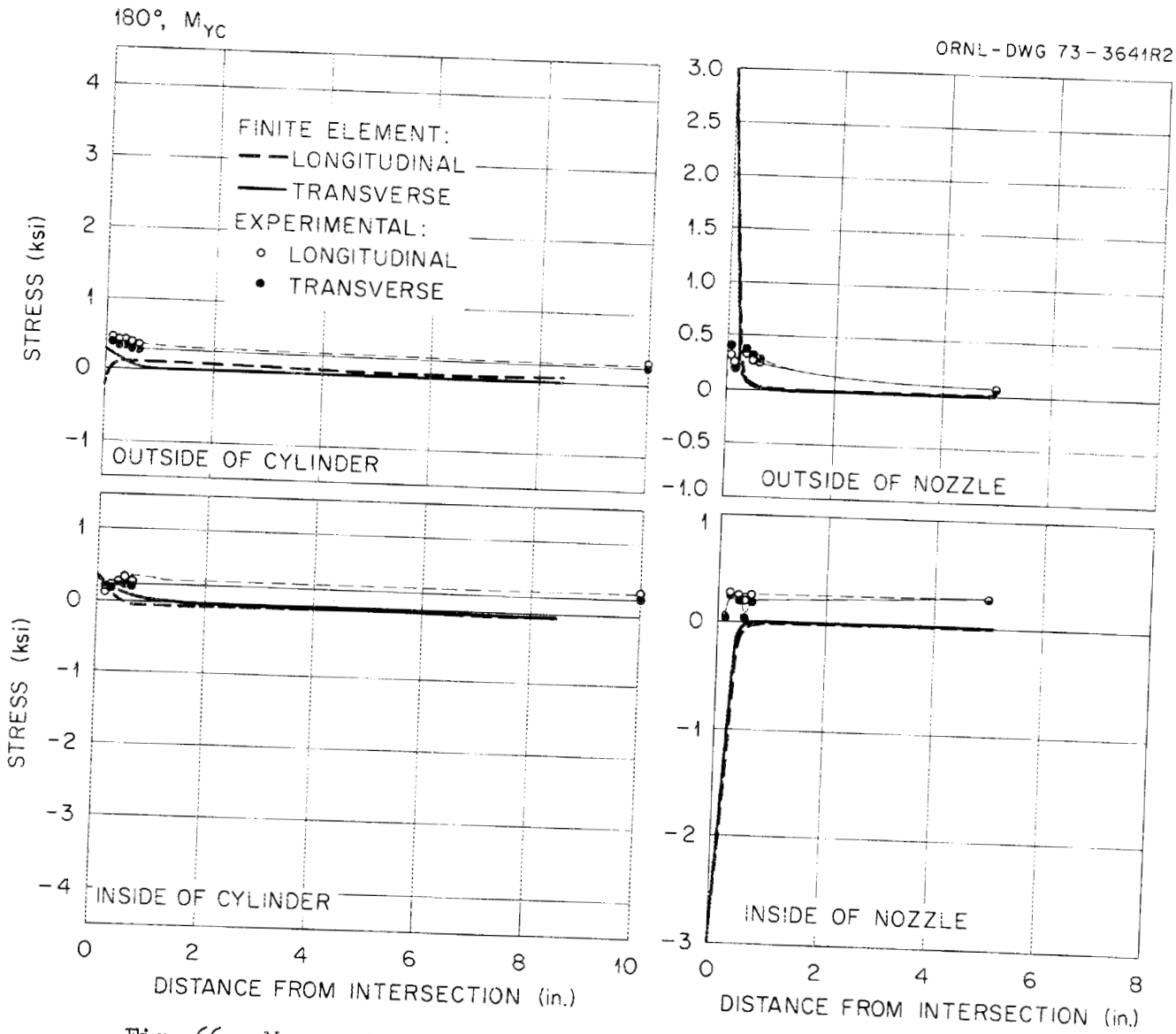

Fig. 66. Measured and predicted stress distributions at 180° for an out-of-plane moment of 40,000 in.-lb on the cylinder.

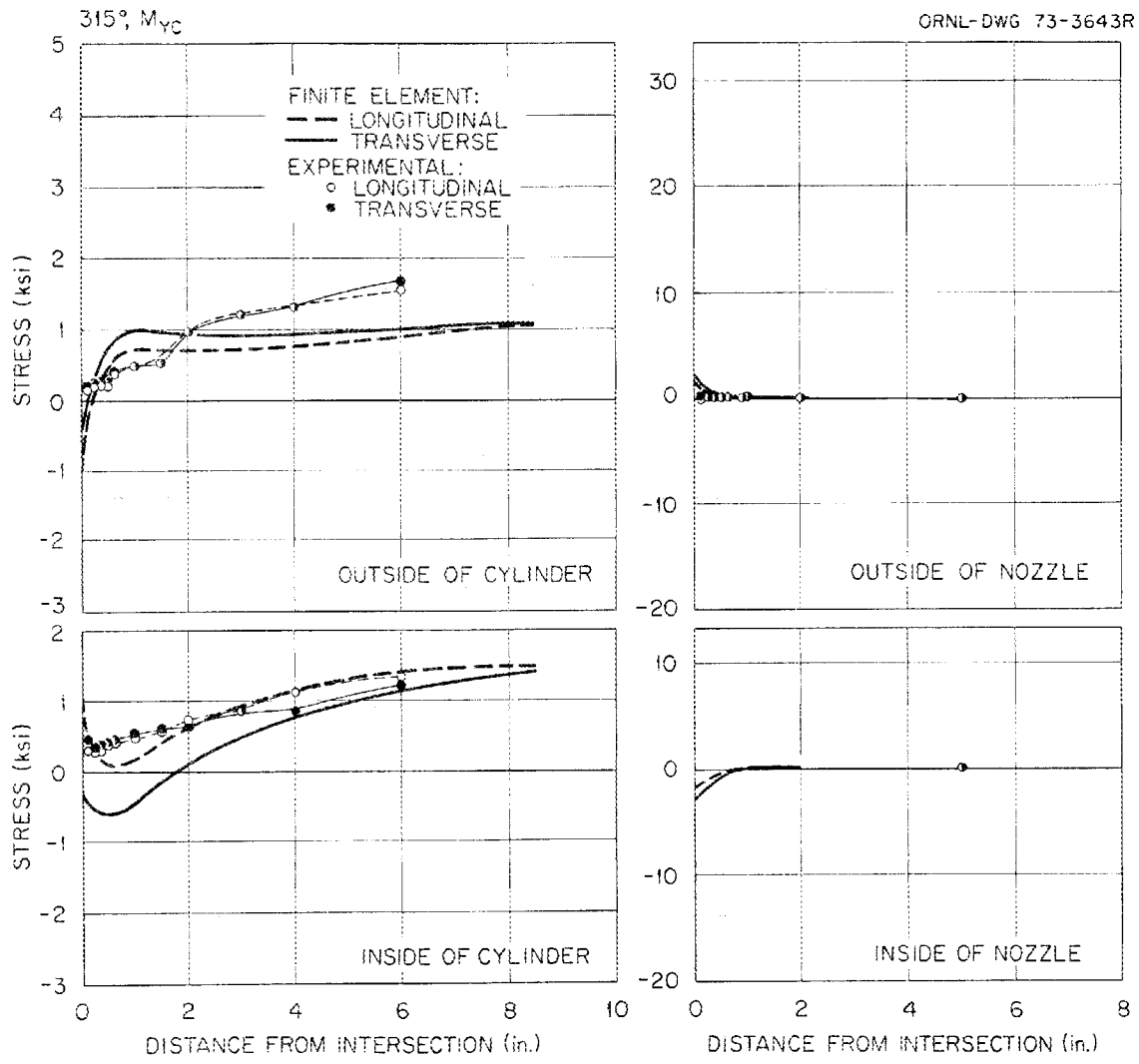

Fig. 67. Measured and predicted stress distributions at 315° for an out-of-plane moment of 40,000 in.-lb on the cylinder.

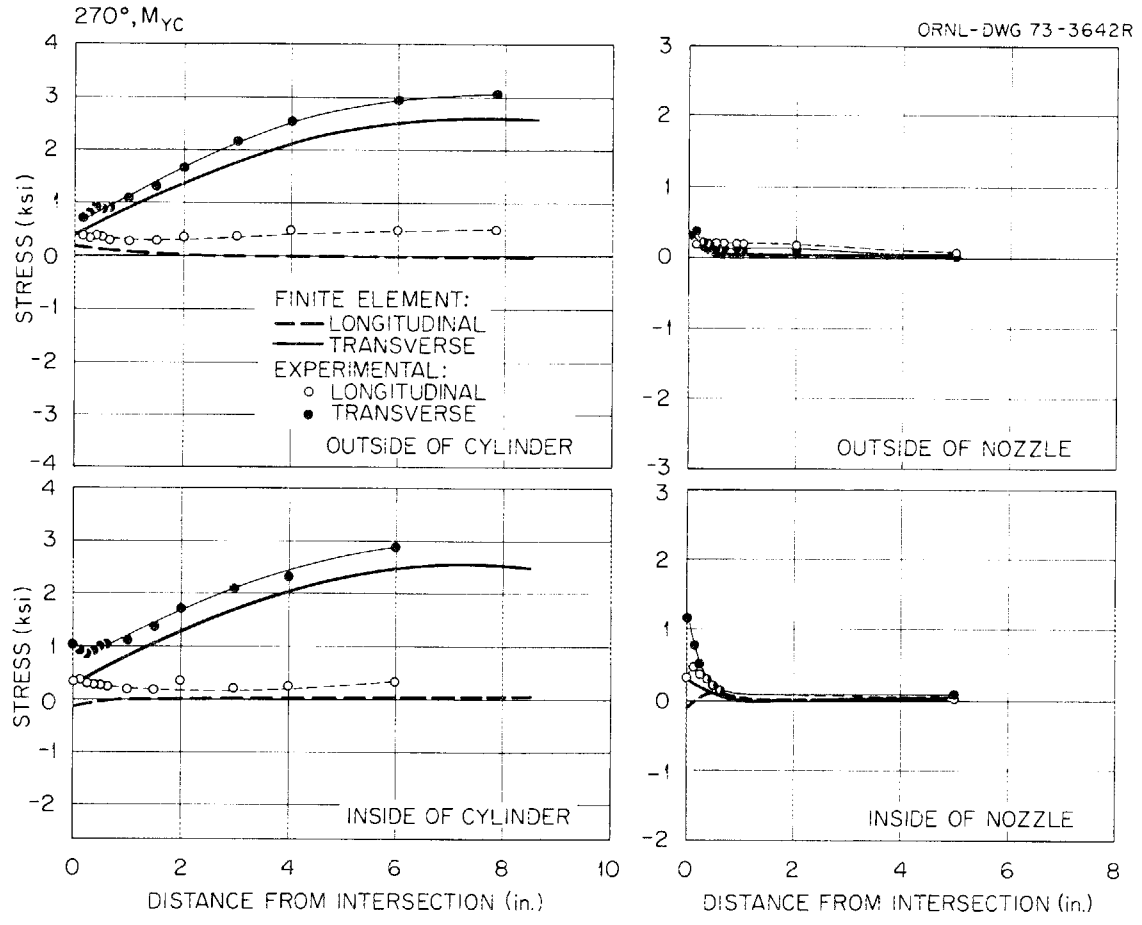

Fig. 68. Measured and predicted stress distributions at 270° for an out-of-plane moment of 40,000 in.-lb on the cylinder.

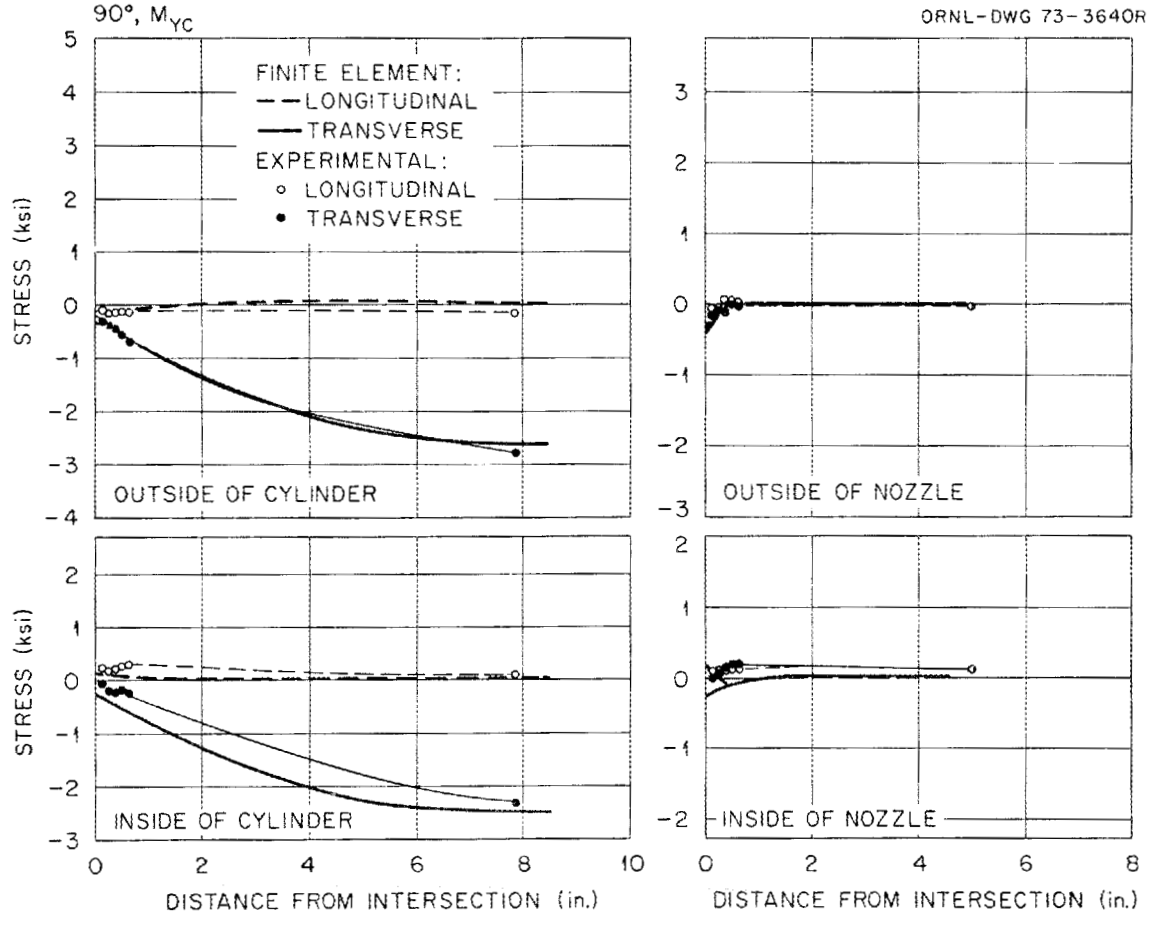

Fig. 69. Measured and predicted stress distributions at 90° for an out-of-plane moment of 40,000 in.-lb on the cylinder.

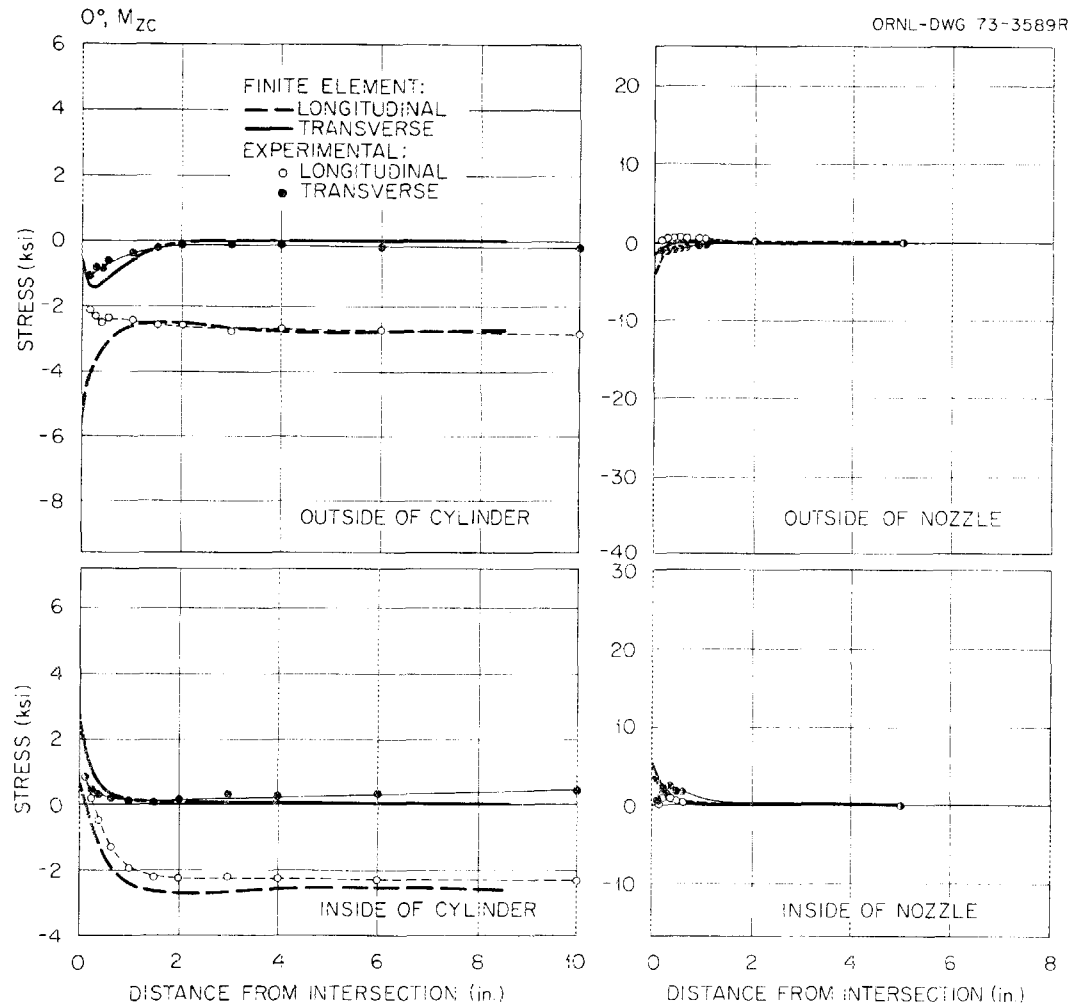

Fig. 70. Measured and predicted stress distributions at 0° for an in-plane moment of 40,000 in.-lb on the cylinder.

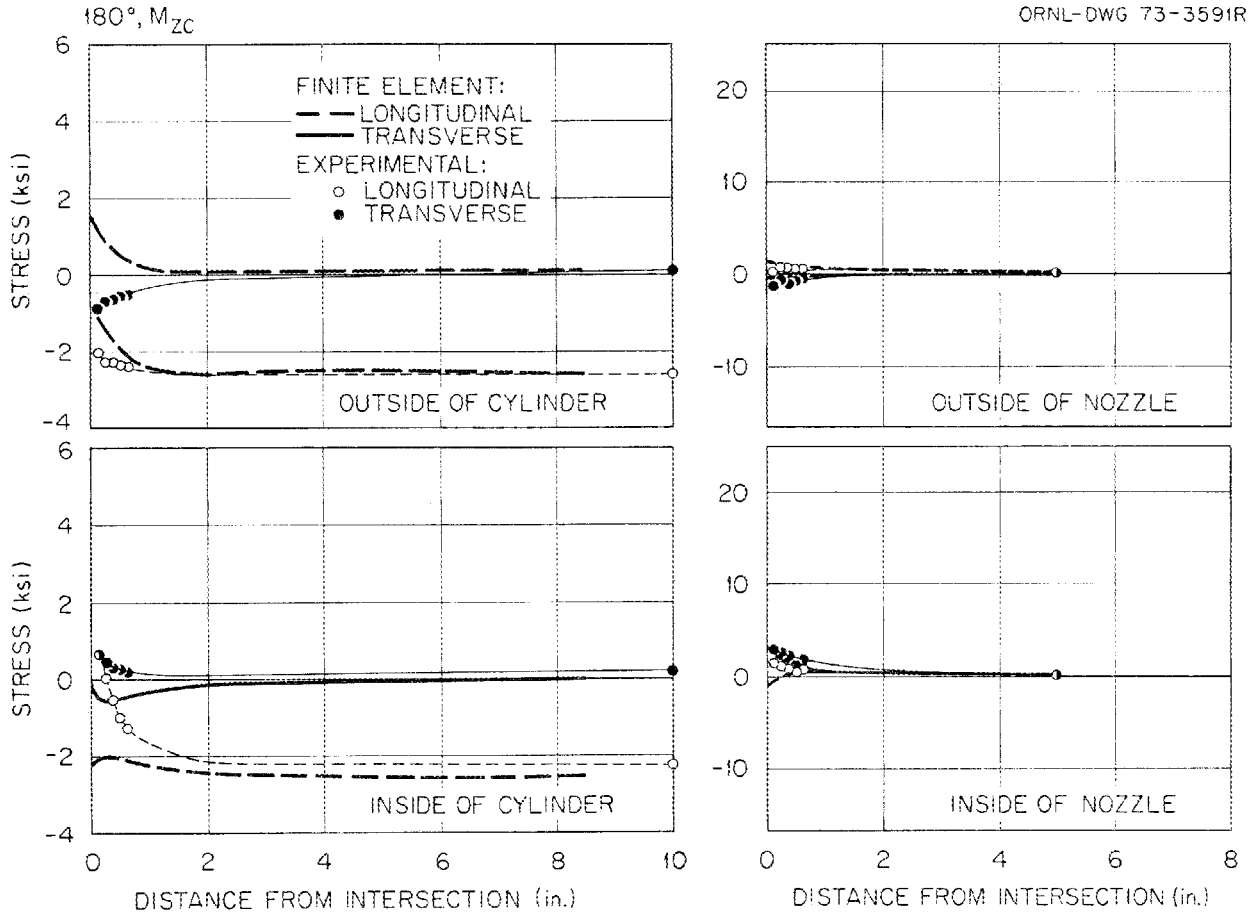

Fig. 71. Measured and predicted stress distributions at 180° for an in-plane moment of 40,000 in.-lb on the cylinder.

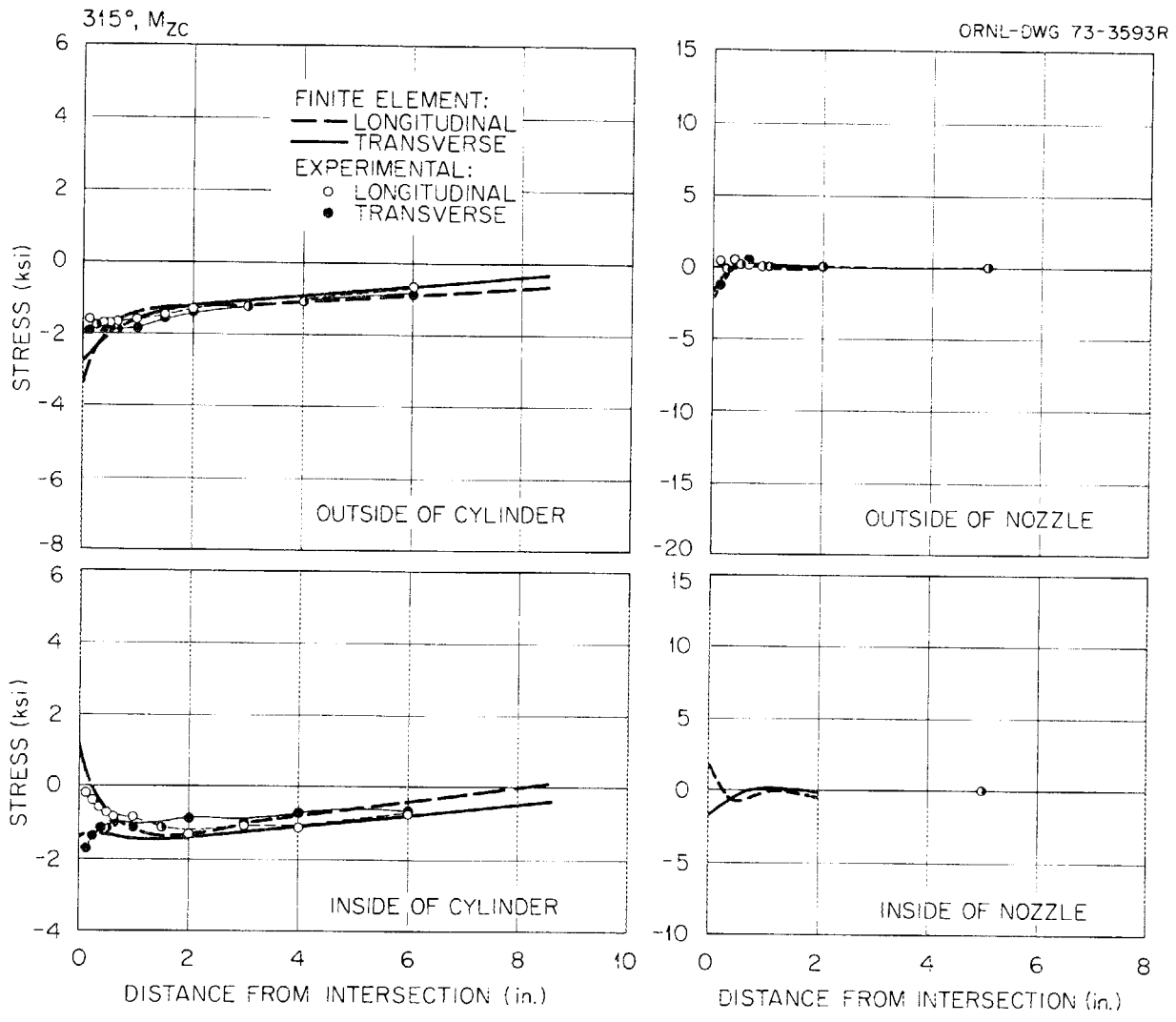

Fig. 72. Measured and predicted stress distributions at 315° for an in-plane moment of 40,000 in.-lb on the cylinder.

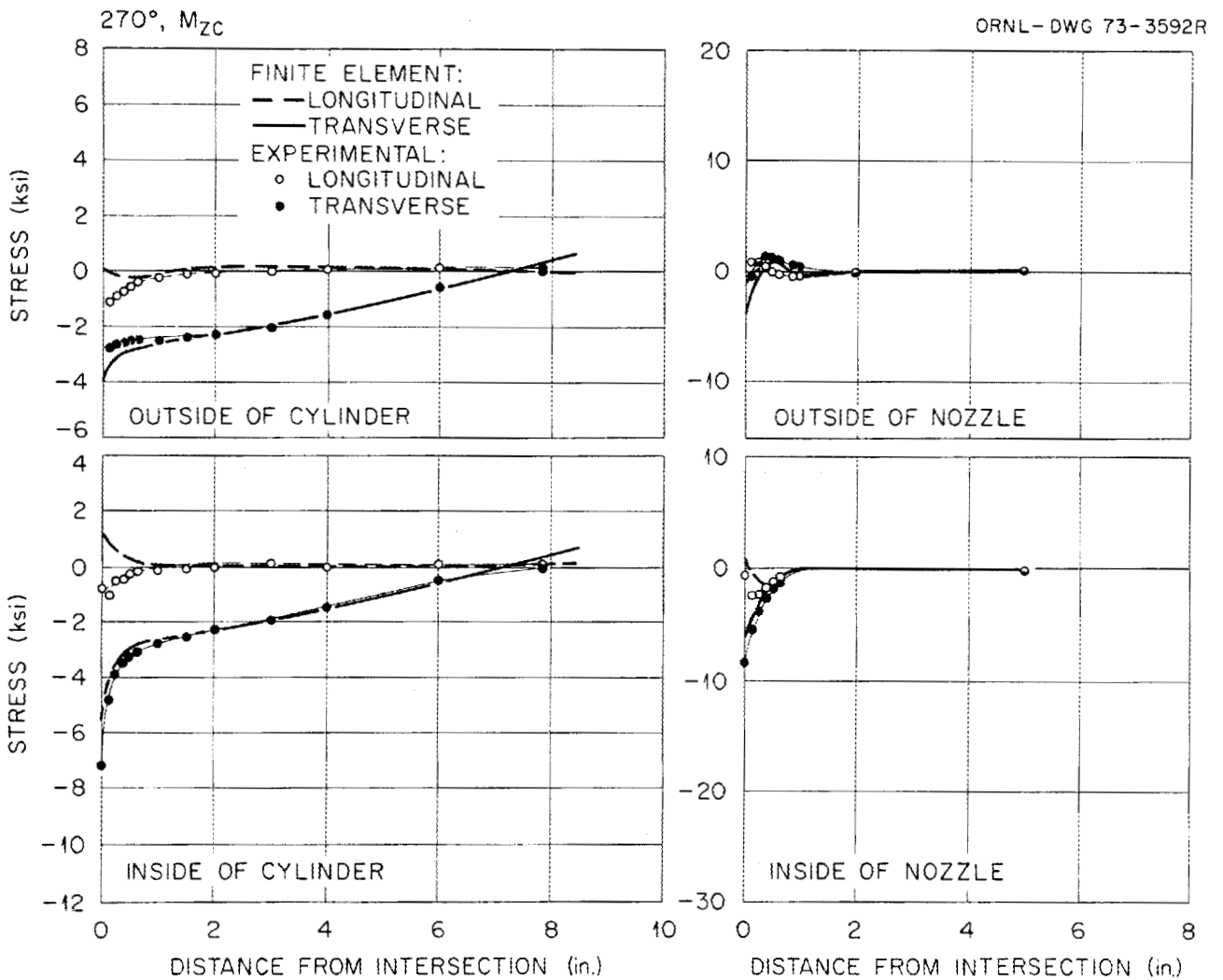

Fig. 73. Measured and predicted stress distributions at 270° for an in-plane moment loading of 40,000 in.-lb on the cylinder.

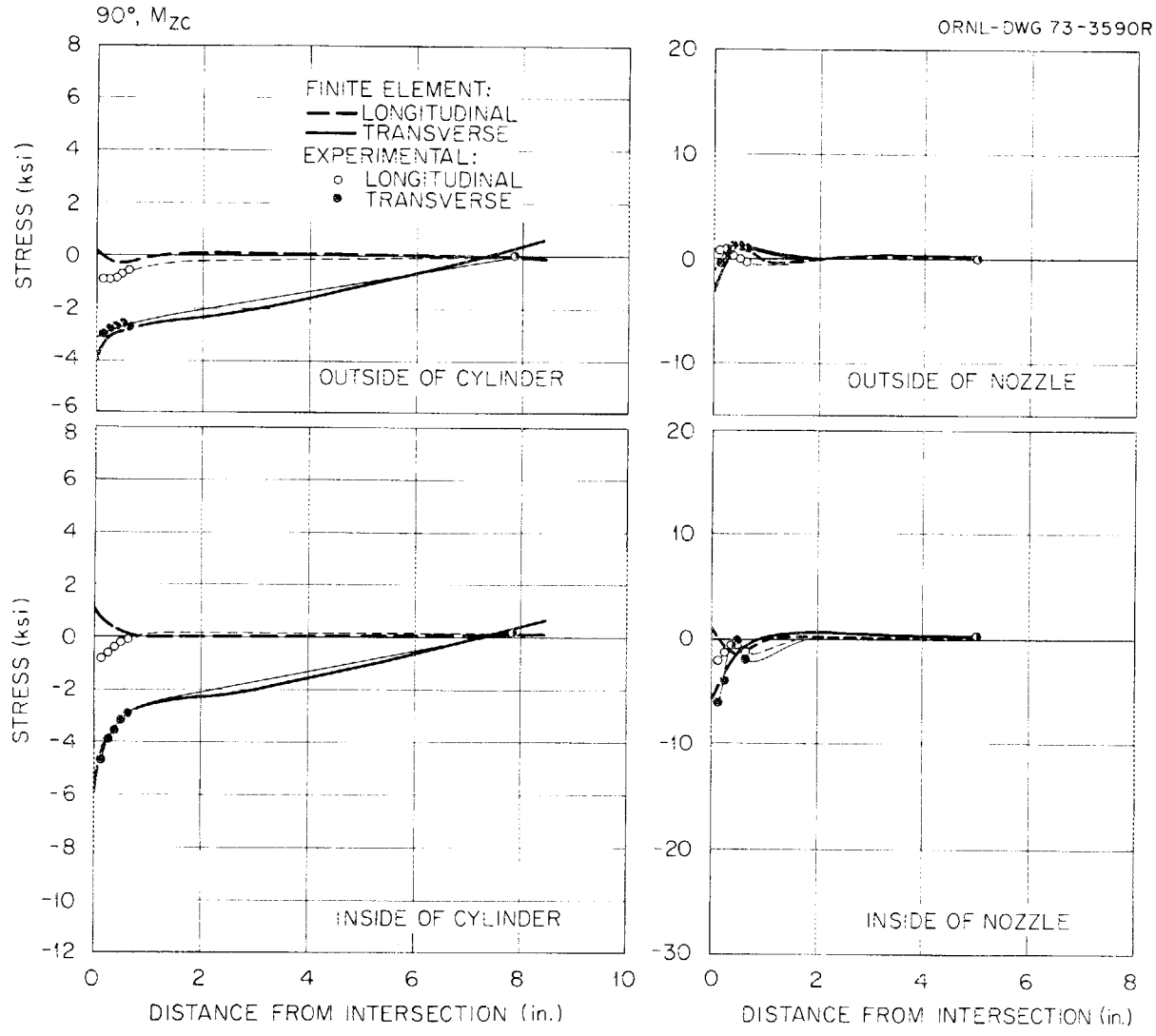

Fig. 74. Measured and predicted stress distributions at 90° for an in-plane moment of 40,000 in.-lb on the cylinder.

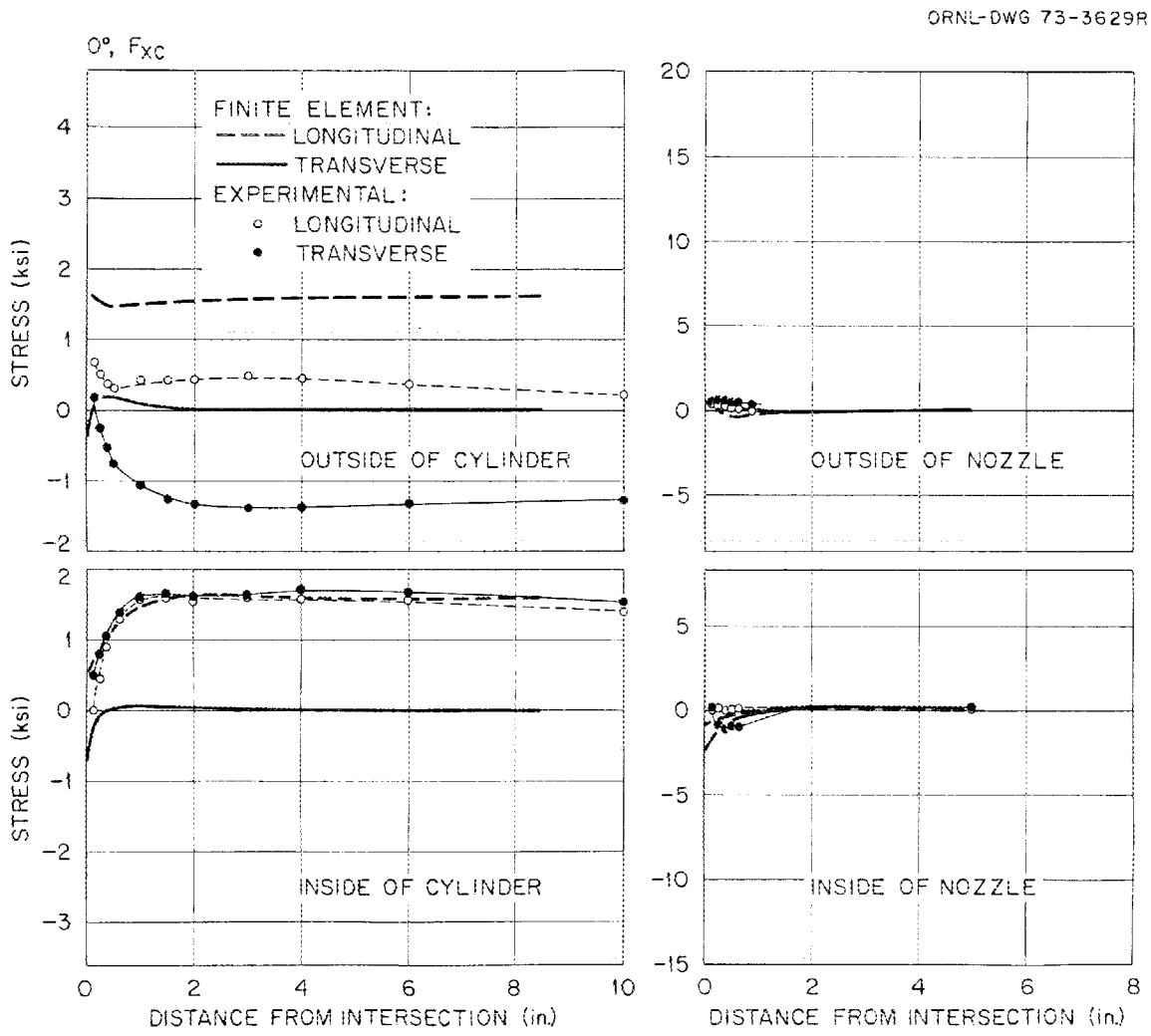

Fig. 75. Measured and predicted stress distributions at 0° for an axial force of 10,000 lb on the cylinder.

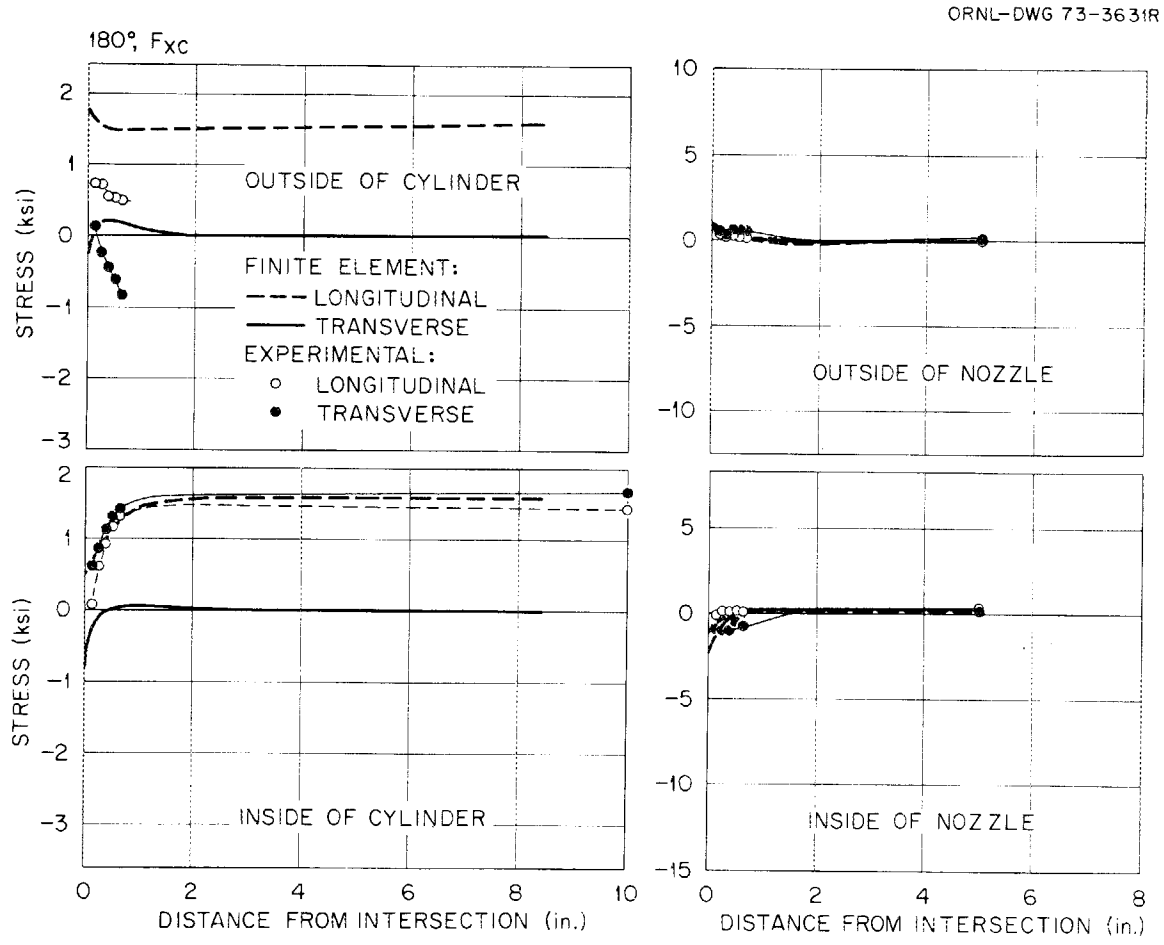

Fig. 76. Measured and predicted stress distributions at 180° for an axial force of 10,000 lb on the cylinder.

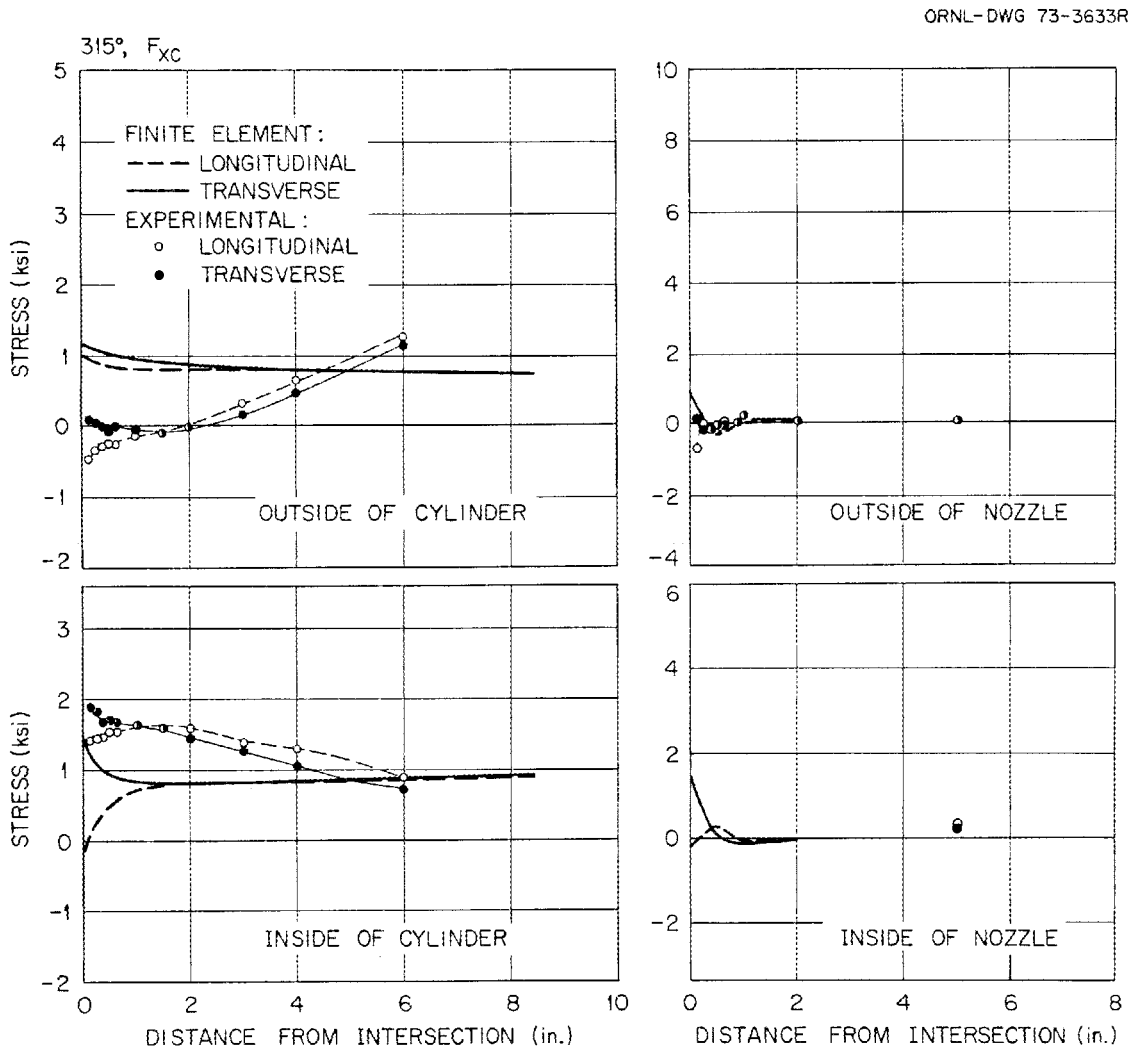

Fig. 77. Measured and predicted stress distributions at 315° for an axial force of 10,000 lb on the cylinder.

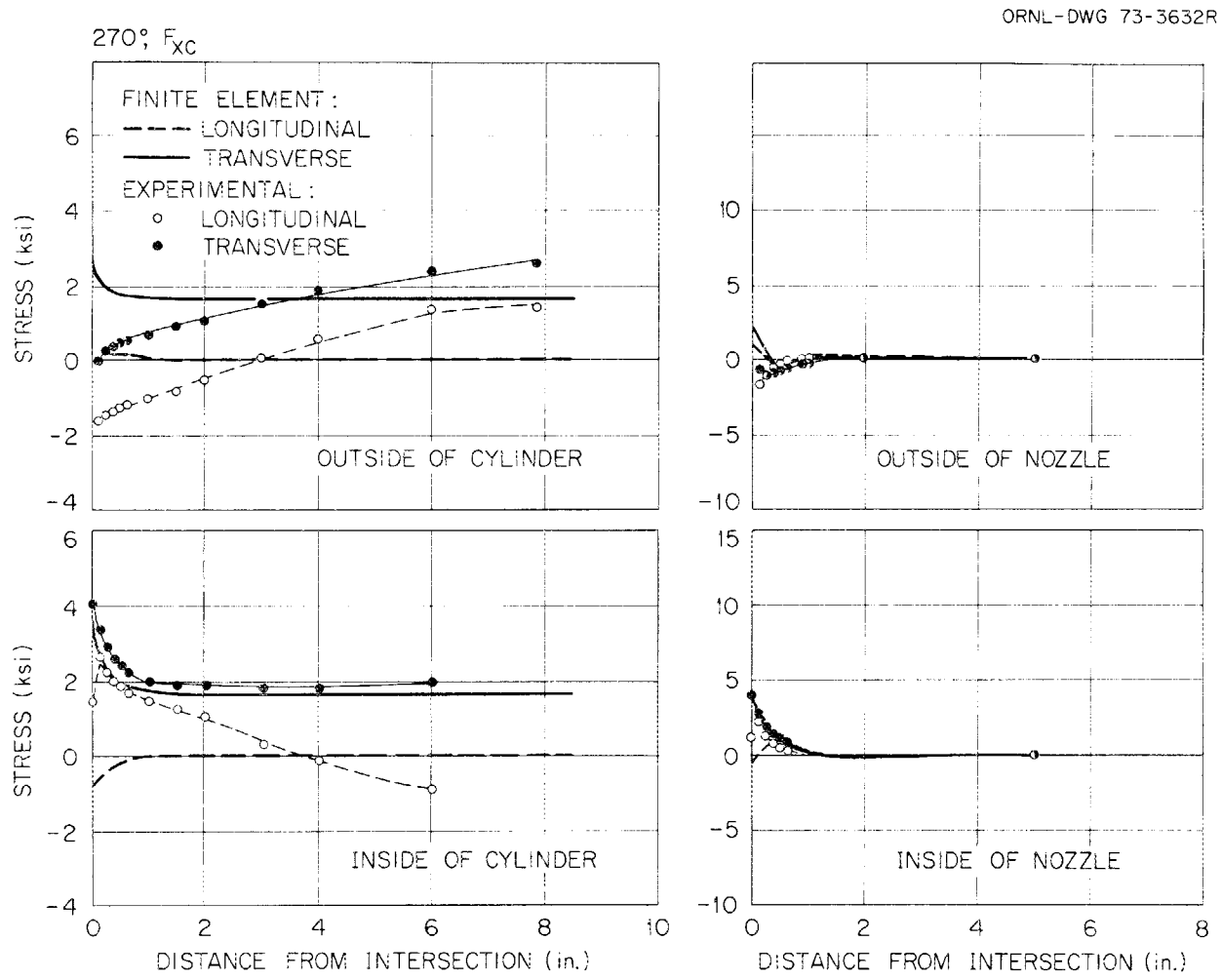

Fig. 78. Measured and predicted stress distributions at 270° for an axial force of 10,000 lb on the cylinder.

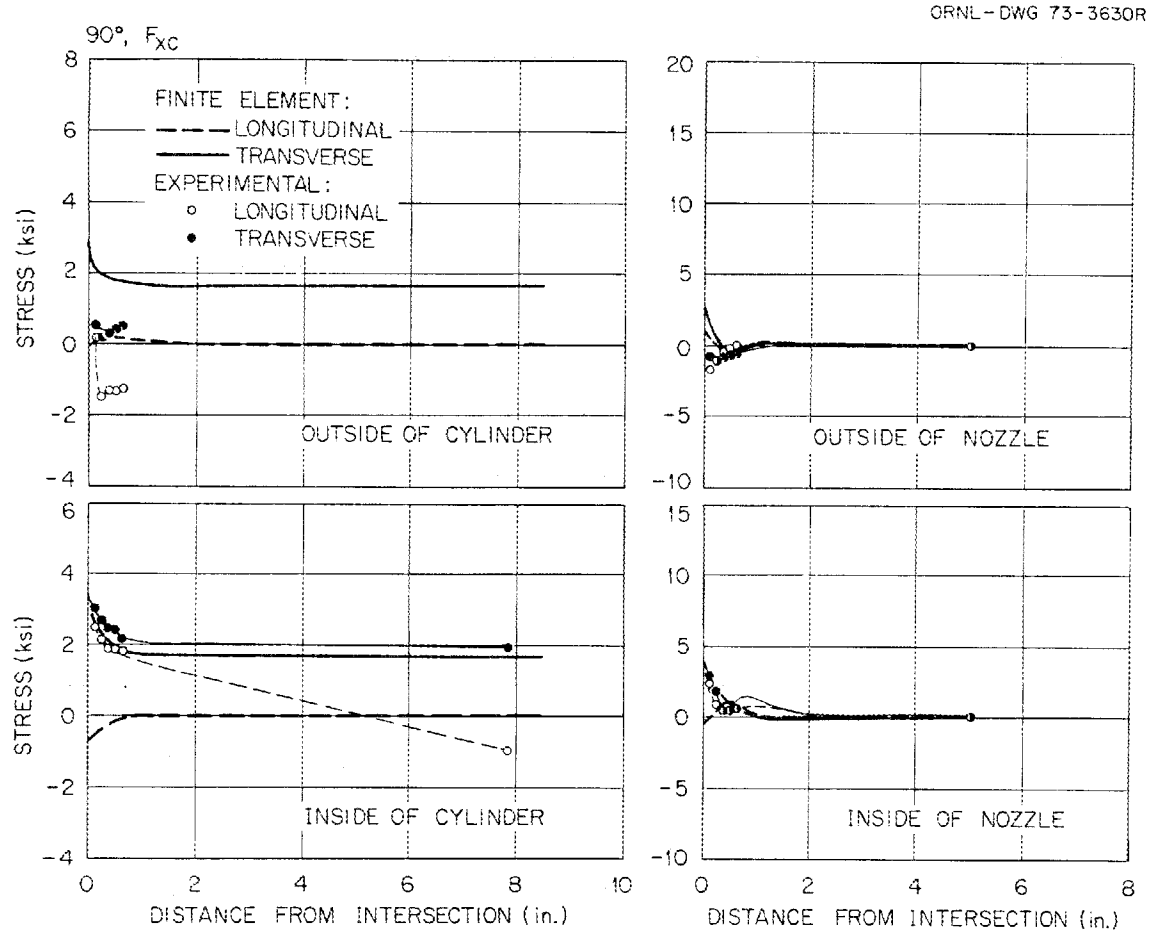

Fig. 79. Measured and predicted stress distributions at 90° for an axial force of 10,000 lb on the cylinder.

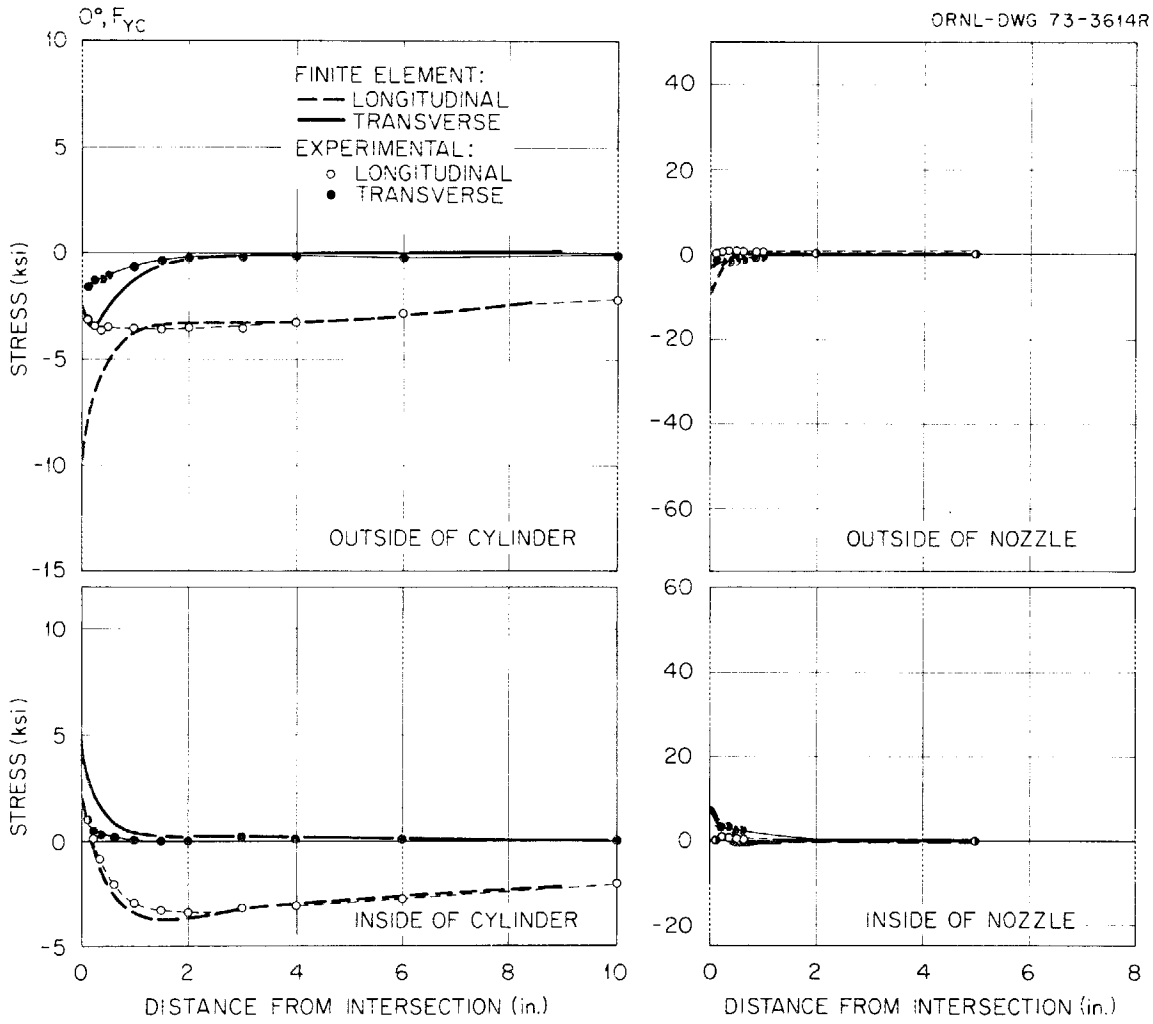

Fig. 80. Measured and predicted stress distributions at 0° for an in-plane force of 3000 lb on the cylinder.

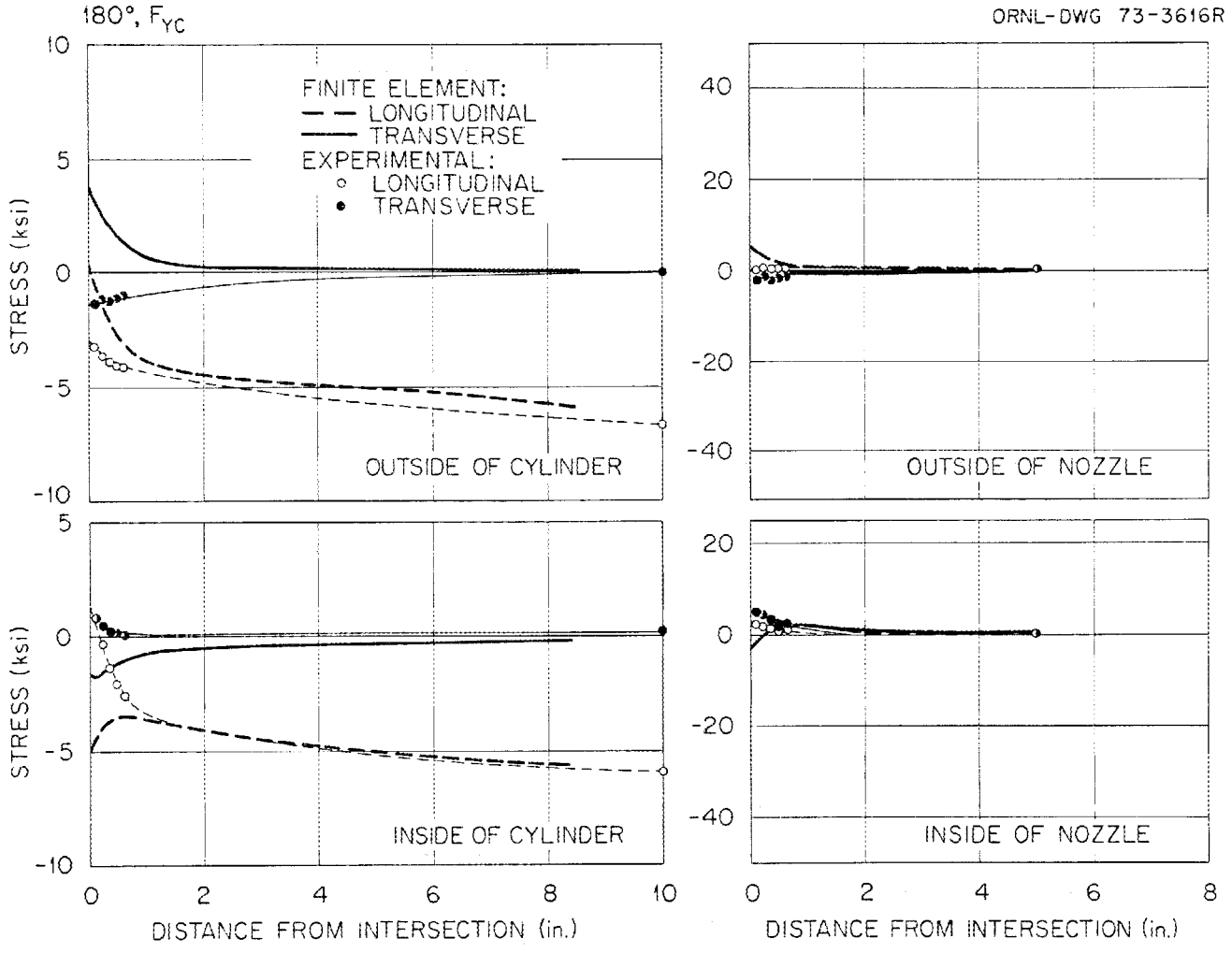

Fig. 81. Measured and predicted stress distributions at 180° for an in-plane force of 3000 lb on the cylinder.

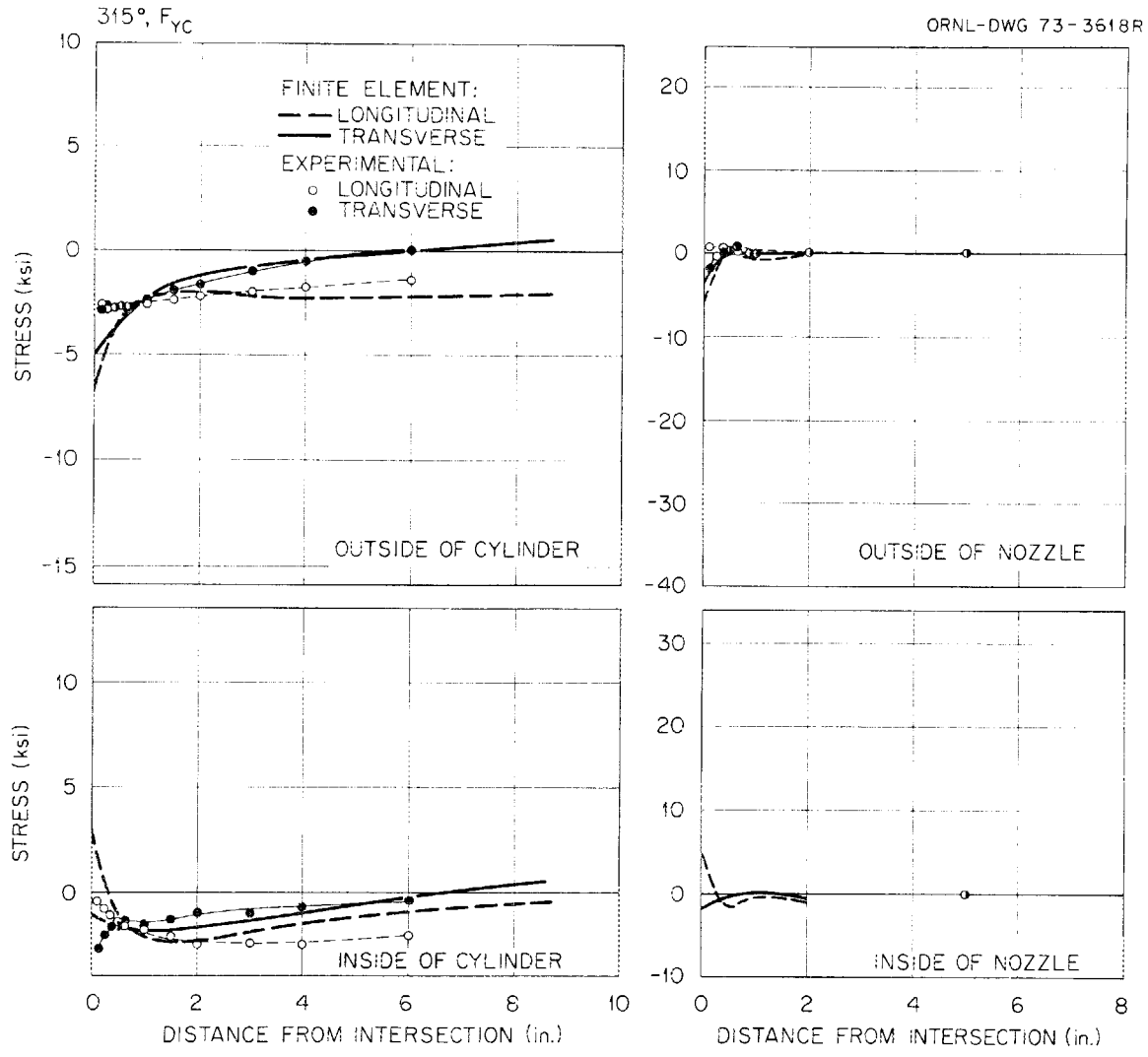

Fig. 82. Measured and predicted stress distributions at 315° for an in-plane force of 3000 lb on the cylinder.

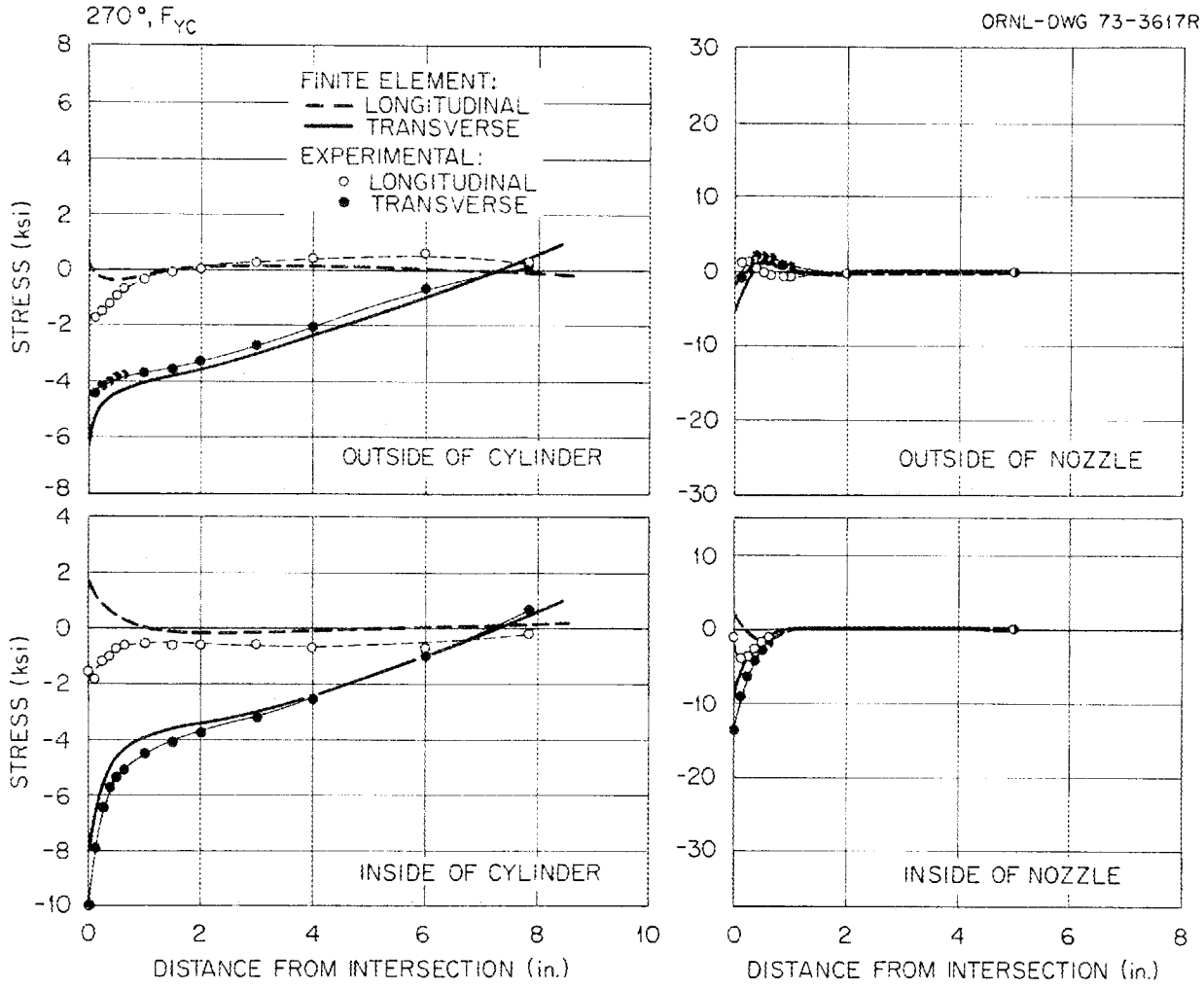

Fig. 83. Measured and predicted stress distributions at 270° for an in-plane force of 3000 lb on the cylinder.

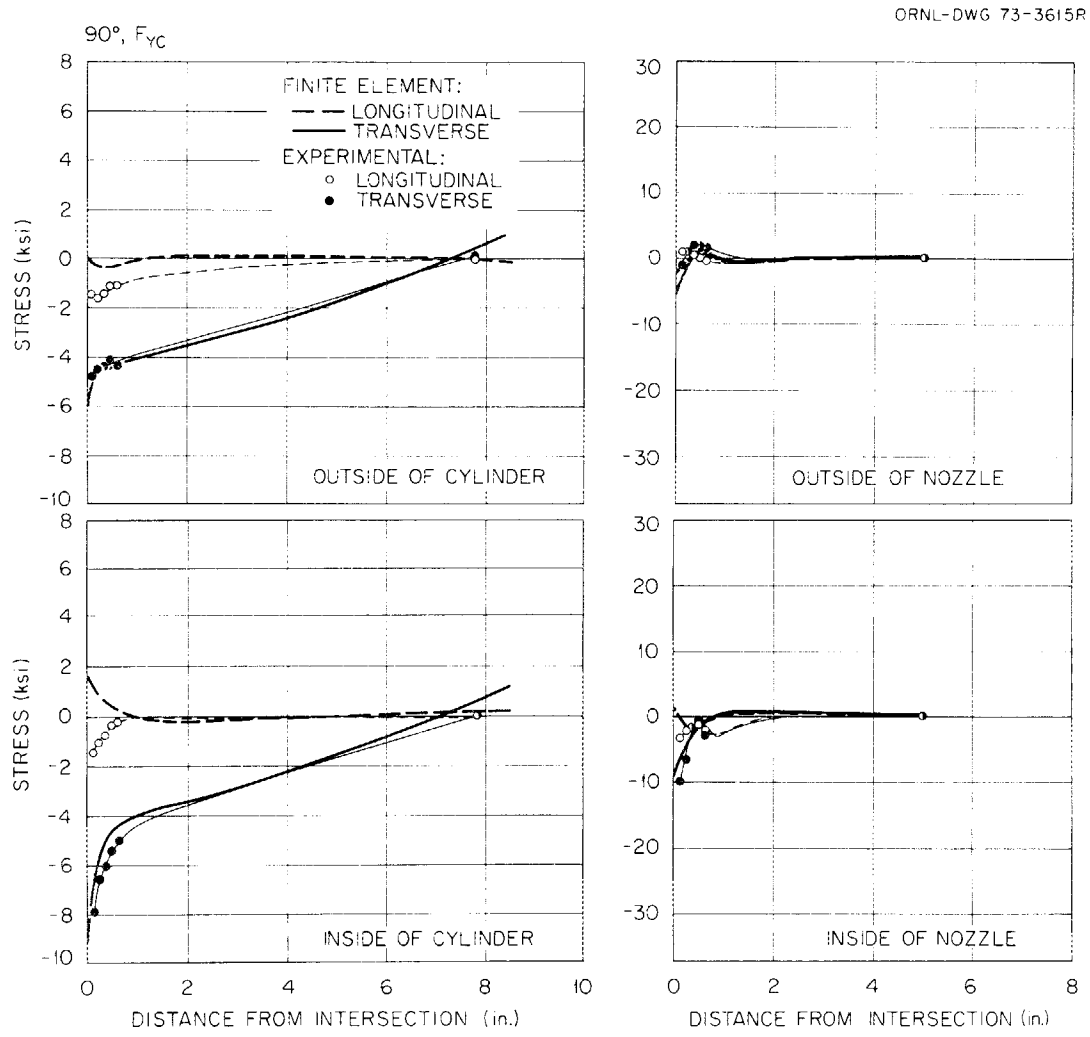

Fig. 84. Measured and predicted stress distributions at 90° for an in-plane force of 3000 lb on the cylinder.

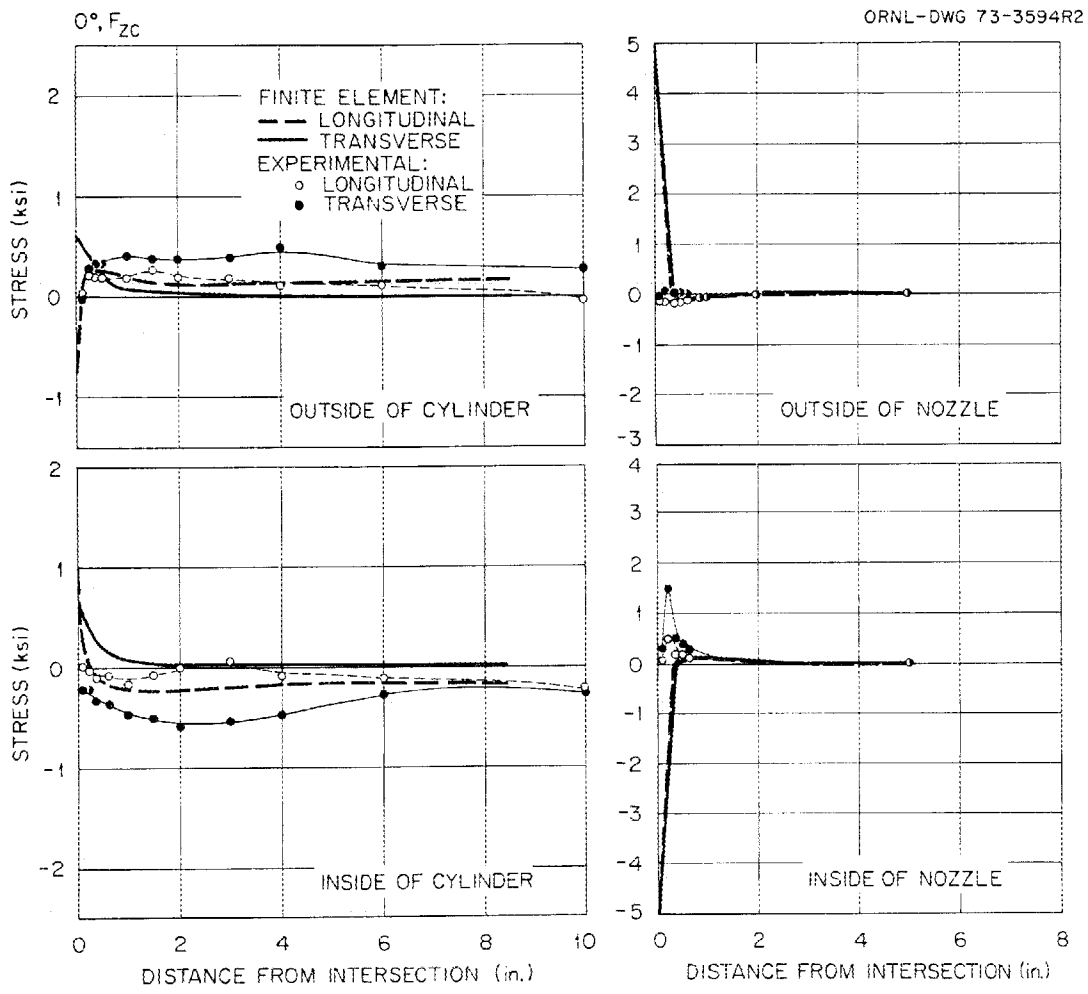

Fig. 85. Measured and predicted stress distributions at 0° for an out-of-plane force of 3000 lb on the cylinder.

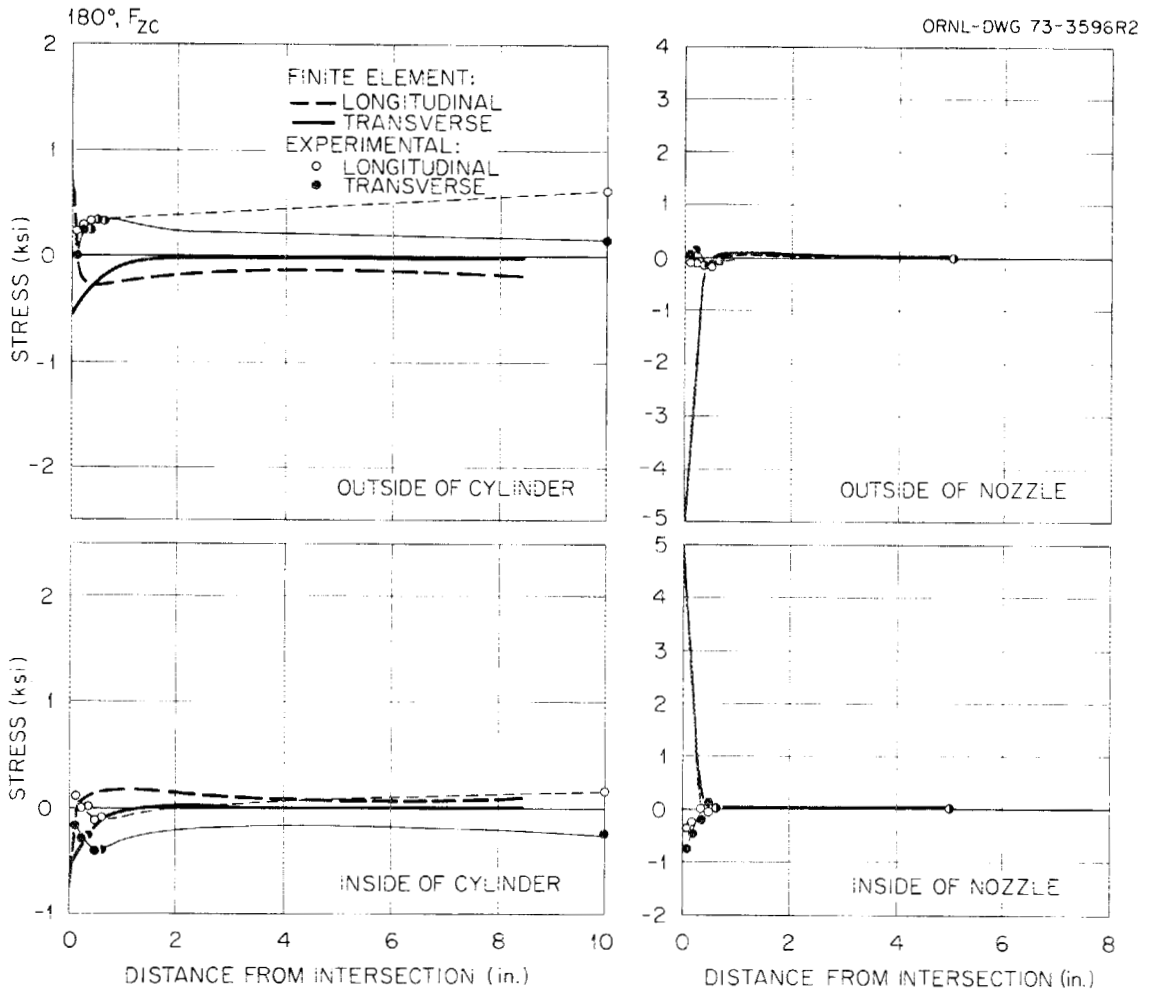

Fig. 86. Measured and predicted stress distributions at 180° for an out-of-plane force of 3000 lb on the cylinder.

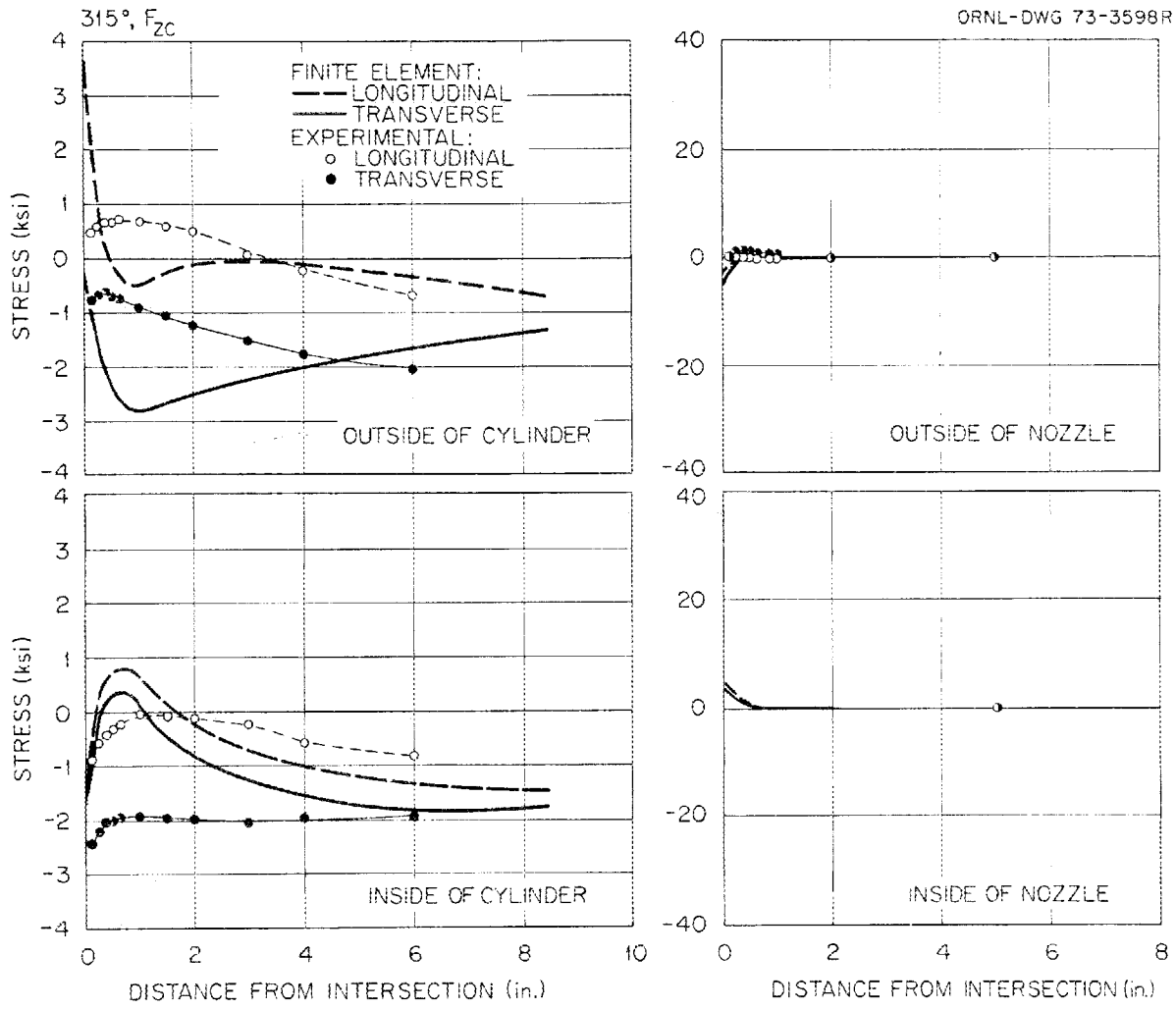

Fig. 87. Measured and predicted stress distributions at 315° for an out-of-plane force of 3000 lb on the cylinder.

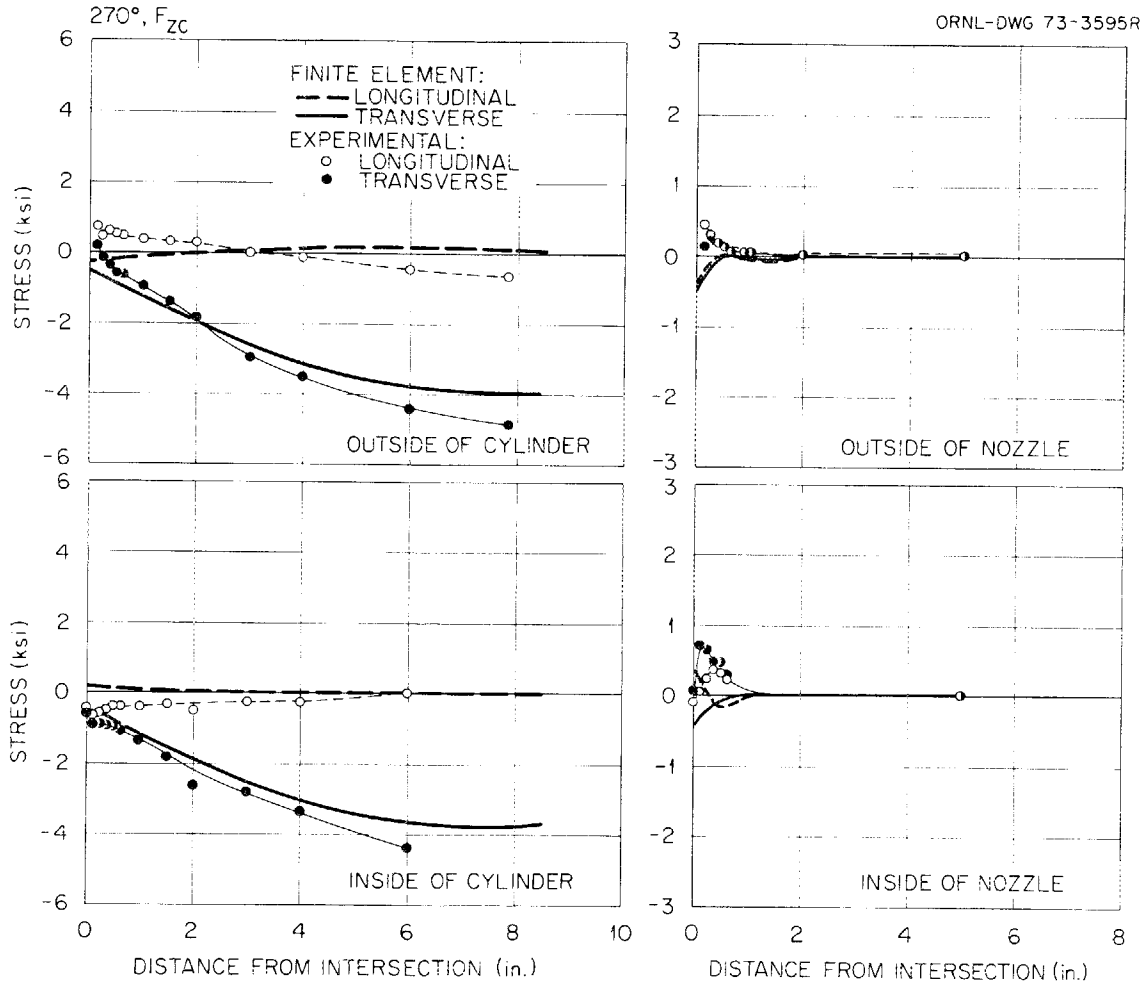

Fig. 88. Measured and predicted stress distributions at 270° for an out-of-plane force of 3000 lb on the cylinder.

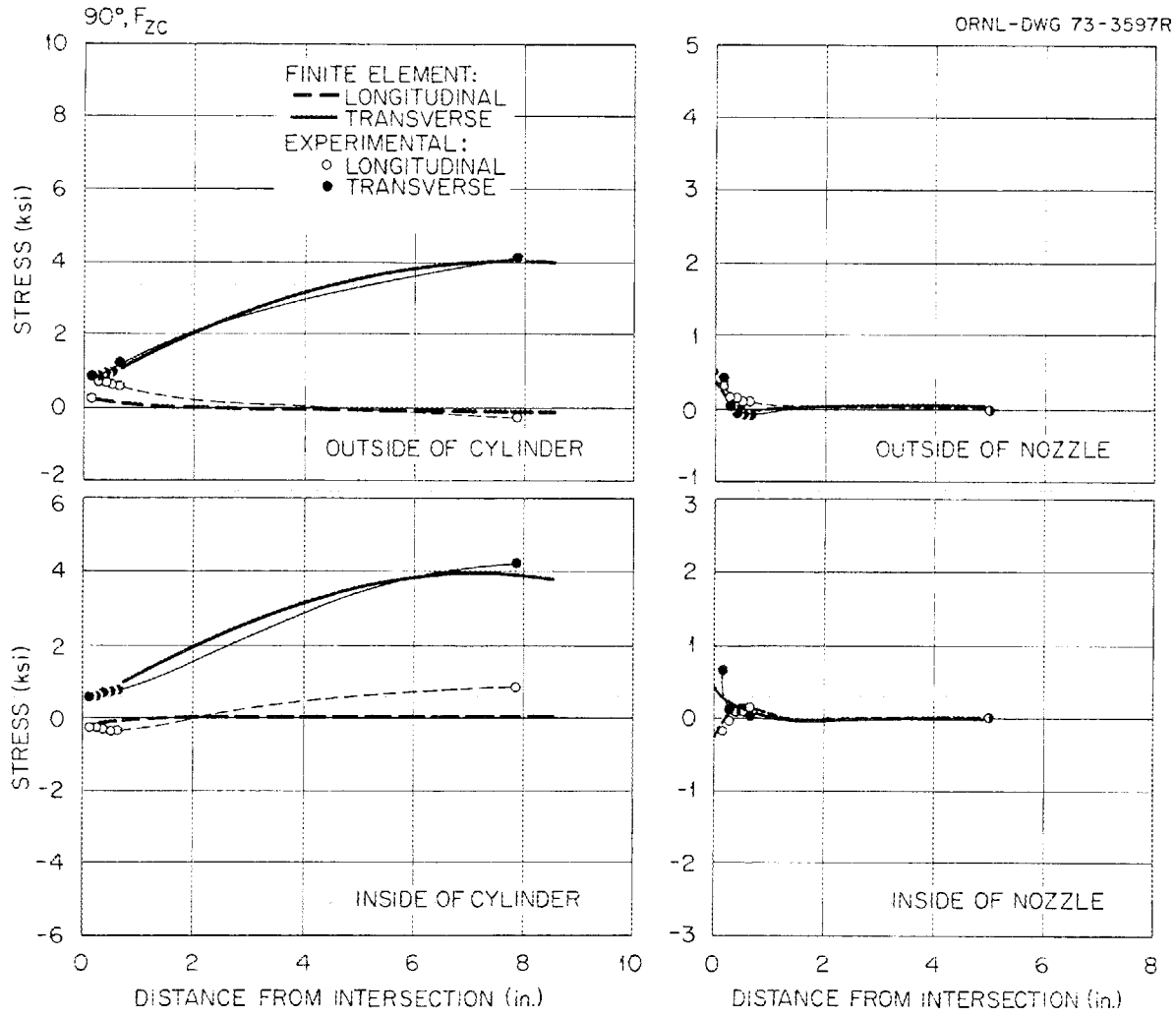

Fig. 89. Measured and predicted stress distributions at 90° for an out-of-plane force of 3000 lb on the cylinder.

5. CONCLUSIONS

Table 2 represents an attempt to summarize the principal findings of this study in terms of maximum principal stress ratios, locations of maximum principal stresses, and the relative overall agreement between theory and experiment for each loading case. The maximum stress ratios are based on the stresses, either measured or predicted, along the five lines of strain gages only and were determined by dividing the maximum absolute principal stress value by a nominal membrane stress value as previously described. The maximum experimental principal stresses were determined by extrapolating the experimentally determined stress distributions to peak stresses at the junction in all but two cases.

The relative overall agreement between the finite-element predictions and the experimental results is rated in the table as excellent, good, fair, or poor. These ratings are, of course, a matter of opinion, but an attempt was made to make an unbiased evaluation by basing them on both the overall qualitative agreement along the gage lines and on the quantitative agreement in areas where the stresses were relatively high.

Table 2 indicates that generally the experimentally determined maximum stress ratios and those based on finite-element predictions are in good agreement. Furthermore, the degree of agreement between the stress ratios generally correlates well with the relative ratings of the overall agreement between theory and experiment. Generally, the agreement was best for cases involving loadings on the nozzle; however, for the torsional moment on the nozzle, the agreement was poor qualitatively and quantitatively.

In all but two loading cases, the maximum experimental stress occurred at the junction of the nozzle and cylinder. One exception was the case of an out-of-plane moment, M_{YC}, on the cylinder, where the maximum occurred on the outside surface of the cylinder at approximately 90° (around at the side of the cylinder) along the transverse plane. The stresses on the inside surface of the cylinder were, however, almost as high as those on the outer surface. The other exception was the out-of-plane force, F_{ZC}, on the cylinder, where the maximum occurred on the outside surface of the cylinder at approximately 90° around on the transverse plane.

Table 2. Summary of maximum stress ratios and locations

Loading case	Experimentally determined maximum stress[a]		Theoretical maximum stress		Overall agreement between theory and experiment
	Stress ratio[b]	Location[c]	Stress ratio[b]	Location[c]	
Internal pressure	2.5	Inside nozzle, 0°	2.3	Outside nozzle, 0°	Good
M_{XN}, out-of-plane moment on nozzle	5.0	Outside cylinder, 270°	7.3	Outside nozzle, 270°	Excellent
M_{YN}, torsional moment on nozzle	1.7	Outside nozzle, 0°	0.6	Inside nozzle, 0°	Poor
M_{ZN}, in-plane moment on nozzle	3.7	Outside cylinder, 0°	5.6	Outside nozzle, 0°	Excellent
F_{XN}, in-plane force on nozzle	4.4	Outside cylinder, 0°	6.2	Outside nozzle, 0°	Excellent
F_{YN}, axial force on nozzle	17.2	Outside cylinder, 270°	19.4	Outside nozzle, 270°	Good
F_{ZN}, out-of-plane force on nozzle	6.6	Outside cylinder, 270°	8.1	Outside nozzle, 270°	Good
M_{XC}, torsional moment on cylinder	2.5	Inside cylinder, 315°	5.6	Outside nozzle, 180°	Poor
M_{YC}, out-of-plane moment on cylinder	1.2	Outside cylinder,[d] 270°	1.1	Outside nozzle, 0°	Fair
M_{ZC}, in-plane moment on cylinder	3.2	Inside nozzle, 270°	2.5	Inside nozzle, 270°	Fair
F_{XC}, axial force on cylinder	2.5	Inside cylinder, 270°	2.5	Inside nozzle, 270°	Poor
F_{YC}, in-plane force on cylinder	3.5	Inside nozzle, 270°	2.6	Inside nozzle, 270°	Good
F_{ZC}, out-of-plane force on cylinder	1.3	Outside cylinder,[d] 270°	1.5	Outside nozzle, 315°	Fair

[a]Based on extrapolation of experimental distributions to a maximum at the junction.

[b]Ratio of maximum absolute principal stress value to nominal stress value.

[c]Maximums all occurred at the junction.

[d]Maximum not at junction; at approximately 90° around on the transverse plane.

In 8 of the 13 cases, the maximum experimental values occurred in the transverse plane of symmetry, while 4 cases produced maximum experimental stresses in the longitudinal plane of symmetry. The torsional moment on the cylinder produced maximum experimental stresses at a point intermediate to the two planes of symmetry. In 6 out of 13 cases the theoretical values occurred in the transverse plane, while 6 occurred in the longitudinal plane. The out-of-plane force on the cylinder produced maximum theoretical stresses at a point intermediate to the two planes of symmetry.

Finally, it should be pointed out that, as would be expected, the out-of-plane moment and force loadings on the nozzle produced quite similar results, as did the in-plane moment and force loadings. The stress distributions were very similar for each pair, and the maximum stress ratios were very close.

In conclusion, the comparison of these finite-element predictions with the experimental results shows reasonably good agreement. It is felt that this analysis would be satisfactory for most engineering purposes.

It should be pointed out that the nozzle wall is thick ($d_o/t = 7.68$) and well outside the range of thin shells; therefore, a thin-shell analysis cannot be expected to give accurate results in all cases, particularly close to the junction on the nozzle. However, the results are satisfactory. The results would be improved by the inclusion of the sixth degree of freedom, at least in the junction region.

ACKNOWLEDGMENTS

The planning and execution of the analytical and experimental study reported here would not have been possible without the assistance and cooperation of many individuals, both within ORNL and outside. The authors are deeply indebted to those people for their contributions.

Special thanks are due J. P. Rudd for the instrumentation of the model, which was a very painstaking task. The finite-element computer program used in the analysis was developed at the University of California, Berkeley.

REFERENCES

1. J. M. Corum and W. L. Greenstreet, "Experimental Elastic Stress Analyses of Cylinder-to-Cylinder Shell Models and Comparisons with Theoretical Predictions," paper No. G2/5, First International Conference on Structural Mechanics in Reactor Technology, Berlin, Sept. 20–24, 1971.

2. J. M. Corum et al., Theoretical and Experimental Stress Analysis of ORNL Thin-Shell Cylinder-to-Cylinder Model No. 1, ORNL-4553 (October 1972).

3. R. C. Gwaltney, J. W. Bryson, and S. E. Bolt, Theoretical and Experimental Stress Analysis of ORNL Thin-Shell Cylinder-to-Cylinder Model 4, ORNL-5019 (in press).

4. D. E. Hardenbergh, S. Y. Zamrik, and A. J. Edmondson, "Experimental Investigation of Stresses in Nozzles in Cylindrical Pressure Vessels," Welding Research Council Bulletin 89, July 1963.

5. D. E. Hardenbergh and S. Y. Zamrik, "Effects of External Loadings on Large Outlets in a Cylindrical Pressure Vessel," Welding Research Council Bulletin 96, May 1964.

6. W. F. Riley, Experimental Determination of Stress Distributions in Thin Walled Cylindrical and Spherical Pressure Vessels with Circular Nozzles, IIT Research Institute Report M6053 (March 1965).

7. C. E. Taylor and N. C. Lind, "Photoelastic Study of the Stresses near Openings in Pressure Vessels," Welding Research Council Bulletin 113, April 1966.

8. M. M. Leven, "Photoelastic Determination of Stresses in Reinforced Openings in Pressure Vessels," Welding Research Council Bulletin 113, April 1966.

9. Ojars Greste, Finite Element Analysis of Tubular K Joints, UCSESM 70-11, University of California, Berkeley (June 1970).

10. W. Reidelbach, "The State of Stress at the Perpendicular Intersection of Two Right Circular Tubes," Ingenieur-Archiv. 30(5), 293–316 (1961).

11. A. C. Eringen, A. K. Naghdi, and C. C. Thiel, "State of Stress in a Circular Cylindrical Shell with a Circular Hole," Welding Research Council Bulletin 102, January 1965.

12. A. K. Naghdi and A. C. Eringen, "Stress Distribution in a Circular Cylindrical Shell with a Circular Cut-Out," Ingenieur-Archiv. 34(3), 161–72 (1965).

13. A. C. Eringen and E. S. Suhubi, "Stress Distribution at Two Normally Intersecting Shells," Nucl. Struct. Eng. 2(3), 253–70 (1965).

14. A. C. Eringen et al., "Stress Concentrations in Two Normally Intersecting Cylindrical Shells Subject to Internal Pressure," Welding Research Council Bulletin 139, April 1969.

15. J. W. Hansberry and N. Jones, "A Theoretical Study of the Elastic Behavior of Two Normally Intersecting Cylindrical Shells," Trans. ASME, J. Eng. Ind. 91B(3), 563–72 (1969).

16. R. F. Maye and A. C. Eringen, "Further Analysis of Two Normally Intersecting Cylindrical Shells Subjected to Internal Pressure," Nucl. Eng. Des. 12(3), 457–74 (1970).

17. J. W. Hansberry and N. Jones, "Elastic Stresses Due to Axial Loads on a Nozzle which Intersects a Cylindrical Shell," Second International Conference on Pressure Vessel Technology, Part 1, Design and Analysis, pp. 129–54, October 1973.

18. P. P. Bijlaard, R. J. Dohrmann, and I. C. Wang, "Stresses in Junction of Nozzle to Cylinder Pressure Vessel for Equal Diameter of Vessel and Nozzle," Nucl. Eng. Des. 5(3), 349–66 (1967).

19. K. C. Pan and R. E. Beckett, "Stress and Displacement Analysis of a Shell Intersection," Trans. ASME, J. Eng. Ind. 92B(3), 303–8 (May 1970).

20. L. R. Herrmann and D. M. Campbell, "A Finite-Element Analysis for Thin Shells," AIAA J. 6(10), 1842–47 (1968).

21. N. Prince and Y. R. Rashid, "Structural Analysis of Shell Intersections," presented at First International Conference on Pressure Vessels and Piping, Sept. 29–Oct. 2, 1969, Delft, The Netherlands.

22. C. P. Johnson, The Analysis of Thin Shells by a Finite Element Procedure, Report 67-22, Department of Civil Engineering, University of California, Berkeley (September 1967).

23. C. P. Johnson and P. G. Smith, A Computer Program for the Analysis of Thin Shells, Report 69-5, Department of Civil Engineering, University of California, Berkeley (August 1967).

24. Ojars Greste, A Computer Program for the Analysis of Tubular K Joints, Report 69-19, Department of Civil Engineering, University of California, Berkeley (November 1969).

25. R. W. Clough and J. L. Tocher, "Finite Element Stiffness Matrices for the Analysis of Plate Bending," Proceedings of Conference on Matrix Methods in Structural Mechanics, AFFDL-TR-66-80, Wright-Patterson Air Force Base (November 1966).

26. R. Bailey and R. Hicks, "Localized Loads Applied to a Spherical Pressure Vessel Through a Cylindrical Insert," J. Mech. Eng. Sci. 2(4), 302 (1964).

Appendix

TABULATION OF EXPERIMENTAL DATA

For the benefit of the reader who would like to compare these experimental data with his own analysis techniques, the data on which the various plots in this report were based are given in Tables A.1 through A.13. Data are tabulated for each loading case for each operable rosette. These data were obtained from the several sets of data taken in each case by the procedures described in Sect. 2.4.

The rosette listings are grouped according to gage lines. For each rosette, the three strain readings are listed first, followed by the normal stress transverse (perpendicular) to the gage line, the normal stress longitudinal (parallel) to the gage line, the shear stress (referred to the gage line as a coordinate axis), and the maximum and minimum principal stresses. The strains are given in microinches per inch, and the stresses are in pounds per square inch.

The nomenclature used to identify and locate each rosette can be explained by considering the following sample designation:

I 180 N-E ,

where the letter I means that the rosette is located on the inner surface of nozzle or cylinder, O denotes an outside rosette, the number 180 indicates that the rosette is located on the 180° gage line (see Fig. 3 or Fig. 4 for the gage line designations). The letter N indicates that the rosette is on the nozzle; C designates a rosette on the cylinder; and E designates the location of the rosette along the gage line according to the following convention:

Rosette designation	Distance from nozzle-cylinder junction (see Fig. 3) (in.)
A	≈0
B	1/8
C	1/4
D	3/8
E	1/2
F	5/8

Rosette designation	Distance from nozzle-cylinder junction (see Fig. 3) (in.)
G	7/8
H	1
J	1 1/2
K	2
L	3
M	4
N	5
P	6
R	7.85
S	10
T	15.7

In every case, the rosettes were positioned on the gage lines so that the leg of the Y lay along the gage line and pointed away from the nozzle-cylinder junction. The convention used can be understood by referring to Fig. 7. The leg of the Y is designated as gage 1 in the tabulations, with gages 2 and 3 being numbered from 1 in the counterclockwise direction.

Finally, in cases where nonlinearity or drift was excessive or where an individual gage or circuit was otherwise obviously malfunctioning, the rosette of which the gage was a part was not used in the final results plotted in this report for the specific loading under consideration. Nonetheless, these data are listed in the tabulations, but they are marked by an asterisk beside the rosette number.

Table A.1. Internal pressure

INTERNAL PRESSURE (300 PSI)

	MICRO-STRAIN			STRESSES			PRIN STRESSES	
ROSETTE	GAGE1	GAGE2	GAGE3	TRANS	LONG	SHEAR	SIGMX	SIGMN
I-0-C-B	-70	332	352	15108	2431	-274	15114	2425
I-0-C-C	-26	263	277	11893	2780	-178	11897	2776
I-0-C-D	16	230	249	10506	3646	-246	10515	3638
I-0-C-F	59	224	217	9634	4662	86	9635	4661
I-0-C-H	73	201	199	8719	4807	18	8719	4807
I-0-C-J	68	180	188	8019	4431	-105	8022	4428
I-0-C-K	52	171	192	7940	3934	-280	7960	3915
I-0-C-L	57	167	191	7798	4046	-316	7824	4019
I-0-C-M	43	174	181	7752	3629	-103	7755	3627
I-0-C-P	50	173	178	7667	3812	-67	7669	3811
I-0-C-S	41	182	171	7724	3553	153	7730	3548
O-0-C-B	122	235	244	10396	6786	-123	10400	6782
O-0-C-C	99	208	218	9261	5738	-132	9266	5733
O-0-C-D	85	191	198	8454	5076	-103	8457	5073
O-0-C-E	58	186	183	8045	4168	32	8045	4168
O-0-C-H	41	150	163	6821	3286	-175	6829	3277
O-0-C-J	47	154	146	6554	3380	108	6558	3376
O-0-C-K	57	150	153	6602	3681	-33	6603	3681
O-0-C-L	59	155	126	6116	3604	386	6174	3546
O-0-C-M	50	158	153	6790	3541	69	6791	3539
O-0-C-P	50	157	150	6677	3503	97	6680	3500
O-0-C-S	47	148	158	6659	3408	-130	6664	3403
I-0-N-B*	0	-52	11	-893	-268	-840	316	-1477
I-0-N-C	59	236	244	10490	4911	-115	10493	4908
I-0-N-D	87	168	181	7566	4874	-176	7577	4862
I-0-N-E	69	97	94	4139	3321	37	4140	3319
I-0-N-F*	-50	64	104	3732	-368	-531	3800	-436
I-0-N-N	6	26	28	1180	523	-38	1182	521
O-0-N-B	-69	103	89	4290	-790	189	4297	-797
O-0-N-C	-49	8	10	441	-1344	-33	442	-1345
O-0-N-D	-14	-20	-18	-822	-665	-19	-663	-824
O-0-N-E	17	-21	-19	-893	244	-28	244	-894
O-0-N-F	33	-13	-9	-537	833	-53	835	-539
O-0-N-G	38	4	6	185	1198	-26	1199	185
O-0-N-H	35	12	12	483	1197	1	1197	483
O-0-N-K	0	19	19	819	246	-3	819	246
O-0-N-N	6	17	16	717	396	18	718	395

Table A.1 (continued)

INTERNAL PRESSURE (300 PSI)

	MICRO-STRAIN			STRESSES			PRIN STRESSES	
ROSETTE	GAGE1	GAGE2	GAGE3	TRANS	LONG	SHEAR	SIGMX	SIGMN
I-90C-B	-36	113	101	4743	331	172	4750	324
I-90C-C	25	98	83	3951	1948	193	3969	1930
I-90C-D	74	88	79	3585	3283	124	3630	3239
I-90C-E	106	82	74	3323	4190	109	4203	3309
I-90C-F	124	70	67	2863	4593	39	4594	2862
I-90C-R	193	75	83	3245	6755	-107	6758	3241
O-90C-B	0	107	114	4844	1453	-92	4847	1451
O-90C-C	142	154	147	6464	6206	101	6499	6171
O-90C-D	152	158	136	6302	6461	293	6685	6078
O-90C-E	162	134	129	5610	6540	65	6544	5606
O-90C-F	179	140	130	5716	7098	132	7111	5704
O-90C-R	172	73	83	3232	6135	-141	6142	3226
I-90N-B	-30	44	47	2033	-295	-52	2034	-296
I-90N-C	-16	10	25	797	-238	-205	837	-278
I-90N-D*	18	-18	-80	-2189	-124	825	165	-2478
I-90N-E*	19	-62	-97	-3509	-470	466	-400	-3578
I-90N-F	22	13	-1	239	718	199	790	168
I-90N-N*	5	-34	26	-184	103	-793	765	-846
O-90N-B	-94	90	91	4067	-1609	-9	4067	-1609
O-90N-C	-112	62	53	2647	-2576	127	2650	-2579
O-90N-D	-98	38	32	1646	-2453	85	1647	-2455
O-90N-E	-67	34	25	1357	-1601	114	1362	-1606
O-90N-F	-48	28	22	1160	-1099	73	1162	-1101
O-90N-N*	5	15	0	322	256	199	491	88

Table A.1 (continued)

INTERNAL PRESSURE (300 PSI)

	MICRO-STRAIN			STRESSES			PRIN STRESSES	
ROSETTE	GAGE1	GAGE2	GAGE3	TRANS	LONG	SHEAR	SIGMX	SIGMN
I180C-B	-47	312	328	14132	2821	-214	14137	2817
I180C-C	-2	257	274	11680	3453	-219	11686	3448
I180C-D	26	240	244	10602	3973	-51	10602	3973
I180C-E	35	224	231	9976	4044	-92	9977	4043
I180C-F	60	214	219	9467	4632	-64	9467	4631
I180C-S	52	187	178	7973	3943	116	7976	3939
O180C-B	104	198	224	9168	5857	-351	9205	5821
O180C-C	86	185	192	8180	5020	-88	8182	5018
O180C-D	77	179	189	8003	4713	-144	8009	4707
O180C-E	63	167	171	7374	4108	-54	7375	4107
O180C-F	54	171	166	7338	3826	62	7339	3825
O180C-S	55	157	148	6646	3642	119	6651	3637
I180N-B	-26	280	339	13633	3313	-775	13691	3255
I180N-C	91	202	234	9491	5570	-424	9536	5525
I180N-D	105	142	148	6259	5026	-74	6263	5021
I180N-E*	77	0	93	1955	2888	-1236	3743	1100
I180N-F	38	108	62	3700	2246	622	3930	2016
I180N-N	4	27	13	876	396	179	936	336
O180N-B	-65	69	98	3727	-844	-385	3760	-876
O180N-C	-46	0	3	111	-1351	-37	112	-1351
O180N-D	-7	-20	-22	-912	-489	27	-487	-913
O180N-E	23	-16	-20	-825	441	52	443	-827
O180N-F	35	-5	-11	-398	927	79	931	-403
O180N-N	6	18	17	750	406	15	750	405

Table A.1 (continued)

INTERNAL PRESSURE (300 PSI)

	MICRO-STRAIN			STRESSES			PRIN STRESSES	
ROSETTE	GAGE1	GAGE2	GAGE3	TRANS	LONG	SHEAR	SIGMX	SIGMN
I270C-A	-108	118	134	5656	-1536	-224	5663	-1543
I270C-B	-32	120	115	5206	591	63	5207	591
I270C-C	27	97	92	4133	2063	70	4136	2061
I270C-D	78	86	82	3611	3415	45	3621	3405
I270C-E	108	85	80	3498	4289	59	4293	3494
I270C-F	135	82	76	3340	5046	78	5050	3337
I270C-H	171	85	72	3263	6103	183	6115	3252
I270C-J	191	88	90	3693	6829	-27	6829	3693
I270C-K*	186	157	92	5263	7162	862	7495	4930
I270C-L	191	89	83	3569	6789	89	6792	3567
I270C-M	191	95	86	3782	6879	116	6884	3778
I270C-P	189	87	90	3685	6773	-47	6774	3685
I270C-R*	211	0	85	1632	6814	-1130	7049	1396
I270C-T*	0	96	89	4061	1218	91	4064	1215
O270C-B	165	177	167	7364	7167	132	7430	7101
O270C-C	175	165	159	6941	7337	84	7354	6924
O270C-D	187	163	158	6843	7673	74	7680	6836
O270C-E	187	160	150	6607	7598	146	7620	6586
O270C-F	188	148	141	6145	7494	105	7503	6136
O270C-H	185	131	129	5513	7191	28	7192	5513
O270C-J	198	111	110	4626	7339	18	7340	4626
O270C-K	194	97	103	4187	7067	-77	7069	4185
O270C-L	210	104	94	4132	7541	131	7546	4127
O270C-M	201	91	89	3740	7144	30	7145	3739
O270C-P	197	81	92	3590	6990	-145	6996	3584
O270C-R	194	84	84	3483	6872	-6	6872	3483
O270C-T	182	92	73	3429	6498	264	6520	3406
I270N-A	-95	85	85	3841	-1697	-10	3841	-1697
I270N-B	10	64	44	2360	999	257	2406	952
I270N-C	52	39	30	1450	1985	122	2011	1424
I270N-D	50	17	13	616	1688	58	1691	613
I270N-E	30	3	5	157	956	-23	957	156
I270N-F	11	5	-1	75	364	87	388	51
I270N-N	0	23	31	1190	357	-110	1204	343
O270N-B	-98	97	91	4231	-1658	74	4232	-1659
O270N-C	-115	59	61	2760	-2633	-29	2761	-2633
O270N-D	-96	39	45	1946	-2301	-86	1948	-2302
O270N-E	-72	27	28	1288	-1763	-15	1288	-1763
O270N-F	-45	26	24	1141	-1014	28	1141	-1015
O270N-G	-25	22	22	989	-455	-3	989	-455
O270N-H	-19	22	20	941	-281	15	941	-281
O270N-K	0	13	14	577	180	-14	578	179
O270N-N	5	17	16	729	367	8	729	367

Table A.1 (continued)

INTERNAL PRESSURE (300 PSI)

	MICRO-STRAIN			STRESSES			PRIN STRESSES	
ROSETTE	GAGE1	GAGE2	GAGE3	TRANS	LONG	SHEAR	SIGMX	SIGMN
I315C-B	-47	116	309	9374	1405	-2569	10130	649
I315C-C	0	90	298	8530	2559	-2772	9619	1470
I315C-D	51	77	260	7335	3743	-2440	8569	2510
I315C-E	74	74	254	7121	4349	-2407	8512	2958
I315C-F	92	72	244	6845	4814	-2286	8331	3328
I315C-H	128	63	215	5975	5637	-2017	7830	3782
I315C-J	132	71	197	5739	5684	-1679	7390	4033
I315C-K	120	81	190	5832	5351	-1456	7068	4116
I315C-L	128	67	180	5297	5439	-1505	6875	3862
I315C-M	111	77	183	5575	4993	-1410	6724	3844
I315C-P	122	62	174	5057	5169	-1482	6596	3630
O315C-B	135	275	97	8016	6448	2373	9731	4733
O315C-C	132	266	94	7753	6271	2296	9425	4600
O315C-D	118	244	91	7228	5720	2040	8649	4300
O315C-E	102	238	87	7039	5181	2020	8333	3886
O315C-F	117	226	71	6398	5425	2070	8038	3785
O315C-H	107	218	66	6119	5052	2022	7676	3495
O315C-J	117	204	65	5787	5236	1852	7384	3639
O315C-K	121	203	67	5786	5351	1815	7397	3741
O315C-L	130	204	69	5843	5638	1803	7546	3935
O315C-M	136	205	70	5894	5854	1802	7676	4072
O315C-P	140	197	64	5581	5860	1765	7491	3951
I315N-N*	-58	-44	-13	-1191	-2101	-420	-1027	-2266
O315N-B	-78	153	42	4356	-1045	1480	4735	-1424
O315N-C*	0	45	45	1972	592	0	1972	592
O315N-D	-63	-1	29	685	-1678	-404	752	-1745
O315N-E	-30	-14	28	339	-813	-572	574	-1048
O315N-F	-8	0	32	706	-41	-422	896	-231
O315N-G	7	-6	31	545	372	-482	948	-31
O315N-H	6	-3	28	561	343	-413	879	25
O315N-K	5	14	19	700	374	-65	713	361
O315N-N	0	16	16	713	214	7	713	214

Table A.2. Out-of-plane moment, M_{XN}, on nozzle

OUT-OF-PLANE MOMENT LOADING, MXN, ON NOZZLE (800 IN-LB)

	MICRO-STRAIN			STRESSES			PRIN STRESSES	
ROSETTE	GAGE1	GAGE2	GAGE3	TRANS	LONG	SHEAR	SIGMX	SIGMN
I-0-C-B	-2	-203	150	-1169	-415	-4710	3933	-5517
I-0-C-C	2	-215	189	-555	-116	-5384	5052	-5724
I-0-C-D	-1	-205	190	-338	-120	-5266	5038	-5497
I-0-C-F	8	-160	154	-143	207	-4183	4218	-4154
I-0-C-H	1	-108	103	-112	4	-2803	2750	-2858
I-0-C-J	0	-75	68	-152	-38	-1913	1819	-2009
I-0-C-K	1	-56	40	-340	-69	-1282	1084	-1493
I-0-C-L	2	-32	24	-187	8	-743	660	-839
I-0-C-M	0	-20	17	-65	-19	-488	446	-530
I-0-C-P	0	-9	12	63	7	-281	318	-248
I-0-C-S	2	-3	6	71	90	-127	207	-47
O-0-C-B	-4	-41	18	-493	-274	-784	408	-1175
O-0-C-C	-6	-85	66	-414	-312	-2016	1654	-2380
O-0-C-D	1	-89	69	-447	-112	-2109	1836	-2395
O-0-C-E	0	-83	69	-303	-102	-2025	1824	-2230
O-0-C-H	1	-51	41	-232	-54	-1225	1085	-1371
O-0-C-J	-3	-29	27	-45	-109	-738	662	-815
O-0-C-K	-1	-20	19	-14	-41	-520	493	-548
O-0-C-L	0	-10	13	56	25	-305	346	-265
O-0-C-M	3	-7	10	55	107	-232	314	-153
O-0-C-P	2	-3	6	65	65	-114	179	-50
O-0-C-S	1	-3	1	-41	10	-56	46	-77
I-0-N-B	0	11	62	1602	481	-691	1931	151
I-0-N-C	-18	-38	114	1684	-48	-2031	3025	-1390
I-0-N-D	4	10	32	904	401	-292	1038	267
I-0-N-E	15	26	1	580	620	324	925	275
I-0-N-F	11	21	-10	232	409	404	734	-93
I-0-N-N	-8	-3	-3	-124	-285	-8	-124	-286
O-0-N-B	-5	70	-88	-391	-262	2102	1777	-2429
O-0-N-C	-1	54	-58	-84	-57	1495	1425	-1566
O-0-N-D	0	32	-36	-101	-30	905	841	-971
O-0-N-E	0	16	-17	-36	-4	435	416	-455
O-0-N-F	-2	6	-4	46	-47	142	149	-149
O-0-N-G	2	-2	2	-6	46	-56	82	-42
O-0-N-H	-1	-4	0	-88	-48	-56	-8	-127
O-0-N-K	0	-4	-3	-145	-44	-21	-39	-150
O-0-N-N	-3	-3	-2	-114	-125	-16	-102	-137

Table A.2 (continued)

OUT-OF-PLANE MOMENT LOADING, MXN, ON NOZZLE (800 IN-LB)

	MICRO-STRAIN			STRESSES			PRIN STRESSES	
ROSETTE	GAGE1	GAGE2	GAGE3	TRANS	LONG	SHEAR	SIGMX	SIGMN
I-90C-B	-449	-284	-276	-11817	-17001	-102	-11815	-17003
I-90C-C	-322	-257	-249	-10759	-12893	-102	-10754	-12898
I-90C-D	-223	-202	-214	-8907	-9366	166	-8853	-9420
I-90C-E	-170	-145	-153	-6341	-7007	106	-6324	-7024
I-90C-F	-125	-128	-121	-5344	-5345	-96	-5249	-5441
I-90C-R	15	-9	8	-41	427	-215	511	-124
O-90C-B*	0	235	209	9752	2926	351	9770	2908
O-90C-C	379	305	274	12317	15052	405	15110	12258
O-90C-D	300	266	229	10546	12169	498	12310	10406
O-90C-E	245	204	194	8486	9893	132	9905	8473
O-90C-F	205	173	169	7304	8328	54	8331	7301
O-90C-R	-9	-9	-7	-345	-387	-23	-335	-397
I-90N-B	-453	-69	-46	-2035	-14209	-299	-2027	-14216
I-90N-C	-58	16	92	2426	-1018	-1014	2702	-1294
I-90N-D	32	33	40	1569	1424	-102	1622	1371
I-90N-E	60	20	4	478	1944	214	1975	448
I-90N-F	154	35	17	965	4906	240	4921	950
I-90N-N	125	-45	6	-986	3450	-673	3550	-1086
O-90N-B	368	272	280	11733	14566	-109	14570	11729
O-90N-C	222	145	167	6623	8652	-296	8695	6580
O-90N-D	123	83	82	3491	4731	19	4731	3491
O-90N-E	130	33	37	1387	4330	-59	4331	1386
O-90N-F	138	10	16	418	4280	-86	4282	416
O-90N-N	169	13	-4	12	5072	239	5083	1

Table A.2 (continued)

OUT-OF-PLANE MOMENT LOADING, MXN, ON NOZZLE (800 IN-LB)

	MICRO-STRAIN			STRESSES			PRIN STRESSES	
ROSETTE	GAGE1	GAGE2	GAGE3	TRANS	LONG	SHEAR	SIGMX	SIGMN
I180C-B	-11	213	-164	1091	12	5022	5603	-4500
I180C-C	-14	234	-186	1088	-98	5593	6120	-5130
I180C-D*	4	205	-175	648	314	5070	5554	-4592
I180C-E	-14	199	-162	835	-183	4811	5163	-4512
I180C-F	-18	158	-139	437	-395	3954	3997	-3955
I180C-S	3	-3	8	106	136	-135	256	-14
O180C-B	-2	35	-53	-403	-188	1168	877	-1468
O180C-C	1	68	-93	-532	-130	2145	1823	-2485
O180C-D	4	66	-97	-677	-96	2177	1810	-2583
O180C-E	0	63	-86	-521	-145	1986	1662	-2328
O180C-F	2	60	-74	-309	-26	1774	1612	-1948
O180C-S	1	5	-1	73	55	84	149	-21
I180N-B	-42	219	-171	1089	-933	5200	5376	-5220
I180N-C	-7	89	-54	760	29	1904	2333	-1544
I180N-D	4	17	5	477	260	162	563	174
I180N-E	9	0	21	460	416	-285	724	152
I180N-F	8	-8	21	291	340	-385	701	-70
I180N-N	22	8	3	213	736	57	742	207
O180N-B	-7	-78	43	-758	-427	-1606	1021	-2207
O180N-C*	-4	0	43	947	155	-571	1246	-144
O180N-D	-5	-35	25	-228	-218	-802	579	-1026
O180N-E	-6	-19	13	-133	-233	-424	244	-610
O180N-F	-6	-8	4	-80	-203	-162	31	-315
O180N-N	-2	-3	-1	-68	-73	-25	-46	-95

Table A.2 (continued)

OUT-OF-PLANE MOMENT LOADING, MXN, ON NOZZLE (800 IN-LB)

	MICRO-STRAIN			STRESSES			PRIN STRESSES	
ROSETTE	GAGE1	GAGE2	GAGE3	TRANS	LONG	SHEAR	SIGMX	SIGMN
I270C-A	133	228	259	10563	7151	-421	10614	7100
I270C-B	447	290	304	12569	17186	-189	17194	12561
I270C-C	308	247	249	10566	12417	-29	12417	10565
I270C-D	222	193	196	8308	9145	-38	9147	8307
I270C-E	162	152	159	6659	6846	-100	6889	6616
I270C-F	119	119	124	5211	5131	-64	5246	5096
I270C-H	57	62	64	2692	2503	-24	2695	2500
I270C-J	2	14	15	634	257	-5	634	257
I270C-K	-18	0	-2	-9	-552	25	-8	-553
I270C-L	-27	-11	-14	-514	-976	34	-511	-978
I270C-M	-26	-11	-14	-521	-933	35	-518	-936
I270C-P	-17	-4	-5	-164	-564	16	-163	-564
I270C-R	-13	0	-4	-69	-412	51	-62	-419
I270C-T	0	-5	-8	-287	-86	31	-81	-292
O270C-B	-519	-321	-330	-13729	-19695	121	-13726	-19698
O270C-C	-394	-274	-267	-11449	-15247	-98	-11446	-15250
O270C-D	-313	-243	-236	-10167	-12440	-91	-10163	-12444
O270C-E	-247	-215	-204	-8944	-10086	-153	-8924	-10107
O270C-F	-199	-175	-168	-7330	-8180	-90	-7321	-8189
O270C-H	-115	-117	-118	-5040	-4967	7	-4966	-5041
O270C-J	-56	-59	-60	-2555	-2458	15	-2456	-2557
O270C-K	-18	-24	-26	-1075	-874	20	-872	-1077
O270C-L	12	6	6	253	450	3	450	253
O270C-M	19	14	14	596	747	-5	747	596
O270C-P	14	10	12	471	555	-17	558	468
O270C-R	9	8	9	375	387	-10	392	370
O270C-T	0	0	1	19	10	-25	40	-11
I270N-A	197	171	148	6801	7953	301	8027	6727
I270N-B	287	6	20	274	8681	-184	8685	270
I270N-C	-4	-68	-56	-2718	-938	-165	-923	-2733
I270N-D	-115	-57	-51	-2243	-4134	-81	-2239	-4137
I270N-E	-153	-36	-45	-1622	-5081	114	-1618	-5084
I270N-F	-157	-22	-26	-871	-4986	56	-870	-4987
I270N-N*	0	-14	2	-270	-81	-219	63	-414
O270N-B	-381	-187	-225	-8647	-14032	511	-8599	-14080
O270N-C	-212	-149	-153	-6393	-8265	55	-6391	-8267
O270N-D	-146	-80	-81	-3371	-5384	12	-3371	-5384
O270N-E	-133	-38	-36	-1480	-4442	-32	-1480	-4443
O270N-F	-135	-16	-12	-469	-4193	-49	-468	-4194
O270N-G	-157	-1	-2	102	-4676	21	102	-4676
O270N-H	-166	-3	-8	-41	-4983	67	-40	-4984
O270N-K	-172	-13	5	2	-5151	-238	13	-5162
O270N-N	-175	-5	-4	-10	-5239	-20	-10	-5239

Table A.2 (continued)

OUT-OF-PLANE MOMENT LOADING, MXN, ON NOZZLE (800 IN-LB)

	MICRO-STRAIN			STRESSES			PRIN STRESSES	
ROSETTE	GAGE1	GAGE2	GAGE3	TRANS	LONG	SHEAR	SIGMX	SIGMN
I315C-B	283	56	364	8919	11159	-4091	14281	5797
I315C-C	191	35	365	8586	8310	-4388	12838	4058
I315C-D	143	14	310	6962	6365	-3945	10620	2708
I315C-E	105	6	286	6319	5055	-3732	9472	1903
I315C-F	76	-1	261	5636	3979	-3490	8394	1220
I315C-H	50	-18	197	3886	2663	-2857	6196	353
I315C-J	15	-5	153	3231	1410	-2112	4621	20
I315C-K	-5	12	117	2843	717	-1402	3539	20
I315C-L	-2	10	75	1874	506	-866	2293	86
I315C-M	-6	15	43	1280	192	-385	1403	70
I315C-P	-7	9	13	484	-65	-57	490	-71
O315C-B	-300	-311	-120	-9137	-11727	-2551	-7571	-13293
O315C-C	-218	-319	-102	-8999	-9251	-2895	-6227	-12023
O315C-D	-153	-293	-93	-8314	-7092	-2668	-4966	-10439
O315C-E	-104	-267	-84	-7608	-5404	-2436	-3832	-9180
O315C-F	-92	-241	-68	-6678	-4764	-2305	-3225	-8217
O315C-H	-48	-190	-59	-5403	-3054	-1748	-2122	-6335
O315C-J	-28	-130	-48	-3878	-2018	-1094	-1512	-4383
O315C-K	-15	-90	-41	-2871	-1320	-658	-1079	-3112
O315C-L	-16	-48	-33	-1777	-1008	-203	-957	-1827
O315C-M	-13	-25	-25	-1086	-722	-1	-722	-1086
O315C-P	-5	0	-10	-216	-203	142	-67	-352
I315N-N	-70	-9	-36	-893	-2362	359	-810	-2445
O315N-B	-242	-128	-205	-7059	-9366	1031	-6666	-9760
O315N-C*	0	-64	-143	-4555	-1367	1060	-1046	-4876
O315N-D	-93	-18	-86	-2182	-3436	897	-1714	-3903
O315N-E	-88	3	-37	-656	-2845	526	-536	-2965
O315N-F	-98	0	-14	-195	-3010	184	-183	-3021
O315N-G	-116	4	2	275	-3399	28	275	-3399
O315N-H	-118	1	-5	39	-3541	71	40	-3543
O315N-K	-119	1	-7	-9	-3578	100	-6	-3581
O315N-N*	0	1	-7	-125	-37	107	35	-197

Table A.3. Torsional moment loading, M_{YN}, on nozzle

TORSIONAL MOMENT LOADING, MYN, ON NOZZLE (2400 IN-LB)

	MICRO-STRAIN			STRESSES			PRIN STRESSES	
ROSETTE	GAGE1	GAGE2	GAGE3	TRANS	LONG	SHEAR	SIGMX	SIGMN
I-0-C-B	5	-27	19	-180	83	-616	581	-678
I-0-C-C	3	-53	51	-40	81	-1382	1404	-1363
I-0-C-D	-1	-46	45	-35	-50	-1212	1170	-1254
I-0-C-F	1	-26	26	8	20	-695	709	-681
I-0-C-H	0	-17	17	1	-2	-445	445	-445
I-0-C-J	1	-15	14	-29	16	-383	377	-390
I-0-C-K	-1	-16	10	-125	-70	-338	241	-436
I-0-C-L	0	-10	7	-71	-28	-231	182	-281
I-0-C-M	1	-6	5	-30	9	-147	138	-159
I-0-C-P	0	-4	3	-33	-19	-92	66	-118
I-0-C-S	-1	-2	2	-18	-32	-53	28	-79
O-0-C-B	-5	265	-246	408	-38	6805	6994	-6624
O-0-C-C	2	108	-102	131	96	2799	2912	-2686
O-0-C-D	-1	76	-68	171	24	1919	2017	-1823
O-0-C-E	0	53	-50	73	7	1375	1415	-1335
O-0-C-H	-1	16	-18	-48	-58	459	406	-513
O-0-C-J	-1	7	-8	-22	-46	190	157	-224
O-0-C-K	-1	3	-5	-30	-25	106	79	-133
O-0-C-L	0	1	-3	-55	-21	50	15	-91
O-0-C-M	1	1	-2	-38	14	37	33	-57
O-0-C-P	1	0	-2	-36	15	23	24	-45
O-0-C-S	0	1	-1	3	13	17	26	-10
I-0-N-B	0	-10	46	803	241	-741	1315	-270
I-0-N-C	-32	-227	196	-635	-1143	-5631	4747	-6526
I-0-N-D	18	-210	213	55	552	-5633	5942	-5335
I-0-N-E	-17	-216	212	-55	-520	-5699	5416	-5991
I-0-N-F	-23	-204	236	722	-472	-5871	6026	-5777
I-0-N-N	-7	-204	216	267	-122	-5605	5681	-5536
O-0-N-B	22	355	-384	-657	454	9852	9766	-9969
O-0-N-C	21	312	-316	-109	587	8372	8619	-8140
O-0-N-D	19	289	-332	-974	289	8268	7950	-8634
O-0-N-E	22	289	-318	-663	451	8085	7999	-8210
O-0-N-F	22	292	-312	-464	533	8042	8092	-8022
O-0-N-G	-2	294	-298	-87	-95	7885	7794	-7977
O-0-N-H	2	308	-296	248	120	8044	8228	-7860
O-0-N-K	0	292	-288	86	26	7728	7784	-7672
O-0-N-N	9	286	-293	-147	216	7714	7751	-7682

Table A.3 (continued)

TORSIONAL MOMENT LOADING, MYN, ON NOZZLE (2400 IN-LB)

	MICRO-STRAIN			STRESSES			PRIN STRESSES	
ROSETTE	GAGE1	GAGE2	GAGE3	TRANS	LONG	SHEAR	SIGMX	SIGMN
I-90C-B	-8	-137	143	142	-207	-3730	3701	-3766
I-90C-C	-9	-148	155	173	-232	-4030	4006	-4065
I-90C-D	-7	-117	123	152	-162	-3198	3197	-3207
I-90C-E	-1	-89	98	192	39	-2484	2601	-2370
I-90C-F	-3	-72	73	24	-83	-1934	1905	-1964
I-90C-R	1	-2	0	-47	24	-26	33	-55
O-90C-B	0	145	-112	724	217	3425	3905	-2964
O-90C-C	-2	122	-89	721	151	2813	3264	-2392
O-90C-D	3	93	-67	582	279	2134	2571	-1709
O-90C-E	3	82	-53	634	272	1807	2269	-1363
O-90C-F	4	72	-53	407	254	1666	1999	-1337
O-90C-R	7	4	5	189	274	-4	274	189
I-90N-B	17	-188	180	-193	457	-4891	5034	-4770
I-90N-C	14	-199	192	-179	364	-5212	5312	-5126
I-90N-D	2	-182	200	380	181	-5088	5370	-4809
I-90N-E	17	-216	165	-1135	156	-5074	4625	-5605
I-90N-F	17	-236	173	-1409	100	-5453	4850	-6159
I-90N-N*	-32	-37	218	4015	237	-3389	6006	-1754
O-90N-B	2	316	-323	-145	7	8510	8441	-8579
O-90N-C	14	257	-268	-274	332	6995	7030	-6972
O-90N-D	17	264	-265	-40	511	7054	7295	-6824
O-90N-E	9	280	-268	259	359	7301	7610	-6992
O-90N-F	13	256	-283	-614	214	7174	6986	-7386
O-90N-N	-31	306	-268	884	-667	7651	7799	-7582

Table A.3 (continued)

TORSIONAL MOMENT LOADING, MYN, ON NOZZLE (2400 IN-LB)

	MICRO-STRAIN			STRESSES			PRIN STRESSES	
ROSETTE	GAGE1	GAGE2	GAGE3	TRANS	LONG	SHEAR	SIGMX	SIGMN
I180C-B	9	-37	28	-199	211	-874	903	-892
I180C-C	7	-56	46	-239	149	-1364	1333	-1422
I180C-D	6	-41	38	-80	145	-1056	1094	-1029
I180C-E	3	-33	28	-104	47	-820	795	-852
I180C-F	2	-25	22	-70	42	-622	610	-638
I180C-S	1	3	-2	25	24	57	81	-32
O180C-B	20	227	-252	-573	421	6384	6327	-6479
O180C-C	11	111	-100	244	412	2812	3141	-2485
O180C-D	7	73	-73	-23	189	1944	2030	-1864
O180C-E	4	51	-52	-35	95	1372	1403	-1344
O180C-F	2	39	-37	35	68	1012	1064	-962
O180C-S	1	1	0	4	20	14	28	-3
I180N-B	31	-128	128	-23	911	-3412	3888	-2999
I180N-C	25	-196	185	-267	667	-5075	5296	-4896
I180N-D	30	-219	197	-525	743	-5546	5690	-5473
I180N-E*	20	0	197	4301	1898	-2621	5982	216
I180N-F	24	-225	194	-695	511	-5582	5522	-5706
I180N-N	-8	-205	186	-408	-348	-5205	4827	-5584
O180N-B	-36	337	-246	2042	-471	7760	8647	-7076
O180N-C*	-25	0	-281	-6147	-2598	3743	-230	-8515
O180N-D	-16	310	-247	1408	-68	7412	8118	-6779
O180N-E	-16	324	-288	809	-251	8154	8450	-7892
O180N-F	-26	311	-284	633	-576	7926	7978	-7921
O180N-N	7	286	-302	-353	112	7834	7717	-7957

Table A.3 (continued)

TORSIONAL MOMENT LOADING, MYN, ON NOZZLE (2400 IN-LB)

	MICRO-STRAIN			STRESSES			PRIN STRESSES	
ROSETTE	GAGE1	GAGE2	GAGE3	TRANS	LONG	SHEAR	SIGMX	SIGMN
I270C-A	19	-79	66	-299	484	-1934	2066	-1881
I270C-B	-4	-141	155	300	-18	-3939	4083	-3802
I270C-C	4	-151	153	30	143	-4056	4143	-3970
I270C-D	2	-118	118	-2	61	-3139	3169	-3109
I270C-E	-1	-94	92	-40	-50	-2475	2430	-2520
I270C-F	0	-70	72	47	14	-1891	1922	-1861
I270C-H	0	-37	39	40	20	-1018	1048	-988
I270C-J	-1	-11	15	76	-6	-341	378	-309
I270C-K	0	0	2	44	6	-16	50	0
I270C-L	0	8	-5	79	11	169	217	-127
I270C-M	-1	7	-2	117	12	118	193	-65
I270C-P	0	3	2	117	20	12	118	19
I270C-R	0	0	4	80	10	-48	104	-15
I270C-T	0	2	0	58	18	22	68	8
O270C-B	-2	198	-236	-843	-299	5778	5213	-6355
O270C-C	1	105	-112	-169	-29	2892	2793	-2991
O270C-D	-6	83	-84	-23	-181	2226	2125	-2329
O270C-E	-4	71	-71	0	-119	1896	1837	-1956
O270C-F	-3	59	-62	-62	-120	1625	1534	-1716
O270C-H	-1	44	-45	-30	-32	1179	1147	-1210
O270C-J	-1	33	-33	2	-21	870	860	-879
O270C-K	-2	23	-21	46	-42	582	586	-582
O270C-L	-1	12	-7	99	0	250	305	-206
O270C-M	0	5	-1	103	37	83	160	-19
O270C-P	0	2	3	116	37	-13	118	35
O270C-R	-1	1	3	80	-1	-19	84	-5
O270C-T	0	-1	0	-14	-14	-9	-5	-23
I270N-A	15	-60	30	-670	259	-1192	1074	-1485
I270N-B	-25	-202	204	64	-730	-5406	5088	-5753
I270N-C	-20	-192	207	351	-500	-5320	5263	-5412
I270N-D	-28	-193	209	379	-716	-5367	5227	-5563
I270N-E	-33	-194	223	671	-789	-5553	5542	-5659
I270N-F*	-68	-193	213	502	-1879	-5406	4847	-6224
I270N-N*	0	-231	183	-1046	-314	-5513	4846	-6205
O270N-B	-7	305	-294	243	-140	7989	8043	-7939
O270N-C	2	267	-258	181	104	6998	7140	-6855
O270N-D	-5	270	-271	-18	-144	7200	7119	-7282
O270N-E	-23	279	-263	378	-577	7214	7130	-7329
O270N-F	-2	275	-265	229	8	7188	7307	-7070
O270N-G	6	272	-284	-258	104	7407	7332	-7486
O270N-H	6	281	-293	-287	91	7645	7550	-7745
O270N-K	-21	305	-275	675	-418	7729	7877	-7620
O270N-N	4	286	-295	-200	54	7746	7674	-7820

Table A.3 (continued)

TORSIONAL MOMENT LOADING, MYN, ON NOZZLE (2400 IN-LB)

	MICRO-STRAIN			STRESSES			PRIN STRESSES	
ROSETTE	GAGE1	GAGE2	GAGE3	TRANS	LONG	SHEAR	SIGMX	SIGMN
I315C-B	-15	-54	137	1840	91	-2545	3657	-1726
I315C-C	-4	-53	144	2007	474	-2618	3969	-1488
I315C-D	7	-34	115	1787	757	-1981	3319	-775
I315C-E	8	-21	99	1699	754	-1594	2889	-436
I315C-F	8	-11	86	1635	742	-1285	2550	-172
I315C-H	11	-3	60	1239	709	-843	1858	91
I315C-J	3	1	42	941	381	-545	1274	48
I315C-K	-4	3	30	718	84	-365	885	-82
I315C-L	-6	-3	16	302	-91	-259	431	-219
I315C-M	-12	-6	3	-40	-373	-120	-2	-412
I315C-P	-11	-6	-4	-221	-382	-21	-218	-385
O315C-B	-2	181	-171	230	10	4685	4806	-4567
O315C-C	-15	89	-109	-423	-585	2637	2134	-3142
O315C-D	-23	49	-93	-947	-973	1883	924	-2843
O315C-E	-27	29	-80	-1087	-1134	1444	334	-2554
O315C-F	-27	13	-74	-1303	-1213	1162	-95	-2421
O315C-H	-28	-5	-57	-1323	-1233	691	-585	-1971
O315C-J	-23	-12	-38	-1062	-1010	342	-693	-1379
O315C-K	-17	-12	-27	-847	-758	201	-597	-1008
O315C-L	-11	-5	-15	-433	-453	139	-303	-582
O315C-M	-7	1	-9	-172	-267	124	-87	-353
O315C-P	-3	5	-2	60	-80	89	103	-123
I315N-N	-53	-161	206	1062	-1276	-4887	4918	-5132
O315N-B	83	325	-380	-1293	2091	9385	9935	-9137
O315N-C*	0	281	-294	-305	-91	7660	7463	-7859
O315N-D	77	274	-311	-894	2055	7800	8518	-7358
O315N-E	58	287	-291	-148	1697	7692	8521	-6972
O315N-F*	58	0	-308	-6843	-302	4109	1680	-8824
O315N-G	31	287	-287	-18	929	7649	8119	-7209
O315N-H	30	295	-285	198	947	7732	8314	-7169
O315N-K	25	282	-293	-264	668	7664	7880	-7476
O315N-N	0	279	-294	-348	-104	7637	7412	-7863

Table A.4. In-plane moment loading, M_{ZN}, on nozzle

IN-PLANE MOMENT LOADING, MZN, ON NOZZLE (1200 IN-LB)

	MICRO-STRAIN			STRESSES			PRIN STRESSES	
ROSETTE	GAGE1	GAGE2	GAGE3	TRANS	LONG	SHEAR	SIGMX	SIGMN
I-0-C-B	-492	-237	-237	-9883	-17715	-1	-9883	-17715
I-0-C-C	-356	-261	-252	-10884	-13937	-112	-10880	-13941
I-0-C-D	-202	-208	-215	-9070	-8777	100	-8747	-9101
I-0-C-F	-39	-142	-142	-6196	-3043	1	-3043	-6196
I-0-C-H	65	-83	-81	-3680	859	-31	860	-3681
I-0-C-J	73	-50	-54	-2369	1475	63	1476	-2370
I-0-C-K	60	-38	-46	-1903	1234	103	1237	-1906
I-0-C-L	23	-29	-39	-1526	228	141	239	-1537
I-0-C-M	7	-22	-26	-1058	-101	58	-97	-1062
I-0-C-P	-5	-19	-17	-782	-399	-25	-398	-784
I-0-C-S	-1	-5	-5	-209	-80	0	-80	-209
O-0-C-B	493	486	478	20644	20995	103	21023	20616
O-0-C-C	327	373	391	16419	14744	-240	16452	14710
O-0-C-D	197	314	330	13937	10077	-218	13949	10065
O-0-C-E	109	282	275	12124	6905	105	12126	6902
O-0-C-H	-5	131	139	5923	1613	-104	5926	1610
O-0-C-J	-21	68	63	2910	251	63	2912	250
O-0-C-K	-1	40	37	1691	463	35	1692	462
O-0-C-L	7	24	26	1088	524	-17	1088	523
O-0-C-M	9	17	16	716	479	24	718	476
O-0-C-P	0	11	12	494	156	-17	495	155
O-0-C-S	1	1	2	76	41	-9	79	39
I-0-N-B	0	43	-30	292	88	979	1174	-794
I-0-N-C	-118	221	103	7265	-1358	1574	7543	-1636
I-0-N-D	103	121	100	4748	4511	274	4928	4331
I-0-N-E	181	77	86	3392	6459	-122	6464	3387
I-0-N-F*	70	42	86	2729	2927	-578	3414	2242
I-0-N-N	194	10	2	51	5848	103	5850	49
O-0-N-B	415	324	322	13733	16585	18	16585	13733
O-0-N-C	250	164	165	6950	9572	-14	9572	6950
O-0-N-D	202	75	81	3214	7017	-73	7018	3212
O-0-N-E	194	16	33	847	6075	-227	6085	837
O-0-N-F	209	-11	12	-228	6208	-305	6223	-242
O-0-N-G	243	-5	-2	-423	7151	-30	7151	-423
O-0-N-H	247	3	3	-147	7367	-8	7367	-147
O-0-N-K*	0	9	4	298	89	62	315	72
O-0-N-N	255	10	12	210	7706	-26	7706	210

Table A.4 (continued)

IN-PLANE MOMENT LOADING, MZN, ON NOZZLE (1200 IN-LB)

	MICRO-STRAIN			STRESSES			PRIN STRESSES	
ROSETTE	GAGE1	GAGE2	GAGE3	TRANS	LONG	SHEAR	SIGMX	SIGMN
I-90C-B	19	258	-284	-577	406	7225	7156	-7326
I-90C-C	28	308	-323	-344	735	8406	8618	-8227
I-90C-D	17	278	-301	-531	350	7714	7636	-7817
I-90C-E	7	253	-274	-458	63	7017	6824	-7219
I-90C-F	10	232	-241	-208	253	6301	6328	-6283
I-90C-R	7	3	5	157	260	-29	268	149
O-90C-B	0	8	-57	-1065	-320	867	251	-1636
O-90C-C	-5	151	-110	907	114	3478	4010	-2990
O-90C-D	-5	135	-105	668	46	3192	3565	-2850
O-90C-E	-4	110	-84	571	58	2579	2906	-2278
O-90C-F	-7	74	-72	50	-192	1936	1869	-2011
O-90C-R	0	1	-1	2	6	36	40	-32
I-90N-B	-3	255	-231	513	55	6475	6763	-6196
I-90N-C	1	78	-51	589	212	1723	2134	-1333
I-90N-D	-1	-13	7	-134	-66	-264	166	-366
I-90N-E	-1	-32	25	-160	-64	-753	643	-867
I-90N-F	-2	-39	26	-297	-139	-864	649	-1085
I-90N-N	17	4	0	66	540	42	544	62
O-90N-B	22	-67	93	552	821	-2130	2821	-1447
O-90N-C	6	-66	85	402	316	-2009	2368	-1651
O-90N-D	-20	-54	53	8	-605	-1433	1167	-1764
O-90N-E	5	-30	32	32	153	-832	927	-741
O-90N-F	8	-10	16	140	276	-349	564	-148
O-90N-N	8	2	0	44	264	32	268	40

Table A.4 (continued)

IN-PLANE MOMENT LOADING, MZN, ON NOZZLE (1200 IN-LB)

	MICRO-STRAIN			STRESSES			PRIN STRESSES	
ROSETTE	GAGE1	GAGE2	GAGE3	TRANS	LONG	SHEAR	SIGMX	SIGMN
I180C-B	510	278	266	11390	18715	158	18718	11387
I180C-C	331	266	268	11371	13332	-20	13332	11370
I180C-D	177	207	209	8941	7981	-18	8941	7981
I180C-E	81	152	169	6960	4505	-233	6982	4483
I180C-F	20	134	144	6098	2423	-135	6103	2418
I180C-S	-6	3	3	139	-126	-10	139	-126
O180C-B	-480	-395	-479	-18661	-20006	1120	-18028	-20640
O180C-C	-332	-360	-366	-15598	-14636	74	-14631	-15604
O180C-D	-201	-314	-323	-13772	-10171	125	-10166	-13777
O180C-E	-121	-267	-261	-11464	-7063	-85	-7061	-11466
O180C-F	-67	-239	-220	-10025	-5010	-246	-4998	-10037
O180C-S	-6	-7	-4	-243	-253	-32	-216	-280
I180N-B	571	11	-96	-2498	16375	1432	16483	-2606
I180N-C	101	-76	-142	-4905	1564	886	1683	-5024
I180N-D	-136	-104	-117	-4717	-5481	176	-4679	-5519
I180N-E	-210	0	-66	-1225	-6657	882	-1085	-6797
I180N-F	-211	-50	-32	-1567	-6789	-243	-1556	-6801
I180N-N	-182	6	14	631	-5266	-112	634	-5268
O180N-B	-375	-232	-201	-9094	-13986	-414	-9059	-14021
O180N-C	-237	0	-139	-2788	-7948	1848	-2194	-8542
O180N-D	-192	-70	-48	-2388	-6484	-287	-2368	-6504
O180N-E	-204	-24	-14	-610	-6292	-127	-607	-6294
O180N-F	-204	-15	7	56	-6111	-286	69	-6124
O180N-N	-259	-1	-10	53	-7747	115	55	-7749

Table A.4 (continued)

IN-PLANE MOMENT LOADING, MZN, ON NOZZLE (1200 IN-LB)

	MICRO-STRAIN			STRESSES			PRIN STRESSES	
ROSETTE	GAGE1	GAGE2	GAGE3	TRANS	LONG	SHEAR	SIGMX	SIGMN
I270C-A	44	-177	151	-616	1142	-4376	4726	-4200
I270C-B	-16	-272	298	593	-301	-7588	7747	-7455
I270C-C	4	-319	324	101	138	-8556	8676	-8437
I270C-D	-3	-294	286	-192	-140	-7730	7564	-7895
I270C-E	-12	-279	253	-567	-536	-7086	6535	-7637
I270C-F	-16	-237	229	-155	-526	-6213	5875	-6556
I270C-H	-3	-171	176	121	-64	-4617	4647	-4590
I270C-J	-4	-93	110	377	-3	-2692	2886	-2512
I270C-K	6	-44	60	335	290	-1390	1703	-1078
I270C-L	4	-8	6	-47	91	-199	232	-189
I270C-M	-3	-1	-13	-305	-177	172	-58	-424
I270C-P	-6	-1	-7	-160	-215	76	-106	-269
I270C-R	-1	0	1	21	-21	-12	24	-25
I270C-T	0	10	6	340	102	51	351	91
O270C-B	10	-84	98	305	403	-2424	2779	-2071
O270C-C	0	-109	124	333	110	-3110	3334	-2891
O270C-D	11	-103	111	166	378	-2845	3119	-2575
O270C-E	6	-89	93	73	196	-2432	2568	-2298
O270C-F	2	-70	72	46	88	-1883	1951	-1816
O270C-H	-2	-31	28	-59	-64	-788	727	-850
O270C-J	0	10	-9	40	5	254	277	-232
O270C-K	-2	24	-25	-19	-54	656	620	-693
O270C-L	1	30	-24	128	66	720	818	-624
O270C-M	-2	12	-15	-62	-81	372	300	-443
O270C-P	0	-1	-5	-129	-43	53	-17	-154
O270C-R	-4	-4	2	-41	-142	-73	-3	-180
O270C-T	1	2	3	106	65	-21	115	56
I270N-A	64	-224	221	-144	1878	-5937	6890	-5156
I270N-B	32	-153	187	717	1182	-4535	5491	-3591
I270N-C	-9	-47	13	-745	-502	-800	185	-1432
I270N-D	-34	-1	-41	-882	-1287	523	-523	-1645
I270N-E	-40	20	-40	-394	-1306	807	77	-1778
I270N-F	-40	17	-28	-215	-1266	601	58	-1538
I270N-N	0	3	5	172	52	-17	174	49
O270N-B	16	95	-74	450	626	2244	2783	-1708
O270N-C	7	87	-74	266	297	2142	2424	-1861
O270N-D	3	59	-59	-21	99	1572	1612	-1534
O270N-E	-5	34	-28	142	-108	820	847	-813
O270N-F	5	19	-17	44	162	471	578	-372
O270N-G	6	8	5	268	268	39	308	229
O270N-H	7	1	0	22	227	10	228	22
O270N-K	-2	-2	-4	-131	-92	14	-88	-136
O270N-N	0	-1	-5	-136	-50	45	-31	-155

Table A.4 (continued)

IN-PLANE MOMENT LOADING, MZN, ON NOZZLE (1200 IN-LB)

	MICRO-STRAIN			STRESSES			PRIN STRESSES	
ROSETTE	GAGE1	GAGE2	GAGE3	TRANS	LONG	SHEAR	SIGMX	SIGMN
I315C-B	-358	-344	-11	-7422	-12967	-4436	-4963	-15426
I315C-C	-213	-316	46	-5703	-8115	-4818	-1943	-11876
I315C-D	-120	-255	74	-3841	-4739	-4380	113	-8693
I315C-E	-51	-206	90	-2479	-2287	-3943	1562	-6327
I315C-F	-5	-153	108	-976	-447	-3482	2781	-4203
I315C-H	74	-70	96	501	2370	-2217	3841	-970
I315C-J	78	-21	73	1055	2653	-1263	3348	360
I315C-K	54	-11	46	718	1846	-758	2227	337
I315C-L	16	-8	28	418	617	-469	997	38
I315C-M	0	-5	24	403	131	-386	676	-142
I315C-P	-4	-2	16	293	-22	-239	421	-151
O315C-B	369	252	278	11246	14432	-353	14471	11207
O315C-C	260	202	268	10050	10806	-880	11386	9470
O315C-D	167	149	229	8128	7462	-1064	8910	6680
O315C-E	102	119	181	6488	5014	-832	6863	4639
O315C-F	65	92	142	5062	3474	-664	5303	3233
O315C-H	13	54	65	2614	1162	-152	2630	1146
O315C-J	-17	3	4	163	-473	-15	164	-473
O315C-K	-13	-24	-18	-910	-676	-79	-652	-934
O315C-L	-4	-33	-26	-1291	-511	-99	-499	-1303
O315C-M	-5	-24	-17	-896	-428	-81	-414	-910
O315C-P	-8	-14	-15	-644	-422	16	-421	-645
I315N-N	95	18	62	1656	3357	-578	3535	1478
O315N-B	338	296	122	8794	12782	2319	13846	7730
O315N-C*	0	208	77	6269	1881	1754	6884	1266
O315N-D	146	111	33	3007	5284	1045	5691	2600
O315N-E	137	50	5	1058	4442	588	4541	959
O315N-F	145	0	1	-138	4301	-13	4301	-138
O315N-G	171	-6	-6	-447	4993	-7	4993	-447
O315N-H	170	-7	6	-204	5029	-169	5034	-209
O315N-K	180	-1	5	-112	5381	-84	5382	-113
O315N-N*	0	-6	9	50	15	-203	236	-171

Table A.5. In-plane force, F_{XN}, on nozzle

IN-PLANE FORCE LOADING, FXN, ON NOZZLE (120 LB)

	MICRO-STRAIN			STRESSES			PRIN STRESSES	
ROSETTE	GAGE1	GAGE2	GAGE3	TRANS	LONG	SHEAR	SIGMX	SIGMN
I-0-C-B	560	263	269	11090	20141	-75	20142	11089
I-0-C-C	415	305	293	12674	16243	165	16250	12666
I-0-C-D	232	237	247	10380	10077	-134	10431	10027
I-0-C-F	33	156	158	6860	3045	-35	6861	3045
I-0-C-H	-79	96	95	4270	-1093	12	4270	-1093
I-0-C-J	-86	62	72	3038	-1659	-129	3041	-1663
I-0-C-K	-61	50	60	2480	-1079	-126	2484	-1084
I-0-C-L	-21	36	42	1756	-97	-79	1760	-100
I-0-C-M	-12	27	27	1207	8	-8	1207	8
I-0-C-P	-7	14	15	653	-1	-10	653	-1
I-0-C-S	-4	6	8	302	-27	-25	304	-29
O-0-C-B	-571	-572	-552	-24083	-24349	-259	-23925	-24507
O-0-C-C	-379	-430	-452	-18963	-17065	298	-17019	-19008
O-0-C-D	-235	-363	-374	-15953	-11833	149	-11827	-15959
O-0-C-E	-123	-319	-310	-13696	-7796	-119	-7794	-13699
O-0-C-H	6	-151	-163	-6901	-1892	163	-1887	-6906
O-0-C-J	17	-83	-75	-3476	-527	-103	-523	-3480
O-0-C-K	4	-45	-47	-2034	-504	24	-504	-2034
O-0-C-L	-12	-27	-28	-1189	-713	8	-713	-1189
O-0-C-M	-9	-21	-21	-918	-535	3	-535	-918
O-0-C-P	-5	-12	-12	-523	-299	-11	-298	-524
O-0-C-S	-2	-7	-5	-256	-138	-18	-135	-259
I-0-N-B*	0	-42	13	-646	-194	-734	348	-1188
I-0-N-C	155	-246	-124	-8296	2169	-1635	2419	-8546
I-0-N-D	-117	-145	-123	-5771	-5227	-288	-5102	-5896
I-0-N-E	-200	-90	-103	-4025	-7194	169	-4016	-7203
I-0-N-F	-116	-45	-94	-2927	-4356	664	-2666	-4617
I-0-N-N	-110	-4	2	84	-3288	-71	86	-3289
O-0-N-B	-461	-363	-363	-15443	-18465	-6	-15443	-18465
O-0-N-C	-269	-184	-183	-7768	-10414	-8	-7768	-10414
O-0-N-D	-206	-78	-88	-3426	-7215	134	-3421	-7219
O-0-N-E	-201	-18	-34	-921	-6320	224	-912	-6330
O-0-N-F	-216	11	-11	227	-6401	292	239	-6414
O-0-N-G	-246	4	-2	311	-7280	72	312	-7280
O-0-N-H	-253	-2	0	236	-7517	-39	236	-7517
O-0-N-K*	0	-7	-4	-241	-72	-41	-63	-251
O-0-N-N	-144	-3	-5	-16	-4336	35	-15	-4336

Table A.5 (continued)

IN-PLANE FORCE LOADING, FXN, ON NOZZLE (120 LB)

	MICRO-STRAIN			STRESSES			PRIN STRESSES	
ROSETTE	GAGE1	GAGE2	GAGE3	TRANS	LONG	SHEAR	SIGMX	SIGMN
I-90C-B	-19	-285	322	817	-330	-8087	8351	-7864
I-90C-C	-21	-338	367	669	-440	-9398	9529	-9300
I-90C-D	-19	-314	337	524	-409	-8662	8732	-8618
I-90C-E	-6	-281	311	669	12	-7877	8224	-7542
I-90C-F	-15	-263	271	184	-401	-7117	7014	-7232
I-90C-R	-1	0	-1	-21	-36	20	-8	-50
O-90C-B*	0	-16	54	848	254	-927	1525	-423
O-90C-C	2	-180	126	-1194	-312	-4086	3357	-4863
O-90C-D	4	-161	117	-987	-183	-3701	3138	-4307
O-90C-E	2	-127	95	-717	-168	-2962	2533	-3417
O-90C-F	1	-92	80	-256	-38	-2288	2144	-2438
O-90C-R	-4	-5	-2	-139	-165	-46	-104	-199
I-90N-B	5	-268	252	-342	42	-6931	6784	-7084
I-90N-C	-3	-71	43	-618	-273	-1514	1079	-1970
I-90N-D	0	29	-26	57	7	736	768	-704
I-90N-E	-2	54	-40	326	31	1252	1439	-1082
I-90N-F	3	67	-41	563	264	1438	1859	-1032
I-90N-N	-6	1	-16	-310	-288	225	-74	-524
O-90N-B	-27	56	-97	-886	-1083	2041	1059	-3028
O-90N-C	-12	60	-86	-558	-518	1946	1408	-2484
O-90N-D	-8	39	-54	-315	-341	1241	913	-1569
O-90N-E	-7	17	-24	-138	-241	540	353	-732
O-90N-F	-6	-1	-5	-123	-205	45	-103	-225
O-90N-N	-2	-15	11	-79	-70	-342	268	-416

Table A.5 (continued)

IN-PLANE FORCE LOADING, FXN, ON NOZZLE (120 LB)

	MICRO-STRAIN			STRESSES			PRIN STRESSES	
ROSETTE	GAGE1	GAGE2	GAGE3	TRANS	LONG	SHEAR	SIGMX	SIGMN
I180C-B	-571	-292	-284	-12049	-20733	-104	-12048	-20734
I180C-C	-359	-280	-287	-12068	-14401	97	-12064	-14405
I180C-D	-186	-219	-229	-9646	-8469	138	-8453	-9662
I180C-E	-84	-168	-189	-7754	-4842	272	-4817	-7780
I180C-F	-19	-133	-155	-6320	-2454	287	-2433	-6341
I180C-S	6	-6	-6	-285	95	-4	95	-285
O180C-B	542	436	483	19603	22150	-623	22295	19458
O180C-C	381	407	415	17645	16715	-99	17655	16705
O180C-D	233	356	364	15561	11652	-98	15564	11650
O180C-E	142	302	293	12917	8121	116	12920	8118
O180C-F	81	267	244	11136	5756	307	11153	5739
O180C-S	6	4	5	203	232	-12	236	198
I180N-B	-647	-11	105	2771	-18591	-1554	2884	-18703
I180N-C	-105	71	169	5381	-1536	-1306	5619	-1774
I180N-D	125	99	142	5143	5308	-577	5808	4643
I180N-E	223	0	64	1154	7032	-848	7152	1034
I180N-F	228	44	25	1249	7209	254	7220	1239
I180N-N	92	-13	6	-264	2694	-261	2717	-287
O180N-B	419	262	229	10327	15674	450	15711	10289
O180N-C	257	0	156	3145	8666	-2078	9361	2450
O180N-D	201	77	63	2847	6892	192	6902	2838
O180N-E	212	28	18	787	6599	133	6602	784
O180N-F	212	16	-5	8	6357	285	6370	-5
O180N-N	147	1	5	-32	4408	-59	4409	-33

Table A.5 (continued)

IN-PLANE FORCE LOADING, FXN, ON NOZZLE (120 LB)

	MICRO-STRAIN			STRESSES			PRIN STRESSES	
ROSETTE	GAGE1	GAGE2	GAGE3	TRANS	LONG	SHEAR	SIGMX	SIGMN
I270C-A	-42	206	-154	1190	-909	4806	5060	-4779
I270C-B	28	308	-308	-24	840	8213	8633	-7817
I270C-C	4	367	-350	354	240	9554	9851	-9257
I270C-D	5	336	-318	398	283	8719	9060	-8379
I270C-E	9	309	-289	427	385	7977	8383	-7571
I270C-F	3	265	-261	71	126	7006	7104	-6907
I270C-H	1	194	-196	-43	18	5203	5190	-5215
I270C-J	7	110	-120	-235	144	3064	3024	-3116
I270C-K	-4	56	-64	-155	-158	1601	1444	-1757
I270C-L	-2	10	-8	42	-39	235	240	-238
I270C-M	0	-6	7	14	-1	-173	179	-166
I270C-P	-1	-3	4	17	-19	-98	99	-101
I270C-R	-1	0	1	22	-33	-12	24	-36
I270C-T	0	5	-1	90	27	85	150	-32
O270C-B	-20	99	-124	-531	-753	2972	2332	-3616
O270C-C	-6	127	-145	-383	-301	3629	3288	-3971
O270C-D	-12	119	-131	-254	-449	3326	2977	-3679
O270C-E	-8	103	-109	-130	-273	2820	2620	-3022
O270C-F	-4	80	-85	-103	-154	2196	2068	-2325
O270C-H	1	33	-36	-70	-6	928	891	-966
O270C-J	1	-10	11	22	28	-269	295	-244
O270C-K	3	-26	30	97	110	-748	851	-645
O270C-L	3	-29	31	28	88	-799	857	-742
O270C-M	1	-14	17	55	49	-416	468	-364
O270C-P	0	-1	2	23	14	-33	51	-15
O270C-R	0	1	0	34	24	18	48	11
O270C-T	0	-1	-2	-62	-22	9	-21	-64
I270N-A	-70	259	-234	634	-1900	6569	6057	-7323
I270N-B*	-53	178	-195	-304	-1675	4964	4021	-6001
I270N-C	-7	48	11	1303	193	502	1496	0
I270N-D	31	-21	59	801	1159	-1056	2051	-90
I270N-E	41	-36	70	691	1424	-1408	2512	-398
I270N-F	43	-34	54	400	1417	-1175	2189	-372
I270N-N	0	-17	11	-117	-35	-376	302	-454
O270N-B	-24	-97	67	-631	-924	-2178	1405	-2960
O270N-C	-16	-91	67	-520	-628	-2110	1537	-2684
O270N-D	-8	-60	44	-344	-351	-1386	1038	-1733
O270N-E	-5	-30	17	-273	-233	-622	369	-876
O270N-F	-5	-8	-1	-210	-209	-91	-118	-301
O270N-G	-5	8	-17	-178	-206	332	140	-525
O270N-H	-6	12	-18	-112	-206	401	245	-562
O270N-K	-4	13	-13	8	-116	342	294	-402
O270N-N	-2	12	-13	-18	-63	340	300	-381

Table A.5 (continued)

IN-PLANE FORCE LOADING, FXN, ON NOZZLE (120 LB)

	MICRO-STRAIN			STRESSES			PRIN STRESSES	
ROSETTE	GAGE1	GAGE2	GAGE3	TRANS	LONG	SHEAR	SIGMX	SIGMN
I315C-B	418	387	19	8463	15083	4891	17679	5867
I315C-C	242	356	-43	6612	9243	5328	13416	2439
I315C-D	128	281	-82	4237	5101	4825	9514	-176
I315C-E	56	232	-95	2940	2549	4355	7104	-1614
I315C-F	3	176	-108	1480	548	3785	4828	-2799
I315C-H	-78	85	-95	-133	-2385	2401	1392	-3911
I315C-J	-86	29	-81	-1041	-2883	1466	-231	-3694
I315C-K	-68	7	-60	-1097	-2359	886	-840	-2815
I315C-L	-27	2	-37	-734	-1044	515	-351	-1427
I315C-M	-6	0	-31	-684	-371	411	-87	-967
I315C-P	1	2	-16	-311	-55	241	90	-456
O315C-B	-426	-294	-320	-13023	-16672	344	-12991	-16704
O315C-C	-299	-229	-302	-11333	-12375	965	-10758	-12950
O315C-D	-193	-175	-265	-9464	-8642	1193	-7792	-10315
O315C-E	-120	-140	-212	-7618	-5884	959	-5459	-8044
O315C-F	-83	-112	-164	-5992	-4286	695	-4039	-6239
O315C-H	-14	-60	-74	-2915	-1301	189	-1279	-2937
O315C-J	20	-2	-1	-96	565	-10	565	-96
O315C-K	20	30	25	1182	941	63	1197	926
O315C-L	8	37	26	1383	647	150	1413	618
O315C-M	4	28	19	1031	418	109	1050	399
O315C-P	5	10	13	495	299	-31	499	294
I315N-N	-54	-15	-19	-694	-1820	56	-691	-1823
O315N-B	-393	-360	-178	-11391	-15193	-2417	-10217	-16367
O315N-C*	0	-227	-96	-7106	-2132	-1752	-1576	-7661
O315N-D	-155	-115	-46	-3385	-5675	-918	-3062	-5998
O315N-E	-139	-43	-19	-1196	-4515	-320	-1165	-4546
O315N-F	-152	0	-11	-66	-4575	141	-61	-4580
O315N-G	-175	12	-9	251	-5183	287	266	-5198
O315N-H	-173	0	-15	-140	-5233	200	-132	-5241
O315N-K	-162	12	-20	-5	-4858	418	30	-4894
O315N-N*	0	10	-14	-69	-21	320	276	-366

Table A.6. Axial force, F_{YN}, on nozzle

AXIAL FORCE LOADING, FYN, CN NOZZLE (500 LB)

	MICRO-STRAIN			STRESSES			PRIN STRESSES	
ROSETTE	GAGE1	GAGE2	GAGE3	TRANS	LONG	SHEAR	SIGMX	SIGMN
I-0-C-B	-77	-10	-49	-1205	-2663	511	-1044	-2824
I-0-C-C	-54	-42	-85	-2727	-2424	574	-1982	-3170
I-0-C-D	-15	-48	-98	-3185	-1416	658	-1199	-3403
I-0-C-F	25	-62	-100	-3594	-340	503	-264	-3670
I-0-C-H	44	-72	-92	-3640	234	268	253	-3659
I-0-C-J	40	-61	-84	-3220	222	310	249	-3248
I-0-C-K	27	-60	-82	-3137	-122	291	-94	-3165
I-0-C-L	8	-50	-66	-2547	-519	209	-498	-2569
I-0-C-M	6	-47	-52	-2182	-460	64	-458	-2184
I-0-C-P	-1	-34	-36	-1538	-505	22	-505	-1538
I-0-C-S	-5	-22	-23	-970	-440	12	-440	-970
O-0-C-B	122	128	118	5273	5249	131	5393	5129
O-0-C-C	91	126	112	5147	4283	185	5185	4245
O-0-C-D	65	121	104	4875	3407	216	4906	3376
O-0-C-E	40	118	98	4701	2608	269	4735	2574
O-0-C-H	15	83	78	3502	1489	66	3504	1486
O-0-C-J	14	70	60	2839	1260	132	2849	1250
O-0-C-K	15	57	54	2425	1162	34	2425	1161
O-0-C-L	15	47	43	1952	1027	47	1955	1025
O-0-C-M	6	39	37	1665	677	31	1666	677
O-0-C-P	3	27	24	1115	437	47	1119	434
O-0-C-S	-3	15	15	662	100	-12	662	100
I-0-N-B	0	11	-3	180	54	193	321	-86
I-0-N-C	-40	86	54	3121	-267	419	3172	-318
I-0-N-D	15	64	60	2713	1254	58	2716	1252
I-0-N-E	29	46	44	1957	1443	23	1958	1442
I-0-N-F	25	32	45	1665	1235	-172	1726	1175
I-0-N-N	28	1	0	-16	838	13	838	-16
O-0-N-B	9	57	66	2704	1074	-125	2714	1064
O-0-N-C	-25	18	29	1056	-431	-136	1069	-444
O-0-N-D	-30	-2	4	80	-869	-70	86	-874
O-0-N-E	-20	-9	-8	-356	-701	-19	-356	-702
O-0-N-F	-6	-13	-11	-527	-336	-20	-335	-529
O-0-N-G	13	-10	-9	-431	275	-19	276	-431
O-0-N-H	19	-7	-9	-375	467	16	467	-375
O-0-N-K	0	-1	-1	-45	-14	-11	-10	-49
O-0-N-N	26	0	2	2	782	-24	782	1

Table A.6 (continued)

AXIAL FORCE LOADING, FYN, ON NOZZLE (500 LB)

	MICRO-STRAIN			STRESSES			PRIN STRESSES	
ROSETTE	GAGE1	GAGE2	GAGE3	TRANS	LONG	SHEAR	SIGMX	SIGMN
I-90C-B	-152	-53	-56	-2228	-5236	39	-2228	-5236
I-90C-C	-90	-56	-37	-1944	-3297	-260	-1896	-3345
I-90C-D	-38	-45	-40	-1826	-1698	-55	-1678	-1846
I-90C-E	-13	-27	-23	-1089	-714	-45	-709	-1095
I-90C-F	7	-17	-13	-679	5	-57	9	-684
I-90C-R	6	-5	-10	-344	91	69	102	-354
O-90C-B*	0	61	90	3306	991	-390	3370	927
O-90C-C	130	109	100	4446	5229	125	5247	4426
O-90C-D	96	92	81	3702	3976	156	4046	3631
O-90C-E	64	62	63	2674	2735	-15	2739	2670
O-90C-F	49	49	49	2106	2109	0	2109	2106
O-90C-R	-7	-17	-12	-635	-405	-64	-389	-651
I-90N-B	-156	13	24	990	-4388	-140	994	-4392
I-90N-C	-19	23	47	1574	-105	-316	1632	-163
I-90N-D	14	12	12	512	560	9	562	510
I-90N-E	20	4	-3	2	599	90	612	-11
I-90N-F	46	-9	-17	-626	1197	106	1203	-632
I-90N-N	20	-8	-1	-221	539	-98	552	-234
O-90N-B	104	101	103	4367	4424	-19	4430	4362
O-90N-C	42	50	58	2327	1971	-110	2359	1940
O-90N-D	-44	25	27	1190	-956	-16	1190	-956
O-90N-E	11	11	14	531	500	-30	550	481
O-90N-F	15	6	8	294	525	-37	530	289
O-90N-N	17	1	1	32	534	0	534	32

Table A.6 (continued)

AXIAL FORCE LOADING, FYN, ON NOZZLE (500 LB)

	MICRO-STRAIN			STRESSES			PRIN STRESSES	
ROSETTE	GAGE1	GAGE2	GAGE3	TRANS	LONG	SHEAR	SIGMX	SIGMN
I180C-B	-84	-79	-24	-2167	-3180	-737	-1779	-3567
I180C-C	-44	-102	-48	-3251	-2284	-715	-1904	-3630
I180C-D	-9	-104	-56	-3518	-1317	-634	-1147	-3688
I180C-E	19	-104	-64	-3712	-558	-545	-467	-3803
I180C-F	29	-99	-67	-3679	-222	-416	-173	-3729
I180C-S	-12	-16	-17	-708	-581	12	-580	-709
O180C-B	116	99	141	5132	5022	-564	5644	4512
O180C-C	88	99	129	4921	4105	-391	5079	3947
O180C-D	62	103	129	5021	3376	-342	5090	3309
O180C-E	43	97	116	4624	2679	-254	4656	2646
O180C-F	31	99	109	4537	2279	-131	4545	2271
O180C-S	-15	15	12	616	-255	35	619	-256
I180N-B	-139	0	57	1392	-3758	-760	1502	-3868
I180N-C	-31	48	76	2775	-85	-374	2823	-133
I180N-D	22	59	63	2662	1468	-59	2665	1465
I180N-E	37	0	35	729	1325	-467	1581	473
I180N-F	34	41	29	1516	1487	162	1664	1339
I180N-N	27	2	-4	-71	779	81	787	-78
O180N-B	12	53	54	2332	1060	-7	2332	1060
O180N-C	-24	0	22	505	-572	-290	577	-646
O180N-D	-25	-1	2	39	-739	-36	40	-740
O180N-E	-13	-12	-9	-437	-516	-44	-417	-536
O180N-F	1	-15	-12	-610	-147	-40	-144	-612
O180N-N	29	-2	3	1	862	-62	867	-4

Table A.6 (continued)

AXIAL FORCE LOADING, FYN, ON NOZZLE (500 LB)

	MICRO-STRAIN			STRESSES			PRIN STRESSES	
ROSETTE	GAGE1	GAGE2	GAGE3	TRANS	LONG	SHEAR	SIGMX	SIGMN
I270C-A*	-96	-72	-79	-3216	-3849	102	-3200	-3865
I270C-B	-247	-116	-129	-5114	-8939	173	-5106	-8947
I270C-C	-154	-104	-110	-4526	-5979	72	-4522	-5983
I270C-D	-90	-79	-83	-3473	-3749	57	-3462	-3760
I270C-E	-47	-58	-63	-2595	-2192	65	-2181	-2605
I270C-F	-16	-40	-43	-1801	-1011	46	-1008	-1804
I270C-H	33	-11	-13	-565	815	31	816	-566
I270C-J	63	8	12	361	1988	-49	1989	359
I270C-K	69	8	18	481	2212	-130	2221	471
I270C-L	64	8	13	393	2050	-63	2052	391
I270C-M	45	-1	2	-16	1342	-36	1342	-17
I270C-P	17	-13	-5	-424	395	-106	409	-437
I270C-R	8	0	-5	-117	190	66	204	-131
I270C-T	0	9	7	351	105	29	355	102
O270C-B	304	202	199	8475	11671	44	11671	8474
O270C-C	227	163	158	6805	8845	66	8847	6802
O270C-D	172	138	134	5795	6902	60	6906	5791
O270C-E	125	118	111	4910	5217	95	5245	4882
O270C-F	93	92	88	3857	3944	49	3965	3836
O270C-H	35	49	49	2119	1684	7	2119	1684
O270C-J	-9	7	7	329	-179	2	329	-179
O270C-K	-31	-15	-17	-686	-1141	26	-685	-1142
O270C-L	-41	-33	-34	-1416	-1655	15	-1415	-1656
O270C-M	-32	-29	-32	-1299	-1344	35	-1279	-1362
O270C-P	-10	-14	-19	-719	-510	59	-494	-735
O270C-R	-2	-7	-14	-456	-195	87	-169	-482
O270C-T	1	10	8	382	151	25	385	149
I270N-A	-133	-29	-26	-1062	-4307	-52	-1061	-4308
I270N-B	-163	32	8	1058	-4560	309	1075	-4577
I270N-C	6	51	38	1939	768	180	1966	740
I270N-D	64	31	23	1127	2272	101	2281	1118
I270N-E	79	7	7	225	2450	0	2450	225
I270N-F	72	-7	-8	-414	2045	15	2045	-414
I270N-N	0	5	-2	52	16	98	133	-66
O270N-B	185	113	136	5280	7137	-313	7188	5229
O270N-C	84	81	86	3577	3607	-72	3665	3519
O270N-D	45	42	46	1879	1902	-59	1950	1830
O270N-E	38	18	20	796	1384	-15	1384	796
O270N-F	40	10	7	334	1302	34	1304	332
O270N-G	48	4	7	204	1499	-36	1500	202
O270N-H	50	7	9	313	1592	-27	1592	311
O270N-K	40	5	3	134	1237	31	1237	132
O270N-N	36	0	2	0	1076	-34	1076	-1

Table A.6 (continued)

AXIAL FORCE LOADING, FYN, CN NOZZLE (500 LB)

	MICRO-STRAIN			STRESSES			PRIN STRESSES	
ROSETTE	GAGE1	GAGE2	GAGE3	TRANS	LONG	SHEAR	SIGMX	SIGMN
I315C-B	-167	-22	-174	-4124	-6250	2022	-2902	-7472
I315C-C	-93	-25	-182	-4457	-4134	2086	-2203	-6388
I315C-D	-50	-20	-159	-3883	-2658	1862	-1311	-5230
I315C-E	-18	-15	-147	-3543	-1589	1750	-562	-4570
I315C-F	7	-10	-137	-3231	-774	1685	83	-4088
I315C-H	29	4	-106	-2282	184	1462	863	-2961
I315C-J	45	-5	-76	-1821	790	941	1094	-2125
I315C-K	47	-16	-48	-1453	968	417	1038	-1523
I315C-L	36	-9	-13	-521	911	57	913	-524
I315C-M	29	-8	15	117	892	-311	1002	8
I315C-P	19	-5	27	473	717	-425	1037	153
0315C-B	204	209	94	6420	8036	1536	8964	5492
0315C-C	153	200	87	6141	6420	1517	7805	4756
0315C-D	106	180	83	5646	4884	1295	6615	3915
0315C-E	73	162	73	5085	3729	1174	5762	3051
0315C-F	63	139	59	4285	3185	1071	4940	2530
0315C-H	30	99	44	3109	1825	731	3440	1494
0315C-J	15	52	28	1741	962	311	1851	854
0315C-K	9	22	21	917	556	15	919	556
0315C-L	5	-8	10	20	144	-239	327	-164
0315C-M	-1	-22	1	-451	-169	-301	22	-642
0315C-P	-9	-30	-8	-831	-520	-289	-346	-1004
I315N-N	24	3	13	324	812	-136	847	289
0315N-B	112	125	87	4522	4717	507	5136	4104
0315N-C	0	73	53	2786	836	267	2822	800
0315N-D	8	33	17	1100	567	217	1177	490
0315N-E	9	14	-2	262	359	215	531	91
0315N-F	19	0	-9	-224	494	124	515	-244
0315N-G	34	2	-7	-150	960	117	972	-162
0315N-H	37	-1	-3	-128	1077	38	1078	-129
0315N-K	37	-2	3	-19	1096	-79	1102	-25
0315N-N	0	0	2	44	12	-17	51	5

Table A.7. Out-of-plane force, F_{ZN}, on nozzle

OUT-OF-PLANE FORCE LOADING, FZN, ON NOZZLE (80 LB)

	MICRO-STRAIN			STRESSES			PRIN STRESSES	
ROSETTE	GAGE1	GAGE2	GAGE3	TRANS	LONG	SHEAR	SIGMX	SIGMN
I-0-C-B	1	-219	169	-1115	-292	-5171	4484	-5890
I-0-C-C	7	-234	207	-598	33	-5879	5605	-6170
I-0-C-D	-2	-229	207	-485	-197	-5812	5473	-6155
I-0-C-F	5	-181	166	-331	53	-4622	4487	-4765
I-0-C-H	-3	-122	110	-252	-174	-3094	2881	-3308
I-0-C-J	-1	-85	72	-286	-130	-2082	1876	-2292
I-0-C-K	3	-58	44	-326	-5	-1356	1200	-1531
I-0-C-L	4	-36	24	-274	48	-793	696	-922
I-0-C-M	-2	-25	17	-189	-114	-557	407	-710
I-0-C-P	-5	-13	7	-117	-183	-268	121	-420
I-0-C-S	-5	-8	1	-139	-197	-113	-51	-285
O-0-C-B	-4	-49	27	-475	-267	-1021	655	-1397
O-0-C-C	-3	-94	77	-352	-209	-2277	1998	-2559
O-0-C-D	5	-96	80	-367	37	-2350	2194	-2523
O-0-C-E	5	-90	79	-256	82	-2256	2176	-2350
O-0-C-H	3	-55	47	-181	25	-1349	1275	-1431
O-0-C-J	-2	-31	31	-1	-60	-818	788	-849
O-0-C-K	-1	-21	21	-10	-25	-553	536	-571
O-0-C-L	-2	-13	11	-34	-77	-320	265	-376
O-0-C-M	-1	-11	8	-61	-42	-247	196	-299
O-0-C-P	-2	-6	4	-47	-61	-140	86	-194
O-0-C-S	-2	-4	2	-39	-61	-82	32	-133
I-0-N-B*	0	-2	66	1422	427	-903	1956	-106
I-0-N-C	-25	-38	118	1797	-225	-2078	3097	-1525
I-0-N-D	5	24	27	1115	496	-53	1120	491
I-0-N-E	17	40	-7	702	724	616	1329	97
I-0-N-F*	-8	36	-18	399	-121	711	896	-618
I-0-N-N	-3	9	-12	-53	-111	273	193	-357
O-0-N-B	-7	66	-90	-507	-374	2079	1640	-2520
O-0-N-C	-5	50	-59	-188	-204	1448	1253	-1644
O-0-N-D	-5	24	-35	-233	-209	795	574	-1016
O-0-N-E	-3	7	-13	-126	-128	267	140	-394
O-0-N-F	-3	-6	-2	-163	-149	-51	-104	-208
O-0-N-G	-3	-14	7	-150	-128	-279	141	-418
O-0-N-H	-3	-13	6	-142	-125	-250	117	-383
O-0-N-K	0	-11	6	-108	-32	-222	155	-296
O-0-N-N	-2	-11	6	-106	-87	-227	130	-324

Table A.7 (continued)

OUT-OF-PLANE FORCE LOADING, FZN, ON NOZZLE (80 LB)

	MICRO-STRAIN			STRESSES			PRIN STRESSES	
ROSETTE	GAGE1	GAGE2	GAGE3	TRANS	LONG	SHEAR	SIGMX	SIGMN
I-90C-B	-501	-315	-306	-13103	-18948	-113	-13101	-18950
I-90C-C	-356	-288	-278	-12049	-14293	-127	-12042	-14300
I-90C-D	-249	-227	-236	-9907	-10436	118	-9882	-10462
I-90C-E	-188	-181	-182	-7790	-7980	12	-7789	-7981
I-90C-F	-144	-136	-143	-5980	-6112	89	-5935	-6156
I-90C-R	6	-4	-6	-222	123	19	124	-223
O-90C-B*	0	167	236	8849	2655	-913	8981	2523
O-90C-C	419	333	303	13529	16623	405	16675	13477
O-90C-D	332	294	252	11656	13463	559	13622	11497
O-90C-E	271	226	217	9443	10976	117	10984	9434
O-90C-F	229	192	188	8109	9306	54	9308	8107
O-90C-R	-4	-6	-5	-235	-199	-12	-196	-239
I-90N-B	-504	-76	-48	-2168	-15775	-363	-2158	-15785
I-90N-C	-64	18	104	2748	-1099	-1138	3059	-1411
I-90N-D	35	42	51	2022	1650	-120	2057	1615
I-90N-E	63	26	9	715	2100	226	2136	680
I-90N-F	166	30	13	771	5199	223	5210	760
I-90N-N	72	-28	0	-709	1952	-370	2003	-759
O-90N-B	408	303	305	12913	16128	-20	16128	12913
O-90N-C	241	160	184	7298	9416	-314	9461	7252
O-90N-D	203	92	86	3690	7211	81	7213	3688
O-90N-E	135	37	40	1542	4509	-41	4510	1541
O-90N-F	143	11	15	415	4419	-59	4420	414
O-90N-N	95	7	-6	-78	2830	169	2839	-87

Table A.7 (continued)

OUT-OF-PLANE FORCE LOADING, FZN, ON NOZZLE (80 LB)

	MICRO-STRAIN			STRESSES			PRIN STRESSES	
ROSETTE	GAGE1	GAGE2	GAGE3	TRANS	LONG	SHEAR	SIGMX	SIGMN
I180C-B	-1	233	-175	1293	372	5435	6287	-4622
I180C-C	-5	255	-193	1386	259	5968	6817	-5172
I180C-D	-12	219	-186	725	-137	5400	5711	-5124
I180C-E	-8	210	-175	782	-7	5125	5527	-4753
I180C-F	-9	178	-152	578	-105	4402	4652	-4179
I180C-S	-2	-5	1	-92	-86	-86	-3	-175
O180C-B	0	50	-69	-429	-132	1584	1310	-1871
O180C-C	1	81	-109	-620	-166	2530	2148	-2933
O180C-D	5	81	-108	-597	-37	2507	2206	-2840
O180C-S	0	4	-5	-9	-1	117	112	-122
I180N-B	-51	232	-183	1119	-1181	5531	5618	-5680
I180N-C	-12	83	-53	670	-162	1818	2119	-1610
I180N-D	2	3	13	354	177	-136	428	104
I180N-E	4	0	30	648	324	-395	913	59
I180N-F	3	-29	27	-32	75	-743	767	-724
I180N-N	7	-12	6	-152	163	-238	291	-280
O180N-B	-12	-79	35	-967	-638	-1520	727	-2332
O180N-C*	-9	0	36	807	-34	-483	1026	-254
O180N-D	-8	-31	17	-300	-318	-650	341	-959
O180N-E	-9	-10	5	-100	-297	-213	36	-433
O180N-F	-8	3	-5	-42	-242	106	3	-288
O180N-N	-5	5	-12	-162	-202	230	49	-413

Table A.7 (continued)

OUT-OF-PLANE FORCE LOADING, FZN, ON NOZZLE (80 LB)

	MICRO-STRAIN			STRESSES			PRIN STRESSES	
ROSETTE	GAGE1	GAGE2	GAGE3	TRANS	LONG	SHEAR	SIGMX	SIGMN
I270C-A*	154	256	289	11801	8157	-439	11853	8104
I270C-B	494	320	338	13910	18986	-233	18996	13899
I270C-C	341	276	276	11758	13742	1	13742	11758
I270C-D	241	215	215	9178	9990	1	9990	9178
I270C-E	172	166	172	7235	7337	-81	7382	7191
I270C-F	122	129	129	5546	5334	-6	5546	5334
I270C-H	49	63	63	2723	2279	-1	2723	2279
I270C-J	-9	13	11	532	-110	17	532	-110
I270C-K	-30	-7	-13	-414	-1037	72	-406	-1045
I270C-L	-41	-20	-22	-883	-1495	30	-881	-1496
I270C-M	-34	-14	-14	-572	-1181	-5	-571	-1181
I270C-P	-17	-1	-4	-100	-552	47	-96	-557
I270C-R	-12	0	-2	-30	-359	26	-28	-362
I270C-T	0	-2	-3	-100	-30	12	-28	-102
O270C-B	-584	-386	-402	-16671	-22533	211	-16664	-22541
O270C-C	-437	-304	-293	-12632	-16890	-146	-12627	-16895
O270C-D	-343	-265	-256	-11062	-13603	-118	-11057	-13608
O270C-E	-268	-236	-218	-9691	-10962	-234	-9650	-11003
O270C-F	-218	-194	-184	-8060	-8951	-128	-8042	-8969
O270C-H	-125	-128	-128	-5488	-5402	1	-5402	-5488
O270C-J	-58	-62	-62	-2661	-2536	-8	-2536	-2661
O270C-K	-15	-23	-23	-999	-751	9	-751	-999
O270C-L	17	9	9	390	621	1	621	390
O270C-M	21	15	16	670	846	-12	847	670
O270C-P	12	9	10	393	487	-15	490	391
O270C-R	6	5	6	246	252	-15	264	234
O270C-T	-1	0	0	3	-26	-3	4	-26
I270N-A	211	182	152	7097	8449	399	8558	6988
I270N-B	320	6	28	402	9735	-301	9745	392
I270N-C	4	-73	-54	-2806	-732	-259	-700	-2838
I270N-D	-120	-67	-54	-2534	-4369	-168	-2519	-4384
I270N-E	-163	-42	-41	-1647	-5382	-3	-1647	-5382
I270N-F	-165	-22	-21	-767	-5166	-16	-767	-5166
I270N-N*	0	-10	4	-142	-43	-183	97	-282
O270N-B	-421	-295	-283	-12243	-16310	-168	-12236	-16317
O270N-C	-227	-161	-168	-6984	-8909	89	-6980	-8913
O270N-D	-154	-84	-89	-3646	-5700	67	-3644	-5702
O270N-E	-136	-39	-40	-1604	-4559	14	-1603	-4559
O270N-F	-138	-14	-12	-414	-4255	-27	-414	-4255
O270N-G	-158	0	-4	76	-4704	53	77	-4704
O270N-H	-165	-1	-8	-18	-4964	93	-17	-4966
O270N-K	-152	-13	2	-71	-4593	-202	-62	-4602
O270N-N	-102	-4	-4	-58	-3090	-2	-58	-3090

Table A.7 (continued)

OUT-OF-PLANE FORCE LOADING, FZN, ON NOZZLE (80 LB)

	MICRO-STRAIN			STRESSES			PRIN STRESSES	
ROSETTE	GAGE1	GAGE2	GAGE3	TRANS	LONG	SHEAR	SIGMX	SIGMN
I315C-B	319	67	400	9906	12542	-4435	15851	6597
I315C-C	214	45	404	9628	9307	-4782	14253	4683
I315C-D	159	21	342	7811	7108	-4271	11745	3174
I315C-E	114	8	311	6897	5481	-4036	10287	2092
I315C-F	78	-1	286	6156	4198	-3824	9124	1230
I315C-H	50	-20	214	4189	2766	-3118	6675	279
I315C-J	11	-8	165	3440	1355	-2299	4923	-127
I315C-K	-11	11	122	2943	560	-1487	3657	-154
I315C-L	-10	4	70	1657	198	-880	2070	-215
I315C-M	-17	10	38	1069	-195	-367	1168	-293
I315C-P	-18	0	3	72	-515	-36	75	-517
O315C-B	-335	-352	-134	-10306	-13154	-2899	-8500	-14960
O315C-C	-246	-354	-114	-10028	-10399	-3197	-7011	-13416
O315C-D	-171	-327	-104	-9284	-7929	-2969	-5561	-11652
O315C-E	-117	-299	-93	-8502	-6075	-2747	-4286	-10292
O315C-F	-102	-266	-73	-7332	-5261	-2563	-3533	-9060
O315C-H	-50	-205	-61	-5799	-3235	-1911	-2216	-6818
O315C-J	-27	-138	-48	-4072	-2040	-1195	-1487	-4625
O315C-K	-15	-94	-40	-2946	-1334	-717	-1061	-3219
O315C-L	-14	-49	-34	-1791	-949	-198	-905	-1835
O315C-M	-11	-24	-24	-1041	-640	5	-640	-1041
O315C-P	-4	2	-11	-202	-183	173	-19	-366
I315N-N	-42	-4	-31	-722	-1470	357	-579	-1613
O315N-B	-272	-175	-237	-8760	-10798	822	-8471	-11088
O315N-C	0	-77	-156	-5112	-1533	1058	-1244	-5401
O315N-D	-99	-25	-91	-2450	-3707	873	-2003	-4154
O315N-E	-93	-3	-36	-759	-3027	439	-677	-3109
O315N-F	-102	0	-12	-146	-3098	156	-137	-3107
O315N-G	-118	-1	5	210	-3470	-87	212	-3472
O315N-H	-118	-3	3	136	-3509	-81	138	-3510
O315N-K	-107	-5	-1	-18	-3221	-61	-17	-3222
O315N-N*	0	-6	1	-123	-37	-92	22	-182

Table A.8. Torsional moment loading, M_{XC}, on cylinder

TORSIONAL MOMENT LOADING, MXC, ON CYLINDER (40000 IN-LB)

	MICRO-STRAIN			STRESSES			PRIN STRESSES	
ROSETTE	GAGE1	GAGE2	GAGE3	TRANS	LONG	SHEAR	SIGMX	SIGMN
I-0-C-B	2	-64	61	-70	39	-1664	1649	-1681
I-0-C-C	5	-69	68	-19	135	-1824	1884	-1768
I-0-C-D	1	-68	68	-15	39	-1810	1822	-1798
I-0-C-F	4	-57	56	-24	102	-1507	1547	-1469
I-0-C-H	2	-50	48	-53	33	-1298	1289	-1309
I-0-C-J	3	-50	46	-105	54	-1281	1258	-1310
I-0-C-K	7	-49	41	-165	146	-1198	1198	-1218
I-0-C-L	11	-53	42	-243	252	-1270	1298	-1289
I-0-C-M	2	-49	46	-88	45	-1267	1248	-1290
I-0-C-P	-1	-44	48	100	-7	-1224	1272	-1179
I-0-C-S	-3	-44	44	7	-86	-1167	1128	-1207
O-0-C-B	-1	92	-87	120	5	2379	2442	-2317
O-0-C-C	3	72	-70	50	114	1886	1969	-1804
O-0-C-D	0	74	-67	154	38	1887	1984	-1792
O-0-C-E	1	70	-65	107	58	1805	1888	-1722
O-0-C-H	-1	58	-57	27	-25	1540	1541	-1539
O-0-C-J	3	52	-56	-90	61	1440	1428	-1456
O-0-C-K	0	50	-54	-89	-28	1390	1332	-1449
O-0-C-L	2	47	-49	-40	42	1284	1286	-1284
O-0-C-M	-1	50	-46	103	7	1278	1334	-1224
O-0-C-P	4	47	-50	-77	88	1301	1309	-1298
O-0-C-S	-2	51	-49	42	-44	1328	1328	-1330
I-0-N-B	0	7	11	394	118	-61	407	105
I-0-N-C	6	27	36	1383	584	-120	1401	566
I-0-N-D	4	12	15	591	307	-33	595	303
I-0-N-E	3	3	18	449	220	-203	568	101
I-0-N-F	2	0	12	250	128	-160	360	17
I-0-N-N	0	0	1	6	-10	-12	13	-16
O-0-N-B	0	27	-30	-65	-32	750	702	-799
O-0-N-C	-1	-1	3	43	-26	-59	76	-60
O-0-N-D	-2	-11	14	81	-38	-332	359	-316
O-0-N-E	-3	-13	17	83	-62	-398	415	-394
O-0-N-F	-2	-14	15	36	-50	-389	384	-398
O-0-N-G	-1	-13	13	1	-18	-340	332	-349
O-0-N-H	-1	-11	11	-7	-43	-292	268	-317
O-0-N-K	0	-2	1	-34	-10	-43	23	-67
O-0-N-N	0	0	-1	-18	-12	14	-1	-29

Table A.8 (continued)

TORSIONAL MOMENT LOADING, MXC, ON CYLINDER (40000 IN-LB)

	MICRO-STRAIN			STRESSES			PRIN STRESSES	
ROSETTE	GAGE1	GAGE2	GAGE3	TRANS	LONG	SHEAR	SIGMX	SIGMN
I-90C-B	5	66	-65	25	150	1739	1827	-1652
I-90C-C	5	70	-70	3	152	1866	1945	-1790
I-90C-D	3	65	-64	10	96	1721	1775	-1669
I-90C-E	0	59	-62	-48	-6	1610	1583	-1637
I-90C-F	2	58	-56	40	71	1509	1565	-1454
I-90C-R	3	39	-49	-208	15	1173	1082	-1275
O-90C-B	0	-49	50	27	8	-1313	1330	-1296
O-90C-C	4	-73	63	-237	53	-1817	1731	-1914
O-90C-D	3	-70	60	-226	12	-1734	1631	-1845
O-90C-E	6	-69	59	-226	110	-1706	1656	-1772
O-90C-F	3	-66	64	-48	79	-1743	1760	-1729
O-90C-R	1	-50	44	-141	-22	-1254	1174	-1337
I-90N-B	-1	0	-1	-10	-37	10	-7	-40
I-90N-C	-1	4	-26	-471	-173	401	106	-750
I-90N-D	0	13	-13	1	-12	337	332	-343
I-90N-E	0	12	-7	112	21	257	327	-195
I-90N-F	-1	6	-1	114	9	85	162	-39
I-90N-N	-1	0	0	5	-18	4	5	-19
O-90N-B	-1	-35	34	-26	-26	-924	897	-950
O-90N-C	1	-4	-2	-127	-22	-33	-12	-137
O-90N-D	3	7	-14	-142	48	279	247	-342
O-90N-E	2	12	-17	-118	38	392	360	-440
O-90N-F	2	12	-17	-119	25	381	341	-435
O-90N-N	0	-1	0	-14	-14	-9	-5	-23

Table A.8 (continued)

TORSIONAL MOMENT LOADING, MXC, ON CYLINDER (40000 IN-LB)

	MICRO-STRAIN			STRESSES			PRIN STRESSES	
ROSETTE	GAGE1	GAGE2	GAGE3	TRANS	LONG	SHEAR	SIGMX	SIGMN
I180C-B	8	-63	66	46	245	-1718	1866	-1576
I180C-C	5	-69	69	-26	153	-1838	1904	-1777
I180C-D	5	-61	65	77	168	-1681	1804	-1559
I180C-E	1	-63	61	-33	10	-1650	1638	-1661
I180C-F	2	-57	56	-18	48	-1496	1511	-1481
I180C-S	0	45	-46	-26	-8	1215	1198	-1231
O180C-B	6	80	-89	-222	104	2253	2201	-2318
O180C-C	4	68	-69	-16	104	1827	1872	-1783
O180C-D	5	67	-70	-83	115	1829	1848	-1816
O180C-E	4	63	-66	-58	111	1720	1748	-1696
O180C-F	3	62	-64	-54	83	1681	1697	-1668
O180C-S	7	43	-50	-150	160	1242	1257	-1246
I180N-B	0	-16	-17	-744	-224	12	-224	-744
I180N-C	-2	-17	-7	-517	-206	-137	-154	-568
I180N-D	-1	-14	-1	-318	-118	-179	-13	-423
I180N-E	0	0	3	61	9	-37	80	-10
I180N-F	1	-8	4	-83	2	-167	132	-213
I180N-N	0	0	0	6	-5	-6	9	-8
O180N-B	-2	18	-16	56	-44	457	465	-454
O180N-C	1	0	2	45	53	-28	78	20
O180N-D	2	-14	5	-216	0	-254	168	-384
O180N-E	2	-16	15	-25	55	-424	440	-411
O180N-F	2	-16	13	-72	44	-394	384	-413
O180N-N	0	-1	-1	-40	-19	9	-16	-43

Table A.8 (continued)

TORSIONAL MOMENT LOADING, MXC, ON CYLINDER (40000 IN-LB)

	MICRO-STRAIN			STRESSES			PRIN STRESSES	
ROSETTE	GAGE1	GAGE2	GAGE3	TRANS	LONG	SHEAR	SIGMX	SIGMN
I270C-A	-9	51	-33	403	-145	1121	1283	-1025
I270C-B	1	69	-67	30	49	1813	1853	-1774
I270C-C	-1	76	-71	104	-10	1963	2010	-1917
I270C-D	-1	69	-64	119	15	1772	1840	-1706
I270C-E	1	64	-60	94	54	1660	1735	-1586
I270C-F	1	59	-56	60	47	1540	1594	-1486
I270C-H	0	54	-51	62	32	1398	1445	-1352
I270C-J	5	47	-49	-49	123	1273	1313	-1239
I270C-K	0	42	-45	-74	-30	1165	1113	-1218
I270C-L	-3	49	-42	150	-45	1204	1260	-1155
I270C-M	-4	48	-42	136	-88	1199	1228	-1179
I270C-P*	4	46	-47	-36	116	1240	1283	-1202
I270C-R*	2	0	-47	-1045	-258	633	93	-1397
I270C-T	0	47	-44	50	15	1209	1242	-1177
O270C-B	-1	-80	89	183	13	-2253	2352	-2157
O270C-C	-4	-69	72	60	-107	-1880	1858	-1905
O270C-D	2	-67	67	2	49	-1790	1815	-1764
O270C-E	1	-67	65	-54	6	-1752	1728	-1777
O270C-F	-1	-63	64	25	-12	-1684	1691	-1678
O270C-H	-2	-57	59	57	-29	-1548	1563	-1535
O270C-J	1	-54	58	80	40	-1488	1548	-1428
O270C-K	4	-47	55	173	166	-1369	1539	-1199
O270C-L	3	-53	51	-55	84	-1385	1401	-1373
O270C-M	1	-47	50	58	60	-1291	1350	-1232
O270C-P	-5	-48	49	31	-132	-1287	1240	-1340
O270C-R	1	-48	49	4	19	-1292	1303	-1280
O270C-T	2	-53	44	-199	-2	-1282	1185	-1386
I270N-A	-7	11	38	1093	110	-362	1212	-9
I270N-B	8	40	31	1557	722	119	1573	705
I270N-C	9	31	20	1118	611	139	1153	575
I270N-D	10	27	11	827	540	203	932	434
I270N-E	7	24	7	659	396	225	788	267
I270N-F	5	19	3	481	294	205	613	162
I270N-N	0	-1	0	-13	-4	-7	0	-17
O270N-B	0	-37	34	-77	-19	-939	892	-988
O270N-C	-1	-2	1	-10	-37	-34	14	-60
O270N-D	-2	12	-10	48	-39	288	296	-286
O270N-E	-1	16	-15	20	-31	404	399	-410
O270N-F	0	14	-12	45	9	354	381	-328
O270N-G	1	12	-12	3	18	315	326	-305
O270N-H	-1	11	-11	-15	-29	293	271	-316
O270N-K	-1	2	-1	24	-15	48	56	-47
O270N-N	0	1	-1	-8	-15	25	14	-37

Table A.8 (continued)

TORSIONAL MOMENT LOADING, MXC, ON CYLINDER (40000 IN-LB)

	MICRO-STRAIN			STRESSES			PRIN STRESSES	
ROSETTE	GAGE1	GAGE2	GAGE3	TRANS	LONG	SHEAR	SIGMX	SIGMN
I315C-B	2	-67	-59	-2781	-769	-104	-764	-2787
I315C-C	16	-58	-50	-2376	-239	-105	-233	-2381
I315C-D	23	-50	-43	-2059	66	-100	71	-2064
I315C-E	30	-48	-41	-1990	298	-94	302	-1994
I315C-F	34	-41	-39	-1809	463	-29	463	-1810
I315C-H	42	-30	-41	-1595	773	143	782	-1603
I315C-J	47	-32	-34	-1511	955	30	956	-1511
I315C-K	54	-38	-27	-1493	1177	-144	1184	-1501
I315C-L	55	-25	-33	-1354	1232	108	1237	-1359
I315C-M	55	-34	-24	-1329	1264	-135	1271	-1336
I315C-P	55	-26	-27	-1233	1286	5	1286	-1233
O315C-B	27	-27	-18	-1016	511	-120	520	-1025
O315C-C	34	-24	-17	-930	751	-96	757	-935
O315C-D	41	-21	-18	-892	950	-37	951	-893
O315C-E	43	-21	-19	-935	995	-22	995	-935
O315C-F	46	-21	-19	-919	1098	-21	1098	-919
O315C-H	51	-21	-24	-1040	1214	35	1215	-1040
O315C-J	54	-25	-21	-1066	1313	-44	1314	-1066
O315C-K	57	-25	-24	-1157	1358	-14	1358	-1157
O315C-L	57	-29	-28	-1321	1324	-7	1324	-1321
O315C-M	59	-31	-28	-1353	1358	-32	1359	-1353
O315C-P	61	-33	-24	-1316	1428	-125	1434	-1322
I315N-N	1	0	0	2	18	1	18	2
O315N-B	6	-3	8	94	200	-149	305	-12
O315N-C	0	23	25	1058	317	-31	1059	316
O315N-D	-17	27	28	1239	-148	-18	1239	-148
O315N-E	-23	26	23	1088	-355	40	1089	-356
O315N-F	-25	0	16	372	-627	-209	415	-669
O315N-G	-21	10	9	447	-503	5	447	-503
O315N-H	-18	9	5	322	-430	45	324	-433
O315N-K	-5	-1	-2	-54	-172	8	-54	-172
O315N-N	0	-1	0	-27	-8	-7	-6	-29

Table A.9. Out-of-plane moment loading, M_{YC}, on cylinder

OUT-OF-PLANE MOMENT LOADING, MYC, ON CYLINDER (40000 IN-LB)

	MICRO-STRAIN			STRESSES			PRIN STRESSES	
ROSETTE	GAGE1	GAGE2	GAGE3	TRANS	LONG	SHEAR	SIGMX	SIGMN
I-0-C-B	5	2	6	173	213	-46	243	143
I-0-C-C	6	5	6	229	235	-7	240	225
I-0-C-D	7	5	4	205	263	15	266	201
I-0-C-F	5	6	5	248	220	15	255	214
I-0-C-H	8	5	4	192	283	16	286	189
I-0-C-J	7	5	4	177	251	16	255	174
I-0-C-K	11	9	5	300	407	58	433	275
I-0-C-L	9	9	6	310	368	46	393	285
I-0-C-M	8	7	5	258	307	33	323	241
I-0-C-P	7	7	6	261	288	11	292	257
I-0-C-S	7	7	6	283	298	9	302	278
O-0-C-B	1	0	-2	-56	8	26	17	-66
O-0-C-C	1	1	-1	-12	27	24	39	-24
O-0-C-D	-2	-4	-1	-112	-103	-41	-67	-149
O-0-C-E	-1	-3	-3	-132	-72	6	-71	-133
O-0-C-H	4	1	-2	-29	108	42	119	-41
O-0-C-J	4	0	-1	-39	95	18	98	-41
O-0-C-K	3	-2	0	-49	76	-24	80	-53
O-0-C-L	3	0	-2	-40	70	30	78	-48
O-0-C-M	2	0	0	9	62	5	63	9
O-0-C-P	3	-3	-2	-97	48	-13	49	-98
O-0-C-S	4	-2	-2	-97	81	7	82	-97
I-0-N-B	0	6	7	297	89	-9	297	89
I-0-N-C	4	3	7	209	182	-58	255	136
I-0-N-D	5	2	5	143	185	-36	206	122
I-0-N-E	6	2	3	111	207	-21	211	107
I-0-N-F	5	2	3	93	180	-11	182	91
I-0-N-N	3	3	2	102	116	20	130	88
O-0-N-B	6	3	10	288	267	-86	365	191
O-0-N-C	6	6	9	323	271	-47	350	244
O-0-N-D	4	3	7	208	184	-60	257	135
O-0-N-E	5	1	4	115	180	-41	200	95
O-0-N-F	1	-1	2	13	24	-33	52	-15
O-0-N-G	-3	0	0	3	-86	6	3	-87
O-0-N-H	-1	0	0	0	-19	1	0	-20
O-0-N-K	0	-1	0	-32	-10	-11	-5	-36
O-0-N-N	-2	-2	-3	-117	-95	6	-94	-119

Table A.9 (continued)

OUT-OF-PLANE MOMENT LOADING, MYC, ON CYLINDER (40000 IN-LB)

	MICRO-STRAIN			STRESSES			PRIN STRESSES	
ROSETTE	GAGE1	GAGE2	GAGE3	TRANS	LONG	SHEAR	SIGMX	SIGMN
I-90C-B	9	-2	0	-58	252	-32	255	-61
I-90C-C	8	-6	-3	-201	189	-34	192	-204
I-90C-D	10	-6	-4	-235	231	-21	232	-236
I-90C-E	11	-6	-2	-187	280	-42	284	-191
I-90C-F	12	-6	-4	-244	301	-21	302	-245
I-90C-R	26	-55	-50	-2337	89	-58	90	-2339
O-90C-B	0	-8	-7	-319	-96	-7	-96	-319
O-90C-C	-1	-9	-9	-382	-140	3	-140	-382
O-90C-D	0	-11	-10	-455	-132	-10	-132	-455
O-90C-E	1	-13	-13	-557	-131	3	-131	-557
O-90C-F	2	-16	-16	-689	-137	2	-137	-689
O-90C-R	22	-59	-67	-2780	-164	110	-159	-2785
I-90N-B	3	0	0	-5	97	2	97	-5
I-90N-C	3	2	2	67	112	0	112	67
I-90N-D	2	3	3	126	109	-7	129	107
I-90N-E	2	4	4	192	132	0	192	132
I-90N-F	2	4	5	191	132	-9	192	131
I-90N-N	3	3	2	125	131	15	143	112
O-90N-B	0	-3	-4	-149	-49	9	-48	-149
O-90N-C	-1	-2	-2	-88	-51	-5	-51	-89
O-90N-D	4	-2	-3	-121	73	11	74	-121
O-90N-E	1	0	0	-5	36	5	37	-5
O-90N-F	1	0	-1	-26	17	9	19	-27
O-90N-N	-1	-1	0	-20	-32	-4	-19	-34

Table A.9 (continued)

OUT-OF-PLANE MOMENT LOADING, MYC, ON CYLINDER (40000 IN-LB)

	MICRO-STRAIN			STRESSES			PRIN STRESSES	
ROSETTE	GAGE1	GAGE2	GAGE3	TRANS	LONG	SHEAR	SIGMX	SIGMN
I180C-B	3	8	2	212	143	86	270	85
I180C-C	5	7	2	192	216	68	273	135
I180C-D	7	8	4	260	282	50	322	220
I180C-E	9	8	3	238	336	57	362	212
I180C-F	7	6	4	224	292	30	303	212
I180C-S	8	6	5	234	312	2	312	234
O180C-B	11	11	8	404	465	30	477	392
O180C-C	11	10	7	347	442	41	457	332
O180C-D	11	8	9	350	437	-20	441	346
O180C-E	11	7	7	300	407	5	407	300
O180C-F	9	7	7	291	367	1	367	291
O180C-S	7	5	7	238	267	-28	285	221
I180N-B	2	2	-1	10	51	33	69	-8
I180N-C	6	7	3	221	241	47	279	183
I180N-D	6	7	3	201	245	55	282	164
I180N-E	6	0	2	45	202	-31	208	39
I180N-F	7	5	4	194	256	2	256	194
I180N-N	6	7	6	281	275	4	282	273
O180N-B	7	10	9	416	327	8	417	326
O180N-C	7	0	9	186	260	-117	346	100
O180N-D	8	10	7	366	340	28	384	322
O180N-E	6	8	6	307	277	18	315	268
O180N-F	6	7	7	282	256	1	282	256
O180N-N	1	2	1	62	61	12	74	50

Table A.9 (continued)

OUT-OF-PLANE MOMENT LOADING, MYC, ON CYLINDER (40000 IN-LB)

	MICRO-STRAIN			STRESSES			PRIN STRESSES	
ROSETTE	GAGE1	GAGE2	GAGE3	TRANS	LONG	SHEAR	SIGMX	SIGMN
I270C-A	1	20	26	1006	329	-74	1014	321
I270C-B	2	20	21	905	343	-20	906	342
I270C-C	1	18	20	844	279	-24	845	278
I270C-D	0	20	21	911	268	-20	912	267
I270C-E	-2	21	24	993	238	-40	995	236
I270C-F	-2	23	24	1019	233	-15	1019	232
I270C-H	-5	26	25	1114	182	12	1114	182
I270C-J	-8	32	30	1375	181	36	1376	180
I270C-K	-6	40	38	1727	333	28	1728	333
I270C-L	-14	48	47	2093	196	15	2093	195
I270C-M	-16	49	56	2323	228	-91	2327	224
I270C-P	-18	68	62	2884	331	72	2886	329
I270C-R*	-18	0	63	1409	-106	-843	1785	-481
I270C-T*	0	0	4	76	23	-59	114	-15
O270C-B	5	17	15	706	366	29	708	364
O270C-C	3	19	18	789	330	13	790	330
O270C-D	3	20	21	890	368	-6	890	367
O270C-E	2	18	22	875	334	-56	881	328
O270C-F	1	21	20	899	289	11	899	289
O270C-H	-2	24	24	1067	255	0	1067	255
O270C-J	-4	30	29	1305	273	11	1306	273
O270C-K	-5	37	38	1664	362	-8	1664	362
O270C-L	-9	47	51	2160	383	-64	2162	381
O270C-M	-10	59	57	2546	476	23	2546	476
O270C-P	-13	68	64	2921	478	56	2922	477
O270C-R	-14	70	68	3058	493	34	3059	492
O270C-T*	6	4	2	128	215	37	229	114
I270N-A	0	26	27	1157	334	-17	1158	334
I270N-B	8	18	17	770	468	14	771	467
I270N-C	7	12	12	506	370	-5	507	370
I270N-D	5	6	6	266	233	-1	266	233
I270N-E	3	4	5	194	160	-5	195	159
I270N-F	3	3	4	145	119	-6	147	118
I270N-N	0	2	1	82	25	15	86	21
O270N-B	2	9	8	373	173	13	374	172
O270N-C	4	4	5	195	182	-3	196	182
O270N-D	5	4	4	160	185	0	185	160
O270N-E	5	3	3	111	187	-3	187	110
O270N-F	5	3	3	109	183	-1	183	109
O270N-G	5	3	3	129	174	-9	176	127
O270N-H	5	2	2	96	186	1	186	96
O270N-K	4	3	2	106	156	14	160	102
O270N-N	2	0	1	34	71	-17	78	27

Table A.9 (continued)

OUT-OF-PLANE MOMENT LOADING, MYC, ON CYLINDER (40000 IN-LB)

	MICRO-STRAIN			STRESSES			PRIN STRESSES	
ROSETTE	GAGE1	GAGE2	GAGE3	TRANS	LONG	SHEAR	SIGMX	SIGMN
I315C-B	6	18	3	459	306	190	588	178
I315C-C	6	17	0	364	289	216	546	107
I315C-D	6	17	1	396	310	221	578	128
I315C-E	9	18	2	427	383	220	626	184
I315C-F	9	21	1	473	419	262	709	183
I315C-H	11	25	0	551	482	328	846	187
I315C-J	13	31	-2	617	577	439	1037	157
I315C-K	18	35	-5	644	734	527	1218	160
I315C-L	20	45	-6	845	863	676	1530	177
I315C-M	29	51	-10	853	1132	813	1818	168
I315C-P	32	67	-11	1207	1318	1040	2304	221
O315C-B	3	-6	14	191	143	-269	437	-103
O315C-C	4	-4	15	230	186	-261	470	-54
O315C-D	5	-4	16	249	215	-271	503	-39
O315C-E	4	-5	17	246	194	-290	512	-71
O315C-F	8	-2	21	404	362	-297	680	85
O315C-H	11	-1	24	495	479	-338	825	149
O315C-J	12	-3	28	533	506	-409	929	110
O315C-K	22	3	42	961	945	-515	1468	437
O315C-L	28	2	53	1182	1209	-672	1868	523
O315C-M	31	0	60	1297	1313	-796	2101	509
O315C-P	35	2	76	1667	1543	-980	2587	623
I315N-N	4	4	3	158	155	8	165	148
O315N-B	-4	-1	9	186	-52	-124	239	-105
O315N-C	0	2	1	77	23	14	81	20
O315N-D	-1	0	0	17	-36	-2	17	-36
O315N-E	1	3	1	86	69	34	112	43
O315N-F	4	0	0	3	119	-5	119	3
O315N-G	1	1	-1	-17	34	27	45	-28
O315N-H	3	3	3	142	132	3	143	131
O315N-K	0	1	1	35	25	4	36	24
O315N-N	0	-3	-3	-119	-36	4	-36	-119

Table A.10. In-plane moment loading, M_{ZC}, on cylinder

IN-PLANE MOMENT LOADING, MZC, ON CYLINDER (40000 IN-LB)

	MICRO-STRAIN			STRESSES			PRIN STRESSES	
ROSETTE	GAGE1	GAGE2	GAGE3	TRANS	LONG	SHEAR	SIGMX	SIGMN
I-0-C-B	20	22	15	796	850	87	915	732
I-0-C-C	2	13	7	438	205	80	463	181
I-0-C-D	-19	8	5	304	-467	43	306	-469
I-0-C-F	-46	4	4	220	-1302	8	220	-1302
I-0-C-H	-66	4	-1	143	-1934	68	145	-1936
I-0-C-J	-74	-1	1	83	-2206	-17	84	-2206
I-0-C-K	-76	-1	4	147	-2227	-77	149	-2229
I-0-C-L	-77	1	10	327	-2210	-128	333	-2216
I-0-C-M	-78	2	7	281	-2258	-78	283	-2260
I-0-C-P	-80	9	3	355	-2303	82	357	-2306
I-0-C-S	-82	11	4	427	-2333	97	431	-2336
O-0-C-B	-59	-25	-26	-1047	-2097	11	-1047	-2097
O-0-C-C	-68	-19	-21	-800	-2290	32	-800	-2291
O-0-C-D	-75	-24	-17	-826	-2509	-88	-822	-2514
O-0-C-E	-73	-19	-13	-619	-2376	-79	-616	-2379
O-0-C-H	-77	-13	-8	-377	-2421	-60	-375	-2422
O-0-C-J	-84	-5	-9	-207	-2570	54	-205	-2571
O-0-C-K	-84	-7	-2	-117	-2561	-61	-116	-2562
O-0-C-L	-91	-4	-6	-119	-2762	19	-119	-2763
O-0-C-M	-88	-6	-3	-102	-2683	-30	-101	-2683
O-0-C-P	-88	-7	-7	-194	-2695	2	-194	-2695
O-0-C-S	-93	-10	-3	-184	-2841	-103	-180	-2845
I-0-N-B	0	7	21	626	188	-180	690	123
I-0-N-C	8	54	55	2392	951	-14	2392	951
I-0-N-D	4	54	58	2456	860	-46	2457	859
I-0-N-E	3	46	39	1868	649	83	1874	643
I-0-N-F	-4	38	44	1793	414	-76	1798	410
I-0-N-N	3	3	2	111	122	7	125	108
O-0-N-B	16	-24	-22	-1015	187	-31	188	-1016
O-0-N-C	27	-28	-27	-1220	456	-15	456	-1220
O-0-N-D	29	-24	-22	-1031	566	-24	566	-1032
O-0-N-E	27	-21	-18	-888	530	-36	531	-889
O-0-N-F	23	-16	-15	-723	483	-16	484	-724
O-0-N-G	17	-9	-9	-417	399	11	400	-418
O-0-N-H	17	-6	-8	-320	408	19	409	-321
O-0-N-K	0	1	1	45	13	-4	45	13
O-0-N-N	1	0	0	9	19	-2	19	9

Table A.10 (continued)

IN-PLANE MOMENT LOADING, MZC, ON CYLINDER (40000 IN-LB)

	MICRO-STRAIN			STRESSES			PRIN STRESSES	
ROSETTE	GAGE1	GAGE2	GAGE3	TRANS	LONG	SHEAR	SIGMX	SIGMN
I-90C-B	19	-109	-104	-4700	-835	-72	-834	-4701
I-90C-C	18	-93	-85	-3921	-644	-103	-641	-3924
I-90C-D	21	-84	-77	-3563	-429	-102	-426	-3566
I-90C-E	24	-77	-67	-3188	-226	-123	-220	-3193
I-90C-F	26	-70	-62	-2927	-96	-109	-92	-2931
I-90C-R	2	6	3	193	116	34	206	103
O-90C-B	0	-78	-58	-2989	-897	-257	-866	-3020
O-90C-C	-4	-67	-62	-2820	-963	-68	-960	-2822
O-90C-D	-2	-63	-61	-2706	-859	-28	-858	-2707
O-90C-E	2	-55	-61	-2570	-708	79	-705	-2573
O-90C-F	7	-59	-64	-2715	-603	56	-602	-2717
O-90C-R	0	-2	-1	-74	-12	-9	-11	-76
I-90N-B	-8	-139	-138	-6087	-2072	-19	-2072	-6087
I-90N-C	-4	-93	-87	-3962	-1315	-79	-1313	-3964
I-90N-D	-19	-20	-11	-664	-773	-126	-581	-856
I-90N-E	-18	-9	-2	-213	-605	-85	-196	-622
I-90N-F	-24	-47	-42	-1926	-1307	-62	-1301	-1932
I-90N-N	3	3	3	129	137	9	143	123
O-90N-B	31	-12	-8	-479	778	-59	780	-482
O-90N-C	18	21	22	923	804	-5	923	804
O-90N-D	-1	30	28	1256	355	28	1256	354
O-90N-E	-12	29	27	1235	17	22	1235	17
O-90N-F	-20	23	21	1003	-298	24	1004	-298
O-90N-N	0	0	0	6	10	7	16	1

Table A.10 (continued)

IN-PLANE MOMENT LOADING, MZC, ON CYLINDER (40000 IN-LB)

	MICRO-STRAIN			STRESSES			PRIN STRESSES	
ROSETTE	GAGE1	GAGE2	GAGE3	TRANS	LONG	SHEAR	SIGMX	SIGMN
I180C-B	14	24	8	690	629	213	875	445
I180C-C	-4	16	3	424	9	184	494	-61
I180C-D	-22	11	1	291	-558	140	314	-581
I180C-E	-37	10	1	281	-1024	115	291	-1034
I180C-F	-45	6	1	200	-1281	62	202	-1283
I180C-S	-78	2	3	178	-2275	-11	178	-2275
O180C-B	-59	-23	-20	-867	-2026	-42	-866	-2027
O180C-C	-69	-20	-15	-694	-2264	-65	-691	-2267
O180C-D	-69	-18	-15	-646	-2257	-48	-645	-2259
O180C-E	-72	-16	-13	-563	-2330	-33	-563	-2330
O180C-F	-74	-16	-10	-502	-2361	-76	-499	-2364
O180C-S	-89	2	-3	90	-2637	68	92	-2638
I180N-B	18	63	68	2860	1390	-74	2864	1387
I180N-C	8	57	62	2613	1037	-70	2616	1034
I180N-D	4	48	54	2243	792	-75	2247	789
I180N-E	6	0	46	995	473	-607	1395	73
I180N-F	7	38	38	1665	718	-1	1665	718
I180N-N	6	5	5	200	230	2	230	200
O180N-B	19	-25	-28	-1184	215	34	216	-1184
O180N-C	29	0	-30	-687	663	397	771	-796
O180N-D	29	-21	-30	-1150	518	113	525	-1158
O180N-E	27	-16	-23	-887	532	84	537	-892
O180N-F	22	-12	-18	-669	468	79	473	-674
O180N-N	0	0	0	-5	-2	-4	1	-8

Table A.10 (continued)

IN-PLANE MOMENT LOADING, MZC, ON CYLINDER (40000 IN-LB)

	MICRO-STRAIN			STRESSES			PRIN STRESSES	
ROSETTE	GAGE1	GAGE2	GAGE3	TRANS	LONG	SHEAR	SIGMX	SIGMN
I270C-A	45	-149	-177	-7208	-812	370	-791	-7229
I270C-B	13	-113	-107	-4851	-1057	-70	-1056	-4852
I270C-C	20	-92	-85	-3924	-563	-88	-561	-3927
I270C-D	19	-82	-76	-3496	-476	-71	-474	-3498
I270C-E	24	-74	-74	-3265	-272	4	-272	-3265
I270C-F	25	-72	-68	-3104	-168	-41	-167	-3105
I270C-H	23	-69	-58	-2823	-147	-137	-140	-2830
I270C-J	23	-63	-52	-2558	-91	-150	-82	-2567
I270C-K	22	-55	-50	-2323	-30	-70	-28	-2325
I270C-L	23	-44	-43	-1927	113	-6	113	-1927
I270C-M	13	-31	-35	-1473	-62	61	-59	-1476
I270C-P	7	-11	-12	-521	66	16	66	-521
I270C-R	3	0	0	3	84	-4	84	3
I270C-T	0	51	68	2600	780	-229	2628	752
O270C-B	-9	-61	-66	-2779	-1115	76	-1111	-2782
O270C-C	-4	-57	-64	-2639	-901	93	-896	-2644
O270C-D	1	-55	-63	-2582	-731	109	-724	-2589
O270C-E	7	-54	-60	-2530	-542	77	-539	-2533
O270C-F	11	-54	-57	-2467	-399	43	-398	-2468
O270C-H	18	-54	-58	-2486	-205	55	-204	-2487
O270C-J	20	-52	-55	-2390	-120	37	-119	-2391
O270C-K	20	-50	-53	-2286	-73	52	-71	-2288
O270C-L	20	-44	-49	-2073	-33	75	-31	-2076
O270C-M	17	-36	-35	-1593	42	-18	42	-1593
O270C-P	10	-15	-12	-612	112	-32	114	-614
O270C-R	2	1	1	41	85	-7	86	40
O270C-T	-25	65	54	2640	42	141	2648	34
I270N-A	68	-184	-192	-8334	-468	109	-466	-8335
I270N-B	-23	-126	-119	-5357	-2289	-84	-2286	-5359
I270N-C	-35	-87	-85	-3728	-2168	-26	-2168	-3728
I270N-D	-28	-58	-58	-2525	-1602	6	-1602	-2525
I270N-E	-18	-36	-41	-1671	-1053	74	-1044	-1679
I270N-F	-10	-24	-27	-1104	-618	49	-613	-1108
I270N-W	0	2	1	65	19	4	65	19
O270N-B	33	-9	-12	-499	847	43	849	-500
O270N-C	18	21	22	921	815	-9	922	814
O270N-D	2	28	33	1336	463	-58	1340	459
O270N-E	-12	26	29	1219	7	-49	1221	5
O270N-F	-18	21	24	1009	-230	-28	1010	-231
O270N-G	-20	11	13	550	-434	-20	551	-434
O270N-H	-18	8	8	370	-438	-10	370	-438
O270N-K	-4	-1	-1	-45	-142	-4	-45	-142
O270N-N	1	0	0	2	32	-2	32	2

Table A.10 (continued)

IN-PLANE MOMENT LOADING, MZC, ON CYLINDER (40000 IN-LB)

	MICRO-STRAIN			STRESSES			PRIN STRESSES	
ROSETTE	GAGE1	GAGE2	GAGE3	TRANS	LONG	SHEAR	SIGMX	SIGMN
I315C-B	11	-106	29	-1710	-188	-1793	999	-2897
I315C-C	1	-98	36	-1372	-395	-1786	968	-2735
I315C-D	-7	-87	34	-1143	-546	-1609	792	-2481
I315C-E	-13	-84	31	-1146	-728	-1525	603	-2477
I315C-F	-18	-77	32	-977	-838	-1457	552	-2366
I315C-H	-17	-77	25	-1116	-841	-1359	387	-2344
I315C-J	-26	-73	25	-1026	-1101	-1304	241	-2368
I315C-K	-35	-67	26	-867	-1307	-1239	171	-2346
I315C-L	-27	-63	19	-952	-1081	-1090	76	-2109
I315C-M	-30	-53	18	-735	-1127	-957	47	-1908
I315C-P	-18	-43	13	-641	-735	-734	48	-1424
O315C-B	-34	35	-124	-1919	-1592	2112	362	-3874
O315C-C	-40	28	-113	-1824	-1753	1881	93	-3670
O315C-D	-38	26	-113	-1878	-1715	1846	52	-3645
O315C-E	-38	21	-108	-1883	-1705	1722	-69	-3518
O315C-F	-37	17	-105	-1895	-1683	1637	-148	-3430
O315C-H	-35	14	-99	-1835	-1604	1504	-211	-3228
O315C-J	-34	12	-87	-1614	-1496	1330	-224	-2886
O315C-K	-30	14	-83	-1474	-1335	1286	-117	-2692
O315C-L	-30	18	-75	-1212	-1266	1234	-5	-2473
O315C-M	-26	16	-67	-1103	-1105	1112	8	-2216
O315C-P	-15	11	-50	-855	-703	815	39	-1597
I315N-N	3	4	3	134	138	11	148	124
O315N-B	27	11	-66	-1232	444	1025	930	-1717
O315N-C	0	-4	-5	-204	-61	19	-59	-207
O315N-D	14	-7	13	111	464	-269	609	-34
O315N-E	7	-11	17	142	246	-373	571	-183
O315N-F	2	0	18	400	183	-244	559	24
O315N-G	-1	-11	13	39	-12	-324	338	-311
O315N-H	2	-7	15	159	118	-290	429	-153
O315N-K	0	-2	3	29	20	-69	94	-45
O315N-N	0	0	-1	-11	-3	12	6	-20

Table A.11. Axial force, F_{XC}, on cylinder

AXIAL FORCE LOADING, FXC, CN CYLINDER (10000 LB)

	MICRO-STRAIN			STRESSES			PRIN STRESSES	
ROSETTE	GAGE1	GAGE2	GAGE3	TRANS	LONG	SHEAR	SIGMX	SIGMN
I-0-C-B	-5	11	11	499	5	-5	499	5
I-0-C-C	7	18	19	802	453	-24	804	451
I-0-C-D	19	24	25	1060	902	-11	1061	901
I-0-C-F	30	33	31	1385	1305	21	1390	1299
I-0-C-H	37	37	38	1602	1577	-10	1606	1574
I-0-C-J	37	38	39	1645	1614	-12	1649	1610
I-0-C-K	36	38	37	1606	1552	20	1613	1545
I-0-C-L	38	38	38	1628	1623	2	1629	1622
I-0-C-M	35	41	39	1713	1574	24	1717	1570
I-0-C-P	35	38	39	1666	1558	-15	1668	1556
I-0-C-S	31	36	35	1525	1386	9	1525	1385
0-0-C-B	21	4	5	177	682	-15	682	177
0-0-C-C	20	-6	-5	-274	503	-17	504	-275
0-0-C-D	18	-14	-10	-535	371	-49	374	-537
0-0-C-E	18	-18	-16	-768	299	-34	300	-769
0-0-C-H	25	-23	-24	-1060	425	11	425	-1061
0-0-C-J	27	-31	-25	-1270	418	-81	422	-1274
0-0-C-K	28	-30	-30	-1341	432	1	432	-1341
0-0-C-L	30	-31	-31	-1390	493	-7	493	-1390
0-0-C-M	29	-30	-31	-1374	451	3	451	-1374
0-0-C-P	26	-30	-29	-1317	374	-9	374	-1317
0-0-C-S	20	-26	-31	-1266	212	66	215	-1269
I-0-N-B	0	7	0	145	44	90	198	-9
I-0-N-C	13	-17	-22	-867	142	61	146	-871
I-0-N-D	12	-25	-27	-1158	22	31	22	-1159
I-0-N-E	11	-23	-18	-923	62	-66	66	-927
I-0-N-F	13	-20	-23	-959	103	42	105	-961
I-0-N-N	3	3	3	113	129	-4	130	112
0-0-N-B	8	10	14	517	386	-47	532	371
0-0-N-C	4	14	14	611	303	0	611	303
0-0-N-D	2	13	14	588	237	-5	588	237
0-0-N-E	0	12	12	513	153	-1	513	153
0-0-N-F	-1	10	10	461	93	0	461	93
0-0-N-G	-4	7	7	320	-30	-5	320	-30
0-0-N-H	-4	5	6	255	-45	-13	255	-45
0-0-N-K	0	0	0	10	3	-4	12	1
0-0-N-N	0	-1	-1	-36	-16	5	-15	-37

Table A.11 (continued)

AXIAL FORCE LOADING, FXC, ON CYLINDER (10000 LB)

	MICRO-STRAIN			STRESSES			PRIN STRESSES	
ROSETTE	GAGE1	GAGE2	GAGE3	TRANS	LONG	SHEAR	SIGMX	SIGMN
I-90C-B	53	72	70	3049	2495	31	3051	2493
I-90C-C	46	63	61	2675	2176	15	2676	2176
I-90C-D	39	56	58	2466	1902	-26	2467	1901
I-90C-E	39	56	55	2391	1889	8	2391	1889
I-90C-F	40	51	50	2184	1852	18	2185	1851
I-90C-R*	-52	47	37	1907	-988	126	1912	-994
O-90C-B	0	19	4	508	152	210	605	55
O-90C-C	-50	0	2	106	-1476	-20	107	-1476
O-90C-D	-47	5	6	279	-1332	-12	279	-1333
O-90C-E	-48	6	10	410	-1330	-48	412	-1331
O-90C-F	-48	8	13	519	-1280	-61	521	-1283
O-90C-R*	21	53	64	2551	1391	-156	2571	1370
I-90N-B	52	69	67	2918	2435	25	2919	2433
I-90N-C	14	47	38	1839	972	120	1855	956
I-90N-D	13	14	10	523	543	56	589	476
I-90N-E	10	15	9	516	462	81	575	404
I-90N-F	9	32	30	1363	664	27	1364	663
I-90N-N	2	4	3	156	120	21	166	110
O-90N-B	-48	-18	-23	-829	-1690	67	-824	-1695
O-90N-C	-28	-22	-26	-1013	-1139	48	-997	-1155
O-90N-D	-12	-21	-20	-899	-639	-13	-639	-899
O-90N-E	-3	-18	-17	-754	-308	-10	-308	-754
O-90N-F	3	-14	-12	-587	-86	-21	-85	-587
O-90N-N	0	-1	-1	-49	-14	-2	-14	-49

Table A.11 (continued)

AXIAL FORCE LOADING, FXC, ON CYLINDER (10000 LB)

	MICRO-STRAIN			STRESSES			PRIN STRESSES	
ROSETTE	GAGE1	GAGE2	GAGE3	TRANS	LONG	SHEAR	SIGMX	SIGMN
I180C-B	-4	12	15	606	66	-34	609	64
I180C-C	11	20	21	880	605	-17	881	604
I180C-D	20	26	26	1134	934	4	1134	934
I180C-E	26	31	31	1320	1171	-2	1320	1171
I180C-F	30	33	33	1413	1323	9	1414	1322
I180C-S	31	39	39	1668	1434	1	1668	1434
O180C-B	23	4	4	142	732	2	732	142
O180C-C	26	-3	-7	-245	698	56	701	-248
O180C-D	23	-9	-10	-442	546	9	546	-442
O180C-E	24	-13	-13	-607	529	-6	529	-607
O180C-F	25	-19	-17	-822	488	-17	489	-822
O180C-S*	21	-29	-24	-1196	282	-68	286	-1199
I180N-B	5	-21	-19	-874	-113	-32	-112	-875
I180N-C	14	-20	-24	-976	118	50	120	-978
I180N-D	13	-20	-26	-1020	70	76	75	-1025
I180N-E	10	0	-24	-531	149	315	272	-654
I180N-F	9	-18	-17	-779	36	-9	37	-780
I180N-N	6	5	6	245	252	-6	256	241
O180N-B	7	12	10	478	353	31	485	345
O180N-C	3	0	14	314	192	-192	455	51
O180N-D	1	14	15	621	228	-11	621	228
O180N-E	0	12	12	539	166	0	539	166
O180N-F	-2	10	12	496	88	-24	497	87
O180N-N	1	0	0	-11	23	5	24	-12

Table A.11 (continued)

AXIAL FORCE LOADING, FXC, CN CYLINDER (10000 LB)

	MICRO-STRAIN			STRESSES			PRIN STRESSES	
ROSETTE	GAGE1	GAGE2	GAGE3	TRANS	LONG	SHEAR	SIGMX	SIGMN
I270C-A	8	86	99	4065	1459	-174	4077	1447
I270C-B	54	78	79	3398	2631	-9	3398	2630
I270C-C	46	69	67	2942	2266	31	2943	2264
I270C-D	41	61	61	2620	2023	2	2620	2023
I270C-E	38	57	57	2459	1884	-4	2459	1884
I270C-F	34	52	51	2237	1703	11	2238	1703
I270C-H	30	48	44	1982	1492	54	1988	1486
I270C-J	23	46	42	1896	1271	59	1901	1266
I270C-K	16	44	42	1881	1047	33	1882	1046
I270C-L	-7	43	41	1838	339	24	1839	339
I270C-M	-22	38	43	1803	-129	-71	1806	-132
I270C-P	-48	48	39	1957	-856	114	1962	-861
I270C-R*	-58	0	41	975	-1437	-553	1096	-1557
I270C-T	0	51	49	2183	655	30	2184	654
O270C-B	-54	-2	-2	-14	-1633	-3	-14	-1633
O270C-C	-50	4	4	236	-1440	-9	236	-1440
O270C-D	-49	6	8	380	-1358	-25	380	-1358
O270C-E	-47	7	10	445	-1262	-40	446	-1263
O270C-F	-45	10	11	517	-1194	-14	518	-1194
O270C-H	-41	15	15	698	-1035	-5	698	-1035
O270C-J	-37	19	19	890	-840	4	890	-840
O270C-K	-29	24	24	1085	-537	-8	1085	-537
O270C-L	-14	32	36	1504	38	-47	1506	36
O270C-M	0	43	41	1845	550	15	1845	550
O270C-P	21	56	53	2373	1336	50	2376	1334
O270C-R	22	61	58	2595	1425	44	2596	1423
O270C-T	-49	19	20	923	-1185	-8	923	-1185
I270N-A	0	93	85	3922	1176	104	3926	1172
I270N-B	46	65	60	2701	2197	63	2709	2189
I270N-C	24	41	42	1802	1268	-11	1803	1268
I270N-D	13	29	31	1295	785	-33	1297	783
I270N-E	5	22	26	1055	457	-55	1060	452
I270N-F	1	17	21	832	281	-60	839	274
I270N-N	0	2	3	120	36	-13	122	34
O270N-B	-51	-16	-15	-622	-1707	-13	-622	-1707
O270N-C	-27	-22	-23	-963	-1096	8	-963	-1097
O270N-D	-12	-20	-22	-910	-624	23	-622	-912
O270N-E	-2	-16	-17	-737	-273	16	-273	-737
O270N-F	2	-14	-14	-610	-112	-1	-112	-610
O270N-G	4	-8	-7	-340	16	-4	16	-340
O270N-H	4	-6	-6	-284	44	3	44	-285
O270N-K	2	-1	-1	-54	33	8	33	-55
O270N-N	0	-1	-1	-43	-8	7	-6	-44

Table A.11 (continued)

AXIAL FORCE LOADING, FXC, ON CYLINDER (10000 LB)

	MICRO-STRAIN			STRESSES			PRIN STRESSES	
ROSETTE	GAGE1	GAGE2	GAGE3	TRANS	LONG	SHEAR	SIGMX	SIGMN
I315C-B	28	47	40	1892	1414	88	1908	1399
I315C-C	30	45	40	1833	1455	63	1843	1444
I315C-D	33	41	37	1673	1477	57	1689	1462
I315C-E	34	40	39	1710	1541	8	1710	1541
I315C-F	35	40	38	1681	1543	27	1686	1538
I315C-H	38	40	36	1619	1637	48	1677	1580
I315C-J	38	42	32	1586	1603	128	1723	1466
I315C-K	39	42	27	1460	1598	196	1737	1322
I315C-L	33	44	16	1275	1385	373	1707	953
I315C-M	33	45	4	1049	1302	544	1735	617
I315C-P	23	53	-20	716	892	976	1784	-176
0315C-B	-16	-50	53	89	-457	-1363	1206	-1574
0315C-C	-12	-46	47	37	-342	-1237	1099	-1404
0315C-D	-10	-46	46	9	-289	-1218	1087	-1367
0315C-E	-7	-46	42	-85	-250	-1173	1008	-1343
0315C-F	-9	-43	43	3	-256	-1152	1033	-1286
0315C-H	-4	-41	38	-52	-137	-1048	954	-1143
0315C-J	-2	-38	32	-113	-95	-930	827	-1034
0315C-K	0	-35	34	-20	5	-914	906	-921
0315C-L	9	-29	36	151	308	-873	1106	-647
0315C-M	17	-18	40	462	636	-784	1337	-240
0315C-P	31	2	50	1124	1253	-644	1836	541
I315N-N	8	6	5	228	300	11	302	226
0315N-B	-26	-25	28	103	-754	-701	496	-1147
0315N-C	0	-11	2	-208	-62	-180	59	-329
0315N-D	-5	-5	-3	-181	-212	-27	-165	-228
0315N-E	-1	-1	-4	-111	-57	32	-41	-126
0315N-F	1	0	-3	-75	21	45	38	-93
0315N-G	1	2	-4	-42	28	87	87	-101
0315N-H	6	8	2	194	223	81	292	126
0315N-K	1	2	-1	24	44	49	84	-16
0315N-N	0	0	1	4	1	-11	14	-8

Table A.12. In-plane force, F_{YC}, on cylinder

IN-PLANE FORCE LOADING, FYC, ON CYLINDER (3000 LB)

	MICRO-STRAIN			STRESSES			PRIN STRESSES	
ROSETTE	GAGE1	GAGE2	GAGE3	TRANS	LONG	SHEAR	SIGMX	SIGMN
I-0-C-B	26	30	17	1005	1086	176	1226	865
I-0-C-C	1	17	5	473	170	166	546	97
I-0-C-D	-31	12	1	321	-846	143	338	-863
I-0-C-F	-70	6	-2	165	-2041	104	169	-2046
I-0-C-H	-98	4	-6	72	-2917	136	78	-2923
I-0-C-J	-109	-2	-2	25	-3250	-7	25	-3250
I-0-C-K	-112	-6	0	-9	-3375	-72	-8	-3377
I-0-C-L	-107	-3	7	204	-3145	-123	208	-3149
I-0-C-M	-104	1	0	124	-3087	9	124	-3087
I-0-C-P	-92	11	-9	134	-2728	264	158	-2753
I-0-C-S	-67	8	-8	55	-1996	212	76	-2018
O-0-C-B	-89	-41	-36	-1577	-3158	-68	-1574	-3161
O-0-C-C	-102	-33	-29	-1254	-3426	-56	-1252	-3428
O-0-C-D	-108	-35	-26	-1204	-3601	-122	-1198	-3607
O-0-C-E	-105	-31	-20	-1006	-3444	-139	-998	-3452
O-0-C-H	-111	-22	-11	-617	-3500	-144	-610	-3507
O-0-C-J	-117	-7	-13	-325	-3606	76	-323	-3608
O-0-C-K	-113	-12	-5	-240	-3471	-86	-238	-3473
O-0-C-L	-114	-8	-7	-194	-3489	-11	-194	-3489
O-0-C-M	-105	-9	-4	-149	-3194	-67	-148	-3196
O-0-C-P	-91	-6	-7	-181	-2793	12	-181	-2793
O-0-C-S	-72	-6	-2	-81	-2170	-52	-80	-2171
I-0-N-B	0	6	23	638	192	-238	741	89
I-0-N-C	6	75	77	3329	1183	-17	3329	1183
I-0-N-D	2	75	83	3477	1092	-113	3482	1086
I-0-N-E	-1	62	57	2630	753	63	2632	751
I-0-N-F	-12	54	65	2620	414	-153	2630	403
I-0-N-N	1	1	0	9	40	18	48	1
O-0-N-B	26	-37	-33	-1563	320	-59	321	-1565
O-0-N-C	42	-43	-40	-1879	708	-47	709	-1880
O-0-N-D	46	-36	-35	-1612	906	-25	907	-1613
O-0-N-E	41	-31	-28	-1360	827	-41	828	-1361
O-0-N-F	36	-27	-22	-1113	747	-56	749	-1115
O-0-N-G	29	-14	-13	-622	685	-15	685	-622
O-0-N-H	26	-9	-11	-479	625	32	626	-480
O-0-N-K	0	3	2	113	34	24	120	27
O-0-N-N	1	0	0	9	25	-5	27	8

Table A.12 (continued)

IN-PLANE FORCE LOADING, FYC, ON CYLINDER (3000 LB)

	MICRO-STRAIN			STRESSES			PRIN STRESSES	
ROSETTE	GAGE1	GAGE2	GAGE3	TRANS	LONG	SHEAR	SIGMX	SIGMN
I-90C-B	32	-182	-177	-7941	-1429	-65	-1428	-7942
I-90C-C	31	-154	-145	-6602	-1038	-111	-1036	-6605
I-90C-D	35	-139	-136	-6082	-789	-38	-788	-6083
I-90C-E	43	-122	-123	-5429	-333	24	-333	-5429
I-90C-F	43	-113	-116	-5091	-243	39	-243	-5091
I-90C-R	-1	38	-41	-77	-47	1047	985	-1109
O-90C-B	0	-123	-93	-4756	-1427	-396	-1380	-4802
O-90C-C	-9	-107	-96	-4453	-1591	-143	-1584	-4460
O-90C-D	-3	-108	-91	-4368	-1391	-218	-1375	-4384
O-90C-E	5	-98	-89	-4106	-1092	-120	-1088	-4111
O-90C-F	8	-105	-93	-4348	-1070	-155	-1063	-4356
O-90C-R	-1	-33	38	99	10	-940	996	-887
I-90N-B	-12	-229	-227	-10012	-3351	-16	-3351	-10012
I-90N-C	-8	-155	-145	-6570	-2196	-135	-2192	-6574
I-90N-D	-34	-42	-27	-1478	-1458	-205	-1263	-1673
I-90N-E	-33	-26	-11	-767	-1218	-195	-695	-1291
I-90N-F	-44	-72	-68	-3036	-2227	-58	-2223	-3040
I-90N-N	1	-1	0	-25	21	-3	21	-25
O-90N-B	45	-25	-13	-892	1087	-161	1100	-905
O-90N-C	25	31	33	1378	1153	-22	1381	1150
O-90N-D	-2	48	43	2010	555	74	2014	552
O-90N-E	-19	47	41	1962	25	76	1965	22
O-90N-F	-31	36	33	1554	-462	49	1555	-463
O-90N-N	0	0	0	3	7	2	8	2

Table A.12 (continued)

IN-PLANE FORCE LOADING, FYC, ON CYLINDER (3000 LB)

	MICRO-STRAIN			STRESSES			PRIN STRESSES	
ROSETTE	GAGE1	GAGE2	GAGE3	TRANS	LONG	SHEAR	SIGMX	SIGMN
I180C-B	17	36	4	857	770	435	1251	377
I180C-C	-16	25	-3	505	-323	376	650	-468
I180C-D	-47	16	-6	287	-1313	291	338	-1364
I180C-E	-72	15	-6	266	-2083	277	299	-2115
I180C-F	-87	6	-5	116	-2584	149	124	-2592
I180C-S	-203	-1	-1	178	-6035	8	178	-6035
O180C-B	-94	-35	-29	-1308	-3222	-77	-1305	-3225
O180C-C	-110	-35	-22	-1115	-3639	-176	-1103	-3651
O180C-D	-116	-33	-26	-1176	-3843	-90	-1173	-3846
O180C-E	-124	-31	-24	-1073	-4029	-106	-1069	-4033
O180C-F	-127	-31	-18	-926	-4103	-176	-917	-4112
O180C-S	-221	1	-12	-18	-6642	173	-13	-6646
I180N-B	28	102	111	4656	2236	-110	4661	2231
I180N-C	7	87	93	3933	1389	-82	3935	1386
I180N-D	0	70	78	3260	986	-111	3266	980
I180N-E	2	0	67	1468	502	-891	1998	-29
I180N-F	4	52	53	2312	802	-15	2312	802
I180N-N	-1	1	1	26	-16	0	26	-16
O180N-B	33	-41	-47	-1960	391	78	393	-1962
O180N-C	50	0	-51	-1173	1144	678	1327	-1356
O180N-D	49	-33	-51	-1900	899	237	919	-1919
O180N-E	45	-26	-36	-1409	939	142	947	-1417
O180N-F	37	-19	-29	-1100	788	126	796	-1108
O180N-N	0	0	-1	-14	5	13	12	-20

Table A.12 (continued)

IN-PLANE FORCE LOADING, FYC, ON CYLINDER (3000 LB)

	MICRO-STRAIN			STRESSES			PRIN STRESSES	
ROSETTE	GAGE1	GAGE2	GAGE3	TRANS	LONG	SHEAR	SIGMX	SIGMN
I270C-A	65	-247	-283	-11718	-1552	468	-1530	-11740
I270C-B	18	-191	-165	-7827	-1813	-344	-1793	-7847
I270C-C	27	-162	-130	-6451	-1135	-431	-1100	-6486
I270C-D	24	-145	-114	-5733	-997	-417	-960	-5770
I270C-E	31	-133	-110	-5371	-678	-312	-657	-5392
I270C-F	31	-131	-100	-5107	-592	-402	-556	-5143
I270C-H	27	-125	-80	-4534	-553	-594	-466	-4621
I270C-J	21	-119	-67	-4126	-618	-691	-487	-4257
I270C-K	18	-108	-62	-3774	-607	-613	-492	-3889
I270C-L	13	-99	-47	-3220	-563	-703	-389	-3395
I270C-M	1	-87	-30	-2577	-743	-750	-475	-2844
I270C-P	-15	-56	9	-1019	-744	-861	-10	-1753
I270C-R	-14	0	29	644	-213	-381	789	-358
I270C-T	0	89	100	4162	1248	-151	4169	1241
O270C-B	-11	-87	-115	-4434	-1672	371	-1623	-4483
O270C-C	-6	-82	-108	-4171	-1440	357	-1395	-4217
O270C-D	1	-77	-106	-4015	-1188	388	-1136	-4068
O270C-E	10	-74	-101	-3856	-870	370	-825	-3901
O270C-F	16	-73	-98	-3786	-652	337	-616	-3822
O270C-H	28	-69	-100	-3730	-288	409	-241	-3778
O270C-J	33	-64	-97	-3565	-75	445	-20	-3621
O270C-K	34	-54	-94	-3281	47	528	129	-3363
O270C-L	36	-33	-89	-2719	279	747	455	-2895
O270C-M	36	-20	-71	-2046	475	683	648	-2219
O270C-P	29	15	-44	-659	663	792	1034	-1030
O270C-R	9	36	-29	148	313	866	1100	-640
O270C-T	-40	98	85	4064	19	165	4071	12
I270N-A	102	-298	-315	-13575	-1009	230	-1005	-13580
I270N-B	-41	-212	-200	-9011	-3928	-155	-3923	-9015
I270N-C	-58	-146	-141	-6255	-3620	-66	-3618	-6256
I270N-D	-48	-96	-96	-4176	-2703	-2	-2703	-4176
I270N-E	-32	-62	-69	-2831	-1815	97	-1806	-2840
I270N-F	-20	-39	-45	-1833	-1155	82	-1145	-1843
I270N-N	0	1	-1	-3	-1	21	19	-22
O270N-B	49	-13	-25	-882	1211	155	1223	-893
O270N-C	27	31	34	1399	1218	-46	1410	1207
O270N-D	1	43	51	2054	660	-111	2063	652
O270N-E	-22	39	46	1890	-107	-98	1894	-111
O270N-F	-30	33	42	1673	-395	-119	1680	-401
O270N-G	-32	16	20	832	-717	-48	834	-718
O270N-H	-30	11	13	580	-715	-25	580	-716
O270N-K	-8	-3	-2	-108	-269	-21	-105	-271
O270N-N	0	0	0	4	1	-9	12	-6

Table A.12 (continued)

IN-PLANE FORCE LOADING, FYC, ON CYLINDER (3000 LB)

	MICRO-STRAIN			STRESSES			PRIN STRESSES	
ROSETTE	GAGE1	GAGE2	GAGE3	TRANS	LONG	SHEAR	SIGMX	SIGMN
I315C-B	12	-166	45	-2656	-450	-2815	1470	-4576
I315C-C	-7	-150	59	-2002	-799	-2780	1444	-4245
I315C-D	-19	-132	55	-1672	-1074	-2496	1141	-3887
I315C-E	-32	-126	50	-1626	-1454	-2347	809	-3889
I315C-F	-39	-115	50	-1387	-1590	-2194	708	-3685
I315C-H	-43	-111	39	-1554	-1749	-1998	349	-3652
I315C-J	-59	-101	38	-1321	-2156	-1857	165	-3642
I315C-K	-73	-85	37	-968	-2475	-1625	70	-3513
I315C-L	-70	-76	28	-991	-2393	-1384	-141	-3243
I315C-M	-76	-55	20	-671	-2484	-997	-231	-2925
I315C-P	-64	-37	15	-422	-2051	-698	-164	-2309
O315C-B	-57	55	-185	-2795	-2538	3201	537	-5870
O315C-C	-66	43	-168	-2678	-2793	2813	78	-5550
O315C-D	-65	39	-166	-2716	-2780	2730	-17	-5478
O315C-E	-64	35	-158	-2635	-2714	2571	-104	-5246
O315C-F	-64	29	-155	-2681	-2736	2449	-259	-5158
O315C-H	-61	26	-139	-2409	-2549	2204	-273	-4684
O315C-J	-59	26	-118	-1960	-2361	1909	-241	-4080
O315C-K	-56	30	-105	-1589	-2144	1803	-43	-3690
O315C-L	-56	39	-84	-925	-1954	1635	275	-3154
O315C-M	-52	42	-68	-522	-1729	1469	462	-2713
O315C-P	-45	42	-40	81	-1333	1093	675	-1927
I315N-N	-1	0	1	27	-14	-7	28	-15
O315N-B	41	19	-101	-1843	683	1596	1456	-2616
O315N-C	0	-7	-12	-410	-123	73	-105	-427
O315N-D	22	-12	18	100	696	-401	898	-101
O315N-E	12	-17	25	161	416	-570	873	-295
O315N-F	4	0	28	604	302	-369	851	55
O315N-G	0	-18	20	47	25	-504	540	-468
O315N-H	0	-16	16	-17	-6	-427	415	-438
O315N-K	-1	-2	3	28	-22	-67	75	-69
O315N-N	0	0	1	19	6	-11	25	-1

Table A.13. Out-of-plane force, F_{ZC}, on cylinder

OUT-OF-PLANE FORCE LOADING, FZC, ON CYLINDER (3000 LB)

	MICRO-STRAIN			STRESSES			PRIN STRESSES	
ROSETTE	GAGE1	GAGE2	GAGE3	TRANS	LONG	SHEAR	SIGMX	SIGMN
I-0-C-B	3	-49	40	-206	25	-1176	1091	-1272
I-0-C-C	1	-53	44	-215	-29	-1293	1175	-1419
I-0-C-D	0	-56	41	-320	-105	-1292	1085	-1509
I-0-C-F	1	-51	35	-361	-74	-1154	946	-1380
I-0-C-H	-1	-48	27	-457	-158	-991	695	-1310
I-0-C-J	3	-49	26	-505	-74	-1007	740	-1319
I-0-C-K	6	-47	21	-580	1	-901	657	-1236
I-0-C-L	7	-46	22	-530	57	-899	709	-1182
I-0-C-M	2	-46	24	-485	-93	-941	673	-1250
I-0-C-P	-1	-42	30	-280	-119	-959	763	-1162
I-0-C-S	-5	-40	27	-284	-243	-898	635	-1162
O-0-C-B	1	62	-63	-20	28	1676	1680	-1672
O-0-C-C	4	54	-40	289	214	1254	1507	-1003
O-0-C-D	3	57	-42	329	186	1309	1568	-1053
O-0-C-E	3	54	-39	334	180	1244	1503	-989
O-0-C-H	2	51	-32	413	183	1096	1400	-803
O-0-C-J	5	47	-30	367	273	1022	1343	-703
O-0-C-K	3	45	-28	365	192	964	1247	-690
O-0-C-L	2	42	-24	385	183	881	1170	-602
O-0-C-M	-1	45	-23	487	115	907	1226	-625
O-0-C-P	1	42	-28	297	111	934	1143	-735
O-0-C-S	-4	41	-29	278	-31	927	1064	-817
I-0-N-B	0	5	6	253	76	-19	255	74
I-0-N-C	2	17	50	1474	490	-446	1646	318
I-0-N-D	2	11	12	507	203	-25	509	201
I-0-N-E	2	5	13	399	177	-110	444	132
I-0-N-F	0	3	10	283	96	-96	323	55
I-0-N-N	0	0	0	9	5	-3	11	3
O-0-N-B	-5	21	-25	-83	-178	604	475	-736
O-0-N-C	-6	1	1	44	-171	2	44	-171
O-0-N-D	-6	-7	8	32	-169	-207	162	-299
O-0-N-E	-5	-10	11	42	-151	-278	240	-349
O-0-N-F	-4	-9	8	-18	-121	-239	174	-314
O-0-N-G	-2	-9	8	-36	-60	-228	181	-277
O-0-N-H	-2	-9	8	-31	-68	-229	180	-279
O-0-N-K	0	-2	1	-22	-7	-45	32	-60
O-0-N-N	-1	0	0	5	-32	11	8	-34

Table A.13 (continued)

OUT-OF-PLANE FORCE LOADING, FZC, ON CYLINDER (3000 LB)

	MICRO-STRAIN			STRESSES			PRIN STRESSES	
ROSETTE	GAGE1	GAGE2	GAGE3	TRANS	LONG	SHEAR	SIGMX	SIGMN
I-90C-B	-15	61	-36	552	-290	1294	1492	-1230
I-90C-C	-16	65	-41	550	-311	1405	1590	-1350
I-90C-D	-18	63	-35	652	-345	1304	1550	-1242
I-90C-E	-20	60	-30	678	-405	1210	1462	-1190
I-90C-F	-19	61	-30	708	-369	1212	1496	-1157
I-90C-R	-15	99	91	4188	808	111	4191	804
O-90C-B	0	-14	53	852	256	-884	1487	-379
O-90C-C	16	-27	66	844	723	-1243	2028	-461
O-90C-D	12	-22	66	952	651	-1174	1985	-382
O-90C-E	10	-21	65	959	599	-1154	1947	-389
O-90C-F	6	-15	72	1230	556	-1157	2098	-312
O-90C-R	-50	89	96	4130	-255	-87	4131	-257
I-90N-B	-13	15	13	639	-187	27	640	-188
I-90N-C	-2	12	-8	93	-37	263	299	-243
I-90N-D	2	11	-8	66	67	255	321	-188
I-90N-E*	37	-28	-42	-1578	650	174	663	-1592
I-90N-F	4	3	-1	30	130	56	155	5
I-90N-N	0	0	0	2	4	7	10	-4
O-90N-B	6	-12	33	437	312	-599	976	-228
O-90N-C	5	1	2	41	159	-14	160	40
O-90N-D	6	5	-8	-62	154	177	253	-161
O-90N-E	4	9	-13	-88	101	289	311	-298
O-90N-F	4	9	-13	-98	90	297	308	-316
O-90N-N	0	0	0	-4	0	8	6	-10

Table A.13 (continued)

OUT-OF-PLANE FORCE LOADING, FZC, ON CYLINDER (3000 LB)

	MICRO-STRAIN			STRESSES			PRIN STRESSES	
ROSETTE	GAGE1	GAGE2	GAGE3	TRANS	LONG	SHEAR	SIGMX	SIGMN
I180C-B	5	-59	52	-158	117	-1469	1454	-1496
I180C-C	3	-63	50	-280	1	-1505	1372	-1651
I180C-D	3	-58	46	-268	21	-1384	1268	-1515
I180C-E	1	-59	41	-407	-107	-1325	1077	-1591
I180C-F	1	-54	36	-392	-87	-1199	969	-1448
I180C-S	8	30	-41	-242	158	950	929	-1012
O180C-B	9	58	-58	1	263	1551	1688	-1424
O180C-C	8	54	-42	257	303	1289	1569	-1010
O180C-D	9	54	-42	251	343	1279	1577	-983
O180C-E	8	54	-39	329	348	1232	1571	-894
O180C-F	8	52	-37	331	326	1184	1512	-855
O180C-S	19	39	-30	156	616	919	1333	-561
I180N-B	-3	-20	-14	-752	-309	-82	-294	-767
I180N-C	-4	-19	-1	-442	-238	-234	-85	-595
I180N-D	3	-10	1	-187	26	-142	97	-258
I180N-E	-2	0	6	128	-27	-76	159	-58
I180N-F	0	-3	5	42	-2	-115	138	-97
I180N-N	1	1	-1	-2	15	15	24	-11
O180N-B	-4	10	-8	41	-97	232	214	-270
O180N-C	-4	0	6	133	-90	-78	158	-115
O180N-D	-3	-12	6	-143	-140	-240	98	-382
O180N-E	-4	-14	10	-91	-153	-315	194	-438
O180N-F	-1	-13	9	-73	-48	-293	232	-353
O180N-N	0	0	1	11	0	-11	18	-7

Table A.13 (continued)

OUT-OF-PLANE FORCE LOADING, FZC, ON CYLINDER (3000 LB)

	MICRO-STRAIN			STRESSES			PRIN STRESSES	
ROSETTE	GAGE1	GAGE2	GAGE3	TRANS	LONG	SHEAR	SIGMX	SIGMN
I270C-A	-9	21	-47	-567	-431	904	408	-1405
I270C-B	-12	32	-73	-891	-635	1403	646	-2171
I270C-C	-10	36	-77	-882	-577	1509	787	-2246
I270C-D	-8	30	-73	-926	-508	1371	670	-2104
I270C-E	-3	27	-71	-968	-395	1300	650	-2013
I270C-F	-3	20	-70	-1103	-416	1192	481	-2000
I270C-H	0	8	-69	-1331	-410	1023	252	-1992
I270C-J	8	-9	-74	-1820	-304	868	91	-2214
I270C-K	9	-39	-79	-2615	-515	530	-389	-2741
I270C-L	20	-37	-90	-2821	-251	712	-67	-3005
I270C-M	25	-50	-103	-3380	-273	707	-119	-3533
I270C-P	44	-93	-106	-4420	5	181	12	-4427
I270C-R*	53	0	-97	-2197	929	1297	1397	-2665
I270C-T*	0	-39	34	-124	-37	-972	892	-1053
O270C-B	23	-55	64	189	743	-1587	2077	-1145
O270C-C	18	-52	47	-149	501	-1320	1536	-1183
O270C-D	24	-55	39	-374	611	-1243	1455	-1218
O270C-E	22	-58	33	-560	502	-1208	1290	-1349
O270C-F	22	-58	31	-617	488	-1179	1238	-1367
O270C-H	22	-62	18	-986	364	-1073	957	-1579
O270C-J	24	-69	6	-1411	297	-1010	765	-1880
O270C-K	27	-74	-9	-1837	270	-868	582	-2148
O270C-L	29	-93	-41	-2971	-34	-699	123	-3129
O270C-M	30	-103	-56	-3524	-145	-621	-34	-3634
O270C-P	29	-113	-87	-4442	-464	-347	-434	-4472
O270C-R	27	-111	-109	-4876	-659	-27	-658	-4876
O270C-T*	13	46	-21	518	541	893	1423	-364
I270N-A	-4	-6	9	66	-101	-190	191	-225
I270N-B	-5	20	12	715	55	109	733	38
I270N-C	2	20	10	638	262	135	681	219
I270N-D	7	16	6	477	367	135	567	277
I270N-E	6	15	7	473	319	105	526	266
I270N-F	5	12	1	275	231	151	405	101
I270N-N	0	0	0	-10	-3	-3	-2	-11
O270N-B	13	-22	29	125	441	-677	978	-412
O270N-C	8	6	4	214	294	21	299	208
O270N-D	4	12	-4	159	176	214	382	-47
O270N-E	3	13	-7	133	116	270	394	-145
O270N-F	2	12	-11	28	70	300	350	-252
O270N-G	1	11	-8	71	38	255	310	-201
O270N-H	2	10	-9	28	59	250	295	-207
O270N-K	0	3	-2	9	10	64	73	-55
O270N-N	1	1	0	20	25	9	31	13

Table A.13 (continued)

OUT-OF-PLANE FORCE LOADING, FZC, ON CYLINDER (3000 LB)

	MICRO-STRAIN			STRESSES			PRIN STRESSES	
ROSETTE	GAGE1	GAGE2	GAGE3	TRANS	LONG	SHEAR	SIGMX	SIGMN
I315C-B	-5	-55	-56	-2448	-883	14	-883	-2448
I315C-C	3	-52	-49	-2234	-583	-43	-582	-2235
I315C-D	6	-50	-43	-2046	-428	-85	-424	-2050
I315C-E	9	-50	-42	-2024	-338	-108	-331	-2030
I315C-F	11	-48	-41	-1968	-255	-106	-248	-1975
I315C-H	17	-48	-39	-1936	-61	-118	-54	-1943
I315C-J	17	-58	-32	-1992	-73	-346	-13	-2052
I315C-K	16	-68	-21	-1982	-129	-622	60	-2172
I315C-L	13	-71	-22	-2065	-236	-658	-24	-2277
I315C-M	0	-86	-3	-1959	-585	-1099	24	-2568
I315C-P	-9	-92	3	-1963	-852	-1262	-29	-2787
O315C-B	24	-7	-27	-773	474	271	530	-830
O315C-C	26	-4	-26	-694	579	293	643	-758
O315C-D	29	0	-28	-650	665	372	763	-748
O315C-E	29	0	-31	-712	661	405	771	-823
O315C-F	32	0	-33	-746	723	437	843	-867
O315C-H	32	1	-41	-916	675	554	849	-1090
O315C-J	30	-1	-45	-1045	597	589	786	-1234
O315C-K	29	1	-55	-1223	497	738	771	-1496
O315C-L	18	2	-71	-1532	79	964	530	-1983
O315C-M	11	1	-81	-1789	-221	1093	340	-2350
O315C-P	-3	-1	-93	-2054	-703	1224	20	-2777
I315N-N	1	-1	-1	-34	15	2	15	-34
O315N-B	11	2	-1	-8	330	39	334	-12
O315N-C	0	18	17	767	230	19	767	229
O315N-D	-11	22	19	908	-72	45	910	-74
O315N-E	-17	19	15	758	-270	62	762	-273
O315N-F	-18	0	11	256	-455	-143	284	-483
O315N-G	-15	7	7	323	-340	11	323	-340
O315N-H	-14	5	4	225	-340	16	225	-340
O315N-K	-2	-2	0	-37	-83	-19	-30	-90
O315N-N	0	0	0	12	4	-1	13	4

ORNL-5020
UC-79, -79h, -79k

INTERNAL DISTRIBUTION

1. R. L. Battiste
2. M. Bender
3. J. J. Blass
4-6. S. E. Bolt
7. R. H. Bryan
8-10. J. W. Bryson
11 J. H. Butler
12. J. P. Callahan
13. R. D. Cheverton
14. C. J. Claffey
15. J. A. Clinard
16. C. W. Collins
17-19. J. M. Corum
20. W. B. Cottrell
21. J. S. Crowell
22. F. L. Culler
23. R. W. Derby
24. W. G. Dodge
25. D. N. Fanning
26. G. G. Fee
27. M. H. Fontana
28. A. P. Fraas
29. W. R. Gall
30. R. H. Gallagher (consultant)
31. M. J. Goglia
32. W. L. Greenstreet
33-42. R. C. Gwaltney
43. W. O. Harms
44. R. F. Hibbs
45. H. W. Hoffman
46. P. P. Holz
47. S. K. Iskander
48. P. R. Kasten
49. K. C. Liu
50. R. N. Lyon
51. R. E. MacPherson
52. W. J. McAfee
53. W. J. McCarthy, Jr.
54. H. C. McCurdy
55. J. G. Merkle
56-70. S. E. Moore
71. D. J. Naus
72. F. M. O'Hara (consultant)
73. T. W. Pickel
74. H. Postma
75. C. E. Pugh
76. M. Raftenberg
77. M. Richardson
78. D. N. Robinson
79. W. K. Sartory
80. R. A. Schmidt
81. M. R. Sheldon
82. J. E. Smith
83. I. Spiewak
84. W. C. T. Stoddart
85. J. J. Taylor
86. D. B. Trauger
87. G. D. Whitman
88. W. J. Wilcox
89. G. T. Yahr
90. ORNL Patent Office
91-93. Central Research Library
94. Document Reference Section
95-100. Laboratory Records Department
101. Laboratory Records, ORNL RC

Subcontractors

102. Atomics International, Canoga Park, CA 91304
103. Auburn University, Auburn, AL 36830
104. Babcock and Wilcox Co., Alliance, OH 44601
105. Battelle-Columbus Laboratories, Columbus, OH 43201
106. Case Western Reserve University, Cleveland, OH 44106
107. Catholic University of America, Washington, DC 20017
108. Combustion Engineering, Chattanooga, TN 37401
109. Combustion Engineering, Windsor, CT 06095
110. General Electric Co., R&D Center, Schenectady, NY 12301
111. Pennsylvania State University, University Park, PA 16802
112. University of Tennessee, Knoxville, TN 37916

EXTERNAL DISTRIBUTION

113-114. Director, Division of Reactor Research and Development, ERDA, Washington, DC 20545
115-116. Director, Office of Nuclear Regulatory Research, NRC, Washington, DC 20555
117. Director, Reactor Division, ERDA, ORO
118. Research and Technical Support Division, ERDA, ORO, Oak Ridge, TN 37830
119-195. Nozzle Analysis and Nuclear Design Criteria – Piping-Pumps-Valves Programs Distribution
196-469. Given distribution as shown in TID-4500 under categories UC-79, -79h, and -79k (25 copies – NTIS)

☆U. S. GOVERNMENT PRINTING OFFICE: 1975-748-189/235